

# INTRODUCTION TO NEUTRINO PHYSICS

*Paolo Lipari*

Dipartimento di Fisica, Università di Roma “la Sapienza”, and I.N.F.N., Sezione di Roma, P.A. Moro 2, I-00185 Roma, Italy

## Abstract

Neutrino Physics in recent times has been going through a revolutionary period. Measurements of neutrinos coming from the sun or produced by cosmic rays in the Earth’s atmosphere have revealed that neutrinos “oscillate”, that is they change their flavor periodically with time. The observation of this phenomenon allows to obtain precious information on the neutrino masses and their mixing, shedding information about the “flavor problem”, that is the origin of the fermion families and of the masses and mixing of quarks and leptons. In these lectures we introduce the subject and review these recent developments.

## 1. INTRODUCTION

In many ways neutrinos are special particles, first of all they are several order of magnitude lighter than all other fermions, and in fact no direct measurement has found evidence for a non zero neutrino mass: for all detected neutrinos one has measured (within errors)  $p c = E$ . Neutrinos are also neutral, do not feel the strong interactions, and interact only weakly, in fact extraordinarily weakly. For example the neutrinos produced in nuclear reactors with energy  $E_\nu \sim 1$  MeV have a cross section of order  $\sigma \sim 10^{-44} \text{ cm}^2$ , this corresponds to a probability  $\sim 10^{-18}$  to interact in a solid detector with the thickness of one meter, or a probability  $\sim 10^{-11}$  to interact inside the Earth traveling along a trajectory that passes through its center.

Neutrinos are then “elusive” particles, but they also are very abundant particles in the universe, and we do not notice them only because they interact so little. We live immersed in a bath of cosmological neutrinos produced when the universe was hot and young, actually ‘immersed’ is probably not a good expression because the neutrino densities inside and outside our bodies are essentially identical. The average number density of cosmological neutrinos is  $n_\nu \simeq 336 \text{ cm}^{-3}$ , and inside our galaxy it can be much larger because of gravitational clustering effects (that are determined by the  $\nu$  mass and are not known). Approximately 60 billions of solar neutrinos, produced in the core of the sun by nuclear reactions, cross each square centimeter of our body every second. A truly fantastic number of neutrinos ( $\sim 10^{58}$ ) is emitted in few seconds following the gravitational collapse of a massive star that triggers one supernova explosion. The sun and the closest supernova in the last three centuries (SN1987A in the Large Magellanic Cloud) have been the first two astrophysical objects to be “seen” in neutrinos, and in the (hopefully) not too far future, new detectors should be able to detect neutrinos from other astrophysical sources, and neutrinos will become a new precious “messenger” from distant objects. The smallness of the neutrino interaction cross section is at the same time the biggest problem for the newly born science of neutrino astronomy, since very massive detectors are required to have appreciable event rates, and also an extraordinary opportunity, because neutrinos can emerge from deep inside the core of astrophysical objects, revealing directly the physical processes that operate there. For example solar neutrinos come directly from the sun inner core, and directly tell us about the nuclear fusion reactions that are the source of the solar luminosity, while the visible photons are emitted from the the surface with a black body spectrum.

Neutrinos have two type of interactions, they can couple with a  $Z^0$  boson, changing their 4-momentum but keeping their identity (neutral current interactions), or they can couple with a  $W^\pm$  boson “transforming” into one of the charged leptons  $e^\pm, \mu^\pm$  or  $\tau^\pm$  (charged current interactions). Of course

the interaction vertices can generate different type of processes. For example the vertex of  $W$  boson, a neutrino and a charged lepton results in processes such as: a charged lepton transforming into a neutrino with the emission of a (virtual)  $W$  boson, or a  $W$  boson that generates a neutrino charged lepton pair. Because of the charged current processes one can define the concept of neutrino flavor. The flavor of a neutrino is simply the type (that is the mass) of the charged lepton that is connected to the same charged current vertex. For example in the decay of a (virtual)  $W^-$  or  $W^+$  one conventionally writes:

$$W^+ \rightarrow \ell^+ + \nu_\ell, \quad W^- \rightarrow \ell^- + \bar{\nu}_\ell, \quad (1)$$

where the label  $\ell = e, \mu, \tau$  of the neutrino correspond to the mass (or type) of the charged lepton. The distinction of  $\nu$  and  $\bar{\nu}$ , and the  $\ell$  label given to the neutrino has a very simple and clear experimental justification. It has been found that a “ $\nu_e$ ”, defined according to the convention of (1), interacting close to its creation point can only produce  $e^-$  (and *not* a  $\mu^-$  or an  $e^+$ ), while a “ $\bar{\nu}_e$ ” can only produce  $e^+$ , a  $\nu_\mu$  only a  $\mu^-$ , and similarly for the other neutrino types. For example a crucial experiment demonstrated that the neutrinos produced in a pair with a  $\mu^+$ , close to their creation point can only generate  $\mu^-$  in the sequence of processes:

$$\begin{aligned} \pi^+ &\rightarrow \mu^+ + \nu_\mu, \\ \nu_\mu + p &\rightarrow \mu^- + \text{hadrons}. \end{aligned} \quad (2)$$

In summary, both the flavor label and the “bar” notation have a well defined phenomenological meaning.

Neutrinos have half integer intrinsic angular momentum (or spin). The extraordinary discovery of the 50’s has been the finding that all “ $\nu$ ” have their spin, within experimental uncertainties, anti-parallel to their momentum, while for all “ $\bar{\nu}$ ” the spin is parallel. In different words all,  $\nu$  are left-handed, and all  $\bar{\nu}$  are right-handed. This is at the basis of the “chiral nature” of the weak interactions, and is the source of the effects of violation of parity observed in nature. This fact opens a fascinating possibility, namely that the states  $\nu$  and  $\bar{\nu}$  are the two different spin states of a two state “Majorana particle” that is the anti-particle of itself, while all the other fermions are “Dirac particles” having 4 states (particle–antiparticle, each with two independent spin states).

A remarkable physical effect, originally predicted by Bruno Pontecorvo [1] has been recently measured in neutrino physics, and is the existence of “flavor oscillations”. To understand this phenomenon let us consider for a moment the decay of a (virtual)  $W$  boson into a quark pair. It is known that this decay is of type:

$$W^- \rightarrow \bar{u} + d', \quad W^- \rightarrow \bar{c} + s', \quad W^- \rightarrow \bar{t} + b', \quad (3)$$

where for example the  $d'$  quark that is produced in association with a  $\bar{u}$  is a linear superposition of the three quark states that have charge  $-1/3$  and well defined mass:  $d$ ,  $s$  and  $b$  (and similarly for  $s'$  and  $b'$ ). The states produced at the  $W$  vertices are connected to the mass eigenstates by the Cabibbo–Kobayashi–Maskawa matrix [2]:

$$\begin{pmatrix} d' \\ s' \\ b' \end{pmatrix} = V^{\text{CKM}} \begin{pmatrix} d \\ s \\ b \end{pmatrix}. \quad (4)$$

It is natural to expect that this “mixing” phenomenon can also happen in the lepton sector, and the neutrinos  $\nu_\ell$  produced in association with the charged lepton  $\ell^-$  will not have a well defined mass but be a linear combination of the states that have a well defined mass:

$$\begin{pmatrix} \nu_e \\ \nu_\mu \\ \nu_\tau \end{pmatrix} = U^{\text{PMNS}} \begin{pmatrix} \nu_1 \\ \nu_2 \\ \nu_3 \end{pmatrix}, \quad (5)$$

where  $U^{\text{PMNS}}$  is the Pontecorvo–Maki–Nakagawa–Sakata matrix [1,3], the leptonic analogous of the

CKM matrix for quarks. In the case of neutrinos, because of the smallness of the neutrino masses a new remarkable quantum-mechanical phenomenon can exist, that is the phenomenon of flavor oscillations. In the case of quarks, the measurement of the final state can easily determine the mass of the quark, on the other hand it is practically impossible to measure the mass of a neutrino, therefore the amplitudes for the production of neutrinos with different mass must be added *coherently*. Since the amplitudes of different mass components evolve differently with space and/or time, acquiring different quantum mechanical phases, it follows that flavor is a *periodical function of time*. In other words if a neutrino of type  $\nu_e$  is produced at a point  $A$ , a measurement close point to this creation point will result in the production of charged leptons of type  $e^-$ , but at a more distant point  $B$  the very same neutrino can generate also  $\mu^-$  or  $\tau^-$  particles if the quantum mechanical phases of its different components have become significantly different from each other. The closer the neutrino masses are to each other, the longer is the time needed to have appreciable phase differences between the different components, and (since neutrinos travel at approximately the speed of light) the probability for a transition to a different flavor becomes significantly different from zero only for a long distance between the production and detection points. On the other hand, experiments with long pathlength allow the measurement of tiny mass differences between the neutrinos.

The remarkable development of the last few years has been the discovery of the phenomenon of flavor oscillations with two type of experiments detecting “atmospheric” and solar neutrinos. The results are consistent with each other, and can be interpreted to give us very constraining information about the neutrino mass splittings and mixing. Additional controversial indications of flavor transitions of type  $\bar{\nu}_\mu \rightarrow \bar{\nu}_e$  have been obtained by the LSND experiment.

These lectures present an introduction to the physics of neutrinos, with particular attention to the discovery of the flavor transitions. The work is organized as follows: in the next Section we discuss general properties of neutrinos, Section 3 gives a rapid overview of the sources of neutrinos in nature, Section 4 discusses the phenomenon of flavor oscillations in vacuum, Section 5 discusses in more detail the quantum mechanics of oscillations, Section 6 discusses neutrino oscillations in matter, Sections 7 and 8 discuss the observations of atmospheric and solar neutrinos, Section 9 and 10 additional observations of reactor and accelerator neutrinos, Section 11 discusses double beta decay, Section 12 presents a phenomenological summary on flavor transitions, Section 13 very briefly discusses model for the neutrino masses.

The bibliography on neutrino physics is very rich. Several good textbooks exist on the subject, for example [4–6]. Recent lectures/reviews of the subjects are: [7–13]. In order to follow the developments of the field two very useful sites on the web are [14] and [15].

## 2. GENERAL PROPERTIES OF NEUTRINOS

### 2.1. Neutrino Flavors:

In the standard model of particle physics there are three neutrino flavors. Each neutrino completes a doublet with the corresponding charged leptons. For example a  $W^+$  gauge boson can couple to the three neutrino/charged-lepton pairs:

$$\begin{aligned} W^+ &\rightarrow e^+ \nu_e, \\ &\rightarrow \mu^+ \nu_\mu, \\ &\rightarrow \tau^+ \nu_\tau. \end{aligned} \tag{6}$$

The label associated to the neutrinos correspond to the flavor, that is the mass of the charged lepton produced in association.

## Electron neutrinos

Historically the first evidence of the neutrinos appeared in the study of nuclear beta decay in the 1920's. Beta decay is a form of radioactivity where a primary nucleus ( $A, Z$ ) decays into a lighter secondary one of the same mass number but charge differing by one unit, and an electron (or positron) and nothing else visible:

$$(A, Z) \rightarrow (A, Z \pm 1) + e^{\mp} + \text{nothing else visible}. \quad (7)$$

An example of this process is the decay of a free neutron into a proton and an electron with a lifetime of approximately 15 minutes (886.7 sec). In the absence of additional invisible particles in the final state, the  $e^{\mp}$  should have a well defined energy  $E_e \simeq Q \equiv M_i - M_f$ , on the contrary experimentalists found a continuum spectrum ranging from  $m_e$  up to the maximum allowed energy  $Q$ . Various explanations were offered for this anomaly (Niels Bohr even arrived to speculate about the possibility that energy conservation was violated) until in December 1930 Wolfgang Pauli suggested that a non-observed particle was emitted in the reaction. This unobserved particle had to be neutral (to conserve electric charge), very light (since  $E_{e,\max} \simeq Q$ ) and with spin 1/2 (to satisfy angular momentum conservation and statistics). In modern notation beta decays are now considered as the processes:

$$\begin{aligned} n &\rightarrow p + e^- + \bar{\nu}_e, \\ A(Z, N) &\rightarrow A(Z + 1, N - 1) + e^- + \bar{\nu}_e, \\ A(Z, N) &\rightarrow A(Z - 1, N + 1) + e^+ + \nu_e. \end{aligned} \quad (8)$$

Soon after the proposal of Pauli, Enrico Fermi [16] proposed a model of beta decay (and weak interactions in general) in terms of the product of two weak "currents", one connecting the initial and final state nucleons, and the other one the final state electron and anti-neutrino. The strength of the interaction was related to the coupling strength  $G_F$ . In Fermi's theory the two currents connected at the same space-time point, assuming that the interaction was very short ranged. In modern language the Fermi constant  $G_F$  can be understood as the effect of the exchange of a virtual but massive heavy "photon", that is the gauge boson  $W^{\pm}$  with a mass  $M_W \simeq 80$  GeV. The weakness of the weak interaction can be understood as the effect of the large mass (and corresponding short range) of the  $W$  boson with  $G_F \simeq e^2/M_W^2$ , or more exactly:

$$\frac{G_F}{\sqrt{2}} = \frac{1}{8} \left( \frac{e}{\sin \theta_W} \right)^2 \frac{1}{M_W^2}, \quad (9)$$

(where  $\theta_W$  is the Weinberg angle). Fermi's theory could successfully describe the observed spectra of electrons and positrons emitted in beta decays, and at the same time it could predict the existence of other processes involving the "weak currents", in particular the existence of the "inverse  $\beta$  decay" processes such as:

$$\begin{aligned} \bar{\nu}_e + p &\rightarrow e^+ + n, \\ \nu_e + n &\rightarrow e^- + p. \end{aligned} \quad (10)$$

The cross section for these processes could be predicted and found to be extremely small. The detection of neutrinos therefore remained elusive for more than 20 years, until the results of Reines and Cowan [17] in 1956. They used the nuclear reactor at Savannah River in South Carolina as an anti-neutrino source and a detector of water with dissolved cadmium chloride; the detection technique was the coincident (with a few  $\mu$ sec delay) observation of a positron emitted in the reaction  $\bar{\nu}_e + n \rightarrow e^+ + n$ , together with a photon emitted in the deexcitation of cadmium after the neutron capture:  $n + {}^{112}\text{Cd} \rightarrow {}^{113}\text{Cd} + \gamma$ . In 1996 Fred Reines received the Nobel prize in physics for this discovery. The study of  $\beta$  decays allowed to establish the "chiral nature" of neutrinos, the  $V-A$  structure of weak interactions, and the existence of Parity non-conservation effects in the weak interactions.

## Muon neutrinos

Muon neutrinos and anti-neutrinos are produced pion and muon decay:

$$\pi^+ \rightarrow \mu^+ + \nu_\mu, \quad (11)$$

$$\mu^+ \rightarrow e^+ + \nu_e + \bar{\nu}_\mu. \quad (12)$$

When the decay  $\pi^\pm \rightarrow \mu^\pm + \nu$  was discovered it was natural to ask the question if the undected particles produced in the decay were identical with the neutrinos produced in  $\beta$  decay. This problem was solved experimentally in 1962 by L. Lederman, M. Schwarz and J. Steinberger [18] who performed the first experiment with accelerator neutrinos. Bombarding a Beryllium target with a 15 GeV primary proton beam, they produced a beam of pions, that because of the decay was the source of a neutrino beam, and then studied the interaction with nucleons of type  $\nu_\mu + N \rightarrow \mu^- + X$  or  $\nu_\mu + N \rightarrow e^- + X$ . Only the first type of interactions were found, demonstrating that  $\nu_e$  and  $\nu_\mu$  are different particles. The reason why the decay  $\pi^+ \rightarrow e^+ \nu_e$  that has a larger phase space available is strongly suppressed (with a branching ratio  $\sim 10^{-4}$ ) is connected to the  $V - A$  nature of the weak interaction, see later in Section 2.4.

## Tau neutrinos

The  $\nu_\tau$  is associated to the third charged lepton, the  $\tau^-$  discovered in 1975 at Stanford. Tau neutrinos and anti-neutrinos are expected to be produced in  $\tau^\pm$  decays.

$$\begin{aligned} \tau^- &\rightarrow \nu_\tau + W^-, \\ &\rightarrow \nu_\tau + e^- + \bar{\nu}_e, \\ &\rightarrow \nu_\tau + \mu^- + \bar{\nu}_\mu, \\ &\rightarrow \nu_\tau + [\bar{u}s']. \end{aligned} \quad (13)$$

## 2.2. Number of light neutrino species

How many families of quarks and leptons exist in Nature? The number of light neutrino species that have the usual electroweak interactions can be determined studying the process:

$$Z^0 \rightarrow \nu_\alpha + \bar{\nu}_\alpha. \quad (14)$$

The partial width of this decay  $\Gamma_{\nu\bar{\nu}}$  is accurately calculable in the standard model:

$$\Gamma_{\nu\bar{\nu}} = 166.9 \text{ MeV} \quad (15)$$

and therefore the  $Z$  will have a branching ratio into invisible final states that is proportional to the number of light neutrino species:

$$\Gamma_{\text{invisible}} = N_\nu \Gamma_{\nu\bar{\nu}}. \quad (16)$$

The invisible width can be obtained experimentally subtracting the contributions of all visible channels from the measured total width:

$$\Gamma_{\text{invisible}} = \Gamma_{\text{tot}} - \Gamma_{\text{vis}} = 498 \pm 4.2 \text{ MeV}. \quad (17)$$

This can be interpreted [19] as the result that the number of the light, active  $\nu$  species is:

$$N_\nu = \frac{\Gamma_{\text{inv}}}{\Gamma_{\nu\bar{\nu}}} = 2.994 \pm 0.012. \quad (18)$$

### 2.3. Sterile neutrinos

Equation (18) gives the number of light particles that have the standard properties of neutrinos with respect to the weak interactions, and therefore does not apply to “sterile neutrinos”. A sterile neutrino is a particle that is a singlet with respect to the  $SU(3) \otimes SU(2) \otimes U(1)$  group of the standard model, but that is mixed or related to neutrinos. As an example (among many) of sterile neutrinos one can consider the “Exact Parity Model” [21], where the gauge group of the universe has the form:

$$\mathcal{G} = \mathcal{G}_1^L \otimes \mathcal{G}_2^R = [SU(3) \otimes SU(2) \otimes U(1)]_1 \otimes [SU(3) \otimes SU(2) \otimes U(1)]_2, \quad (19)$$

and each fermion has a mirror partner, so that the ordinary fermions are singlet with respect to the subgroup  $\mathcal{G}_2^R$ , while the mirror particles are singlet with respect to  $\mathcal{G}_1^L$ . Because of the existence of the mirror particles the model is symmetric with respect to parity. In this model there are three “mirror neutrinos”, that do not interact with the ordinary  $W$  and  $Z$  bosons and are coupled only to the mirror gauge bosons  $\tilde{W}$  and  $\tilde{Z}$ . Clearly the bound (18) is not relevant for these particles. It can be shown that in this model the eigenstates of the Hamiltonian are linear combinations of type  $\nu_{1,2} = (\nu \pm \tilde{\nu})/\sqrt{2}$  of standard and sterile states, and therefore one expects for all three flavors oscillations  $\nu_\ell \leftrightarrow \tilde{\nu}_\ell$  (with a mixing angle  $\simeq 45^\circ$ ).

An (indirect) limit on the existence of sterile neutrinos mixed with ordinary ones comes from cosmology, and in particular from Big–Bang nucleosynthesis. From the measured primordial abundances of helium-4 and other light nuclear species, one can obtain an estimate of the energy density of the universe at the epoch of nucleosynthesis, that can be translated in an estimate of  $N_\nu^{\text{eff}}$  that is equivalent number of light ( $m < 1$  MeV) species that are *in thermal equilibrium* at this epoch. For a larger  $N_\nu^{\text{eff}}$  the evolution of the universe becomes faster and the helium abundance grows. From the observed primordial helium abundance one can then extract an upper limit:

$$N_\nu^{\text{eff}} < 3.3, \quad (20)$$

(but perhaps more conservatively 4  $\nu$  species can still be tolerated). In the absence of mixing, sterile neutrinos that interact only extremely weakly will not be in thermal equilibrium with the cosmic soup at the nucleosynthesis epoch, and therefore the limit (20) cannot in general exclude their existence, however oscillations between standard and sterile neutrinos can generate a significant population of sterile neutrinos. If the mixing is sufficiently large and the oscillations sufficiently fast (that is if the mass differences are sufficiently large) one can violate the bound (20). Therefore the bound (20) be used to set limits on the existence of oscillations between standard and sterile neutrinos.

### 2.4. Chirality and Helicity

It has been observed that all neutrinos have (within errors) spin parallel to their momentum, while for anti-neutrinos spin and momentum are antiparallel. This is a consequence of the  $V - A$  structure of the weak interaction. In this theory the spinor of the fermions (anti-fermions) produced in a  $W^\pm$  vertex are projected with  $(1 \mp \gamma_5)$  ( $\gamma_5$  is a Dirac matrix). In words, particles are produced in weak interaction vertices with a well defined *chirality*. For a particle with  $m/E$  small, a state of left chirality (that is the projection  $(1 - \gamma_5)$ ) corresponds to an amplitude  $\sim 1$  of having the spin antiparallel to the momentum and an amplitude  $\sim m/E$  of having the opposite spin state. For right chirality the situation is reversed. Clearly in the case of massless particles chirality (that is the  $(1 \pm \gamma_5)$  projections of a fermion state), and helicity (that is the projection of the spin parallel to the fermion momentum) coincide, however in general the two concepts are different, and this difference can have very important consequences.

An example one can consider the decay of the charged pion. This decay has two possible modes:

$$\begin{aligned}\pi^+ &\rightarrow \mu^+ + \nu_\mu, \\ \pi^+ &\rightarrow e^+ + \nu_e.\end{aligned}$$

The strong suppression of the second mode, is an outstanding manifestation of the  $V - A$  nature of the charged current weak interactions, and a clear illustration of the difference between the chirality and the helicity. Let us consider (see Fig. 1) the decay of pions at rest:  $\pi^+ \rightarrow \ell^+ + \nu_\ell$ . The  $V - A$  structure

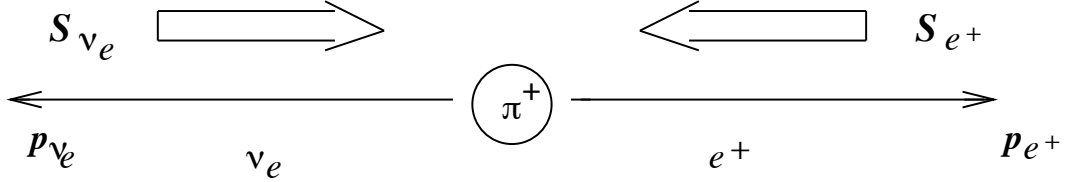


Fig. 1: Charged pion decay in the rest frame of the pion.

of weak interactions requires the emitted  $\nu_\ell$  to be of left handed chirality. For  $m_\nu \simeq 0$  this also means that it has the left handed (or negative) helicity (spin antiparallel to its momentum). Conservation of total angular momentum then requires  $\ell^+$  to be of negative helicity. However, the  $\ell^+$  is an antiparticle, and again for the  $V - A$  structure of weak interactions it must be produced in a state of right-handed chirality. Therefore the amplitude of the process must be proportional to the admixture of left handed (negative) helicity for a right-handed chirality charged-lepton, that is proportional to its mass:  $A(\pi^+ \rightarrow \ell^+ + \nu_\ell) \propto m_\ell$ . Including phase space effects  $\propto (m_\pi^2 - m_\ell^2)$  one has the expectation:

$$R_\pi \equiv \frac{\Gamma(\pi^+ \rightarrow e^+ + \nu_e)}{\Gamma(\pi^+ \rightarrow \mu^+ + \nu_\mu)} = \left( \frac{m_e}{m_\mu} \right)^2 \left( \frac{m_\pi^2 - m_e^2}{m_\pi^2 - m_\mu^2} \right)^2 = 1.28 \times 10^{-4}. \quad (21)$$

In agreement (after including a 4% radiative correction) with the experimental value:  $R_\pi = (1.230 \pm 0.004) \times 10^{-4}$ .

## 2.5. Limits on the Neutrino masses

### Direct Measurements

A direct measurement of the neutrino masses is in principle possible, with kinematical methods, determining the momentum and energy of a neutrino. These methods have only produced upper limits for the neutrino masses [19].

For  $\nu_e$  (or more precisely  $\bar{\nu}_e$ ) the most sensitive method is the study of the shape of the high energy part of the  $\beta$  decay spectrum. The “end point” of the spectrum (the highest kinematically allowed energy for the electron) depends on the  $\nu$  mass ( $E_e^{\max} \simeq Q - m_\nu$ ). The most studied decay (because of a low  $Q$  value) is the decay of Tritium:



The current limits<sup>1</sup> are

$$\begin{aligned}m_{\nu_1} &< 2.5 \text{ eV at 95% c.l. (Troitsk)}, \\ &< 6 \text{ eV at 95% c.l. (Mainz)}, \\ &< 15 \text{ eV at 95% c.l. (PDG suggestion)}.\end{aligned} \quad (23)$$

---

<sup>1</sup> $\nu_1, \nu_2$  and  $\nu_3$  are the primary mass components of  $\nu_e, \nu_\mu$  and  $\nu_\tau$ , respectively.

A limit on the mass of  $\nu_\mu$  can be obtained studying the decay  $\pi^+ \rightarrow \mu^+ \nu_\mu$ . In the pion rest frame the momentum of the muon is:

$$E_\mu^* = \frac{m_{\pi^\pm}^2 + m_\mu^2 - m_\nu^2}{2 m_{\pi^\pm}}. \quad (24)$$

The neutrino mass can be obtained from measurements of the masses  $m_\pi$ ,  $m_\mu$  and the momentum  $p_\mu$  of the final state muon in the pion rest frame. This results in an upper limit:

$$m_{\nu_2} < 170 \text{ keV at 90% c.l..} \quad (25)$$

For  $\nu_\tau$  the limit is obtained measuring the missing 4-momentum in decays like  $\tau^- \rightarrow 5\pi^\pm \nu_\tau$  where all particles except the neutrino are measured. This results in the limit:

$$m_{\nu_3} < 18.2 \text{ MeV at 95% c.l..} \quad (26)$$

### Neutrinoless double beta decay

The non observation of the neutrinoless double beta decay allows to set a limit on the combination:

$$\langle m_{\nu_e} \rangle_{\text{eff}} = \sum_j U_{ej}^2 m_j \lesssim 0.4 \text{ eV}, \quad (27)$$

(for more discussion see Section 11.). This limit applies only to the case where neutrinos are Majorana particles (see Section 2.6). Note also that the limit depends on the neutrino mixing matrix and since the  $U_{ej}$  are complex numbers cancellations are possible and  $\langle m_{\nu_e} \rangle_{\text{eff}}$  is a lower limit for the highest neutrino mass.

### Supernova SN1987A

The measurements of a small number of  $\bar{\nu}_e$  from supernova 1987A in February 1987 has allowed to obtain a limit  $m_{\bar{\nu}_e} \lesssim 20 \text{ eV}$  (see Section 3.2).

### Cosmological limit

The most stringent limits on the neutrino masses can be obtained from cosmology (for more discussion see Section 3.1). The energy density in neutrinos can be very reliably estimated as:

$$\Omega_\nu = \frac{\rho_\nu}{\rho_c} = \frac{1}{h^2} \frac{\sum_j m_j}{93 \text{ eV}}, \quad (28)$$

where  $\rho_c$  is the critical density that makes the universe flat, and  $h \simeq 0.65$  is the Hubble constant in units of 100 Km/s/Mpc. The measured flatness of the universe gives a limit  $\Omega_{\text{tot}} h^2 \lesssim 0.4$  that results in:

$$\sum_j m_j \lesssim 37 \text{ eV}. \quad (29)$$

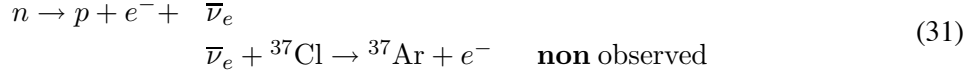
A more stringent (but more model dependent) limit can be obtained from studies of structure formation in the universe. From these studies emerges a broad consensus that most of the energy density of the universe is in form of “dark energy” ( $\Omega_\Lambda \sim 0.7$ ), and “cold dark matter” ( $\Omega_{CDM} \simeq 0.25$ ), leaving only a smaller amount available for neutrinos. Recent measurements of the anisotropies of the Cosmic Microwave Background Radiation by WMAP [20] have been interpreted as giving a limit on the contribution of Hot Dark Matter in the universe:

$$\Omega_\nu h^2 \leq 0.0076 \quad (95\% \text{ C.L.}). \quad (30)$$

This corresponds to the limit  $\sum_j m_j \leq 0.7 \text{ eV}$ .

## 2.6. DIRAC or MAJORANA particles ?

Can neutrinos be their own antiparticles? If this is the case they are “Majorana” particles, if not they are “Dirac” particles like the quarks and the charged leptons. It is known experimentally that neutrinos emitted in  $\beta^-$  decay (which we conventionally call  $\bar{\nu}_e$ ) are not captured in reactions which are caused by  $\nu_e$ . That is the sequence of reactions:



is not observed even if the reaction  $\nu_e + {}^{37}\text{Cl} \rightarrow {}^{37}\text{Ar} + e^-$ , does exist in nature. This does *not* imply that  $\nu_e$  and  $\bar{\nu}_e$  are different objects, because the weak interactions that are responsible for neutrino interactions are chiral (or have a  $V - A$  structure). The particles which we call  $\bar{\nu}_e$  are right-handed, while the particles that are absorbed by  ${}^{37}\text{Cl}$  are left-handed, and therefore the non observation described in (31) could simply be due to a strong dynamical suppression (of order  $\sim (m_\nu/E)^2$ ), even if  $\nu_e$  and  $\bar{\nu}_e$  are in fact the same object. The sequence of reactions described in (31) is therefore possible if two conditions are met:

- $\nu_e$  and  $\bar{\nu}_e$  are identical particles (that is the neutrino is a Majorana particle)
- The neutrino mass is non vanishing, so that the helicity suppression is large but not complete.

Something like the sequence of reactions in (31) could be observable in the process of neutrinoless double beta decay (see Section 11.), and the study of this process appears the best way to verify the nature (Dirac or Majorana) of the neutrino.

## 3. NEUTRINO SOURCES

Neutrinos are very common particles in the universe, and play a very important role in many objects and events in astrophysics and cosmology. Figure 2 shows a plot of the energy spectrum of neutrinos that reach the surface of the Earth. The spectrum extends for more than 20 orders of magnitude in both energy and intensity. “Naturally” produced neutrinos have several components: particle accelerators.

### 3.1. Cosmological Neutrinos

The relic neutrinos, i.e. the neutrinos left over from the early epochs of the evolution of the universe, have a number density of about  $56 \text{ cm}^{-3}$  for each neutrino species ( $\nu_e, \bar{\nu}_e, \nu_\mu, \bar{\nu}_\mu, \nu_\tau, \bar{\nu}_\tau$ ) and a black-body spectrum with a temperature  $T_\nu \simeq 1.947$  Kelvins (or an average kinetic energy of  $5 \times 10^{-4}$  eV). [For a general review of cosmology see for example [22,23].]

The spectrum of relic *photons* from the big bang has been well studied by the COBE satellite and other detectors and has a temperature  $T_\gamma^{\text{now}} = 2.728$  Kelvin. This corresponds to a number density:

$$n_\gamma = \frac{2}{(2\pi\hbar)^3} \int d^3 p_\gamma \frac{1}{e^{E/T} - 1} \simeq 412 \text{ cm}^{-3}. \quad (32)$$

An analogous neutrino spectrum must exist from the early universe. In fact, when the universe was sufficiently hot, neutrinos were kept in equilibrium with the photons with reactions such as  $\gamma\gamma \rightarrow \nu_\alpha \bar{\nu}_\alpha$ . Neutrinos dropped out of thermal equilibrium when the temperature dropped below  $T \sim 10^{10}$  Kelvin, and from this point remained essentially decoupled from the rest of the universe, but proceeded to cool as the universe expanded. The neutrino temperature is cooler than the photon one, because the photon component was “reheated” by the annihilation of the electron and positron components of the ‘cosmic

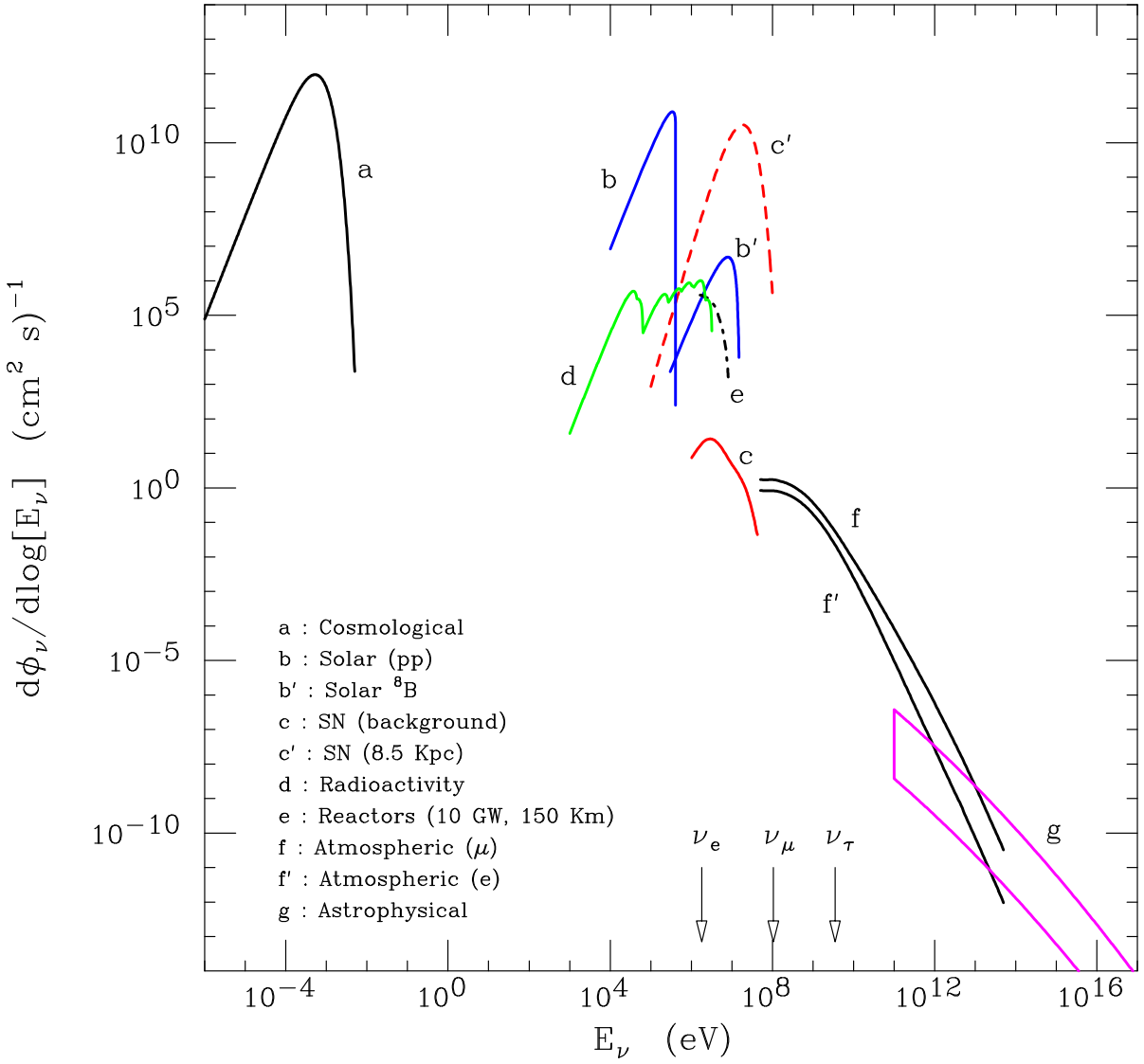


Fig. 2: Flux of neutrinos at the surface of the Earth. The three arrows show the energy thresholds for charged current interactions on a free proton target. The line that refers to cosmological neutrinos assumes that the neutrino mass is vanishing. For massive neutrinos the flux is modified since gravitational clustering enhances the density, the  $\nu$  velocity is decreased and the energy spectrum is modified. The line that refers to Supernova neutrinos describes  $\bar{\nu}_e$ . Different neutrino species have similar spectra, with differences difficult to appreciate in the figure. The line that describes geophysical neutrinos includes the  $^{238}\text{U}$  and  $^{232}\text{Th}$  decay chains, the flux weakly depend on geographical location. The atmospheric neutrino fluxes are calculated for the Kamioka location. Only the lowest energy part depends on the location. A range of prediction for the flux of astrophysical neutrinos is shown.

soup' that happened at a temperature  $T_\gamma \simeq m_e$ . Since the entropy of the photon gas after the  $e^\pm$  annihilation is equal to the sum of the entropy of the three components ( $\gamma, e^+, e^-$ ) before annihilation, one has<sup>2</sup>:

$$T_\gamma^3 \times 2 = T_\nu^3 \times \left[ 2 + 4 \times \frac{7}{8} \right] \quad (33)$$

or

$$T_\nu = \left( \frac{4}{11} \right)^{\frac{1}{3}} T_\gamma. \quad (34)$$

This corresponds to a neutrino number density:

$$n_\nu = \frac{1}{(2\pi\hbar)^3} \int d^3p \frac{1}{e^{E/T} + 1} \simeq 56 \text{ cm}^{-3}. \quad (35)$$

Note that in the last equation we have considered a single spin state for the neutrino. If the neutrino is massive and is a Dirac particle, also an additional neutrino (and anti-neutrino) spin state exists, however since these 'wrong helicity' states are singlet with respect to the standard model, they interact extremely weakly, and are present in negligible number in the cosmic soup, so that the neutrino number density of neutrinos does not depend on whether they are Dirac or Majorana particles. For completeness we also observe that our derivation of the neutrino number density has assumed that  $n_\nu \simeq n_{\bar{\nu}}$ . More in general, it is possible to construct models where the universe has a large net lepton number and  $(n_\nu - n_{\bar{\nu}})/(n_\nu + n_{\bar{\nu}})$  is large. In these cases the neutrino number density is modified.

The cosmological neutrino *energy* density depends critically on the  $\nu$  masses. For  $m_\nu \gg T_\nu^{\text{now}} \simeq 1.6 \times 10^{-4}$  eV, the kinetic energy of the neutrinos is negligible and the  $\nu$  energy density is simply  $\rho_\nu = m_\nu n_\nu$ . In units of the critical density  $\rho_c = \frac{3}{8\pi G} H^2$  (the density that makes the universe flat) one has:

$$\Omega_\nu = \frac{\rho_\nu}{\rho_c} = \frac{1}{h^2} \frac{\sum_j m_j}{93 \text{ eV}}, \quad (36)$$

where  $h \simeq 0.65$  is the Hubble constant in units of 100 Km/sec/Mpc. Measurements of the age of the universe and of its expansion rate give a limit  $\Omega h^2 \lesssim 0.4$  that sets the most stringent limit on the neutrino masses. On the other hand equation (36) tell us that if the neutrinos masses are of order of few eV's or more they can be an important, or even the dominant component of the dynamics of the universe solving the so called "Dark Matter Problem", one of the most important puzzles in Physics today.

If neutrinos are an important component of the mass of the universe they also play a crucial role in the formation of its observed structures (galaxies, clusters of galaxies, and larger scale coherent structures). At early times the universe was extremely smooth as demonstrated by the tiny amplitude of the temperature fluctuations of the cosmic microwave background radiation across the sky, gravity however enhances the density contrast of the irregularities in the density field, generating the observed structures. The outcome of this evolution depends on the initial spectrum of density fluctuations, but also on the composition of the cosmic fluid. If the matter that composes the cosmic fluid can move around easily, it can wipe out the fluctuations of the smaller scales. Neutrinos that are weakly interacting and that, because of their small mass, remain relativistic until later times are very efficient at erasing the initial fluctuations up to large scale, while other forms of dark matter, for example the WIMPS (Weakly Interacting Massive Particles) that move more slowly because of their larger mass are less efficient.

The recent measurements of the anisotropies of the Cosmic Microwave Background Radiation by WMAP [20] have been interpreted as giving a limit on the contribution of Hot Dark Matter in the universe:  $\Omega_\nu h^2 \leq 0.0076$  (at 95% C.L.). This corresponds to the limit  $\sum_j m_j \leq 0.7$  eV.

---

<sup>2</sup>The entropy per unit volume of a bosonic degree of freedom is  $s_B = (2\pi^2/45) T^3$ , and for a fermionic degree of freedom is  $s_F = (7/8) s_B$ .

## Limits on sterile neutrinos

Big bang nucleosynthesis [25] is one of the pillars of cosmology. According to the theory four elements: deuterium, helium-3, helium-4 and lithium-7 were formed when the universe was hot ( $T \sim 1$  MeV) and young ( $t \lesssim 100$  seconds). The calculated abundances of these elements, depend on the baryon density of the universe, and to reproduce the observed abundances one needs to conclude that baryonic matter is only a small fraction of the present energy density of the universe. This calculation allows also to put a limit on the “effective number” of light species (or “neutrinos”) in the universe. The fraction of the baryonic mass that is transformed into helium (that is observed to be approximately 25%) grows with the number of effective neutrino species. This can be understood qualitatively observing that the evolution of the universe is speeded up if more particles species are present and the density is therefore larger, in a faster expansion the neutrons in the cosmic soup have less time to decay and end up forming more helium. Comparing the calculation with the observed helium abundance one obtains the result:

$$N_\nu^{\text{eff}} \lesssim 3.3. \quad (37)$$

As discussed before, the measurements of the width of the  $Z$  boson at LEP set a very stringent limit on the number of neutrinos  $N_\nu = 2.994 \pm 0.012$ , however the cosmological limit is more general because it applies to all light particle that are in thermal equilibrium in the universe, independently from their interaction properties, and therefore it applies to standard (or active) neutrinos, but also to any other light particles, including for example “sterile neutrinos”.

Does then the bound (37) rule out the existence of light sterile neutrinos, such as those implied by the LSND results? It is not necessarily so. The limit refer to a particle in *thermal equilibrium* with the soup of photons electrons and positron at the epoch of nucleosynthesis. A light sterile neutrinos that is interacting “super-weakly”, can only be put in thermal equilibrium with the rest of the matter by oscillations with ordinary neutrinos. Therefore the bound is effective only if the mixing of the sterile neutrino with an ordinary one is sufficiently large and if the squared mass difference is sufficiently large (so that oscillations have time to develop). Oscillations in the dense medium of the universe are controled by subtle matter effects whose calculation is still controversial, it is therefore still not clear what is the precise range of mixing parameters that can be excluded with the cosmological bound (37), and if they are in contrast with explanations in terms of sterile neutrinos of the LSND result<sup>3</sup>.

A very interesting topic that we cannot cover here is the role that neutrinos could play in baryogenesis. The observed excess of baryons over antibaryons in the universe may be related to decays of heavy Majorana neutrinos. For a review of the physics of cosmological neutrinos see [28].

## 3.2. Supernovae

Type II Supernovae explosions (for reviews and references see [29]) mark the end of the life of massive stars (with  $M \gtrsim M_\odot$ ) that have developed an iron core surrounded by several onion-like burning shells and an outer envelope of hydrogen and helium. Iron is the most strongly bound nucleus in nature, and no additional burning can generate energy to support the star core. A stellar iron core is supported by the electron degeneracy pressure, a quantum mechanical effect related to the Heisenberg uncertainty principle:  $\Delta p \Delta x \simeq \hbar$ , that gives momentum to fermions squeezed in a small volume. When enough ‘nuclear ash’ has accumulated, and the iron core of the star reaches the Chandrasekhar limit of  $\sim 1.4$  solar masses, it becomes unstable, and collapses. The collapse is very rapid (can be approximated by free fall) and lasts only a small fraction of a second. The compressed core heats, ‘boiling’ the iron nuclei into separate nucleons, then it becomes energetically favorable to capture the electrons on free protons in the

---

<sup>3</sup>More conservative analysis conclude that the bound of nucleosynthesis can be relaxed to  $N_\nu^{\text{eff}} < 4$ , in this case one light sterile neutrino can certainly exist without conflict with cosmological data.

neutronization process

$$e^- + p \rightarrow n \rightarrow \bar{\nu}_e , \quad (38)$$

that converts nearly all protons in the collapsing core into neutrons. The  $\nu_e$  produced in these reaction rapidly escape from the core generating a “neutronization burst” of  $\nu_e$ ’s. When the collapsing core reaches nuclear density (at a radius  $R \sim 10$  Km) the implosion is halted because of the stiffness of nuclear density matter. At this point a shock wave is formed that propagates outward ejecting the outer layers of the star and producing the spectacular visible explosion. The newly formed proto-neutron star has a radius  $R_{\text{n.s.}} \simeq 10$  Km (and therefore the density is of the same order of nuclear matter), and contains a kinetic energy of order

$$E_{\text{kin}} = -E_{\text{grav}} = \frac{GM^2}{R_{\text{n.s.}}} \simeq 3 \times 10^{53} \text{ erg} . \quad (39)$$

Nearly all (99%) of the energy is radiated away in the form of neutrinos, with only  $\sim 1\%$  going into producing the spectacular explosion as kinetic energy of the ejected layers and electromagnetic radiation. It is likely that the neutrinos emitted by the proto neutron star play a crucial role in the explosion, depositing enough energy near the outward propagating shock to “push” it out of the star, generating the explosion.

All six neutrino species contribute approximately equal to the energy outflow, since they are produced in the hot core by “flavor blind” processes like  $\gamma\gamma \rightarrow \nu_\alpha \bar{\nu}_\alpha$ . The energy spectra are thermal, with average energies  $\langle E(\nu_e) \rangle \simeq 11$  MeV,  $\langle E(\bar{\nu}_e) \rangle \simeq 15$  MeV, and  $\langle E(\nu_{\mu,\tau}) \rangle \simeq \langle E(\bar{\nu}_{\mu,\tau}) \rangle \simeq 25$  MeV. The neutrino emission lasts a time of order  $\Delta t \simeq 10$  seconds that is determined by the time needed for neutrinos to “random walk” out of the core undergoing many scatterings in the dense material<sup>4</sup>. The different average energies of the different components are the consequence of the different cross sections for elastic scattering with electrons (that still exist in the star). Electron neutrinos have the largest cross section, and are emitted from closer to the surface of the stars, while  $\nu_{\mu,\tau}$ ’s and  $\bar{\nu}_{\mu,\tau}$  with a smaller cross section are emitted from deeper inside the stars and are “hotter”.

The theory of neutrino emission in supernova explosions has had a dramatic confirmation the 23rd february 1987, when the neutrinos and the radiation of supernova (SN1987A) that had exploded 170,000 years before in the Large Magellanic Cloud (a small satellite galaxy of our Milky Way) reached the Earth (see Fig. 3). Two detectors: Kamiokande in Japan and IMB in the US detected [30] a few events (11 Kamiokande, 7 IMB) in coincidence with each other and in a time interval of 13 seconds. These events that can be interpreted as the detections of positrons from the reaction  $\bar{\nu}_e + p = e^+ + n$ . From the number and energy spectrum of the observed events, it is possible to extract (with large statistical errors) a fluence and a temperature for the  $\bar{\nu}_e$  emitted by the supernova with results in reasonable agreement with the theoretical predictions.

The handful of events detected from SN1987A have allowed to determine (or put limits) on several neutrino properties, and in particular on its mass. The velocity of a neutrino is given by:

$$v = \frac{p_\nu}{\sqrt{p_\nu^2 + m_\nu^2}} \simeq 1 - \frac{m_\nu^2}{2E_\nu^2} . \quad (40)$$

Therefore two neutrinos of different energy emitted at the same time from a source at a distance  $L$  will reach the detector with a relative time delay:

$$\Delta t = t_1 - t_2 = \frac{L}{v_1} - \frac{L}{v_2} \simeq L \left( \frac{m_1^2}{2E_1^2} - \frac{m_2^2}{2E_2^2} \right) . \quad (41)$$

---

<sup>4</sup>Most of these interactions are elastic scatterings with the neutrons in the star, where the energy of the neutrino changes, but little energy is transferred because of the neutron mass is much larger than the neutrino energy.

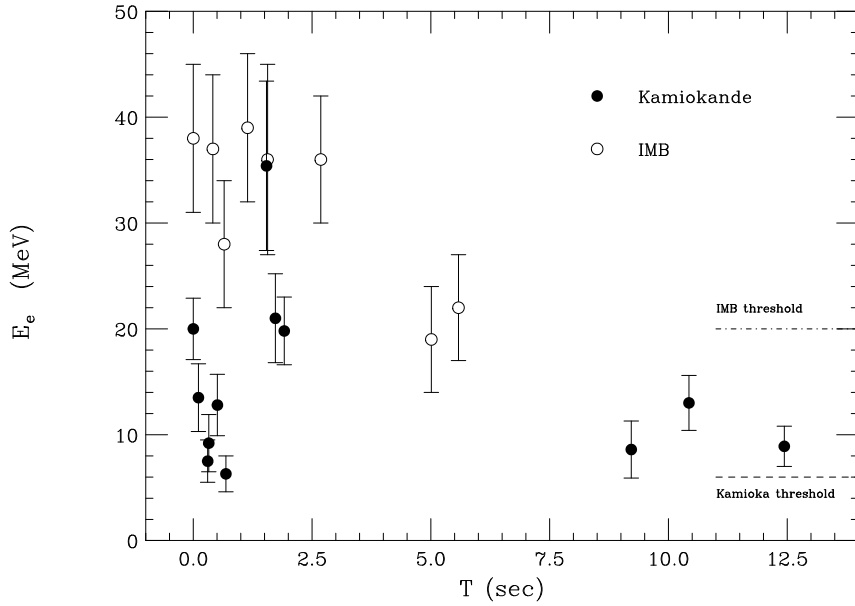


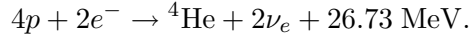
Fig. 3: Time and energy of the events detected the 23rd of february 1987 by the Kamiokande and IMB detectors that are associated with the explosion of the supernova SN1987A in the Large Magellanic cloud, approximately 170 thousand light years away.

Inserting appropriate numerical values one can see that for a mass of 10 eV, a 10 MeV neutrinos emitted from SN1987A ( $L \simeq 55$  Kpc  $\simeq 1.7 \times 10^{21}$  cm) will have a delay of 2.8 seconds with respect to a high energy neutrino. An analysis of the data, shows no correlation of energy with time of arrival, and an overall duration of the signal in agreement with prediction, and therefore no indication of a non vanishing mass. From these considerations one can obtain a conservative limit:<sup>5</sup>

$$m_{\bar{\nu}_e} \lesssim 20 \text{ eV}. \quad (42)$$

### 3.3. Stars

Neutrinos are copiously produced in thermonuclear reactions which occur in the stellar interior and in particular in our sun. The reaction that liberates nuclear binding energy is the effective fusion reaction



So the sun luminosity implies a  $\nu_e$  flux at the Earth of approximately  $6 \times 10^{10} (\text{cm}^2 \text{ s})^{-1}$ . The detailed spectrum of the emitted neutrinos depends on the “path” taken by the nuclear reactions to burn hydrogen into helium. Most of the solar neutrinos have energy below 0.41 MeV, but a smaller component (of order  $5 \times 10^6 (\text{cm}^2 \text{ s})^{-1}$ ) due to the beta decay of boron-8 extends up to 14 MeV, and plays a very important role in the detection of solar neutrinos. The measurements of solar neutrinos and their implications are discussed in Section 8.

### 3.4. Natural Radioactivity neutrinos

The Earth emits approximately 40 TeraWatt of energy, approximately 40% of this energy outflow is due to the decay of radioactive nuclei, 90% of this is due to decay chains due to the Uranium and Thorium decay chains. A  ${}^{238}\text{U}$  nucleus initiates a cascade of 8  $\alpha$  and 6  $\beta$  transitions that terminates in

---

<sup>5</sup>This limit corresponds to the assumption that electron neutrinos have a single dominant mass component.

the stable nucleus  $^{206}\text{Pb}$ , while  $^{232}\text{Th}$  initiates a cascade of 6  $\alpha$  and 4  $\beta$  transitions that terminates with  $^{208}\text{Pb}$ . In each  $\beta$  decay is emitted a  $\bar{\nu}_e$ , with a maximum energy of 3.27 MeV. These decays induce at the surface of the Earth a flux of  $\sim \text{few} \times 10^6 (\text{cm}^2 \text{ s})^{-1}$ . The flux will depend on the location of a detector, because we expect that chemical processes during the formation of the Earth have concentrated Uranium and Thorium in the Earth's crust and (less strongly) mantle, depleting the core. Since the thickness of the crust is variable (being thicker under the continents and thinner under the oceans) the flux is dependent on detector location, for example being larger in Italy than in Japan. The high energy tail (above the threshold energy of 1.8 MeV) of this “geophysical”  $\bar{\nu}_e$  flux can be in principle observed studying the capture on free protons followed by the detection of the neutron capture:  $(\bar{\nu}_e + p \rightarrow e^+ + n, n + p \rightarrow \gamma + d)$ . New large mass detectors for the first time have a chance to measure the geophysical neutrinos. The KamLand detector in the Kamioka observatory in Japan with 1 Kton of  $\text{CH}_2$  scintillator could measure a predicted rate of 50–100 events/year, while the Borexino detector in Italy with 300 tons of  $\text{C}_9\text{H}_{12}$  scintillator could measure a rate of 10–20 events/year. These measurements can give information on the geophysical structure, dynamics and evolution of the present Earth [31].

### 3.5. Atmospheric Neutrinos

The Earth receives an approximately isotropic and constant flux of cosmic rays (with an intensity of approximately 0.5 particles/ $(\text{cm}^2 \text{ sec sr})$ ). The primary cosmic rays, interacting in the upper atmosphere generate a number of secondary particles including charged pions and kaons that in turn generate neutrinos in decays of the type

$$\pi^+ \rightarrow \mu^+ + \nu_\mu, \quad \mu^+ \rightarrow e^+ + \nu_e + \bar{\nu}_\mu \quad (43)$$

(and charged conjugate decays).

### 3.6. Astrophysical Neutrinos

Until today two astrophysical objects have been observed in neutrinos, the sun and the supernova SN1987A. In the future one expects the detection of other astrophysical sources of very high energy neutrinos. Very large ( $\text{Km}^3$ ) neutrino telescopes [32,33] are currently under construction for the detection of high energy astrophysical neutrinos with  $E_\nu \gtrsim 10^{12}$  eV (that is a Tera-electronVolt (TeV) and beyond). The motivation [32–33] for the existence of these very high energy neutrinos is the fact that fluxes of cosmic rays up to energy as high as  $10^{20}$  eV are known to exist, and therefore must be produced somewhere, even if their sources have not been clearly established. Perhaps the best candidates as sources of the “Ultra High Energy” (UHE) cosmic rays are Active Galactic Nuclei or Gamma Ray Bursts. Our poor understanding of the origin of the cosmic rays is mostly due to the fact, that electrically charged particles are bent in the galactic ( $|\vec{B}_{\text{gal}}| \simeq 3 \mu\text{Gauss}$ ) and inter-galactic magnetic fields and therefore do not point back to their sources. It is natural, in fact essentially unavoidable that the sources of UHE cosmic rays sources are also sources of neutrinos. This can be easily understood observing that in general a cosmic ray accelerator must contain a non negligible amount of “target material” in the form of gas, or also of photons in an environment filled with high densities of radiation. When an accelerated proton interacts with a target particle it will produce several charged pions (and kaons) that will then decay into neutrinos (with chains such as  $\pi^+ \rightarrow \mu^+ \nu_\mu$  followed by  $\mu^+ \rightarrow e^+ \nu_e \bar{\nu}_\mu$ <sup>6</sup>). The flux of astrophysical neutrinos has a harder energy spectrum than the flux of atmospheric ones, and one expects that it should become dominant at energies above 1–10 TeV. Since we expect that most neutrino sources are extragalactic one expects a diffuse, approximately isotropic flux, due to the superposition of all sources in the universe, with the most powerful objects visible as neutrino point-like sources.

---

<sup>6</sup>In an astrophysical environment the density is in most case so low that even long lived particles can decay before reinteraction.

In order to detect these astrophysical neutrinos one needs very large and massive detectors. The most promising method is based on the detection of Cherenkov light in water or ice. Water (or ice) is naturally a beautiful candidate as a neutrino detector: it is dense, abundant and cheap, relativistic charged particles emit efficiently Cherenkov photons traveling in the medium, that is transparent in the relevant wavelength range (blue light). To construct a neutrino telescope it is therefore sufficient to distribute in a sufficiently large volume of water a number of photo-sensible devices (Photo Multipliers Tubes or PMT's) capable to detect the Cherenkov photons of particles produced in neutrino interactions. The telescope must be screened from the background of the charged cosmic ray radiation, placing it deep under the Earth surface. The original concept of a very large water telescope for high energy neutrinos was developed by the DUMAND group, that originally planned to build a detector in the deep ocean (at a depth of  $\sim 4500$  meters in the Hawaii archipelago) made of “strings” of photomultipliers. Each string should be anchored to ocean floor, and supported by buoyancy. Similar concepts are now pursued by three groups in the Mediterranean (the NESTOR (Greece), ANTARES (France), and NEMO (Italy) projects). The most advanced project (AMANDA) is located in Antarctica, at the South Pole and is based on the same Cherenkov method but uses ice instead of liquid water. Ice at sufficiently low temperature and high pressure, becomes transparent and is a good Cherenkov medium, and can be used also as the mechanical structure that supports the photomultipliers, that are placed in deep holes melted in the ice before its permanent refreezing.

### 3.7. Reactor and Accelerator neutrinos

Two important types of man-made sources of neutrinos also exist, namely: reactor neutrinos (see Section 9) and accelerator neutrinos (see Section 10).

## 4. NEUTRINO OSCILLATIONS IN VACUUM

The probability of finding a neutrino created in a given flavor state to be in the same state (or any other flavor state) can oscillate with time. The idea of the possible existence of neutrino oscillations was first introduced by Pontecorvo [1]. This remarkable phenomenon is the consequence of simple Quantum Mechanics. The neutrinos are produced in charged-current weak interactions in association with a charged lepton are weak-eigenstates:  $\nu_e$ ,  $\nu_\mu$  or  $\nu_\tau$ . In general these weak eigenstates do not have a well defined mass, and can be written as linear superpositions of three states  $\nu_1$ ,  $\nu_2$  and  $\nu_3$  each having mass ( $m_1$ ,  $m_2$  and  $m_3$ ). In general we can write:

$$|\nu_\alpha\rangle = \sum_j U_{\alpha j}^* |\nu_j\rangle , \quad (44)$$

where we have indicated the flavor and mass eigenstates using respectively using greek and latin indices, and  $U$ , the neutrino mixing or Pontecorvo–Maki–Nakagawa–Sakata (PMNS) matrix, is a unitary matrix. The unitarity of  $U$  follows from the fact that the three flavor (and mass) eigenstates are orthogonal to each other.

If the matrix  $U$  is non trivial, it is simple to demonstrate that the phenomenon of flavor oscillation must exist. For simplicity let us assume that at time  $t = 0$  a neutrino is produced as the flavor eigenstate  $|\nu_\alpha\rangle$  with a well defined<sup>7</sup> 3-momentum  $\vec{p}$  and consider the probability to find the neutrino in a different flavor state  $|\nu_\beta\rangle$  at a later time  $t$ . The initial state at  $t = 0$  can be written as a superposition of mass

---

<sup>7</sup>The condition that the neutrino is produced with a well defined momentum is used here for pedagogical simplicity, and can be dropped. This is discussed together with additional details in Section 5.

eigenstates as:

$$|\nu(0)\rangle = |\nu_\alpha\rangle = \sum_j U_{\alpha j}^* |\nu_j\rangle. \quad (45)$$

Note that the energy of our neutrino state is not well defined since each component will have an energy  $E_j = \sqrt{p^2 + m_j^2}$ . The time evolution of a mass eigenstates (that has a well defined energy) is simply a phase factor  $e^{-iE_j t}$ , and for our state created with well defined flavor the time evolution gives:

$$|\nu(t)\rangle = \sum_j U_{\alpha j}^* e^{-iE_j t} |\nu_j\rangle. \quad (46)$$

Now the different components acquire different phases, and this results in non trivial effects. The probability amplitude of finding the neutrino at the time  $t$  in a flavor state  $|\nu_\beta\rangle$  is (we will now use the convention that repeated indices are summed over):

$$\begin{aligned} A(\nu_\alpha \rightarrow \nu_\beta; t) &= \langle \nu_\beta | \nu(t) \rangle \\ &= \{U_{\beta k} \langle \nu_k | \} \left\{ e^{-iE_j t} U_{\alpha j}^* |\nu_j\rangle \right\} \\ &= U_{\beta k} U_{\alpha j}^* e^{-iE_j t} \langle \nu_k | \nu_j \rangle \\ &= U_{\beta j} U_{\alpha j}^* e^{-iE_j t}, \end{aligned} \quad (47)$$

(where we have used  $\langle \nu_k | \nu_j \rangle = \delta_{jk}$ ). The oscillation probability is obtained squaring the amplitude:

$$P(\nu_\alpha \rightarrow \nu_\beta; t) = |A(\nu_\alpha \rightarrow \nu_\beta; t)|^2 = |U_{\beta j} U_{\alpha j}^* e^{-iE_j t}|^2, \quad (48)$$

is periodical in time and clearly is non vanishing even for  $\beta \neq \alpha$ .

#### 4.1. Two flavor case

It is instructive to consider in more detail the simpler case of the mixing of only two neutrino flavors (for example  $\nu_e, \nu_\mu$ ). In this case we have only two mass eigenstates ( $\nu_1, \nu_2$ ) and two mass eigenvalues ( $m_1$  and  $m_2$ ). The relation between flavor and mass eigenstates can then be written in matrix form as:

$$\begin{bmatrix} |\nu_e\rangle \\ |\nu_\mu\rangle \end{bmatrix} = \begin{bmatrix} c & s \\ -s & c \end{bmatrix} \begin{bmatrix} |\nu_1\rangle \\ |\nu_2\rangle \end{bmatrix}, \quad (49)$$

where we have used the compact notation  $c = \cos \theta$ ,  $s = \sin \theta$ , with  $\theta$  the mixing angle. Let us now assume now that an electron neutrino is created at time  $t = 0$  with momentum  $p$ . This corresponds to the initial state:

$$|\nu(t=0)\rangle = |\nu_e\rangle = c|\nu_1\rangle + s|\nu_2\rangle.$$

The two mass components of the neutrino have energies  $E_1$  and  $E_2$  given by:

$$E_i = \sqrt{p^2 + m_i^2} \simeq p + \frac{m_i^2}{2p} \simeq E + \frac{m_i^2}{2E}, \quad (50)$$

After a time  $t$  the neutrino state will be:

$$|\nu(t)\rangle = c e^{-iE_1 t} |\nu_1\rangle + s e^{-iE_2 t} |\nu_2\rangle. \quad (51)$$

The phase difference between the two components result in a non-trivial flavor evolution of the neutrino. For example the probability of finding the neutrino with the muon flavor can be obtained as:

$$\begin{aligned}
P(\nu_e \rightarrow \nu_\mu; t) &= |\langle \nu_\mu | \nu(t) \rangle|^2 \\
&= | \{ -s \langle \nu_1 | + c \langle \nu_2 | \} | \nu(t) \rangle |^2 \\
&= c^2 s^2 \left| e^{-iE_2 t} - e^{-iE_1 t} \right|^2 \\
&= 2 c^2 s^2 \{ 1 - \cos[(E_2 - E_1)t] \} \\
&= \sin^2 2\theta \sin^2 \left[ \frac{\Delta m^2}{4E} t \right],
\end{aligned} \tag{52}$$

where we have used the notation  $\Delta m^2 = m_2^2 - m_1^2$ . For relativistic neutrinos one can also approximate  $L \simeq t$ . Another convenient form of the expression for the transition probability is

$$P(\nu_e \rightarrow \nu_\mu; L) = \sin^2 2\theta \sin^2 \left[ 1.27 \Delta m^2 \frac{L}{E} \right], \tag{53}$$

where  $L$  is in meters and  $E$  in MeV (or  $L$  is in km and  $E$  in GeV).

Examples of these 2-flavor oscillation probabilities are shown in Figs. 4 and 5. Note how the shape of the probability is defined by two parameters: the amplitude of the sinusoidal oscillations that is equal to  $\sin^2 2\theta$  where  $\theta$  is the mixing angle, and the oscillation length, that is the distance between any two closest minima or maxima of the oscillation probability. The oscillation length is inversely proportional to the squared mass difference  $|\Delta m^2|$  and is linear with the neutrino energy  $E$ :

$$\ell_{\text{osc}} = \frac{4\pi E}{|\Delta m^2|} \simeq 2.48 \frac{E \text{ (MeV)}}{|\Delta m^2| \text{ (eV}^2)} \text{ meters} = 2.48 \frac{E \text{ (GeV)}}{|\Delta m^2| \text{ (eV}^2)} \text{ Km.} \tag{54}$$

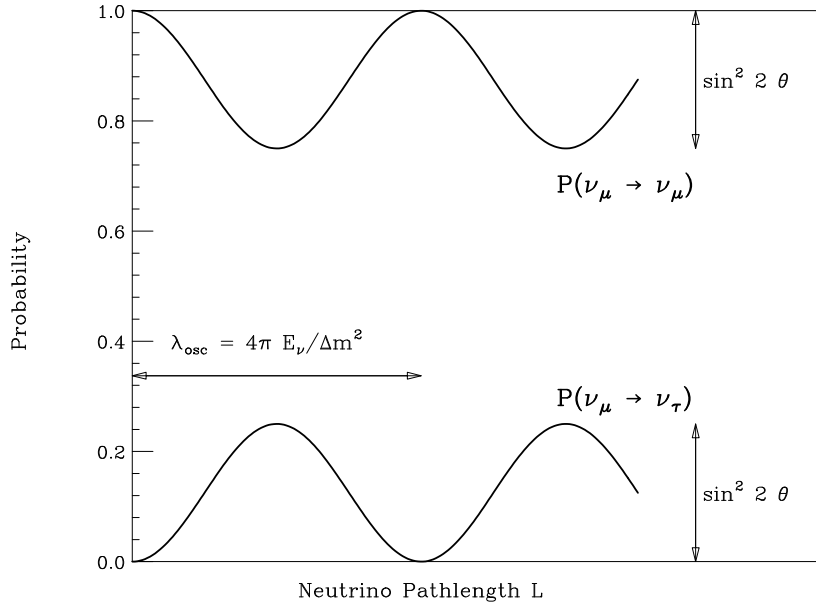


Fig. 4: Plot of the oscillation probabilities as function of the neutrino pathlength  $L$  for the transitions  $\nu_\mu \rightarrow \nu_\mu$  and  $\nu_\mu \rightarrow \nu_\tau$  in the approximation of two flavor mixing. The energy of the neutrino is fixed.

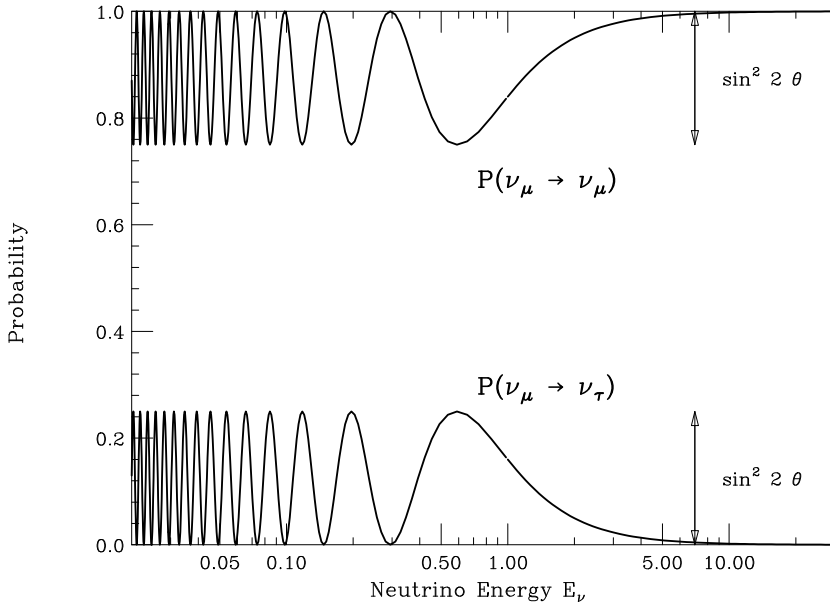


Fig. 5: Example of the shape of the the oscillation probabilities  $P(\nu_\mu \rightarrow \nu_\mu)$  and  $P(\nu_\mu \rightarrow \nu_\tau)$  as function of the neutrino energy  $E_\nu$  for a fixed neutrino pathlength  $L$ . In the example we have chosen  $\Delta m^2 = 1 \times 10^{-3} \text{ eV}^2$  (approximately one third the value indicated by the atmospheric neutrino experiments) and  $L = 730 \text{ Km}$  (the  $\nu$  pathlength of the Fermilab to Minos and Cern to Gran Sasso projects).

#### 4.2. Dirac and Majorana Phases

In the case of three flavors, the neutrino mixing matrix  $U$  can be parametrized in terms of 3 mixing angles, one CP violating phase and, if the neutrinos are Majorana particles, 2 additional ‘‘Majorana phases’’. In the mos general case ( $n$  flavors) one has  $n(n - 1)/2$  mixing angles,  $(n - 1)(n - 2)/2$  ‘‘Dirac phases’’ and (possibly)  $(n - 1)$  additional Majorana phases.

The most general  $n \times n$  complex matrix depends on  $2n^2$  real parameters; If the matrix is unitary  $n^2$  parameters can be eliminated using the set of equations  $U_{\alpha j} U_{\beta j}^* = \delta_{\alpha\beta}$ . The  $n^2$  remaining parameters can be divided into  $n(n - 1)/2$  angles and  $n(n + 1)/2$  phases. If the neutrinos is a Dirac particle,  $2n - 1$  phases can be removed with a proper rephasing of the left handed fields. This is easy to see, considering the set of equations that relate the flavor and mass eigenstates:

$$\begin{aligned} |\nu_e\rangle &= U_{e1}^* |\nu_1\rangle + U_{e2}^* |\nu_2\rangle + U_{e3}^* |\nu_3\rangle, \\ |\nu_\mu\rangle &= U_{\mu 1}^* |\nu_1\rangle + U_{\mu 2}^* |\nu_2\rangle + U_{\mu 3}^* |\nu_3\rangle, \\ |\nu_\tau\rangle &= U_{\tau 1}^* |\nu_1\rangle + U_{\tau 2}^* |\nu_2\rangle + U_{\tau 3}^* |\nu_3\rangle. \end{aligned}$$

We can make any matrix element real rephasing a flavor eigenstate. For example the value  $U_{e1} = |U_{e1}| e^{i\varphi_{e1}}$  can be made real (and positive) redefining the electron neutrino state  $|\nu_e\rangle \rightarrow |\nu_e\rangle e^{i\varphi_{e1}}$ , and similarly an entire column  $(U_{ej}, U_{\mu j}, U_{\tau j})$  can be made real redefining the three flavor eigenstates and eliminating 3 (or more in general  $n$ ) phases from the matrix. If the neutrino is a Dirac particle we are also allowed to rephase the mass eigenstates, and therefore we can make real one line  $(U_{\alpha 1}, U_{\alpha 2}, U_{\alpha 3})$  in the matrix eliminating other 2 (or more in general  $n - 1$ ) phases. Therefore for Dirac neutrino the rephasing eliminates  $(2n - 1)$  phases from the mixing matrix leaving a total of

$$N_{(\text{physical phases})}^{\text{Dirac}} = \frac{n(n + 1)}{2} - (2n - 1) = \frac{(n - 1)(n - 2)}{2}. \quad (55)$$

For  $n = 2$  one has  $N(\text{phases}) = 0$  and the mixing matrix is real, for  $n = 3$  one phase is present.

If the neutrinos are Majorana particles, there is less freedom to rephase the fields, since one cannot arbitrarily change the phase of the matter fields  $|\nu_j\rangle$ . This can be understood observing that the Majorana mass term in the Lagrangian is of the form  $\nu_L \nu_L + h.c.$  rather than of the form  $\bar{\nu}_R \nu_L + h.c.$  and so the phases of neutrino mass fields cannot be canceled by a rephasing. Therefore only  $n$  phases can be eliminated from the matrix and one remains with additional  $(n - 1)$  “Majorana” phases. These Majorana phases are common to an entire column of the mixing matrix, and for this reason they have no effect on neutrino flavor transitions. This can be easily understood observing that the Hamiltonian that controls the flavor evolution has the form (in the flavor basis):  $\mathcal{H} = \frac{1}{2E_\nu} U \text{diag}[m_1, m_2, m_3] U^\dagger$  or in components:

$$\mathcal{H}_{\alpha\beta} = \frac{1}{2E_\nu} \sum_j U_{\alpha j} U_{\beta j}^* m_j \quad (56)$$

and any phase that is common to an entire column (defined by the index  $j$ ) cancels in flavor evolution. These additional phases can however be important in other processes, in particular in double beta decay.

In the case of three flavors, the mixing matrix can then be parametrized with three mixing angles and one CP violating phase (two additional Majorana phases have no influence on the flavor evolution). The most commonly used parametrization has the form:

$$\begin{aligned} U &= \begin{pmatrix} 1 & 0 & 0 \\ 0 & c_{23} & s_{23} \\ 0 & -s_{23} & c_{23} \end{pmatrix} \begin{pmatrix} c_{13} & 0 & s_{13} e^{-i\delta} \\ 0 & 1 & 0 \\ -s_{13} e^{i\delta} & 0 & c_{13} \end{pmatrix} \begin{pmatrix} c_{12} & s_{12} & 0 \\ -s_{12} & c_{12} & 0 \\ 0 & 0 & 1 \end{pmatrix} \\ &= \begin{pmatrix} c_{12}c_{13} & s_{12}c_{13} & s_{13}e^{-i\delta} \\ -s_{12}c_{23} - c_{12}s_{13}s_{23}e^{i\delta} & c_{12}c_{23} - s_{12}s_{13}s_{23}e^{i\delta} & c_{13}s_{23} \\ s_{12}s_{23} - c_{12}s_{13}c_{23}e^{i\delta} & -c_{12}s_{23} - s_{12}s_{13}c_{23}e^{i\delta} & c_{13}c_{23} \end{pmatrix}, \end{aligned} \quad (57)$$

where the mixig angles are denoted  $\theta_{12}, \theta_{13}, \theta_{23}$  and have used the notation:  $c_{jk} = \cos \theta_{jk}, s_{jk} = \sin \theta_{jk}$ , and the  $CP$  violating phase is  $\delta$ .

### 4.3. CP and T violating effects

In general the neutrino oscillation probability can violate the  $CP$  or  $T$  symmetry, that is in general:

$$P(\nu_\alpha \rightarrow \nu_\beta) \neq P(\bar{\nu}_\alpha \rightarrow \bar{\nu}_\beta), \quad (58)$$

$$P(\nu_\alpha \rightarrow \nu_\beta) \neq P(\nu_\beta \rightarrow \nu_\alpha). \quad (59)$$

On the other hand the  $CPT$  theorem imposes (in vacuum) the condition:

$$P(\nu_\alpha \rightarrow \nu_\beta) = P(\bar{\nu}_\beta \rightarrow \bar{\nu}_\alpha). \quad (60)$$

The study of the existence of  $CP$  and  $T$  violation effects in neutrino physics is clearly a fascinating and very important topic.

To see how the oscillation probabilities can violate the  $CP$  and  $T$  symmetries, let us consider

again the general (3 flavors) oscillation probability.

$$\begin{aligned}
P(\nu_\alpha \rightarrow \nu_\beta) &= \left| \sum_j U_{\beta j} U_{\alpha j}^* e^{-i m_j^2 \frac{L}{2E\nu}} \right|^2 \\
&= \sum_{j=1,3} |U_{\beta j}|^4 |U_{\alpha j}|^4 \\
&\quad + \sum_{j < k} 2 \operatorname{Re}[U_{\beta j} U_{\beta k}^* U_{\alpha j}^* U_{\alpha k}] \cos\left(\frac{\Delta m_{jk}^2 L}{2E}\right) \\
&\quad + \sum_{j < k} 2 \operatorname{Im}[U_{\beta j} U_{\beta k}^* U_{\alpha j}^* U_{\alpha k}] \sin\left(\frac{\Delta m_{jk}^2 L}{2E}\right),
\end{aligned} \tag{61}$$

where we have used the notation

$$\Delta m_{jk}^2 = m_k^2 - m_j^2. \tag{62}$$

We can see that in general the oscillation probability is composed of a constant term plus 3 “cosine” terms, and 3 “sine” terms. One can immediately see some symmetry properties of the oscillation probability:

- To obtain the oscillation probabilities for anti-neutrinos (replacing neutrinos with anti-neutrinos correspond to a  $CP$  transformation) we have simply to replace the matrix  $U$  with its complex conjugate  $U^*$  in the expression of the probability. After the replacement  $U \rightarrow U^*$  in equation (61) the “sin” terms change sign while the “cos” terms remain invariant. We can therefore see that the oscillation probability can violate  $CP$  if and only if the mixing matrix has a non vanishing imaginary part, that is if and only of  $\delta$  is different from the values 0 or  $\pi$ .
- The oscillation probability for the time reversed channel (that is the probability for the transition  $\nu_\beta \rightarrow \nu_\alpha$ ) can be obtained from equation (61) simply with the interchange of indices  $\alpha \leftrightarrow \beta$ . One can immediately see that under this operation the “sin” terms change sign, and the “cos” terms remain invariant. Therefore as in the previous case the oscillation probability can violate  $T$  reversal symmetry if and only  $U$  has a non vanishing imaginary part, or equivalently if and only if  $\delta$  is different from the values 0 or  $\pi$ .
- A CPT transformation correspond to the replacement of  $\nu$  with  $\bar{\nu}$  and the interchange of the initial and final flavors, that is formally with the replacements:  $U \rightarrow U^*$ , and  $\alpha \leftrightarrow \beta$ . It is easy to see that under these transformations expression (61) remains invariant. Therefore the general expression for the oscillation probability respect  $CPT$  invariance as it should.
- Inspection of equation (61) also shows that the coefficients of the “sine” terms vanish when  $\alpha = \beta$ . Since it is the “sine” terms that are not symmetric under a  $CP$  and  $T$  operations, it follows that  $CP$  and  $T$  violating effects do not exist for the “diagonal” transitions ( $\nu_e \rightarrow \nu_e$ ,  $\nu_\mu \rightarrow \nu_\mu$ ,  $\nu_\tau \rightarrow \nu_\tau$ ). This is as it should be, since it is necessary to satisfy the  $CPT$  theorem.

The expression for the oscillation probabilities can be rewritten in a more compact form using the properties of a unitary matrix  $U$   $U^\dagger = U^\dagger U = I$ . The unitarity definition can be written more explicitly as:

$$\sum_j U_{\alpha j} U_{\beta j}^* = \delta_{\alpha\beta}, \tag{63}$$

$$\sum_\alpha U_{\alpha j} U_{\alpha k}^* = \delta_{jk}. \tag{64}$$

Using these relations it is possible to obtain relations between the coefficients of the “sine” and “cosine” terms in the expression for the oscillation probability. The most important result is about the quantities

$J_{jk}^{\alpha\beta} = -\text{Im} [U_{\alpha j} U_{\alpha k}^* U_{\beta j}^* U_{\beta k}]$  that are the coefficients of the “sine” terms in the oscillation probability and control the CP and T violation effects. These quantities have obviously the symmetry properties:

$$J_{jk}^{\alpha\beta} = -J_{kj}^{\alpha\beta} = -J_{jk}^{\beta\alpha} \quad (65)$$

and

$$J_{jj}^{\alpha\beta} = J_{jk}^{\alpha\alpha} = 0. \quad (66)$$

With some simple algebra using the unitarity conditions<sup>8</sup> one can also obtain the additional relations:

$$J_{12}^{\alpha\beta} = J_{23}^{\alpha\beta} = J_{31}^{\alpha\beta}, \quad (67)$$

$$J_{jk}^{e\mu} = J_{jk}^{\mu\tau} = J_{jk}^{\tau e}. \quad (68)$$

It follows that (in the case of three neutrinos) there is a single independent coefficient  $J_{jk}^{\alpha\beta}$  the “Jarlskog parameter”:

$$J = J_{12}^{e\mu} = -\text{Im}[U_{e1} U_{\mu 1}^* U_{e2} U_{\mu 2}] \quad (69)$$

$$= c_{13}^2 s_{13} s_{12} c_{12} s_{23} c_{23} \sin \delta. \quad (70)$$

All other non vanishing coefficients (those with  $\alpha \neq \beta$  and  $j \neq k$ ) are equal or opposite to  $J$ . We can therefore finally write the most general form of the probability for the  $\nu_\alpha \rightarrow \nu_\beta$  transition (for  $\alpha \neq \beta$ ) as:

$$\begin{aligned} P_{\nu_\alpha \rightarrow \nu_\beta} &= A_{\alpha\beta}^{12} \sin^2 \left( \frac{\Delta m_{12}^2 L}{4 E_\nu} \right) + A_{\alpha\beta}^{23} \sin^2 \left( \frac{\Delta m_{23}^2 L}{4 E_\nu} \right) + A_{\alpha\beta}^{13} \sin^2 \left( \frac{\Delta m_{13}^2 L}{4 E_\nu} \right) \\ &\quad \pm 8 J \sin \left( \frac{\Delta m_{12}^2 L}{4 E_\nu} \right) \sin \left( \frac{\Delta m_{23}^2 L}{4 E_\nu} \right) \sin \left( \frac{\Delta m_{13}^2 L}{4 E_\nu} \right). \end{aligned} \quad (71)$$

In this equations we have used the unitarity conditions to obtain the result that the constant term in (61) vanishes (it is unity for  $\alpha = \beta$ ) and have rewritten the CP and T violating part of the probability using the symmetry relations for “sine” coefficients and the trigonometric identity:

$$\sin a + \sin b - \sin(a + b) = 4 \sin \left( \frac{a}{2} \right) \sin \left( \frac{b}{2} \right) \sin \left( \frac{(a+b)}{2} \right). \quad (72)$$

We have also used the notation

$$A_{\alpha\beta}^{jk} = -4 \text{Re}[U_{\alpha j} U_{\beta j}^* U_{\alpha k}^* U_{\beta k}]. \quad (73)$$

The CP and T violation effects are described by the last term that changes sign under a CP or T reversal operation. From the expression (70) of  $J$  as a function of the mixing matrix parameters and the form of the oscillation probability, one can see that in order to have observable CP and T violation effects one needs to have three conditions:

- [1] The phase  $\delta$  must be non trivial (that is  $\delta \neq 0$  and  $\delta \neq \pi$ )
- [2] All mixing angles must be non vanishing:  $\theta_{12} \neq 0, \theta_{23} \neq 0, \theta_{13} \neq 0$ .
- [3] All three oscillations must be “active”, that is all three phases  $\Delta m_{jk}^2 L / 4E$  must be appreciably different from zero.

---

<sup>8</sup>The “trick” to use is to note each  $J$  can be seen as the product of two terms of the form  $U_{\alpha j} U_{\beta k}^*$  that can be expressed as a function of each other using the unitarity constraints such as:  $U_{e1} U_{\mu 1}^* = -(U_{e2} U_{\mu 2}^* + U_{e3} U_{\mu 3}^*)$ .

#### 4.4. One Mass scale dominance

The expressions for the oscillation probabilities become simpler in the approximation that one squared mass difference is much smaller than the other two. This is realized if the neutrino masses are “hierarchical”, that is:

$$m_1 \ll m_2 \ll m_3. \quad (74)$$

In this case one has

$$|\Delta m_{12}^2| \ll |\Delta m_{23}^2| \simeq |\Delta m_{13}^2|. \quad (75)$$

In this situation there is a range of  $E_\nu$  and  $L$  where the “short” oscillations are operating but the “long” ones have not developed (and  $|\Delta m_{12}^2| L/4E \ll 1$ ). The oscillation probability can then be well approximated for non-diagonal transitions ( $\alpha \neq \beta$ ) as:

$$P(\nu_\alpha \rightarrow \nu_\beta) = 4|U_{\alpha 3}|^2 |U_{\beta 3}|^2 \sin^2 \left( \frac{\Delta m_{13}^2}{4E} L \right), \quad (76)$$

that is a form similar to the similar to 2-flavor case. The probabilities oscillate with a single frequency related to the squared mass difference  $\Delta m_{13}^2 \simeq \Delta m_{23}^2$ . The amplitudes of the probability oscillations for the different transitions depends only on the elements of the third column of the lepton mixing matrix  $U$ . Explicitely the oscillation probabilities are:

$$\begin{aligned} P(\nu_e \rightarrow \nu_\mu; L) &= 4|U_{e 3}|^2 |U_{\mu 3}|^2 \sin^2 \left( \frac{\Delta m_{13}^2}{4E} L \right) \\ &= s_{23}^2 \sin^2 2\theta_{13} \sin^2 \left( \frac{\Delta m_{13}^2}{4E} L \right), \end{aligned} \quad (77)$$

$$\begin{aligned} P(\nu_e \rightarrow \nu_\tau; L) &= 4|U_{e 3}|^2 |U_{\tau 3}|^2 \sin^2 \left( \frac{\Delta m_{13}^2}{4E} L \right) \\ &= c_{23}^2 \sin^2 2\theta_{13} \sin^2 \left( \frac{\Delta m_{13}^2}{4E} L \right), \end{aligned} \quad (78)$$

$$\begin{aligned} P(\nu_\mu \rightarrow \nu_\tau; L) &= 4|U_{\mu 3}|^2 |U_{\tau 3}|^2 \sin^2 \left( \frac{\Delta m_{13}^2}{4E} L \right) \\ &= c_{13}^4 \sin^2 2\theta_{23} \sin^2 \left( \frac{\Delta m_{13}^2}{4E} L \right). \end{aligned} \quad (79)$$

The survival probability for diagonal transitions take also the simple form: (for example for  $\nu_e$ ):

$$\begin{aligned} P(\nu_e \rightarrow \nu_e) &= 1 - [1 - |U_{e 3}|^2] |U_{e 3}|^2 \sin^2 \left( \frac{\Delta m_{13}^2}{4E} L \right) \\ &= 1 - \sin^2 2\theta_{13} \sin^2 \left( \frac{\Delta m_{13}^2}{4E} L \right). \end{aligned} \quad (80)$$

$$= 1 - \sin^2 2\theta_{13} \sin^2 \left( \frac{\Delta m_{13}^2}{4E} L \right). \quad (81)$$

It coincides with the  $\nu_e$  survival probability in the 2-flavor case with the substitutions:  $\Delta m^2 \rightarrow \Delta m_{13}^2$  and  $\theta \rightarrow \theta_{13}$ .

Another limiting case is relevant for very long baseline reactor experiments (such as KamLand),

and corresponds to the situation

$$\frac{\Delta m_{13}^2}{2E}L \simeq \frac{\Delta m_{23}^2}{2E}L \gg 1. \quad (82)$$

(that is very fast oscillations due to the mass squared differences  $\Delta m_{13}$  and  $\Delta m_{23}$  with averaged effect). The  $\nu_e$  survival probability is then:

$$P(\nu_e \rightarrow \nu_e) \simeq c_{13}^4 P + s_{13}^4, \quad (83)$$

with

$$P = 1 - \sin^2 2\theta_{12} \sin^2 \left( \frac{\Delta m_{21}^2}{4E} L \right). \quad (84)$$

that is the  $\nu_e$  survival probability in the 2-flavor case with the mass squared difference  $\Delta m^2 = \Delta m_{21}^2$  and mixing angle  $\theta = \theta_{12}$ .

## 5. QUANTUM MECHANICS OF NEUTRINO OSCILLATIONS

The phenomenon of flavor oscillations is a fascinating demonstration of quantum mechanical effects in the macroscopic world, and a detailed discussion of its origin can illustrate (and also requires) several important quantum mechanical concepts like coherence, decoherence, wave packets and so on. In this lectures we are concentrating on the phenomenology of the neutrino oscillations and possible interpretations, so we do not have enough space for a careful analysis of these more theoretical aspects. In particular, the derivation of the flavor oscillation formula that we have outlined before, based on the assumption that neutrinos are emitted with a well defined momentum, is simple and elegant, and gives the correct answer for essentially all possible practical applications, however it is not theoretically very solid, it is also not correct in all possible circumstances, and raises several conceptual questions: for example the assumption of a mass independent momentum for neutrinos is in general not correct, and the concept of creation and detection “points” is problematic in a quantum world with an uncertainty principle  $\Delta p \Delta x \gtrsim 1$ . A better theoretical treatment of neutrino flavor transitions requires a wave packet treatment of the neutrinos, or more rigorously a quantum field approach. A detailed description of these problems is beyond the scope of these lectures and we refer to [4,37,40] for more discussion and additional references. We include however here a brief discussion to illustrate a few most important points.

### 5.1. Energy and Momentum of Oscillating Neutrinos

The assumption that the neutrinos are produced with a momentum independent from their mass that was used in our (standard) derivation of the oscillation formula is in general not valid. To have a concrete example, let us consider the neutrinos produced in the decay  $\pi^+ \rightarrow \mu^+ \nu_\mu$  in the rest frame of the parent pion. In this frame, a massless neutrino has an energy (and momentum)

$$E = p = \frac{m_\pi}{2} \left( 1 - \frac{m_\mu^2}{m_\pi^2} \right). \quad (85)$$

If the neutrino has mass  $m_j$  the energy and momentum are modified, and can be obtained exactly from 4-momentum conservation:

$$E_j = E + \frac{m_j^2}{2m_\pi} = E + \frac{m_j^2}{2E} \left( 1 - \frac{m_\mu^2}{m_\pi^2} \right), \quad (86)$$

$$p_j = \sqrt{E_j^2 - m_j^2} \simeq E - \frac{m_j^2}{2E} \left( 1 + \frac{m_\mu^2}{m_\pi^2} \right). \quad (87)$$

In these equations we have neglected terms of order  $m_j^4/E^3$  or higher, and  $E$  is always given by equation (86). Note that both the momentum and the energy of the emitted neutrino depend on its mass. More in general neutrinos produced in different processes will have an energy and a momentum that depend on their mass and can be well approximated by the expressions:

$$E_j = E + \frac{m_j^2}{2E} \xi, \quad p_j = E - \frac{m_j^2}{2E} (1 - \xi), \quad (88)$$

where  $E$  is the energy calculated assuming  $m_\nu = 0$  and  $\xi$  is a dimensionless parameter of order unity that depends on the process we are considering<sup>9</sup>, in the example that we have discussed  $\xi = (1 - m_\mu^2/m_\pi^2) \simeq 0.43$ . The expression for flavor transitions will however turn out to be *independent* from the value of  $\xi$ .

The wavefunction of the neutrino state at production can then be represented as the superposition of neutrinos with different masses  $m_j$  each with appropriate momentum  $p_j$  and energy  $E_j$ , and amplitudes given by the mixing matrix. A neutrino produced at time  $t_0$  with flavor  $\nu_\alpha$  has then the wavefunction:

$$|\psi(x, t_0)\rangle = \sum_j U_{\alpha j}^* |p_j; \nu_j\rangle = \sum_j U_{\alpha j}^* |p_j\rangle |\nu_j\rangle = \sum_j U_{\alpha j}^* e^{ip_j(x-x_0)} |\nu_j\rangle, \quad (89)$$

where we have represented the eigenstate of momentum  $|p_j\rangle$  as a plane wave:  $|p_j\rangle = e^{ip_j(x-x_0)}$  with  $x_0$  the position of  $\pi$  decay. Using the Schrödinger equation for time evolution one can easily write the wavefunction at a later time  $t$  as:

$$|\psi(x, t)\rangle = \sum_j U_{\alpha j}^* e^{ip_j(x-x_0)} e^{-iE_j(t-t_0)} |\nu_j\rangle. \quad (90)$$

If we now want to see what is the probability to find a neutrino with flavor  $\beta$  at a distance  $L = x - x_0$  from the decay point and a time  $T = t - t_0$  from the decay point we have to compute:

$$\begin{aligned} P_{\nu_\alpha \rightarrow \nu_\beta}(L, T) &= |\langle \nu_\beta | \psi(x, t) \rangle|^2 = \left| \left\langle \sum_k U_{\beta k} \langle \nu_k | \right\rangle | \psi(x, t) \rangle \right|^2 \\ &= \sum_j |U_{\beta j}|^2 |U_{\alpha j}|^2 + \sum_{k>j} 2\text{Re} \left[ U_{\alpha k}^* U_{\alpha j} U_{\beta k} U_{\beta j}^* e^{i(p_k-p_j)L-i(E_k-E_j)T} \right]. \end{aligned} \quad (91)$$

This expression is identical to what we have obtained in the with the assumption that the neutrinos are emitted with a fixed (mass independent) momentum, except that the phase  $\varphi_{jk}$  associated to the product  $U_{\alpha k}^* U_{\alpha j} U_{\beta k} U_{\beta j}^*$  is now:

$$\begin{aligned} \varphi_{jk} &= (p_k - p_j)L - (E_k - E_j)T \simeq [(p_k - p_j) - (E_k - E_j)]L \\ &= \frac{1}{2E} \left[ -(m_k^2 - m_j^2)(1 - \xi) + (m_k^2 - m_j^2)\xi \right] L = \frac{(m_k^2 - m_j^2)}{2E} L. \end{aligned} \quad (92)$$

We can see that the phases (and therefore the expressions for the oscillation probabilities) do not depend from the quantity  $\xi$ , and we have exactly the same result obtained before with a derivation based on the fixed momentum assumption.

---

<sup>9</sup>The expressions (88) respects the condition that the neutrino is on a mass shell ( $E_j^2 = p_j^2 + m_j^2$ ) up to higher order corrections of order  $m_j^4/E^3$ .

## 5.2. Momentum resolution in the $\nu$ measurement

The phenomenon of flavor oscillation of neutrinos, that is the time (or pathlength) dependence of the probability to find a certain flavor is the consequence not only of mixing, but also of the fact that the neutrino masses are so tiny, that experimentally it is extremely difficult to obtain a resolution that is sufficiently good to determine the neutrino mass, therefore the different amplitudes (corresponding to the different masses) have to be summed coherently, and the quantum interference effects result in the space-time flavor oscillations.

It is instructive to note that *in principle* the situation could be different, and one can imagine a *gedanken* experiment measurement capable to determine the mass of an observed neutrino. As an illustration let us consider again the  $\nu_\mu$  produced in the decay of a  $\pi^+$  at rest. As discussed before the wavefunction of the final state is a superposition of neutrinos of different mass, each having a well defined different momentum. It is in principle possible to perform a measurement with a resolution smaller than the difference in momentum between different mass eigenstates:  $\Delta p < |p_k - p_j|$ . In this case however, according to the Heisenberg uncertainty principle the measurement cannot be localized in space better than  $\Delta x \gtrsim 1/\Delta p$ . This has the consequence that:

$$\Delta x \gtrsim \frac{1}{\Delta p} \gtrsim \frac{1}{|p_k - p_j|} \simeq \frac{2E}{|m_k^2 - m_j^2|} \simeq L_{\text{osc}}^{jk}. \quad (93)$$

In other words, if the resolution is sufficiently good to determine the mass of the neutrino, then the uncertainty in the position of the observation must be larger than the oscillation length, and no quantum interference can be observed. Therefore, in principle, an extremely precise measurement of the momentum of the neutrino can resolve three distinct values of the momentum  $p_1, p_2$  and  $p_3$ , each corresponding to the three neutrino mass eigenvalues. The three results are obtained each with a probability  $P_j = |U_{\mu j}|^2$  that is independent from the neutrino pathlength. The measurement of the neutrino momentum can be performed detecting charged current interactions, and each neutrinos detected with a certain momentum will be in general found not to have a well defined flavor, and the probability to measure the flavor  $\alpha$  for neutrinos with momentum  $p_j$  (and therefore mass  $m_j$ ) will be  $P_\alpha^{(j)} = |U_{\mu j}|^2 |U_{\alpha j}|^2$ , again independently from the distance between the pion decay and the position of the detector.

This argument explains why in the quark sector one can measure the mixing of weak eigenstates, for example observing that a  $u$  quark makes weak transitions to a state  $d'$  that is a linear combination of the quarks  $d, s$  and  $b$  with measurable coefficients, however one does not observe quark oscillations<sup>10</sup>. In fact measuring the flavor of a quark is exactly equivalent to the measurement of its mass, and as in the case of neutrinos, resolving the mass destroys the oscillations. Of course in the quark case the mass measurement is enormously easier because of the very large mass differences between different flavors, and viceversa it would be extremely hard to identify experimentally the weak eigenstates  $d', s'$  and  $b'$ .

## 5.3. Wave-packet treatment

The localization of the neutrino source and detection points implies that the neutrinos cannot be described as plane waves, but they must be described as *wave packets*. The size of the wave packet is determined by the size of the region within which the neutrino production process is localized. Obviously because of the uncertainty principle it follows that even a mass eigenstates cannot be described as having a well defined 3-momentum. The wave-packet treatment is discussed in more detail for example in the textbook of Kim and Pevsner [4]. The introduction of the wave-packet for neutrino also leads to the concept of the “coherence length” for the oscillations.

---

<sup>10</sup>Oscillations are observed between particle/anti-particle pairs such as  $K^\circ \leftrightarrow \bar{K}^\circ$ ,  $D^\circ \leftrightarrow \bar{D}^\circ$  or  $B^\circ \leftrightarrow \bar{B}^\circ$ .

## 5.4. Coherence Length

It is important to discuss the concept of the coherence length for neutrino oscillations. Neutrinos with different masses will have different velocities given by:

$$v_j = \frac{p_j}{E_j} \simeq 1 - \frac{m_j^2}{2E^2}. \quad (94)$$

The neutrino emitted in a certain process can be seen as a wave packet with a size  $\sigma_x$  that is determined by the size of the region where the neutrino production is localized. One can approximate the wave packet as a gaussian of size  $\sigma_x$ , and correspondingly the momentum distribution of the neutrino will also be a gaussian with width  $\sigma_p = 1/\sigma_x$  and centered at a value  $p_j$ . The wave packet of a neutrino created with a certain flavor, will be in general the superposition of three overlapping wave packets corresponding to the three  $\nu$  masses. The three components of the wave functions will propagate with different group velocities  $v_j \simeq 1 - m_j^2/(2E^2)$ , and therefore during propagation the different components will separate. The overlap between two components  $\nu_j$  and  $\nu_k$  will remain significant only if the separation of the centers of their wave packets is smaller than  $\Delta x \sim 2\sigma_x$ ; this will be correct only for a pathlength smaller than

$$L \lesssim L_{\text{coh}}^{jk} = \sqrt{2} \frac{2\sigma_x}{|v_j - v_k|} \simeq \frac{4\sqrt{2} E^2 \sigma_x}{|\Delta m_{jk}^2|}, \quad (95)$$

(the factor  $\sqrt{2}$  at this point is arbitrary). For  $L > L_{\text{coh}}$  the wave packets that corresponds to the different neutrinos are separated (see Fig. 6) the coherence between the different neutrinos is lost and oscillations are not present any more. An observer at a distance  $L \gg L_{\text{coh}}$  from a neutrino source that generates neutrinos of flavor  $\alpha$  will detect neutrinos of all flavors, but with probabilities independent from  $L$ .

The coherence length is in practical not important except for the neutrinos produced in distant supernovae.

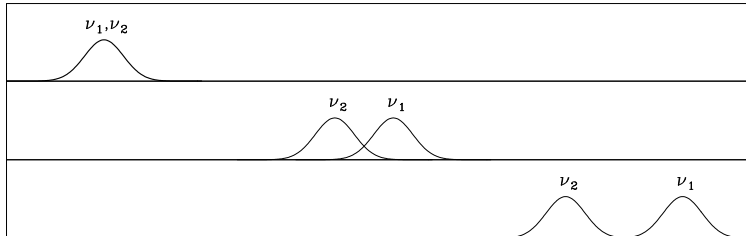


Fig. 6: Scheme of the decoherence of a neutrino wave packet during propagation. The components of the packet that corresponds to the masses  $m_1$  and  $m_2$  propagate with different group velocity  $v_1$  and  $v_2$  and after a distance of order  $L_{\text{coh}} \sim \sigma_x / |v_2 - v_1|$  the packets do not overlap any more and the phenomenon of oscillation stops. An observer will receive separate neutrino pulses that corresponds to the different neutrino masses.

## 5.5. More General Formula

The effects that we have discussed above can be included in the formula for the probability  $\nu_\alpha \rightarrow \nu_\beta$  using a wave packet, or more rigorously a quantum field theory treatment with the result [40]:

$$P_{\nu_\alpha \rightarrow \nu_\beta}(x) = \sum_j |U_{\beta j}|^2 |U_{\alpha j}|^2 + \sum_{k>j} 2\text{Re} \left[ U_{\alpha k}^* U_{\alpha j} U_{\beta k} U_{\beta j}^* e^{i2\pi \frac{x}{L_{\text{osc}}^{jk}}} \right] e^{-\left(\frac{x}{L_{\text{coh}}^{jk}}\right)^2} e^{-2\pi^2 \xi^2 \left(\frac{\sigma_x}{L_{\text{osc}}^{jk}}\right)^2}, \quad (96)$$

where  $L_{\text{osc}}^{jk} = 4\pi E / |\Delta m_{jk}^2|$  is the usual oscillation length and  $L_{\text{coh}}^{jk}$  was defined in (95), and  $\sigma_x$  is the combination of the spatial uncertainties in the neutrino production and observation points. This formula

is identical to the “standard” one that we have discussed before except for the last two factors, that are both unity when  $x \ll L_{\text{coh}}$  or  $\sigma_x \ll L_{\text{osc}}^{jk}$ . The first one is related to the decoherence of the neutrinos that we have just discussed, and the second one is related to the simple condition that the neutrino must be localized better than an oscillation length. In all the problems that we will consider in this work  $L_{\text{coh}}$  is much longer than the neutrino pathlength, and  $\sigma_x$  can be safely assumed to much shorter than the oscillation lengths, and therefore the standard formula that neglects the effects discussed here is valid to a very good approximation.

## 5.6. Do charged leptons oscillate ?

In charged current interactions the neutrinos are always produced in association with a charged lepton, and it is natural to ask the question if some sort of oscillatory behaviour is also associated to these charged leptons. For example since in the decay  $\pi^+ \rightarrow \nu_\mu + \mu^+$  the probability to observe a  $\nu_\mu$  is a function of the distance  $L$  from the decay point, should the probability of detecting a muon also have a non trivial  $L$  dependence that is the combination of an exponential behaviour (the muon is an unstable particle) with some oscillations? In other words: can “muon oscillations” exist? The answer is no, they cannot exist. The probability of detecting a charged lepton at a certain distance from its production point (in vacuum) is either a constant (for  $e^\pm$ ) or a simple exponential (for  $\mu^\pm$  and  $\tau^\pm$ ). In the literature there are actually claims to the contrary [41], that however have been solidly refuted [37,40].

It is easy to convince oneself of the non existence of charged lepton oscillations with considerations that are similar to those outlined before. The  $e$ ,  $\mu$  and  $\tau$  states are eigenstates of mass, and therefore the identification of a charged lepton is exactly equivalent to a measurement of its mass. As in the case of quarks, the coherence in the production is immediately lost, and no oscillations are present. Note also that the charged lepton equivalent of the neutrino weak eigenstates are those linear combinations of  $e$ ,  $\mu$  and  $\tau$  that are produced in association with the neutrino mass eigenstates  $\nu_1$ ,  $\nu_2$  or  $\nu_3$ , and experimentally is is essentially impossible to measure these states.

It would be instructive to consider the amplitude of the evolution of a two particle final state composed of a neutrino and a charged lepton (as for example in  $\pi^\pm$  decay) and study what correlations can exist between measurements of the two particles. This interesting study is in fact an example of the Einstein, Rosen, Podolsky (EPR) phenomenon, and mathematically it follows analogous steps as for the study of correlations in the processes  $\phi \rightarrow K\bar{K}$  or  $\Upsilon(4s) \rightarrow B\bar{B}$  that are at the basis of  $CP$  violation studies in the quark sector. A careful analysis shows that, as expected, no muon oscillations are visible also in the case of measurements of both neutrino and charged lepton (see [40]).

## 6. NEUTRINO OSCILLATIONS in MATTER

The discussion of the previous Section was relevant for neutrinos propagating in vacuum, however in many (actually in most) circumstances, neutrinos propagate in a medium filled with material. For example solar neutrinos are created in the center of the sun, and have to travel across a lot of solar material, many of the atmospheric neutrinos have to cross a thick layer, or even the entire Earth before reaching the detector, even reactors and accelerator neutrinos, can have to cross thick layers of material. The presence of matter can have a profound effects on the oscillation probabilities [42,43].

### 6.1. Neutrino Effective Potential in matter

Neutrinos have an extremely feeble interaction with matter, and therefore one could naively expect that the presence of matter should have a negligible effect on their propagation, however this is not so because one must consider the *coherent* effect of forward scattering from many particles on the propagation of

a neutrino. The effect of coherent forward scattering can be described as an index of refraction for neutrinos in matter, or equivalently as the presence of an *Effective Potential* due to the presence of matter. Ordinary matter is composed of electrons, protons and neutrons, and the effective potential receives contributions from all target particles. The interaction can proceed with  $Z^0$  exchange, resulting in the effective potentials:

$$\begin{aligned} V_{\nu_\mu e} = V_{\nu_\tau e} &= V_{\nu_e e}^Z = -\frac{\sqrt{2}}{2} G_F N_e, \\ V_{\nu_\mu p} = V_{\nu_\tau p} &= V_{\nu_e p} = +\frac{\sqrt{2}}{2} G_F N_p, \\ V_{\nu_\mu n} = V_{\nu_\tau n} &= V_{\nu_e n} = -\frac{\sqrt{2}}{2} G_F N_n. \end{aligned} \quad (97)$$

The effective potential for  $\nu_e$  is different because the scattering (see Fig. 7) can also proceed with  $W$  exchange:

$$V_{\nu_e e} = V_{\nu_e e}^Z + V_{\nu_e e}^W = -\frac{\sqrt{2}}{2} G_F N_e + \sqrt{2} G_F N_e. \quad (98)$$

The total effective potential is the sum of the three contributions (for example  $V_{\nu_e} = V_{\nu_e e} + V_{\nu_e p} + V_{\nu_e n}$ ). The crucial role is played by the *difference of potential* between the  $\nu_e$  and  $\nu_{\mu,\tau}$ :

$$V \equiv V_{\nu_e} - V_{\nu_\mu} = V_{\nu_e} - V_{\nu_\tau} = +\sqrt{2} G_F N_e. \quad (99)$$

This potential difference is proportional to the electron density  $N_e$ , and has the numerical value:

$$V = +\sqrt{2} G_F N_e = +\sqrt{2} G_F \frac{\rho}{M_p} Y_e = 3.8 \times 10^{-14} \left( \frac{\rho}{\text{g cm}^{-3}} \right) \left( \frac{Y_e}{0.5} \right) \text{eV}, \quad (100)$$

(where  $Y_e$  is the electron number per nucleon). It is important to note that for anti-neutrinos the effective potential reverse its sign:

$$V_{\bar{\nu}_\alpha} = -V_{\nu_\alpha}. \quad (101)$$

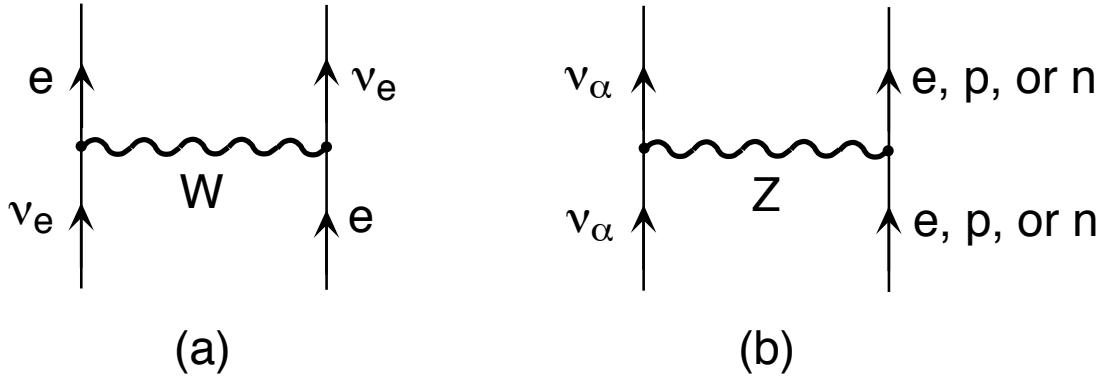


Fig. 7: Feynman diagrams for the forward elastic scattering of a  $\nu$  from a particle of matter. (a)  $W$ -exchange-induced scattering from an electron, possible only for  $\nu_e$ . (b)  $Z$ -exchange-induced scattering from an  $e^-$ ,  $p$  or  $n$ . possible for all flavors with equal amplitude.

## 6.2. Flavor Evolution Equation

In the presence of matter the flavor evolution of neutrinos is described by an effective Hamiltonian that is the sum of a free Hamiltonian plus a matter induced term that includes the effective potential and that therefore changes sign for neutrinos and antineutrinos:

$$\mathcal{H}(\nu) = \mathcal{H}_0 + \mathcal{H}_m, \quad (102)$$

$$\mathcal{H}(\bar{\nu}) = \mathcal{H}_0^* - \mathcal{H}_m. \quad (103)$$

Writing more explicitly for neutrinos one has:

$$\mathcal{H}(\nu) = U \begin{bmatrix} E_1 & 0 & 0 \\ 0 & E_2 & 0 \\ 0 & 0 & E_3 \end{bmatrix} U^\dagger + \begin{bmatrix} V_e & 0 & 0 \\ 0 & V_\mu & 0 \\ 0 & 0 & V_\tau \end{bmatrix}. \quad (104)$$

This Hamiltonian enters a Schrödinger equation that controls the flavor evolution:

$$i \frac{d}{dx} \nu_\alpha = \mathcal{H} \nu_\alpha. \quad (105)$$

The subtraction from the Hamiltonian of a term proportional to the unit matrix, clearly does not change the flavor evolution, therefore all that counts for the matter term is a matrix of form  $\mathcal{H}_m = \text{diag}[V, 0, 0]$ . It should be clear that when  $V$  is comparable to the energy differences  $|E_j - E_k| \simeq |\Delta m_{jk}^2|/(2E_\nu)$  the  $\nu$  flavor evolution is strongly modified.

It can be useful to note that the potential can be seen as having the effect of changing the mass of the neutrino. In fact we can write:

$$E - V = \sqrt{p^2 + m^2} \simeq p + \frac{m^2}{2p} \quad (106)$$

and approximating  $p \simeq E$  one finds that the effect of the potential is equivalent to a shift in the squared mass:

$$m^2 \rightarrow m^2 + 2EV. \quad (107)$$

Quantitatively the potential difference is therefore equivalent to a shift in the squared mass difference:

$$(\Delta m^2)^{\nu_e(\bar{\nu}_e)}_{\text{matter}} = \pm 2E_\nu V \simeq \pm 0.76 \times 10^{-4} \left( \frac{\rho}{\text{g cm}^{-3}} \right) \left( \frac{E_\nu}{\text{GeV}} \right) \frac{Y_e}{0.5} \text{ eV}^2. \quad (108)$$

Note that electron neutrinos (anti-neutrinos) acquire effectively a larger (smaller) squared mass. Of course a more complete discussion must include mixing (see below).

In general the matter term in equation (105) can vary along the neutrino trajectory. If the density is constant however the flavor evolution can be solved analytically calculating the eigenvalues and eigenvectors of the (time independent) Hamiltonian.

## 6.3. Two flavor case

In the following we will discuss the simpler case where  $\nu_e$  is mixed with  $\nu_\mu$  and  $\nu_\tau$ , and study the structure of the eigenvalues and eigenvectors in matter as a function of the potential  $V$ . This will turn out to be of more than academic interest, because it applies to a good approximation to the oscillation of solar neutrinos (where in fact  $\nu_e$  is mixed with a linear combination of  $\nu_\mu$  and  $\nu_\tau$ ).

## Hamiltonian in vacuum

For pedagogical purposes let us reconsider the free Hamiltonian in the case of two neutrino species. Writing explicitly the mixing matrix (with the compact notation  $c = \cos \theta, s = \sin \theta$ ) one has:

$$\begin{aligned}
\mathcal{H}_0 &= U \text{diag}[E_1, E_2] U^\dagger \\
&= \begin{bmatrix} c & s \\ -s & c \end{bmatrix} \begin{bmatrix} E_1 & 0 \\ 0 & E_2 \end{bmatrix} \begin{bmatrix} c & -s \\ s & c \end{bmatrix} \\
&= \frac{1}{2E} \begin{bmatrix} c & s \\ -s & c \end{bmatrix} \begin{bmatrix} m_1^2 & 0 \\ 0 & m_2^2 \end{bmatrix} \begin{bmatrix} c & -s \\ s & c \end{bmatrix} + \lambda \mathbf{I} \\
&= \frac{\Delta m^2}{4E} \begin{bmatrix} c & s \\ -s & c \end{bmatrix} \begin{bmatrix} -1 & 0 \\ 0 & +1 \end{bmatrix} \begin{bmatrix} c & -s \\ s & c \end{bmatrix} + \lambda' \mathbf{I} \\
&= \frac{\Delta m^2}{4E} \begin{bmatrix} -c^2 + s^2 & 2cs \\ 2cs & c^2 - s^2 \end{bmatrix} + \lambda' \mathbf{I} = \frac{\Delta m^2}{4E} \begin{bmatrix} -\cos 2\theta & \sin 2\theta \\ \sin 2\theta & \cos 2\theta \end{bmatrix} + \lambda' \mathbf{I},
\end{aligned}$$

(the terms  $\lambda \mathbf{I}$  or  $\lambda' \mathbf{I}$  are proportional to the unit matrix and can be dropped.

## Hamiltonian in matter

We can now add the matter Hamiltonian, that we can recast in the form:

$$\mathcal{H}_{\text{mat}} = \begin{bmatrix} V_e & 0 \\ 0 & V_\mu \end{bmatrix} = \begin{bmatrix} V & 0 \\ 0 & 0 \end{bmatrix} + \lambda'' \mathbf{I} = \frac{V}{2} \begin{bmatrix} +1 & 0 \\ 0 & -1 \end{bmatrix} + \lambda''' \mathbf{I}, \quad (109)$$

where the terms proportional to the unit matrix  $I$  can be dropped because are irrelevant for the flavor evolution. Adding the matter potentials to the free Hamiltonian one obtains:

$$\mathcal{H} = \mathcal{H}_0 + \mathcal{H}_{\text{mat}} = \frac{\Delta m^2}{4E_\nu} \begin{bmatrix} -\cos 2\theta + \xi & \sin 2\theta \\ \sin 2\theta & +\cos 2\theta - \xi \end{bmatrix}, \quad (110)$$

where we have defined

$$\xi = \frac{2VE}{\Delta m^2} = \frac{2\sqrt{2}G_F N_e}{\Delta m^2}. \quad (111)$$

It is now straightforward to diagonalise the matter hamiltonian, comparing with the form of the free one. In fact dividing and multiplying by  $\sqrt{\sin^2 2\theta + (\cos 2\theta - \xi)^2}$  we can rewrite:

$$\begin{aligned}
\mathcal{H} = \mathcal{H}_0 + \mathcal{H}_{\text{mat}} &= \frac{\Delta m^2}{4E_\nu} \begin{bmatrix} -\cos 2\theta + \xi & \sin 2\theta \\ \sin 2\theta & +\cos 2\theta - \xi \end{bmatrix} \\
&= \frac{(\Delta m^2)_{\text{eff}}}{4E_\nu} \begin{bmatrix} -\cos 2\theta_m & \sin 2\theta_m \\ \sin 2\theta_m & +\cos 2\theta_m \end{bmatrix}, \quad (112)
\end{aligned}$$

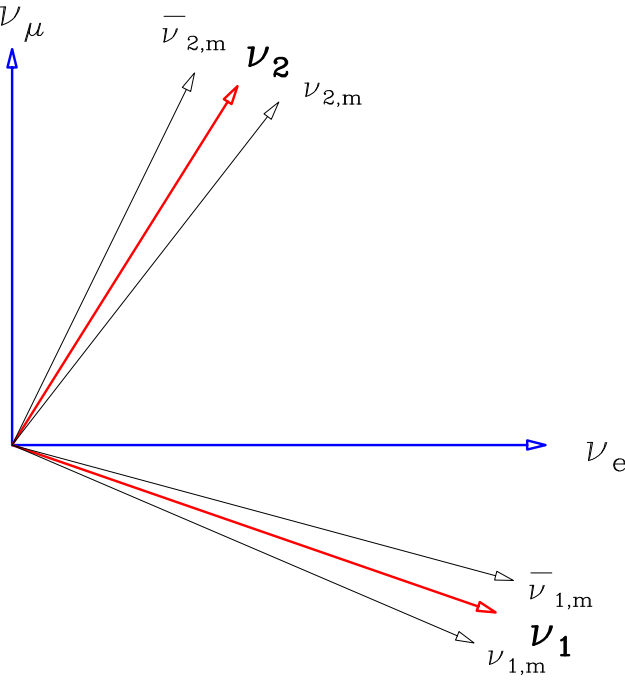


Fig. 8: This figure shows a scheme of the relation between the flavor, mass and propagation eigenstates in the case of two neutrino mixing. For neutrinos (antineutrinos) propagating in matter the propagation eigenstates do not coincide with the mass eigenstates. We have labeled the mass eigenstates so that  $m_1 < m_2$  (and therefore  $\Delta m^2 = m_2^2 - m_1^2 > 0$ ). With this convention for the labeling of the mass eigenstates, for neutrinos  $\theta_m^\nu > \theta$ , while for antineutrinos  $\theta_m^{\bar{\nu}} < \theta$ . In the limit of very large matter effects ( $(E \times V) \gg \Delta m^2$ )  $\theta_m^\nu \rightarrow \pi/2$  and  $\theta_m^{\bar{\nu}} \rightarrow 0$ . In the case shown (where  $\theta = 25^\circ$ )  $\theta_m^\nu$  becomes  $45^\circ$  for a certain value of  $(E \times V)$  and a “MSW resonance” is present for neutrinos (and not anti-neutrinos). For  $\theta > 45^\circ$  the resonance exists for anti-neutrinos.

where

$$\sin^2 2\theta_m = \frac{\sin^2 2\theta}{\sin^2 2\theta + (\cos 2\theta - \xi)^2} \quad (113)$$

and

$$(\Delta m^2)_{\text{eff}} = \Delta m^2 \times \sqrt{\sin^2 2\theta + (\cos 2\theta - \xi)^2}. \quad (114)$$

In matter the neutrino and anti-neutrino mixing are different because  $\nu$  and  $\bar{\nu}$  have opposite effective potentials. The eigenvalues/eigenvectors solutions for anti-neutrinos can be obtained with the replacement  $V \rightarrow -V$ , that is  $\xi \rightarrow -\xi$ . The situation is illustrated in Fig. 8.

### The MSW resonance

It is very instructive to study the behaviour of effective mixing parameters in matter as a function of the quantity  $\xi = 2VE/\Delta m^2$  (see Fig. 9). Note that  $\xi$  is proportional to the density  $V$  and to the neutrino energy  $E$ . Without loss of generality it is possible to assume that  $\Delta m^2$  is positive, if the mixing angle  $\theta$  can vary in the interval  $\theta \in [0, \frac{\pi}{2}]$ . In this case  $\theta = 0$  corresponds to the situation where the lightest neutrino state is a pure  $\nu_e$  and  $\theta = \frac{\pi}{2}$  to the situation where the lightest state is a  $\nu_{\mu,\tau}$ <sup>11</sup>. With this convention  $\xi$  is always positive for neutrinos always negative for antineutrinos.

---

<sup>11</sup>For two flavor mixing it is also possible to use a different convention, reducing the range of variability of  $\theta$  in the range  $[0, \pi/4]$ , and considering both positive and negative  $\Delta m^2$ . In this convention the  $\nu_1$  is always the state with the largest overlap with  $\nu_e$ ; while in the other convention  $\nu_1$  is the eigenstate with the lowest mass.

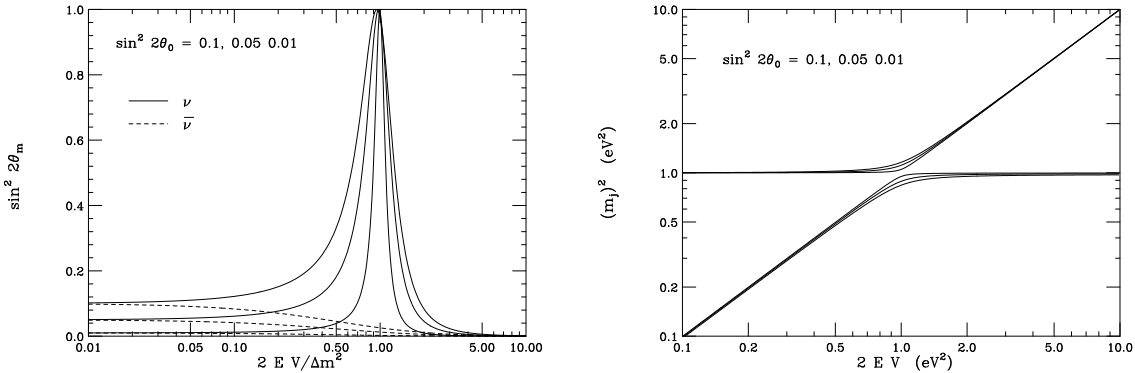


Fig. 9: The left panel shows the effective mixing parameter in matter  $\sin^2 2\theta_m$ , in the case of two flavor ( $\nu_e-\nu_\mu$  or  $\nu_e-\nu_\tau$ ) mixing, plotted as a function of  $\xi = (2 E V)/\Delta m^2$ . The right panel shows the effective squared masses in matter for neutrinos in the case of two flavor  $\nu_e-\nu_\mu$  (or  $\nu_e-\nu_\tau$ ) mixing. The mass eigenvalues are taken as  $m_1^2 = 0.1 \text{ eV}^2$  and  $m_2^2 = 1 \text{ eV}^2$ .

The main features of the effective mixing in matter in Fig. 9, can be readily understood from equation (113):

- [1] The low density limit can be obtained for  $\xi \rightarrow 0$ , it is easy to see that one recovers the vacuum case.
- [2] The limits  $\xi \rightarrow \pm\infty$  correspond to very high energy (or very large density) for neutrinos or antineutrinos. The effective mixing parameters become:

$$\sin^2 2\theta_m^{\nu(\bar{\nu})} \rightarrow \frac{\sin^2 2\theta}{\xi^2} \simeq \sin^2 2\theta \left( \frac{\Delta m^2}{2EV} \right)^2 \rightarrow 0, \quad (115)$$

$$(\Delta m^2)_{\text{eff}}^{\nu(\bar{\nu})} \rightarrow \Delta m^2 \times \xi = \pm 2EV. \quad (116)$$

It can be seen that equation (115) corresponds to  $\theta_m \rightarrow \frac{\pi}{2}$  for  $\nu$  and to  $\theta_m \rightarrow 0$  for  $\bar{\nu}$ . In other words when the potential difference  $V$  becomes much larger than the energy differences  $\Delta m^2/(2E)$  the  $\nu_e$  or  $\bar{\nu}_e$  become eigenvectors of propagation: the  $\nu_e$  (with  $V > 0$ ) corresponds to the heaviest eigenvector  $|\nu_{2,m}\rangle$ , while  $\bar{\nu}_e$  (with  $V < 0$ ) corresponds to the lightest eigenvector  $|\nu_{1,m}\rangle$ .

- [3] The mixing parameter  $\sin^2 2\theta_m$  becomes unity (that is  $\theta_m$  becomes  $\pi/4$ ) for the condition

$$\xi = \cos 2\theta, \quad (117)$$

that is:

$$2V E = \Delta m^2 \cos 2\theta. \quad (118)$$

This condition can be satisfied with  $\xi > 0$  (that is for neutrinos) when  $\theta < \pi/4$ ; and with  $\xi < 0$  (that is for anti-neutrinos) when  $\theta > \pi/4$ .

- [4] The width of the “resonance region”, that is the range of  $\xi$  for which  $\sin^2 2\theta_m$  is larger than 0.5 is  $\xi \in [\cos 2\theta - \sin^2 \theta, \cos 2\theta + \sin^2 \theta]$  and shrinks with decreasing  $\theta$ .

The relation between flavor, mass and propagation eigenstates can be pictured geometrically observing that with increasing density the mixing angle  $\theta_m^\nu$  for neutrinos “rotates” monotonously anti-clockwise from the vacuum value  $\theta$  (for a vanishingly small density) toward increasing values, reaching for very large densities the asymptotic value  $\theta_m^\nu \rightarrow \frac{\pi}{2}$ . For antineutrinos the mixing angle  $\theta_m^{\bar{\nu}}$  rotates in the opposite direction toward the asymptotic value  $\theta_m^{\bar{\nu}} \rightarrow 0$ . Clearly the mixing angle in matter must become “maximal” (that is take the value  $\theta_m = 45^\circ$ ) for neutrinos *or* antineutrinos, for a particular value of the product  $E_\nu N_e$ . This condition will be present for neutrinos when  $\theta < 45^\circ$  that is when the highest mass state is predominantly a  $\nu_e$  as it is naively expected “normal” ordering of the neutrino masses, or for anti-neutrinos if  $\theta > 45^\circ$  that is for an inverted hierarchy of the  $\nu$  masses<sup>12</sup>.

<sup>12</sup>In the other convention of having the angle  $\theta$  limited to the region  $\theta \in [0, \pi/4]$ , one would conclude that the MSW resonance is present for neutrinos for  $\Delta m^2 > 0$  or for anti-neutrinos for  $\Delta m^2$  negative. The statements have of course the identical physical meaning.

Figure 9 shows a plot of the effective mixing angle  $\theta_m$  and of the effective mixing parameter  $\sin^2 2\theta_m$  for neutrinos and anti-neutrinos. One can see that the mixing parameter has a “resonance like” behaviour around the value  $\xi = \cos 2\theta$  where the mixing becomes maximal. The “MSW” resonance (from the initials of Mikheyev, Smirnov and Wolfenstein [42] that discovered it) has a width (half width at half maximum)  $\delta\xi = \sin 2\theta$  that becomes narrower with decreasing  $\sin 2\theta$ .

In Fig. 9 we plot an example of the effective squared mass eigenvalues as a function of the product  $2VE$ . This illustrates that at the resonance  $\Delta m_{\text{eff}}^2$  has a minimum and becomes  $\Delta m_{\text{eff}}^2 = \Delta m^2 \sin 2\theta$ . The  $\Delta m_{\text{eff}}^2$  at the resonance vanishes for  $\theta = 0$  or  $\theta = 90^\circ$ . This can be easily understood observing that in the case of no mixing ( $\theta = 0^\circ$ ) the effective squared masses in matter are simply  $M_{1,2}^2 = m_{\nu_e}^2 + 2EV$  and  $M_{2,1}^2 = m_{\nu_\mu}^2$ . In this case the “resonance” corresponds simply to a level crossing at  $2EV = (m_{\nu_\mu}^2 - m_{\nu_e}^2)$ . Below the “resonance” or crossing point the heaviest propagation eigenvector is a  $\nu_\mu$ , above the crossing point it becomes a  $\nu_e$ .

In the presence of a small non vanishing  $\theta$ , there is no more a “crossing” of the levels, however something very similar happens in the flavor content of the propagation eigenstates. For example the propagation eigenstates that correspond to the largest (heaviest) eigenvalue correspond to a nearly pure  $\nu_\mu$  for small  $\xi$  and to a nearly pure  $\nu_e$  for large  $\xi$ . This phenomenon is possibly the key mechanism in the oscillation of solar neutrinos.

#### 6.4. Variable density

In many cases of interest neutrinos propagate in non homogeneous matter. Examples of this problem are:

- [1] Solar neutrinos that are created near the center of the sun, where the density is of order  $130 \text{ g cm}^{-3}$ , and travel to the surface with the density decreasing approximately exponentially along the trajectory.
- [2] Atmospheric neutrinos can cross the Earth, where the density is approximately  $2.7 \text{ g cm}^{-3}$  near the surface but higher than  $12 \text{ g cm}^{-3}$  near the center.
- [3] Supernova neutrinos have also to cross a large column density of material with a rapidly varying electron density.

In general the transition probabilities can be easily calculated numerically solving the flavor evolution equation:

$$\begin{aligned} i \frac{d}{dx} \begin{pmatrix} \nu_e \\ \nu_\mu \\ \nu_\tau \end{pmatrix} &= [\mathcal{H}_0 + \mathcal{H}_{\text{mat}}(x)] \begin{pmatrix} \nu_e \\ \nu_\mu \\ \nu_\tau \end{pmatrix} \\ &= \left\{ \frac{1}{2E} U \begin{bmatrix} m_1^2 & 0 & 0 \\ 0 & m_2^2 & 0 \\ 0 & 0 & m_3^2 \end{bmatrix} U^\dagger + \begin{bmatrix} V(x) & 0 & 0 \\ 0 & 0 & 0 \\ 0 & 0 & 0 \end{bmatrix} \right\} \begin{pmatrix} \nu_e \\ \nu_\mu \\ \nu_\tau \end{pmatrix}, \quad (119) \end{aligned}$$

where  $V(x) = V_e(x) - V_\mu(x) = \sqrt{2} G_F N_e(x)$  is the effective matter potential. The initial condition of the equation can be taken as a flavor eigenstate (for example  $|\nu_e\rangle$ ):  $|\nu_{\text{ini}}\rangle = \delta_{\alpha,e}$ , and the probability  $P_{\nu_e \rightarrow \nu_\alpha}$  is obtained squaring the final neutrino  $\alpha$  component.

## 7. ATMOSPHERIC NEUTRINOS

Atmospheric neutrinos are produced in the collisions of cosmic rays with the Earth's upper atmosphere. Cosmic rays are relativistic charged particles that reach the Earth with an isotropic flux of approximately 1 particle/(cm<sup>2</sup> sec sr). They are produced in astrophysical sources whose nature, after nearly a century of research, is still in question (the most likely sources are the blast waves produced by supernovae explosions), most cosmic rays are protons with contributions of completely ionized nuclei, and smaller components of electrons, anti-protons and positrons. Cosmic rays have a spectrum that to a good approximation follows a power law behaviour:  $\phi_A(E) \propto E^{-\alpha}$  with  $\alpha \simeq 2.7$ , extending up to extremely high energies  $E \sim 10^{20}$  eV. The galactic magnetic fields trap the cosmic rays for a long (energy dependent) time of order of millions of years, and during this time the directions of the particles are completely scrambled, so that the flux is to a very good approximation isotropic and uniform in time, because time variations in the source intensity are averaged over a long time. Primary cosmic ray interact in the upper atmosphere, with the air nuclei producing secondary particles:

$$p + A_{\text{Air}} \rightarrow p, n, \pi^\pm, \pi^\circ, K^\pm, \dots$$

that initiate showers in the atmosphere. Neutrinos are abundantly produced in these showers, the dominant source is the decay of  $\pi^\pm$ , and the subsequent decay of  $\mu^\pm$ , such as:

$$\begin{aligned} \pi^+ &\rightarrow \mu^+ + \nu_\mu \\ &\downarrow \\ &e^+ + \nu_e + \bar{\nu}_\mu \end{aligned} \tag{120}$$

(and charge conjugate channels), similarly neutrinos are also produced in the decay of kaons.

For a review on atmospheric neutrinos see [44].

### 7.1. Robust properties of the predicted fluxes

The detailed calculation of the atmospheric neutrino fluxes is a non trivial problem (for reviews see [45,46]), that requires the following elements:

- [1] A description of the primary cosmic rays  $\phi_A^{\text{c.r.}}(E)$ , with fits to the measurements obtained from balloon and satellites experiments.
- [2] A model of hadronic interactions to compute the multiplicity and energy and angular distributions of the final state particles produced in hadron-nucleus and nucleus-nucleus interactions.
- [3] A calculation scheme (usually a montecarlo method) to compute the development of the showers taking into account all relevant processes, like the energy losses of charged particles, the competition between interaction and decay for unstable hadrons, and the weak decays of mesons and muons.

Independently from the details of this calculation, and using the assumption that the flavor of the neutrinos does not change during propagation from the creation point to the detector, one can obtain two fundamental and very robust properties of the fluxes

- The flux of  $\nu_\mu + \bar{\nu}_\mu$  is approximately twice as large as the flux of  $\nu_e + \bar{\nu}_e$

$$[\phi_{\nu_\mu}(E_\nu, \Omega_\nu) + \phi_{\bar{\nu}_\mu}(E_\nu, \Omega_\nu)] \simeq 2 \times [\phi_{\nu_e}(E_\nu, \Omega_\nu) + \phi_{\bar{\nu}_e}(E_\nu, \Omega_\nu)]. \tag{121}$$

- The fluxes of all neutrino species are up-down symmetric:

$$\phi_{\nu_\alpha}(E_\nu, \theta_\nu) = \phi_{\nu_\alpha}(E_\nu, \pi - \theta_\nu). \tag{122}$$

The condition (121) is a simple consequence of equation (120), that tell us that, after the completion of the chain decay, for each  $\pi^+$  ( $\pi^-$ ) there is one  $\nu_\mu$ , one  $\bar{\nu}_\mu$  and one  $\nu_e$  ( $\bar{\nu}_e$ ) that have approximately the same average energy. The last remark about the average energy of the neutrinos is necessary to insure that the relation (121) between the neutrino fluxes is valid not only for the total number of neutrinos, after integration over all energies, but also for the differential fluxes at each neutrino energy. One could naively think that the “second generation” neutrinos produced in muon decay will have on average a lower energy than the  $\nu_\mu$  produced directly in the  $\pi^+$  decay, however this is not the case, because in the first decay the muon carries away a large fraction of the pion energy since  $m_\mu$  is close to  $m_\pi$ :  $\langle E_{\mu^+} \rangle / E_{\pi^+} = (1 + m_\mu^2/m_\pi^2)/2 \simeq 0.787$ , and the average energy of the three neutrinos are very similar. Ignoring the energy loss of the muon before decay one has  $\langle E_{\nu_\mu} \rangle / E_{\pi^+} = 0.213$ ,  $\langle E_{\bar{\nu}_\mu} \rangle / E_{\pi^+} = 0.265$ ,  $\langle E_{\nu_e} \rangle / E_{\pi^+} = 0.257$ . Equation (121) ceases to be valid at high energy ( $E_\nu \gtrsim 3$  GeV for vertical neutrinos) when, because of relativistic effects, the muon decay length becomes longer than the thickness of the atmosphere, and muons reach the ground dissipating their energy in ionization.

The prediction of the up-down symmetry (equation (122)) is even more robust, and in fact can be demonstrated as a simple *geometry theorem* from the (quasi-exact) spherical symmetry of the problem that can be restated as:

- [1] the Earth can be well described as a perfect sphere.
- [2] the primary cosmic rays are isotropic, that is the fluxes that arrive at different points on the Earth are all equal.

The demonstration is simple. The neutrinos that enter a sphere with zenith angle  $\theta_z^{\text{down}}$  will exit the sphere with zenith angle  $\theta_z^{\text{up}} = \pi - \theta_z^{\text{down}}$  (see Fig. 10). The absorption of neutrinos inside the Earth is a negligible effect (of order  $\sim 10^{-6}$  for vertical  $\nu_{\mu,e}$  at 1 GeV), and therefore the number of neutrinos that enter the Earth with a given energy and zenith angle  $\theta_z$  is equal to the number of neutrinos that exits with zenith angle  $\pi - \theta_z$  and the same energy:

$$N_{\nu_\alpha}^{\text{in}}(E, \theta_z) = N_{\nu_\alpha}^{\text{out}}(E, \pi - \theta_z). \quad (123)$$

For spherical symmetry (isotropic primary cosmic rays) the neutrino flux is equal for all points on the Earth, and can be related to the total number of crossing neutrinos as

$$\phi_{\nu_\alpha}(E, \theta_z) = \frac{N_{\nu_\alpha}^{\text{in(out)}}(E, \theta_z)}{4\pi R_\oplus^2 |\cos \theta_z|}, \quad (124)$$

where  $4\pi R_\oplus^2$  is the Earth surface and the factor  $|\cos \theta_z|$  takes into account the orientation of the surface with respect to the neutrino direction. The equality of the fluxes follows immediately. It is clear that this prediction of up-down symmetry for the neutrino fluxes, offers a gold-plated method to study flavor oscillations. The pathlengths for up-going and down-going neutrinos are very different (by a factor of order  $10^3$  for the vertical directions) and in the presence of oscillations one expects that the two fluxes are modified in different ways. Therefore, if oscillations exist, the up-down symmetry will be broken and the effect can be easily observed measuring a difference in the rates of up-going and down-going events.

Since the up-down symmetry (or lack of) plays a crucial role in the evidence for oscillations in atmospheric neutrinos it is worthwhile to consider what is the maximum size of the asymmetry that can be expected in the absence of oscillations. The sources of asymmetry are the following:

- [1] The largest violations of spherical symmetry is due to the presence of the geomagnetic field. The field bends the trajectories of the primay particles, so that low rigidity particles cannot reach the surface of the Earth. The effect is stronger at the magnetic equator (where the cosmic ray flux

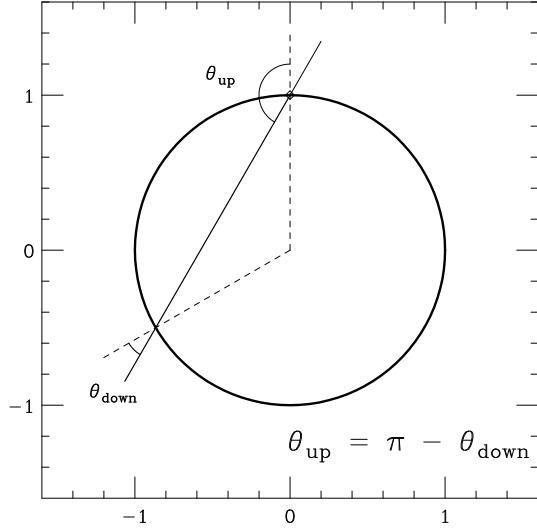


Fig. 10: The geometrical origin of the up-down symmetry of the atmospheric neutrino fluxes. The symmetry is present in the absence of neutrino oscillations.

is minimum and vanishes at the magnetic pole (where the cosmic ray is maximum). This effect influences also the lowest energy neutrinos, because high rigidity cosmic rays are not influenced by the geomagnetic field. For a detector placed near the magnetic equator (like Super-Kamiokande in Japan), the effect is a suppression of the down-going hemisphere (where the equatorial field is operating) relative to the up-going one (since the average effect of the geomagnetic field is weaker). The effect is reversed for detectors placed near a magnetic pole.

- [2] The Earth is not a perfect sphere, and its general shape can be approximated as an ellipsoid of rotation, however it can be shown that this effect is entirely negligible. More important are those small ‘irregularities’ represented by mountains. The number of neutrinos produced in showers that develop above a mountain is (slightly) reduced because of the reduced thickness of air. Since most ( $\sim 0.7$ ) of the Earth surface is at sea level, while most neutrino detectors are placed below a mountain (that is used as an absorber), this results in a small reduction of the down-going flux.
- [3] A third (smaller effect) is due to the average density profile of the atmosphere that changes with latitude. Since the profile has also seasonal variations, the size of this effect can be constrained by the (non)-observations of seasonal effects.

## 7.2. Detectors

The event rate for atmospheric neutrinos is of order  $\sim 0.5$  events/(Kton day), and to have appreciable rates one needs very massive detectors. Moreover, to reduce the background due to secondary cosmic rays that at the surface (at sea level) have a flux  $\sim 200$  particles/ $(m^2 \text{ sec})$ , the detectors have to be placed deep underground. The component of  $\gamma$ ,  $e^\pm$  and hadrons can be absorbed with few meters of rock, but to reduce significantly the flux of the penetrating muons, one needs a coverage of order of 1 Km of rock. Detectors for atmospheric neutrinos have been constructed using essentially two techniques: iron calorimeters with a segmentation of order 1 cm (such as Frejus, Nusex and Soudan-2) and Water Cherenkov detectors like Kamiokande, IMB and Super-Kamiokande. Relativistic charged particles moving in water with a velocity larger than  $\beta_c = 1/n \simeq 0.75$  (where  $n \simeq 1.33$  is the refractive index of the material) emit Cherenkov radiation; when  $\beta \rightarrow 1$  the light is emitted in a cone of semi-angle  $\theta_C = \cos^{-1} n \simeq 42^\circ$ . Since water is transparent to the Cherenkov radiation, the photons can be detected with sensitive elements (photo multiplier tubes or PMT’s) placed at the surface of the detector. This method allows the construction of large detectors at a relatively low cost.

The largest sample of data on atmospheric neutrinos has been obtained by the Super-Kamiokande detector (see Fig. 11). The detector is a stainless steel cylinder with 42 meters of height and 39 meters of diameter that contain 50 Ktons of water. A two meters layer of water is used as a veto counter, while the inner volume (32 Kton) can be used to detect neutrino interactions. The surface of the inner volume is instrumented with 11146 PMT's each one with a diameter of 50 cm that look “inside”, while 1885 PMT's with 20 cm diameter look “outside” instrumenting the veto detector. The Super-Kamiokande detector has taken data from april 1996 until november 2001, when the implosion of one phototube, started a chain reaction, that destroyed approximately two thirds of the other PMT's. The detector is currently being repaired and will start taking data again in 2003.

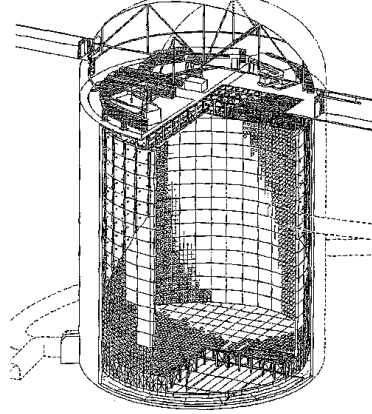


Fig. 11: The Super-Kamiokande detector.

The most important class of atmospheric neutrino events are quasi-elastic interactions of type:

$$\begin{aligned} \nu_\ell + n &\rightarrow \ell^- + p, \\ \bar{\nu}_\ell + p &\rightarrow \ell^+ + n. \end{aligned} \quad (125)$$

With increasing  $E_\nu$ , events with the production of additional particles in the final state also become possible (see Fig. 12).

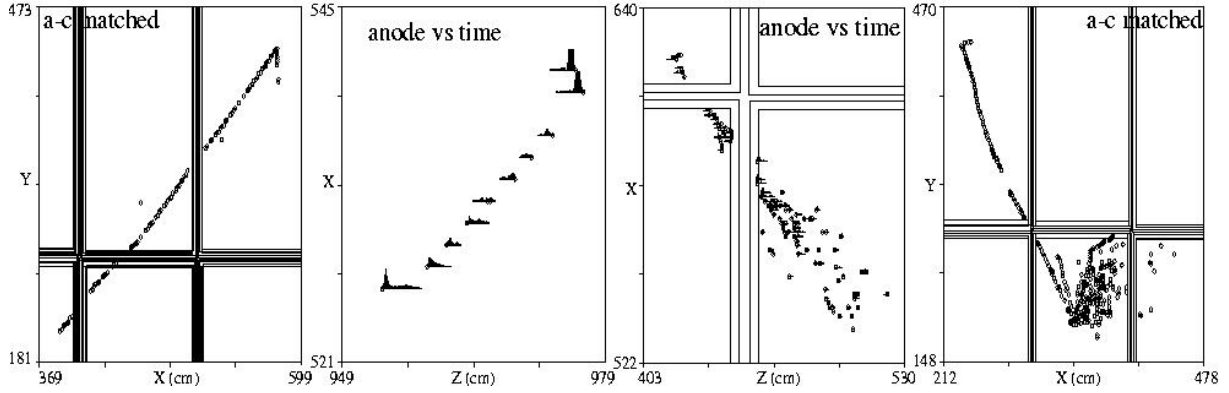


Fig. 12: Atmospheric neutrino events detected by the Soudan-2 detector. The events at the left can be interpreted as  $\nu_\mu + n \rightarrow \mu^- + p$  because of the  $\mu$ -like track and the short proton recoil. The next event is the other view of an event of the same type. The next event can be interpreted as a “single shower” event of type  $\nu_e + n \rightarrow e^- + p$  or  $\bar{\nu}_e + p \rightarrow e^+ + n$ . The last event is a multiprong  $\nu_\mu$  (or  $\bar{\nu}_\mu$ ) interaction.

Muons in water lose energy continuously and emit Cherenkov light until they reach the critical velocity, near the end of their range:  $L_\mu \simeq 5 E_{\text{GeV}}$  meters. This results in a ‘ring’ of Cherenkov light at the surface of the detector. From the shape and brightness of the ring it is possible to determine the point of creation of the particle and its direction and energy. Electrons in water undergo bremsstrahlung and originate an electromagnetic shower, so that their energy is dissipated in the ionization of several  $e^\pm$  particles, each one generating a Cherenkov ring that overlap in a single visible ring that is more ‘fuzzy’ than those produced by muons, because of multiple scattering effects. The difference between the ‘sharp’ ( $\mu$ -like) and ‘fuzzy’ ( $e$ -like) rings allows to determine the flavor of the charged lepton (see Fig. 13). The

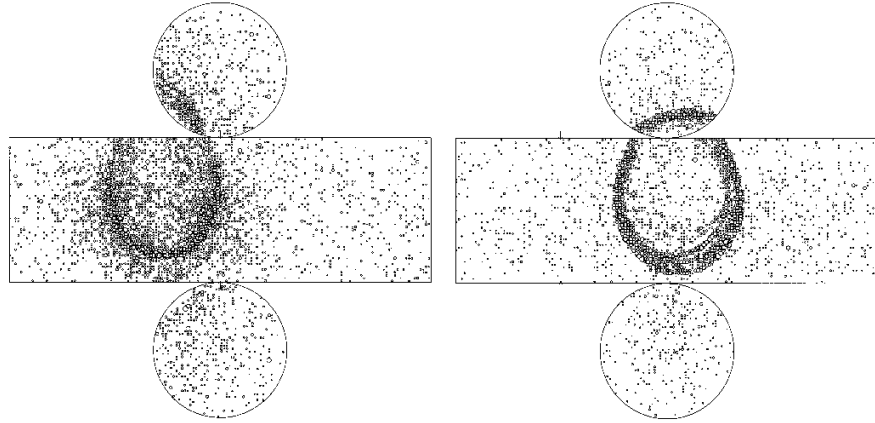


Fig. 13: Single-ring events in Super-Kamiokande. The event on the left is  $e$ -like, the one on the right  $\mu$ -like.

flavor identification is easier when a single ring is present in the event, and for this reason “single ring” events have been selected by SK at some cost in efficiency at higher neutrino energy when the production of additional particles in the final state becomes more important. The results of Super-Kamiokande are shown in Fig. 14. the 6 panels show the results for different classes of events. The first 4 classes of events are “fully contained events”, that is events where the neutrino interacts inside a detector fiducial volume (2 meters away from the detector walls for a fiducial mass of 22.5 Ktons) and no particle exits from the detector. The events are divided into 4 categories according to the flavor identification ( $e$  or  $\mu$ ) and the amount of visible energy (smaller or larger than 1.33 GeV). The other two classes of events are throughgoing and stopping upward going muons. These are events generated by the charged current interactions of  $\nu_\mu$  and  $\bar{\nu}_\mu$  in the rock below the detector.

The results of SK Fig. 14 are shown together with a standard model prediction (in the absence of  $\nu$  oscillations), and a with a prediction that assumes the existence of  $\nu_\mu \leftrightarrow \nu_\tau$  oscillations. In this case the prediction depends on the two parameter  $\Delta m^2$  and  $\sin^2 2\theta$ , and the lines shown correspond to the best fit values  $\Delta m^2 = 2.5 \times 10^{-3} \text{ eV}^2$  and  $\sin^2 2\theta = 1$ .

Several points appear clearly from an inspection of Fig. 14. The first one is that for  $e$ -like events, the data and the standard model (no oscillation) prediction are in good agreement with each other, note in particular that the data exhibits the predicted up-down symmetry. On the other hand for all 4 categories of  $\mu$ -like events there is a significant deficit with respect to the prediction. Moreover these deficits exhibit some very interesting dependence on the zenith angle. The most spectacular effect, and the key for the interpretation of the result is the zenith angle distribution of the multi-GeV  $\mu$ -like events, where the number of up-going events (with zenith angle  $\cos \theta_z < 0$ ) is only 1/2 of the number of down-going ones ( $\cos \theta_z > 0$ ).

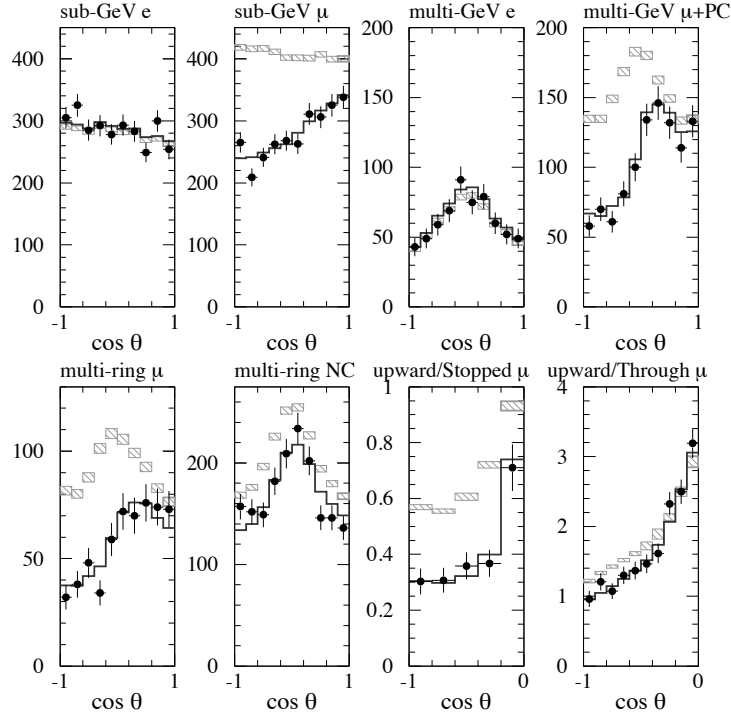


Fig. 14: Zenith angle distribution of Super-Kamiokande FC, PC and UPMU samples. Dots, solid line and dashed line correspond to data, MC with no oscillation and MC with best fit oscillation parameters, respectively.

### 7.3. The $\nu_\mu \leftrightarrow \nu_\tau$ interpretation.

It is simple to understand qualitatively how the assumption of  $\nu_\mu \leftrightarrow \nu_\tau$  oscillations can provide a good description of the data. Under this assumption the neutrino fluxes at the detector are related to the no-oscillation ones by:

$$\begin{aligned} \phi_{\nu_e} &\rightarrow \phi_{\nu_e}, \\ \phi_{\nu_\mu} &\rightarrow [1 - \langle P_{\nu_\mu \rightarrow \nu_\tau} \rangle] \phi_{\nu_\mu}, \\ \phi_{\nu_\tau} \simeq 0 &\rightarrow \langle P_{\nu_\mu \rightarrow \nu_\tau} \rangle \phi_{\nu_\mu}, \end{aligned} \quad (126)$$

and similarly for anti-neutrinos. In this equation, the brackets  $\langle \rangle$  correspond to an average over the position of the creation points of the neutrinos (and therefore the pathlength). After this average the the oscillation probability will depend on the *neutrino* energy and direction, with a form that is determined by the two parameters  $\Delta m^2$  and  $\sin^2 2\theta$ :

$$\langle P_{\nu_\mu \rightarrow \nu_\tau} \rangle = \langle P_{\nu_\mu \rightarrow \nu_\tau} \rangle(E_\nu, \cos \theta_z; \Delta m^2, \sin^2 2\theta).$$

Matter effects are ineffective in the case of two-flavor  $\nu_\mu \leftrightarrow \nu_\tau$  oscillations and one has the simple formula:

$$P_{\nu_\mu \rightarrow \nu_\tau}(L, E_\nu) = \sin^2 2\theta \sin^2 \left[ \frac{\Delta m^2 L}{4E_\nu} \right]. \quad (127)$$

This probability takes some simple form in the limits of large or small  $L/E_\nu u$  (where large or small is defined comparing with  $1/\Delta m^2$ ):

$$P_{\nu_\mu \rightarrow \nu_\mu} = \begin{cases} 0 & \text{for } L \text{ small,} \\ 1 - \frac{\sin^2 2\theta}{2} & \text{for } L \text{ large.} \end{cases} \quad (128)$$

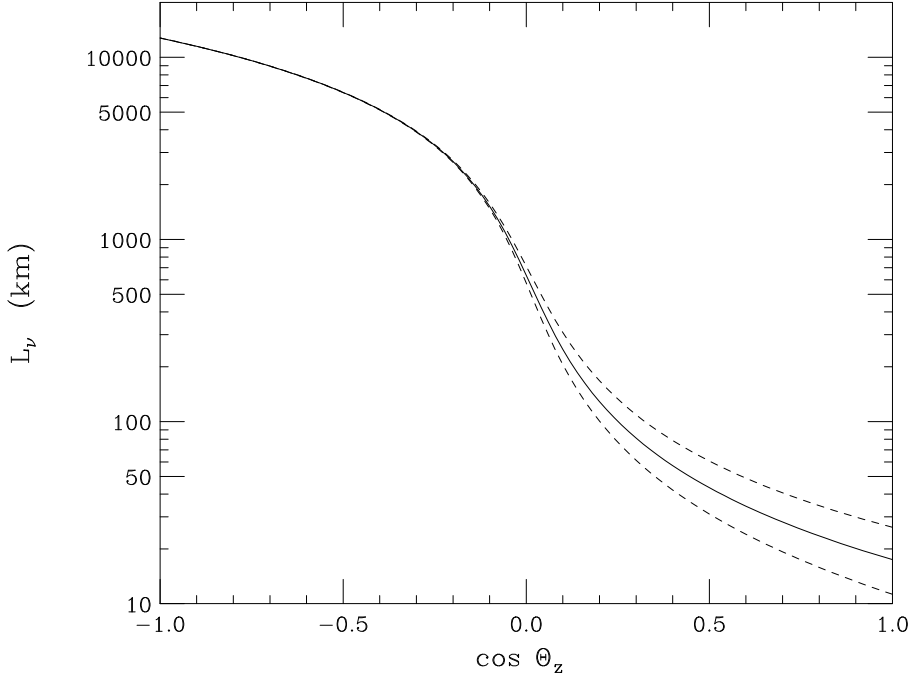


Fig. 15: Neutrino pathlength as a function of the neutrino zenith angle. The solid line is the most likely distance, the dashed lines correspond to  $\pm 34\%$  of the events.

In the case of large  $L$  we have averaged over fast oscillations.

Evidence for the presence of oscillations in the  $\nu_\mu \leftrightarrow \nu_\tau$  case can be obtained either observing the appearance of events with a  $\tau^\mp$  in the detector, or observing a suppression of the rate of  $\mu$ -like events. The threshold of charged current interactions for  $\nu_\tau$  and  $\bar{\nu}_\tau$  is  $E_{\nu_\tau}^{\text{thresh}} \simeq m_\tau + m_\tau^2/(2m_p) \simeq 3.5$  GeV, and the cross section is severely suppressed close to the kinematical threshold, therefore the flux of  $\nu_\tau$  and  $\bar{\nu}_\tau$  generated by the oscillations is very difficult to observe, while the disappearance effects can be more easily detected. Clearly a detectable effect is a suppression of the rate of  $\mu$ -like events with respect to the no-oscillation prediction or, to eliminate systematic uncertainties, with respect to the  $e$ -like rate, moreover it can be expected that disappearance effects can be a function of the zenith angle and energy of the neutrinos, reflecting the functional form of the probability (127).

The neutrino pathlength  $L$  is very strongly correlated with the zenith angle  $\theta_z$  (see Fig. 15). For a first order analysis it is sufficient to observe that neutrinos are produced at a typical height  $h \sim 20$  Km, with only a weak dependence on the energy, flavor and zenith angle (see [47] for more discussion) and therefore to a reasonable approximation

$$L \simeq -R_\oplus \cos \theta_z + \sqrt{(R_\oplus \cos \theta_z)^2 + 2 R_\oplus h + h^2}. \quad (129)$$

This expression ranges from  $L \sim h \sim 20$  Km for vertically down-going neutrinos ( $\cos \theta_z = 1$ ) to  $L \simeq 2 R_\oplus + h \simeq 12740$  Km for up-going  $\nu$  ( $\cos \theta_z = -1$ ). For horizontal neutrinos the pathlength is  $L_{\text{hor}} \simeq \sqrt{2R_\oplus h} \sim 500$  Km. A natural expectation is that up-going neutrinos, that travel for a longer distance will have larger oscillation probabilities than down-going ones, and therefore the rate of up-going events will be more suppressed.

In order to understand the parameters  $\Delta m^2$  and  $\sin^2 2\theta$  that can fit the atmospheric neutrino data it is best to look first at the multi-GeV data. Defining “Up” as the up-going rate (with  $\cos \theta_{z,\mu} < -0.4$ )

and “Down” as the down-going rate (with  $\cos \theta_{z,\mu} > 0.4$ ), the ratio is approximately one half:

$$\left( \frac{\text{Up}}{\text{Down}} \right)_{\text{multiGeV}} = 0.54 \pm 0.04 \pm 0.01. \quad (130)$$

Experimentally one measures the direction of the charged leptons ( $e$  or  $\mu$ ) and not of the neutrino, however the two directions are correlated, and the average angle  $\langle \theta_{\ell\nu} \rangle$  shrinks with increasing energy  $\propto E_\ell^{-1}$ . For sub-GeV events  $\langle \theta_{\ell\nu} \rangle \sim 60^\circ$ , the correlation is rather poor, while for multi-GeV events  $\langle \theta_{\ell\nu} \rangle \sim 10^\circ$ , the correlation is much more strict, and to first approximation one can assume  $\theta_{z,\mu} \simeq \theta_{z,\nu}$ . It is then quite easy to see how data and prediction can be reconciled, assuming the presence of  $\nu_\mu \leftrightarrow \nu_\tau$  oscillations and choosing appropriately the parameters  $\sin^2 2\theta$  and  $\Delta m^2$  so that down-going events have negligible suppression while down-going events have the average suppression as in equation (128). A rough estimate of the oscillation parameters is easy to obtain. The up/down ratio allows to estimate the mixing parameter from:

$$1 - \frac{\sin^2 2\theta}{2} \simeq \left( \frac{\text{Up}}{\text{Down}} \right)_{\text{multiGeV}} \sim 0.5, \quad (131)$$

giving  $\sin^2 2\theta \simeq 1$ . To estimate  $\Delta m^2$  one can use the fact that the critical length that separates “long” (no-oscillation) from “short” (averaged oscillations) pathlengths correspond to the horizontal directions:

$$L^* \simeq \frac{\lambda_{\text{osc}}^*}{2} \simeq \frac{2\pi \langle E_\nu \rangle}{|\Delta m^2|} \simeq 1000 \text{ Km}. \quad (132)$$

For multi-GeV events, in first approximation one has  $\langle E_\nu \rangle \sim 3 \text{ GeV}$ , with an estimate:

$$|\Delta m^2| \simeq \frac{2\pi (\hbar c)}{L^*} \simeq 3 \times 10^{-3} \text{ eV}^2. \quad (133)$$

A measurement of the average suppression of the  $\nu_\mu$  and  $\bar{\nu}_\mu$  flux can be obtained from the ratio  $(\mu)_{\text{Data}} / \mu_{\text{MC}}$  between the measured and predicted event rate. In order to reduce the systematic uncertainty in the prediction it is useful to consider the “Double ratio”

$$R = \left( \frac{(\mu)_{\text{Data}}}{(e)_{\text{Data}}} \right) / \left( \frac{(\mu)_{\text{MC}}}{(e)_{\text{MC}}} \right). \quad (134)$$

Since as discussed before (see equation (121)) the ratio between  $\mu$ -like and  $e$ -like events can be reliably predicted in the double ratio systematic uncertainties such as the absolute normalization of the flux cancel. For multi-GeV events the double ratio measured by SK is:

$$R_{\text{multiGeV}} = 0.68 \pm 0.03 \text{ (stat)} \pm 0.08 \text{ (sys)}, \quad (135)$$

this corresponds to best estimate for the oscillation probability averaged over all zenith angles and energies for this class of events.

The sub-GeV events are nicely consistent with this interpretation. The average oscillation probability can be obtained from the double ratio  $R$ :

$$R_{\text{subGeV}} = 0.64 \pm 0.02 \text{ (stat)} \pm 0.05 \text{ (sys)} \quad (136)$$

is close to the one measured for the multi-GeV events, as it is expected. In this case the correlation between the muon and the neutrino direction is less good, and therefore the up/down asymmetry for muon events is less marked, but it still clearly visible.

The results of a detailed fit to the SK data results in the allowed region (at 90% C.L.) shown in

Fig. 16, give the result:

$$\begin{cases} |\Delta m^2| \sim (1.6 - 4.5) \times 10^{-3} \text{ eV}^2, \\ \sin^2 2\theta \geq 0.90, \end{cases} \quad (137)$$

that corresponds to the qualitative estimate that we have discussed.

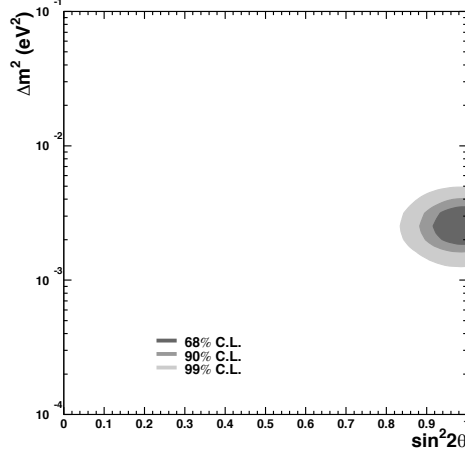


Fig. 16: Allowed regions at the 68,90 and 99% confidence level for the  $\nu_\mu \leftrightarrow \nu_\tau$  oscillation hypothesis obtained by Super-Kamiokande.

#### 7.4. Upward-going muons

A different method to detect fluxes of  $\nu_\mu$  and  $\bar{\nu}_\mu$  is the observation of neutrino induced upward-going muons. In these events the neutrino interaction happens in the rock below the detector, and the  $\mu^\mp$  produced in charged current interactions propagate to the detector. In through-going events the muons cross the detector, while in stopping events the muons range out inside the detector volume. Because of the up-down symmetry of the atmospheric neutrino fluxes one expects (in the absence of oscillations, and if the detector is placed at a sufficient depth) an equal number of  $\nu$ -induced up-going and down-going muon events, however down-going events cannot be separated from the flux of atmospheric muon events, where the muon is produced directly in the atmosphere, and therefore only up-going events can be used to study the neutrino fluxes, with the exception of exceptionally deep detectors. For a threshold energy of order 1 GeV, The flux of  $\nu$ -induced upgoing events is of order:

$$\langle \phi_{\mu\uparrow} \rangle \simeq 2 \times 10^{-13} (\text{cm}^2 \text{ sec sr})^{-1} \simeq 60 [(1000 \text{ m}^2) \text{ year sr}]^{-1}. \quad (138)$$

For a rock overburden of order  $h \sim 1$  Km, the atmospheric muon flux is still approximately  $10^5$  times larger than the  $\nu$ -induced one. The two fluxes become comparable for a thickness of approximately 5 Km of rock.

The range of a muon in rock is  $R_\mu \simeq 1.7 E_{\text{GeV}}$  meters, therefore high energy neutrinos can produce up-going muons even if they interact far from the detector. For  $\nu_\mu$  and  $\bar{\nu}_\mu$  with energy larger than  $\gtrsim 10$  GeV (the precise number depends of course on the dimension and geometry of the detector) the event rate in up-going muons is larger than the rate of interactions inside the detector. The neutrino energy that contribute to the fluxes of up-going muons is shown in Fig. 17: the median neutrino energy is of order  $E_\nu \sim 10$  GeV for stopping events, and  $E_\nu \sim 100$  GeV for through-going events. In the presence of  $\nu_\mu \leftrightarrow \nu_\tau$  oscillations with  $\Delta m^2$  of the order suggested by the contained events one can expect that the

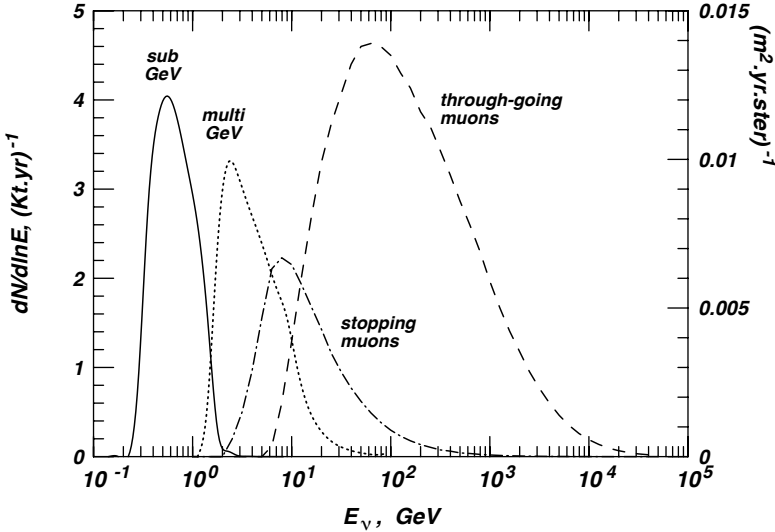


Fig. 17: Event rates as a function of neutrino energy for fully contained events, stopping muons, and through-going muons at SuperKamiokande.

flux of the (lower energy) passing events is suppressed by the averaged factor  $1 - \sin^2 2\theta$  for all zenith angles except for directions very close to the horizontal plane, while for the higher energy through-going events the suppression should be smaller, and with a non trivial dependence on the zenith angle, being largest for the vertical direction.

Up-going muons have been the first type of atmospheric neutrino events to be observed [54] with simple detectors placed in very deep mines in South Africa and in India. Larger samples of up-going muons have been obtained by several detectors: Baksan [55], Frejus [56], MACRO [57], Kamiokande [50] and Super-Kamiokande [52]. The first two detectors have measured fluxes that are compatible with the no-oscillation hypothesis, while Kamiokande, MACRO and Super-Kamiokande have measured deviations from the no-oscillation hypothesis that can be well explained with the existence of  $\nu_\mu \leftrightarrow \nu_\tau$  oscillations with parameters that are compatible with those indicated by the contained events observations. In the case of up-going muon events one cannot use the two “robust methods” (the  $\mu/e$  ratio and the up-down comparison) available for the contained events, since one can observe only  $\nu_\mu$  and  $\bar{\nu}_\mu$  in the up-going hemisphere, and therefore the systematic uncertainties are more important. In particular the uncertainty in the prediction of the absolute rate of the fluxes is large of order of 15–20%, however some measurements are affected by smaller uncertainties, and allow to test for the existence of  $\nu$  flavor transitions. The most robust prediction is the shape of the zenith angle distribution of the  $\phi_{\mu\uparrow}$ . In the absence of oscillations the shape of the distribution has a minimum (maximum) for the vertical (horizontal) direction(s). This is a consequence of the fact that the decay of the  $\pi^\pm$  and  $K^\pm$  that generate the neutrinos is more probable for horizontal mesons. This can be understood observing that mesons can decay only during an interval in their trajectory that corresponds to an interaction length; this interval is longer for horizontal mesons that are produced and travel higher in the atmosphere where the air density is lower. This competition between interaction and decay is controlled by geometry and can be predicted accurately. In the presence of oscillations, vertical neutrinos that correspond to longer pathlength can oscillate more, and are more suppressed than horizontal ones and the ratio vertical/horizontal becomes smaller than in the no-oscillation case. This distortion of the predicted shape of the up-going muon flux has been observed by Kamiokande, MACRO (see Fig. 18) and Super-Kamiokande (see Fig. 14.).

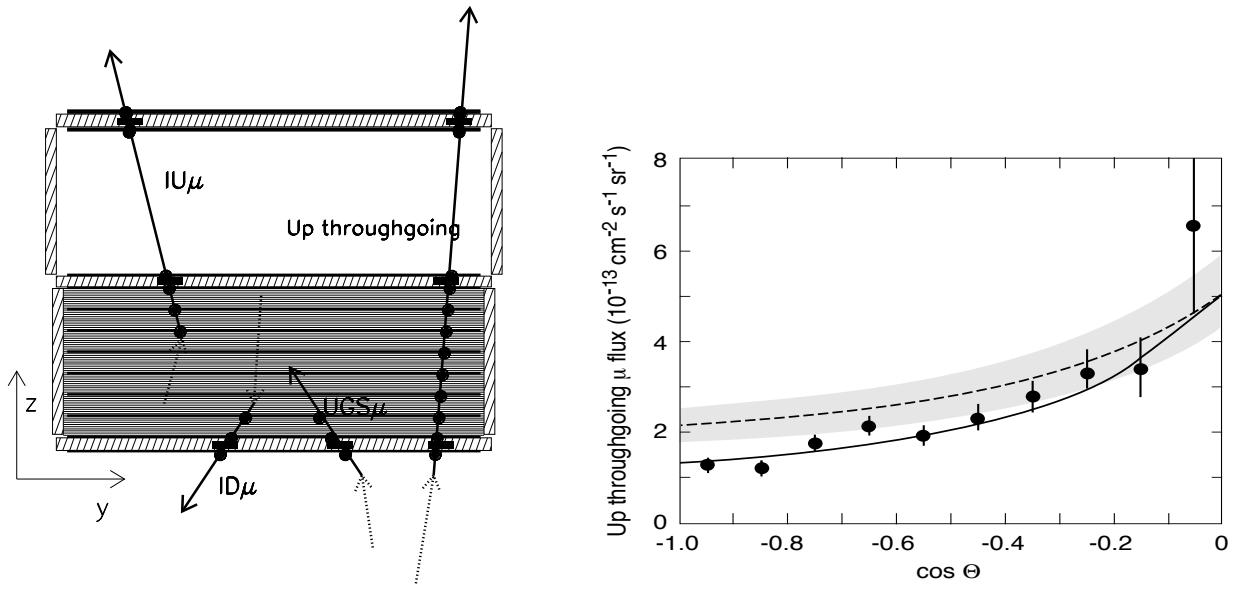


Fig. 18: The left panel shows a scheme of the MACRO detector, and a scheme of the three classes of atmospheric neutrino events. The right panel shows the measurement of the flux of through-going muons compared with predictions with and without the presence of oscillations.

### 7.5. The MACRO data

The MACRO detector that was located in Hall B of the Gran Sasso Laboratory, under a minimum rock overburden of  $3150 \text{ hg/cm}^2$  was a large rectangular box of dimensions  $76.6 \times 12.3 \text{ m}^3$ , divided longitudinally in six supermodules and vertically in a lower part ( $4.8 \text{ m}$  high) and an upper part ( $4.5 \text{ m}$  high) (Fig: 18a). It had three types of detectors which gave redundancy of informations: liquid scintillation counters, limited streamer tubes and nuclear track detectors. This last detector was used only for new particle searches.

The MACRO detector could measure three classes of atmospheric neutrino interactions (see Fig. 18):

- The “Up throughgoing muons” (with  $E_\mu > 1 \text{ GeV}$ ) are generated by  $\nu_\mu$  and  $\bar{\nu}_\mu$  interactions in the rock below the detector. The tracking is performed with streamer tubes hits; the time information, provided by scintillation counters, allows the determination of the direction (versus) by the time-of-flight measurement.
- The “Internal Upgoing” (IU) events come from  $\nu_\mu$  interactions inside the lower apparatus. Since two scintillation counters are intercepted, the Time of Flight method can be applied to identify the upward going muons. The median parent neutrino energy for these events is  $\sim 4 \text{ GeV}$ . If the atmospheric neutrino anomalies are the results of  $\nu_\mu$  oscillations with maximal mixing and  $10^{-3} < \Delta m^2 < 10^{-2} \text{ eV}^2$ , one expects a reduction of about a factor of two in the flux of IU events, without any distortion in the shape of the angular distribution.
- The “Up-going Stopping muons” (UGS) are due to  $\nu_\mu$  interactions in the rock below the detector yielding upgoing muon tracks; The “semicontained downgoing muons” (ID) are due to  $\nu_\mu$  induced downgoing tracks with vertex in the lower MACRO. The events are found by means of topological criteria; the lack of time information prevents to distinguish between the two subsamples. An almost equal number of UGS and ID events is expected. In case of oscillations, a similar reduction in the flux of the up stopping events and of the semicontained upgoing muons is expected; no reduction is instead expected for the semicontained downgoing events (which come from neutrinos which travelled  $\sim 20 \text{ km}$ ).

A summary of the results of MACRO is given in Fig. 18 and in the Table below:

---

	Events	MC no osc	$R = (\text{Data}/\text{MC no osc})$
Upthroughgoing	809	$1122 \pm 191$	$0.721 \pm 0.026_{\text{stat}} \pm 0.043_{\text{sys}} \pm 0.123_{\text{th}}$
IU	154	$285 \pm 28_{\text{sys}} \pm 71_{\text{th}}$	$0.54 \pm 0.04_{\text{stat}} \pm 0.05_{\text{sys}} \pm 0.13_{\text{th}}$
ID+UGS	262	$375 \pm 37_{\text{sys}} \pm 94_{\text{th}}$	$0.70 \pm 0.04_{\text{stat}} \pm 0.07_{\text{sys}} \pm 0.17_{\text{th}}$

---

The results are consistent with the existence of  $\nu_\mu \leftrightarrow \nu_\tau$  oscillations with a best fit point of  $\sin^2 2\theta = 1$  and  $\Delta m^2 = 2.5 \times 10^{-3} \text{ eV}^2$  (by coincidence very similar to the best-fit of SK). The data/prediction rates for the three classes of events can be explained qualitatively very simply:

- [1] The suppression of the rate of internal up-going (IU) events, that are produced by neutrinos with very long pathlength and low energy, can be explained with averaged oscillations, (no distortions of the zenith angle distribution) and the suppression of  $\sim 0.5$  corresponds to maximal mixing ( $\sin^2 2\theta \sim 1$ ).
- [2] The higher energy through-going events have a smaller suppression that is effective mostly for vertical (very long pathlength) events. This can be interpreted as a consequence of the functional dependence of the oscillation probability on the combination  $\Delta m^2 L/E_\nu$ . These high energy data allow to determine a range of possible  $\Delta m^2$  from the shape of the distortion of the zenith angle distribution.
- [3] The events belonging to the last class (ID + UGS) are a combinations of two sources. The first source (ID) due to internal interactions of down-going neutrinos is little affected by oscillations (because of the short pathlength). The second source (stopping up-going muons) that are suppressed with average oscillations. The combination of the two effects give the average effect  $\simeq 0.70$  the

The region in the plane  $(\sin^2 2\theta, \Delta m^2)$  allowed by the MACRO data is shown in Fig. 19, together with the results of other measurements. All results are in reasonable agreement.

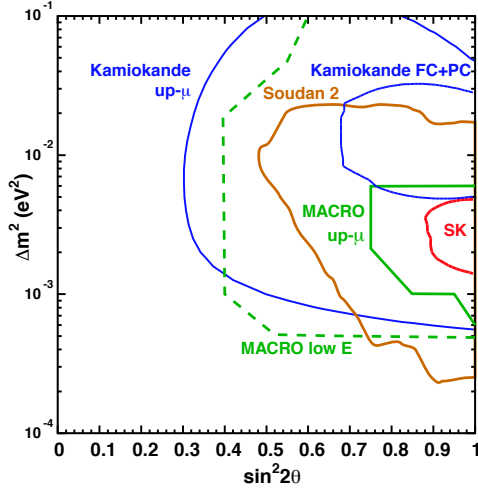


Fig. 19: 90% C.L. allowed region contours for  $\nu_\mu \longleftrightarrow \nu_\tau$  oscillations obtained by the Kamiokande, SuperKamiokande, MACRO and Soudan 2 experiments.

## 7.6. Three flavor analysis

In the discussion we have performed until now we have discussed an interpretation of the data in terms of a simple two-flavor mixing between  $\nu_\mu$  and  $\nu_\tau$ , with  $\nu_e$  a non-mixed state that corresponds to a mass eigenstate. This simple hypothesis does allow a very successful description of the experimental results, however it is clearly a very special situation. In the most general case the oscillations are controlled by three (two independent) squared mass differences, three mixing angles and one phase, and the discussion is quite complex. The situation simplifies considerably if one assumes that one squared mass difference (that without loss of generality can be labeled as  $\Delta m_{12}^2$ ) is so small that is unobservable. For atmospheric neutrino experiments this corresponds to the condition:

$$\Delta m_{12}^2 \left( \frac{L}{E} \right)_{\max} \simeq \Delta m_{12}^2 \left( \frac{R_\oplus}{(0.3 \text{ GeV})} \right) \ll 1, \quad (139)$$

that corresponds to  $\Delta m_{12}^2 \lesssim 10^{-4} \text{ eV}^2$ . In this situation (the “one mass scale dominance” approximation), as discussed in Section 4.4, the oscillation probabilities depend on three parameters:

- One squared mass difference:  $\Delta m^2 \simeq \Delta m_{23}^2 \simeq \Delta m_{13}^2$ .
- Two mixing angles  $\theta_{13}$  and  $\theta_{23}$  that describe the flavor content of the “isolated” (that does not belong to a quasi-degenerate doublet) state that we have labeled  $\nu_3$ :

$$|\nu_3\rangle = \sin \theta_{13} |\nu_e\rangle = \sin \theta_{13} \cos \theta_{23} |\nu_\mu\rangle = \sin \theta_{13} \sin \theta_{23} |\nu_\tau\rangle.$$

The two-flavor discussion that we have developed until now corresponds to the special case  $\theta_{13} \simeq 0$  (with the relabeling  $\theta \equiv \theta_{23}$ , and the results obtained tell us that the “isolated” state  $\nu_3$  is a linear combination of  $\nu_\mu$  and  $\nu_\tau$  with approximately equal weight (since  $\sin^2 2\theta_{23} \simeq 1$  corresponds to  $\theta_{23} = 45^\circ$ ).

It is clearly of considerable interest to study both angles  $\theta_{23}$  and  $\theta_{13}$ . It turns out that the best measurement of  $\theta_{13}$  has been obtained not with atmospheric neutrinos but with neutrinos from reactors (see Section 9.), and gives an upper limit  $\sin^2 \theta_{13} < 0.05$ . Therefore “a posteriori” the two-flavor analysis of atmospheric neutrinos turns out to be a surprisingly good approximation. Analysis of the atmospheric neutrino data in terms of three flavor oscillations in the framework of the one mass scale dominance approximation have been performed by SK. The result (see Fig. 33) gives allowed intervals for  $\Delta m^2$  and  $\theta_{23}$  that are very close to the intervals obtained in the two-flavor analysis, while for the other angle  $\theta_{13}$  one obtains only an upper limit  $\sin^2 \theta_{13} \leq 0.75$ . The upper limit for the angle  $\theta_{13}$  may seem surprisingly large considering that these angle controls the oscillations of electron neutrinos, and all  $e$ -like events are compatible with the absence of oscillations. The poor limit if  $\theta_{13}$  can be understood as the consequence of an interesting cancellation effect. After inclusion of oscillations, the flux of  $e$ -like events can be schematically written as:

$$e = e_0 [1 - P_{\nu_e \rightarrow \nu_\mu} - P_{\nu_e \rightarrow \nu_\tau}] + \mu_0 P_{\nu_\mu \rightarrow \nu_e} \quad (140)$$

in the limit of small  $\Delta m_{12}^2$  one has the relations:

$$\begin{aligned} P_{\nu_e \rightarrow \nu_\mu} &= P_{\nu_\mu \rightarrow \nu_e}, \\ P_{\nu_e \rightarrow \nu_\mu} \sin^2 \theta_{23} &= P_{\nu_e \rightarrow \nu_\tau} \cos^2 \theta_{23}. \end{aligned} \quad (141)$$

Using the result  $\sin^2 \theta_{23} \simeq \cos^2 \theta_{23} \simeq 0.5$  (that follows from  $\sin^2 2\theta_{23} \simeq 1$ ) one obtains:  $P_{\nu_\mu \rightarrow \nu_e} = P_{\nu_e \rightarrow \nu_\mu} \simeq P_{\nu_e \rightarrow \nu_\tau} \simeq P$ , and substituting into (140) one obtains:

$$e \simeq e_0 [1 - 2P] + \mu_0 P \simeq e_0 \left\{ [1 - 2P] + \left( \frac{\mu_0}{e_0} \right) P \right\} \simeq e_0, \quad (142)$$

where we have used the result that before oscillations  $\mu_0/e_0 \simeq 2$ . Therefore even if the oscillations of electron neutrinos are rather large, the effect on the flux is small because one has a disappearance effect that has two channels ( $\nu_e \rightarrow \nu_\mu$  and  $\nu_e \rightarrow \nu_\tau$ ) with approximately equal probability, and one appearance effect ( $\nu_\mu \rightarrow \nu_e$  with the same transition probability, but a source that is twice as large, and to first order the two effects cancel.

### 7.7. The $\nu_\mu \leftrightarrow \nu_{\text{sterile}}$ hypothesis

Since the effect observed in atmospheric neutrinos is the disappearance of  $\mu$ -like events, it is natural to ask the question if the physical process observed is in fact due to transitions  $\nu_\mu \rightarrow \nu_\tau$ , or if it is instead due to transitions  $\nu_\mu \rightarrow \nu_{\text{sterile}}$ , where  $\nu_{\text{sterile}}$  is a singlet under the  $SU(2) \otimes U(1)$  group of the electroweak interactions that is a particle that does not interact with the  $W$  and  $Z$  bosons and is therefore completely invisible.

The two type of oscillations can be distinguished using three methods:

- (i) The most straightforward method is of course the detection of  $\tau^\pm$  leptons, that can be produced by the charged current interactions of  $\nu_\tau$  and  $\bar{\nu}_\tau$  in the case of  $\nu_\mu \leftrightarrow \nu_\tau$  oscillations, but are absent in the case of  $\nu_\mu \leftrightarrow \nu_{\text{sterile}}$ . However the expected rate of production of  $\tau^\pm$  is expected to be small because only high energy neutrinos above threshold can contribute, and the identification of these events is experimentally very difficult.
- (ii)  $\nu_\tau$  and  $\bar{\nu}_\tau$  can interact with neutral current interactions, while a sterile neutrino is by definition non interacting; therefore in the hypothesis of  $\nu_\mu \rightarrow \nu_{\text{sterile}}$  oscillations, one should also observe a suppression of the rate of neutral current interactions.
- (iii) Another method to distinguish  $\nu_\mu \leftrightarrow \nu_\tau$  and  $\nu_\mu \leftrightarrow \nu_{\text{sterile}}$  oscillations is the fact that in this second hypothesis the oscillation probability is modified by matter effects. As discussed before matter effects are absent in the case of  $\nu_\mu \leftrightarrow \nu_\tau$  oscillations since the effective potentials for  $\nu_\mu$  and  $\nu_\tau$  are equal:

$$V(\nu_\mu) = V(\nu_\tau) = \sqrt{2} G_F \left[ \frac{N_p}{2} - \frac{N_e}{2} - \frac{N_n}{2} \right] = -\sqrt{2} G_F \frac{N_n}{2}, \quad (143)$$

where  $N_p$ ,  $N_e$  and  $N_n$  are the densities of protons, electrons and neutrons, and we have used the condition of electric neutrality ( $N_e = N_p$ ). On the other hand, the absence of interactions results in  $V(\nu_{\text{sterile}}) = 0$ , with a potential difference:

$$V_{\mu s} = -\sqrt{2} G_F \frac{N_n}{2} \simeq -10^{-13} \text{ eV} \left( \frac{\rho}{5 \text{ g cm}^{-3}} \right). \quad (144)$$

Note that the potential difference  $V_{\mu s}$  differs by a factor of 2 and by a sign from the potential difference  $V_{e\mu} = V_{e\tau}$ .

The potential difference becomes significant when it is comparable or larger than the energy difference between different neutrinos eigenmass states:

$$|V_{\mu s}| \geq |E_2 - E_1| \simeq \frac{|\Delta m^2|}{2E_\nu}, \quad (145)$$

that is for a neutrino energy larger than:  $E_\nu \geq |\Delta m^2|/(2|V_{\mu s}|) \sim 60 \text{ GeV}$ , where we have used  $|\Delta m^2| = 3 \times 10^{-3} \text{ eV}^2$  and a density  $\sim 5 \text{ g cm}^{-3}$  for the numerical estimate. It follows that the matter effects are a negligible effect for the sub-GeV and multi-GeV events and become important (and then dominant) only at higher energy. In this case the most important consequence of the matter effects is a suppression of the oscillation probability at large energy. This suppression can be understood from the expression for

the effective mixing parameter in matter  $\sin^2 2\theta_m$ , that for maximal mixing in vacuum is:

$$\sin^2 2\theta_m = \frac{1}{1 + (2V_{\mu s} E_\nu / \Delta m^2)^2}, \quad (146)$$

that is suppressed  $\propto E_\nu^{-2}$  at large neutrino energies.

Super-Kamiokande has analysed its data to test if the  $\nu_\mu \leftrightarrow \nu_{\text{sterile}}$  oscillation hypothesis can provide a valid answer. In order to test this hypothesis the collaboration has analysed three samples of data:

- (i) A neutral current (NC) enriched sample constructed as a set of contained events where the highest energy particle (ring) is  $e$ -like. This sample of events contains only a small contamination of  $\nu_\mu (\bar{\nu}_\mu)$  CC interactions, and is composed by a combination of  $\nu_e (\bar{\nu}_e)$  CC interactions and NC (neutral current) interactions.
- (ii) A sample of large energy,  $\mu$ -like, contained events selected with large visible energy:  $E_{\text{vis}} > 5 \text{ GeV}$ .
- (iii) The through-going upward-going muon events.

The first type of events allows to study if neutral current interactions are suppressed (oscillations with  $\nu_{\text{sterile}}$ ) or not (oscillations with  $\nu_\mu$ ). In the first case one should observe an up-down asymmetry of the events due to the disappearance of up-going neutral current interactions. The second and third classes of events select high energy neutrinos. The oscillation of these high energy neutrinos is suppressed in the  $\nu_\mu \leftrightarrow \nu_{\text{sterile}}$  case, because of the existence of matter effects. The data (see Fig. 20) shows no evidence for an up-down asymmetry of the neutral current events, and no evidence for a suppression of the mixing parameter  $\sin^2 2\theta$  with energy, and this has allowed the SK collaboration [53] to eliminate the  $\nu_\mu \leftrightarrow \nu_{\text{sterile}}$  hypothesis at more than 3 sigmas. This results is confirmed by the analysis of throughgoing muons of the MACRO collaboration [59].

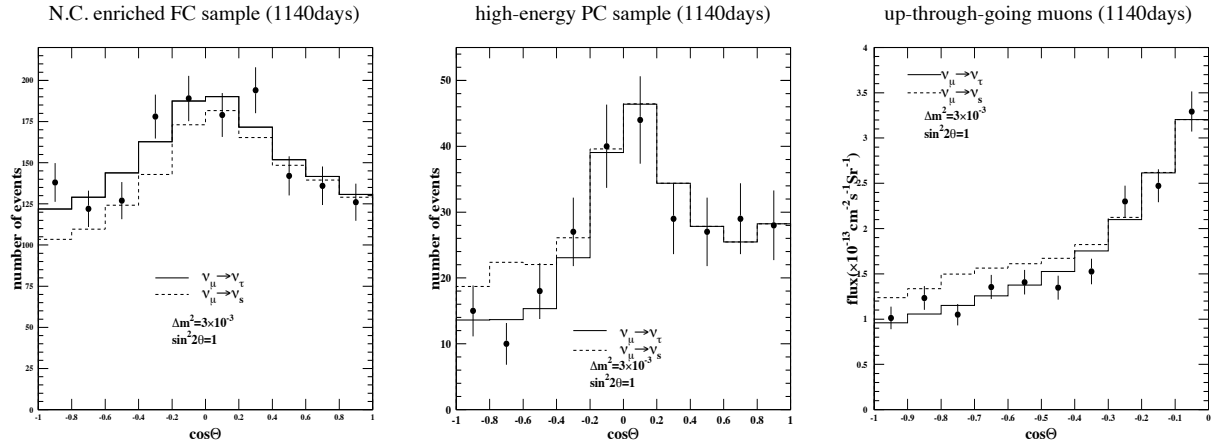


Fig. 20: Zenith angle distributions of left: NC enriched sample, center: high-energy PC sample, right: up-through-going muon sample (from [53]).

It is natural to consider a more general situation where muon (anti-)neutrinos oscillate into a linear combination of type  $\cos \xi \nu_\mu + \sin \xi \nu_{\text{sterile}}$ . A preliminary analysis of SK results in a 90% C.L. upper limit  $\sin^2 \xi \leq 0.25$  (see then bottom panel of Fig. 21).

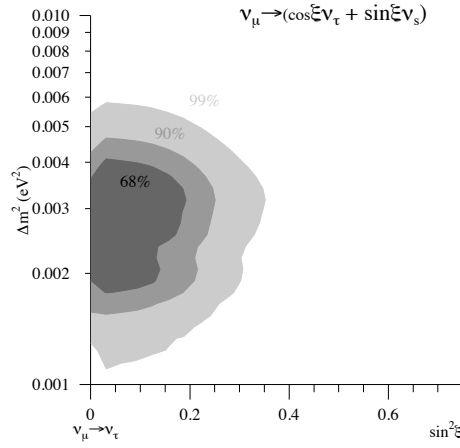


Fig. 21: Limit on the Sterile Content of Atmospheric Neutrino Oscillations. The limit on the sterile content is  $\sin^2 \xi < 0.25$  at 90% C.L.

### 7.8. Alternative explanations

Several alternative mechanisms have been proposed as explanations of the atmospheric neutrino data, based for example on the possibility of neutrino decay [62], violations of the equivalence principle [63,64], the existence of Flavor Changing Neutral Currents (FCNC) [65], or the effect of large extra dimensions [66–68]. Most of these models are excluded by the data (for reviews see [60,61]). The reason for this is that atmospheric neutrino data probe three decades in pathlength  $L$  and four decades in energy  $E$ . Such a wide dynamical range severely constrains deviations from the standard  $L/E$  behavior of the  $P_{\mu\tau}$  transition probability. Therefore,  $P_{\mu\tau}$  seems to be (dominantly) a function of  $L/E$ . Models that still give a reasonable fit are those that have a probability that is a function of  $L/E$  but with a non-oscillatory behaviour, such as in neutrino decay ([62]), or in the decoherence scenario of [69]. In these models the survival probability (after averaging) has the same “asymptotic” form for large  $L/E$ , but a monotonic behaviour. The large energy-angle smearing of SK prevents a clear discrimination (see Fig. 22).

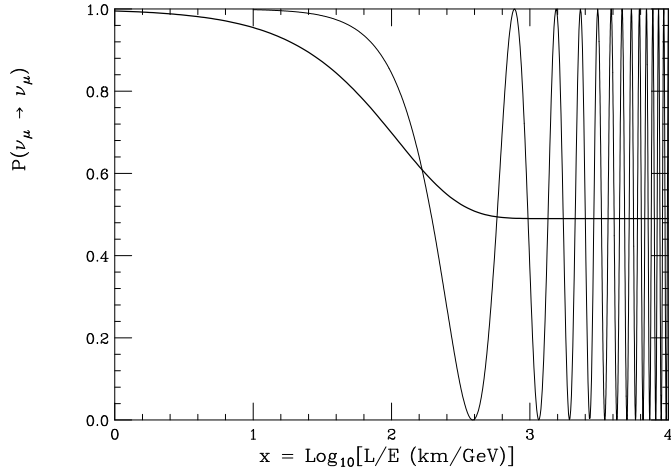


Fig. 22: Survival probability  $P_{\nu_\mu \rightarrow \nu_\mu}$  capable of explaining the atmospheric neutrino data. The oscillating curve is the result of a standard oscillation scenario (with best fit parameters). The solid curve can be obtained in a neutrino decay scenario [62].

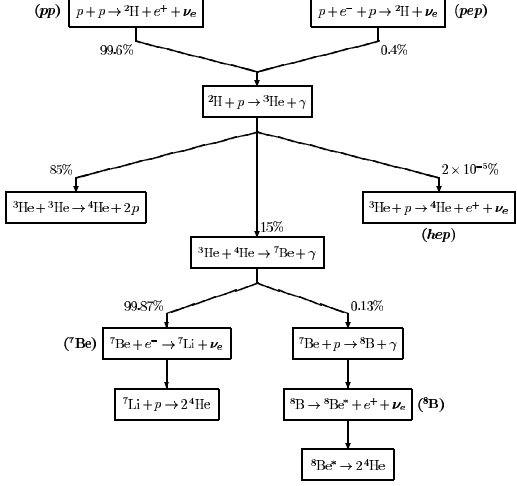


Fig. 23: The  $pp$  fusion cycles for the burning of hydrogen in the sun (and other main sequence stars). For each branch is indicated the probability calculated in the standard solar model. In parenthesis are indicated the different sources of neutrinos ( $pp$ ,  $pep$ ,  $^7\text{Be}$ ,  $^8\text{B}$  and  $hep$ ).

## 8. SOLAR NEUTRINOS

### 8.1. The Solar neutrino fluxes

The energy of the sun is produced in nuclear fusion reactions (for reviews see [70,71]). The process that generates the energy is the combination of 4 protons and 2 electrons to produce a helium-4 nucleus and two neutrinos:

$$4p + 2e^- \rightarrow {}^4\text{He} + 2\nu_e. \quad (147)$$

Each one of these reactions releases a total energy energy  $Q$ :

$$Q = 4m_p^2 + 2m_e^2 - m_{He} = 26.73 \text{ MeV}, \quad (148)$$

this energy is shared as kinetic energy among all final state particles. The neutrinos produced in the reaction escape from the sun, carrying away a fraction of the released energy, while the kinetic energy of the other particles is the source of the thermal energy of the sun. The flux of solar neutrinos is then given by the equation:

$$\Phi_{\nu_e} \simeq \frac{1}{4\pi d_\odot^2} \frac{2L_\odot}{(Q - \langle E_\nu \rangle)}, \quad (149)$$

where  $L_\odot = 3.842 \times 10^{33}$  erg/s is the solar luminosity,  $d \simeq 1.495 \times 10^{13}$  cm is the sun–earth distance, and  $\langle E_\nu \rangle \simeq 0.3$  MeV is the average energy carried away by neutrinos in a fusion cycle. Equation (149) predicts that there is an enormous flux ( $\phi_{\nu_\odot} \sim 6 \times 10^{10} (\text{cm}^2 \text{s})^{-1}$ ) of solar neutrinos that reaches the Earth. The fusion reaction (147) can happen with different sets (or “cycles” of reactions) that produce the same final particles, but that result in different energy distributions for the neutrinos, therefore for a detailed prediction of the neutrino fluxes one needs to build a model of the sun and compute the contributions of the different cycles.

Main sequence stars burn their hydrogen into helium with three  $pp$  cycles (see Fig. 23) and/or with a CNO bi-cycle. The  $pp$  cycles are the dominant mechanism for energy production in cooler (lower mass) stars while the CNO bi-cycle mechanism is dominant for hotter (larger mass) stars. In the sun  $\sim 98.5\%$  of the energy is produced with the  $pp$  cycles and only  $1.5\%$  with the CNO bi-cycle (that to a good approximation can be neglected).

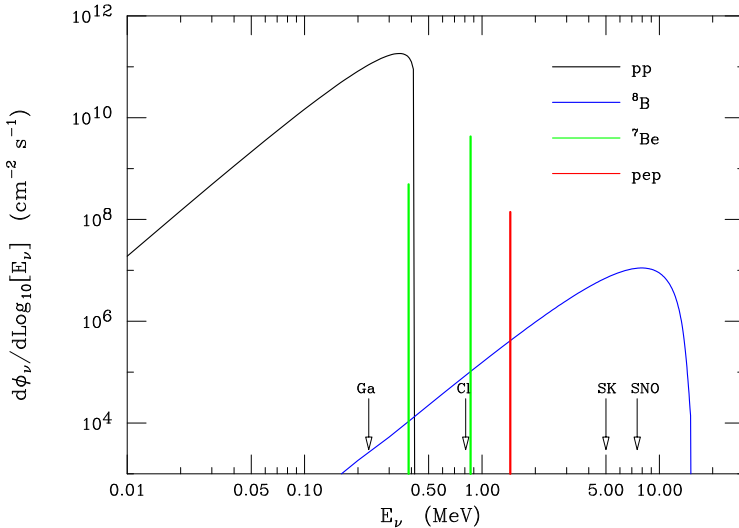


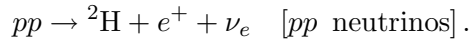
Fig. 24: Energy spectrum of solar neutrinos for the 4 most important sources: *pp*,  $^8\text{B}$ ,  $^7\text{Be}$  and *pep*. calculated according to the standard solar model of [72]. The arrows indicate the energy threshold of the 4 experiments that have reported measurements of solar neutrinos. The Gallium experiments have the lowest threshold and are sensitive to all sources, including the most abundant *pp* neutrinos. The (heavy) water cherenkov detectors Super-Kamiokande and SNO are sensitive only to the highest energy  $^8\text{B}$  neutrinos.

In order to compute the relative importance of the different fusion cycles, and to obtain a precise prediction for the fluxes of neutrinos emitted by the sun, it is necessary to compute in detail the structure of the sun, that is the profiles of its density, temperature and composition, and the rates for the different nuclear reactions (that also depend on the position inside the sun). This is the task of the “Standard Solar Model” [72,74] that uses well known physics and some approximations, notably spherical symmetry and the absence of rotation, to compute the structure of the sun and predict the neutrino fluxes. The initial condition of the problem is a total mass of material and an initial composition that is estimated as equal to the present composition at the surface (the fraction of helium is not measured and is a free parameter). The solar mass form an hydrodynamical equilibrium configuration, the compression of the core generates heat, that allow the beginning of nuclear fusion reactions that release additional energy. The composition of the core evolves with time according to the rates of the nuclear reactions, and the structure slowly evolves according to these changes. The observed solar radius and energy output are constraints in the calculation.

### 8.1.1. The *pp* cycles

The main components of the solar neutrino flux are shown in Fig. 24, and are also tabulated in Table 1. The different components are the result of different cycles of nuclear burning that all result in the same effect of combining 4 protons and two electrons to produce a helium-4 and two neutrinos, but produce neutrino with different energy distributions.

A brief description of the *pp* cycles can be summarized as follows. The first step in the *pp* cycles is the formation of deuterium ( $^2\text{H}$ ). This happen most of the time with the weak interaction two-body reaction:



This reaction is the source of the so called *pp* neutrinos. In the dense environment of the solar core also the three body reaction

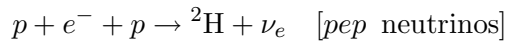
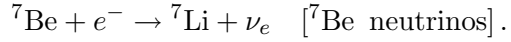


Table 1: Predictions of the solar neutrino fluxes.

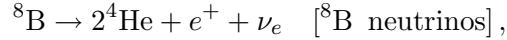
Source	Reaction	$\langle E_\nu \rangle_\odot$ (MeV)	Flux (cm <sup>2</sup> sec) <sup>-1</sup>	Cl (SNU)	Ga (SNU)
pp	$p + p \rightarrow {}^2\text{H} + e^+ + \nu_e$	0.2668	$5.95 \cdot 10^{10}$	0.0	69.7
pep	$p + e^- + p \rightarrow {}^2\text{H} + \nu_e$	1.445	$1.40 \cdot 10^8$	0.22	2.8
hep	${}^3\text{He} + p \rightarrow {}^4\text{He} + e^+ + \nu_e$	9.628	$9.30 \cdot 10^3$	0.04	0.1
<sup>7</sup> Be	${}^7\text{Be} + e^- \rightarrow {}^7\text{Li} + \nu_e$	0.814	$4.77 \cdot 10^9$	1.15	34.2
<sup>8</sup> B	${}^8\text{B} \rightarrow {}^8\text{Be} + e^+ + \nu_e$	6.735	$5.05 \cdot 10^6$	5.76	12.1
<sup>13</sup> N	${}^{13}\text{N} \rightarrow {}^{13}\text{C} + e^+ + \nu_e$	0.706	$5.48 \cdot 10^8$	0.09	3.4
<sup>15</sup> O	${}^{15}\text{O} \rightarrow {}^{15}\text{N} + e^+ + \nu_e$	0.996	$4.80 \cdot 10^8$	0.33	5.5
<sup>17</sup> F	${}^{17}\text{F} \rightarrow {}^{17}\text{O} + e^+ + \nu_e$	0.999	$5.63 \cdot 10^6$	0.0	0.1
Total				$7.6_{-1.1}^{+1.3}$	$128_{-6.0}^{+6.5}$

can happen and results in an approximately monochromatic neutrino line (*pep* neutrinos with  $E_\nu = 1.41$  MeV). The deuterium generated in these reactions rapidly absorbs one proton with the reaction  $d + p \rightarrow {}^3\text{He} + \gamma$ , producing Helium-3. The  ${}^3\text{He}$  is consumed in interactions with another  ${}^3\text{He}$  or with a  ${}^4\text{He}$  nucleus. In the first case (the 3–3 branch) the reaction is:  ${}^3\text{He} + {}^3\text{He} \rightarrow {}^4\text{He} + \gamma$  that completes the cycle (*pp*–I chain) with the formation of helium-4. In the other (3–4) branch one has the reaction  ${}^3\text{He} + {}^4\text{He} \rightarrow {}^7\text{Be} + \gamma$  producing beryllium-7. The two possible fates of the beryllium nuclei determine an additional branching. The most likely event is an electron capture reaction:



The lithium nucleus is formed in the ground state or in an excited one, and therefore the  ${}^7\text{Be}$  neutrinos form two lines with 0.8631 MeV (89.7%) and 0.3855 MeV (10.3%). The Lithium then absorbs a proton to produce two  ${}^4\text{He}$  nuclei completing the (*pp*–II) cycle.

The second branch for the Beryllium nuclei is the absorption of a proton to produce  ${}^8\text{Boron}$ , that undergoes a beta decay into two  ${}^4\text{He}$  nuclei:



completing the (*pp*–III) cycle. The  ${}^8\text{B}$  neutrinos extend up to the highest energy of 14 MeV, and even if they are only a fraction  $10^{-4}$  of the flux, play a very important role in the detection of the solar neutrinos. It is important to understand that the kinetic energy of the interacting particles is of order  $E_{\text{kin}} \sim T_{\text{center}} \simeq 1.5 \times 10^7$  Kelvin  $\simeq 1.5$  KeV is small with respect to the energy released in the reaction, therefore the shape of the neutrino spectra emitted in each reaction is determined uniquely by particle physics, with no dependence from the modeling of the sun that has simply the role of determining the relative importance of the different branches.

## 8.2. Detection of Solar Neutrinos

Measurements of the solar neutrino fluxes have been reported from several experiments using four different methods of detection. They all have reported measurements smaller than the prediction.

### The Chlorine experiment

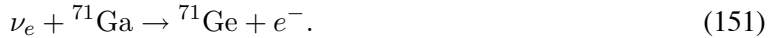
In the “Chlorine experiment” one exposes  $^{37}\text{Cl}$  to solar neutrinos, and detect the argon-37 (a radioactive unstable nucleus) produced in the reaction



This reaction has a threshold energy of 0.814 MeV. An experiment based on this technique, has been constructed by Raymond Davis and his collaborators in the Homestake mine in South Dakota (US), and has been taking data from 1969 to 1993. This detector first reported a deficit in the neutrino flux [75].

### The Gallium experiment

A lower energy threshold ( $E = 0.214$  MeV) can be obtained using a Gallium target, and the reaction



The Chlorine and Gallium experiments are known as *Radio-chemical methods*, they both are sensitive only to electron neutrinos, in fact since an  $e^-$  is present in the final state  $\nu_\mu, \nu_\tau$  and anti-neutrinos cannot induce the nuclear transitions (150) and (151). Two detectors based on the gallium technique have been taking data: GALLEX [76] in the Gran Sasso underground laboratory and SAGE [77] in Russia.

The quantity that is measurable in the radiochemical experiments such as the Chlorine and Gallium experiments is a capture rate, that is the probability per unit time that a target nucleus exposed to the solar neutrinos “captures” a solar neutrino with a reaction of the type (150) or (151). The capture rate can be calculated as:

$$C_j = \int dE \phi_{\nu_\odot}(E) \sigma_j(E) , \quad (152)$$

where  $\phi_{\nu_\odot}(E)$  is the flux of solar neutrinos with energy  $E$  and  $\sigma_j(E)$  is the cross section (the subscript  $j$  indicates the reaction considered). The capture rate is measured in units of  $\text{sec}^{-1}$ . It has become customary to use the unit:

$$1 \text{ SNU} \equiv 1 \text{ Solar Neutrino Unit} = 10^{-36} \text{ sec}^{-1} . \quad (153)$$

In Table 1 we show the estimates for the capture rates in chlorine and gallium, and the contributions of the different components of solar neutrinos. Note that the Chlorine experiment is mostly sensitive to the intensity of the boron and beryllium neutrinos, while the most abundant  $pp$  neutrinos are below threshold, while more than half the rate for Gallium experiments is predicted to be generated by  $pp$  neutrinos.

### Electron Scattering

Solar neutrinos are also detectable observing the Elastic Scattering on electrons:



This reaction does not have a threshold, however it is detectable above the natural radioactivity background only when the final state electron has a sufficiently high energy. Threshold as low as  $E > 5$  MeV, have been obtained. This method can only reveal the highest energy ( $^8\text{B}$ ) solar neutrinos. The electron scattering method is sensitive to all neutrino types, however the cross section for  $\nu_e$  is approximately 7 larger than for  $\nu_\mu$  and  $\nu_\tau$ . The final state electron in the reaction (154) is emitted in a direction strongly correlated with the neutrino one. This technique has been first used by the Kamiokande [79] detector in Japan, and then by the larger size Super-Kamiokande [83] detector. The cross section for neutrino

electron-scattering is given by the expression:

$$\frac{d\sigma_{\nu_e e}}{dT} = \frac{2G_F^2 m_e^2}{\pi} \left[ g_L^2 + g_R^2 \left( 1 - \frac{T}{E_\nu} \right)^2 - g_L g_R \frac{m_e c^2 T}{E_\nu^2} \right], \quad (155)$$

where  $T$  is the kinetic energy of the final state electron and the constants  $g_L^2$  and  $g_R^2$  have values:

$$g_L^2 = \begin{cases} \left(\frac{1}{2} + \sin^2 \theta_W\right)^2 & \simeq 0.536 , \quad \nu_e \\ \sin^4 \theta_W & \simeq 0.0538 , \quad \bar{\nu}_e \\ \left(-\frac{1}{2} + \sin^2 \theta_W\right)^2 & \simeq 0.0719 , \quad \nu_i \\ \sin^4 \theta_W & \simeq 0.0538 , \quad \bar{\nu}_i \end{cases}$$

$$g_R^2 = \begin{cases} \sin^4 \theta_W & \simeq 0.0538 , \quad \nu_e \\ \left(\frac{1}{2} + \sin^2 \theta_W\right)^2 & \simeq 0.536 , \quad \bar{\nu}_e \\ \sin^4 \theta_W & \simeq 0.0538 , \quad \nu_i \\ \left(-\frac{1}{2} + \sin^2 \theta_W\right)^2 & \simeq 0.0719 , \quad \bar{\nu}_i \end{cases}$$

For electron neutrinos the cross section is approximately  $\sigma(\nu_e e) \simeq 1.0 \times 10^{-44} E_{\text{MeV}} \text{ cm}^2$  while for  $\nu_\mu$  and  $\nu_\tau$  the cross section is  $\sigma(\nu_{\mu,\tau}) \simeq 0.15 \times 10^{-44} E_{\text{MeV}} \text{ cm}^2$  is approximately 7 times smaller.

### Heavy Water

Two other methods to measure solar neutrinos make use of a deuterium target. The Sudbury Neutrino Observatory (SNO) detector in Canada [85] contains 1 Kton of heavy water. One could expect that the reaction  $\nu_e + n \rightarrow e^- + p$  plays an important role in the detection of solar neutrinos, however free neutrons do not exist in nature, therefore this reaction can only be observed with bound neutrons in nuclei, and for nearly all nuclei the threshold for the reaction  $\nu_e + (A, Z) \rightarrow e^- + (A, Z + 1)$  is too high for solar neutrinos. The deuterium nucleus with its small binding energy (2.2 MeV) is the closest approximation of free neutrons, and the reaction



has an energy threshold of only 1.44 MeV. The positron detected in the reaction can be observed. The reaction (156) is only sensitive to  $\nu_e$ .

Deuterium allows also to detect solar neutrinos with the neutral-current reaction:



where deuterium is broken up into its nucleon constituents. This reaction has a threshold of 2.2 MeV, and a cross section that is identical for all flavors; it can be detected observing the photons emitted in the capture of the final state neutron:  $n + (A, Z) \rightarrow (A + 1, Z) + \gamma$ .

### 8.3. Experimental Results

In Fig. 25 is shown the distribution of the angle  $\theta_{\text{sun}}$  (angle with respect to the sun direction) for all particles detected particles in Super-Kamiokande with an energy larger than 5 MeV. There is clear evidence for a contribution due to solar neutrinos above a flat background. With the electron scattering technique the sun is “seen” in neutrinos in the sense that a real image (even if rather blurry) can be constructed using neutrinos.

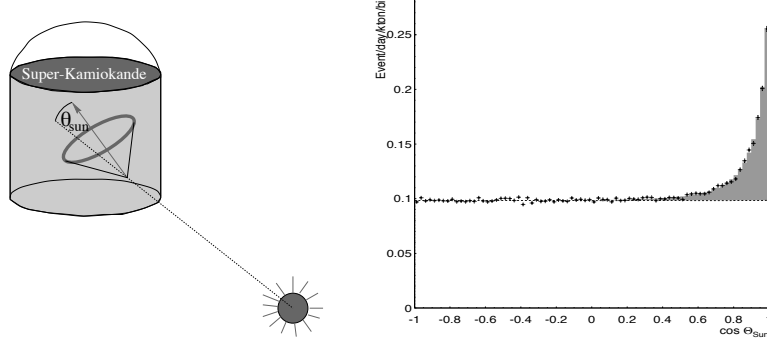


Fig. 25: Distribution of  $\cos \theta_{\text{sun}}$  of Super-Kamiokande events. The peak at  $\cos \theta_{\text{sun}} \simeq 1$  is the contribution of events generated by electron scattering:  $\nu + e^- \rightarrow \nu + e^-$ , superimposed on a flat background.

The energy and zenith angle distribution of the SK events are shown in Fig. 26. It should be noted that there are not statistically significant distortions with respect to a no-oscillation prediction. This sets important constraints on possible solutions in terms of  $\nu$  oscillations.

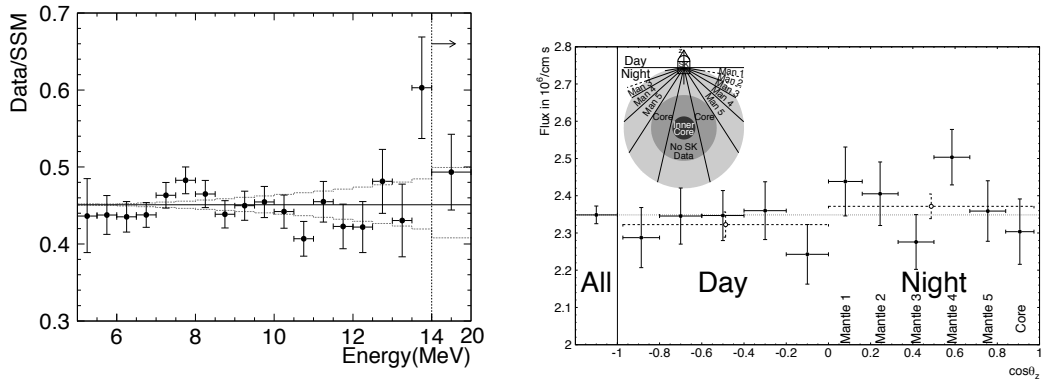


Fig. 26: The left panel shows the energy spectrum of the events measured by Super-Kamiokande in the solar neutrino signal plotted as the ratio to the Standard Solar Model calculation of [72]. The horizontal solid line is the ratio for the total flux, the dotted band around this line is the systematic uncertainty due to the energy scale. There is no evidence for a spectral distortion. A flat ratio gives a  $\chi^2/\text{d.o.f.} = 19.0/18$ . The right panel shows the zenith angle distribution of the Super-Kamiokande events in the solar neutrino signal. Neutrinos detected during the night have traveled inside the Earth. From [83].

The Sudbury Neutrino Observatory (SNO) in Canada uses as sensitive material one kiloton of heavy water ( $\text{D}_2\text{O}$ ) contained in a transparent acrylic shell of 12 meter diameter. The Cherenkov photons emitted by charged particles are detected by a system of 9546 PMT's mounted on a geodesic structure of 17.8 meters of diameter. The geodesic structure is also immersed in ultra-pure water to provide shielding. The right panel of Fig. 27 shows results obtained with the SNO detector. The top panel shows the distribution in  $\cos \theta_{\odot}$  of all events with energy larger than 5 MeV. For a heavy water detector one has three different contributions:

- Events due to electron scattering ( $\nu_e + e^- \rightarrow \nu_e + e^-$ ) that have an angular distribution peaked at small  $\theta_{\odot}$ .
- Events due to the charged current scattering process  $\nu_e + d \rightarrow e^- + p + p$ . In this process the electron is produced with an energy  $E_e \simeq E_{\nu} - 1.44 \text{ MeV}$  and an approximately flat angular distribution with a small negative slope in  $\cos \theta_{\text{sun}}$ , so that the most likely scattering is backward.
- Finally the 6.5 MeV photons produced in the neutron capture process  $n + d \rightarrow T + \gamma$  give an isotropic (flat in  $\cos \theta_{\odot}$ ) distribution. Most neutrons are produced by the neutral current reaction  $\nu_x + d \rightarrow \nu_x + p + n$

One can see that because of the different angular, and energy (see the bottom panel in Fig. 27) it is possible to disentangle the three contributions.

The central panel in Fig. 27 shows that in the inner fiducial volume the event rate is uniform, as expected for neutrino interactions (while background events induced by radioactivity is concentrated near the outer region).

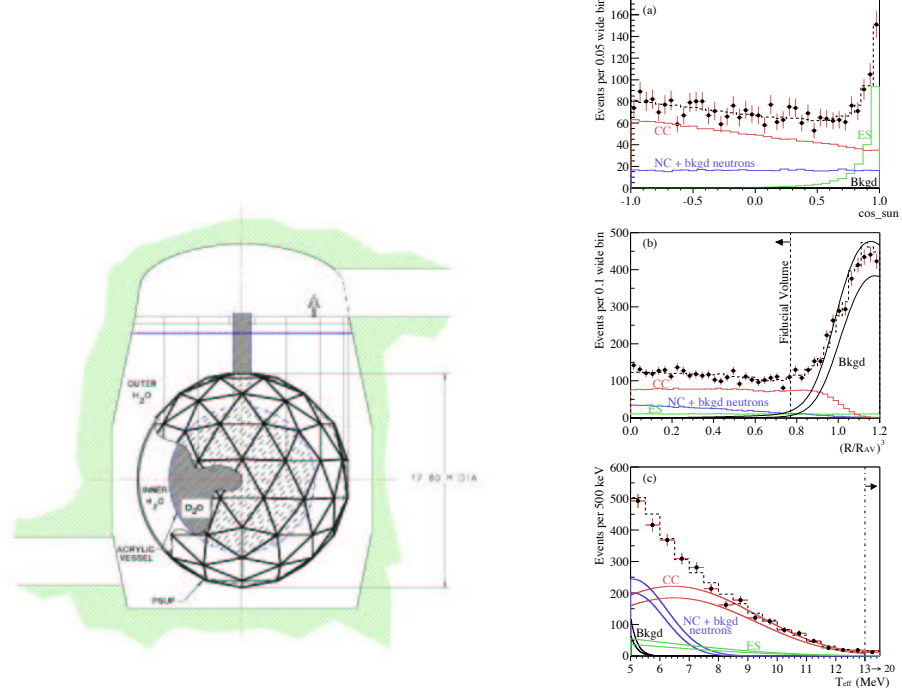


Fig. 27: Left panel: the SNO detector. The inner vessel contains 1 Kton of ultra-pure heavy water. Right panels: (a) Distribution of  $\cos \theta_\odot$  of the detected events in the inner fiducial volume ( $R < 0.55$  m). (b) Distribution of the volume weighted variable. (c) Kinetic energy distribution of the events in the inner fiducial volume. Also shown are the Monte Carlo prediction for the three classes of events: CC ( $\nu_e + d \rightarrow e^+ + p + n$ ), Electron Scattering (ES:  $\nu_x + e^- \rightarrow \nu_x + e^-$ ), and Neutral currents ( $\nu_x + d \rightarrow p + n$ ). The shapes of the curves is fixed, but the relative normalization is fitted to the data. The bad indicated  $\pm 1\sigma$  uncertainties. The dashed lines are the sum of all contributions. All distributions are for a detected kinetic energy larger than 5 MeV. From [86].

In Table 2 we show the results of the different measurements of solar neutrinos and compare with the predictions based on the solar model of Bahcall et al [72]. The last column in the Table shows the ratio of the measured rate with the theoretical prediction based on the no-oscillation hypothesis. All experiments detect a significant deficit.

The top part of Table 2 gives the results for the radiochemical experiments: the chlorine one [75], and the two Gallium experiments GALLEX [76,78] and SAGE [77]. For this part of the Table the unit used for both data and prediction is SNU (or  $10^{-36}$  neutrino captures per nucleus and per second). The bottom part of the Table gives results of the measurement of the highest energy part of the solar neutrino flux, where only neutrinos from Boron-8 decay contribute, and the unit used for both measurement and prediction is a flux: [ $10^6 (\text{cm}^2 \text{s})^{-1}$ ]. This mean that the results are given in term of an *undistorted* flux of neutrinos with only the absolute normalization free. The flux of <sup>8</sup>B neutrinos has been measured with three different techniques: (i) electron elastic scattering (ES), (ii) CC  $\nu_e$ -deuterium scattering ( $\nu_e + d \rightarrow e^- pp$ ), and (iii) the observations of the capture of neutrons produced in the NC reactions  $\nu_x + d \rightarrow \nu_x + p + n$ . The electron scattering experiment has been performed by three experiments

Table 2: Measurements of solar neutrinos and comparison with no-oscillations predictions.

Experiment	Prediction	Data	Data/Prediction
Chlorine	$7.6^{+1.3}_{-1.1}$	$2.56 \pm 0.23$	$0.34 \pm 0.06$
GALLEX + GNO	$128^{+9}_{-7}$	$74.1^{+6.7}_{-7.8}$	$0.58 \pm 0.07$
SAGE	$128^{+9}_{-7}$	$75.4^{+7.8}_{-7.4}$	$0.59 \pm 0.07$
$^8\text{B}$ -ES [Kamiokande]	$5.05^{+1.0}_{-0.8}$	$2.80 \pm 0.40$	$0.55 \pm 0.13$
$^8\text{B}$ -ES [SuperKamiokande]	$5.05^{+1.0}_{-0.8}$	$2.40^{+0.09}_{-0.07}$	$0.48 \pm 0.09$
$^8\text{B}$ -ES [SNO]	$5.05^{+1.0}_{-0.8}$	$2.39 \pm 0.24$	$0.47 \pm 0.12$
$^8\text{B}$ -CC [SNO]	$5.05^{+1.0}_{-0.8}$	$1.76 \pm 0.06$	$0.35 \pm 0.08$
$^8\text{B}$ -NC [SNO]	$5.05^{+1.0}_{-0.8}$	$5.09 \pm 0.44$	$1.0 \pm 0.20$

(Kamiokande [82], Super-Kamiokande [83] and SNO [85] the measurements using deuterium have been performed by SNO alone.

Inspecting Table 2 and comparing the measurements to the predictions one can make several important points:

- [1] There is a statistical very significant deficit of neutrinos that is observed by all measurements, except for the measurement that involves neutral currents. This is evidence for the “disappearance” of  $\nu_e$
- [2] The deficit is not equal for different experiments that probe different energy regions of the spectrum. The Gallium experiments, that probes the lowest energy solar neutrinos, observes the smallest deficit, while the chlorine experiment observes the largest deficit. This is evidence for a non trivial energy dependence of the disappearance probability  $P(\nu_e \rightarrow \nu_x)$ .
- [3] The three measurements of the highest energy ( $^8\text{B}$ ) neutrinos with the electron-scattering technique are all in good agreement with each other, however the measurement of SNO using CC interactions on deuterium indicates a *larger deficit*. A careful statistical analysis [85] shows that the measurements of the ES and CC method differ by 3.3 standard deviations. This can be explained assuming that the “disappearing”  $\nu_e$  are transformed into  $\nu_\mu$  or  $\nu_\tau$  that can still contribute a suppressed but non zero contribution to the electron scattering event rate (see Fig. 28).
- [4] This interpretation is confirmed by the agreement of prediction and observations for the neutral current events.

The “real-time” experiments of Super-Kamiokande and SNO, also give a time distribution and an energy spectrum of the detected neutrino events. This allows also to perform more detailed studies, searching for effects such as:

- [1] A deformation of the energy spectrum of the neutrinos with respect to a prediction that depend *uniquely* on particle physics. No significant deformation has been observed (see Fig. 26).
- [2] A difference of the detected rate between day and night (or more in general on the orientation of the sun with respect to the detector, that is on the sun zenith angle). Neutrinos detected during the night have traversed the Earth, and it is possible that the presence of the Earth matter modifies the flavor transition probabilities.

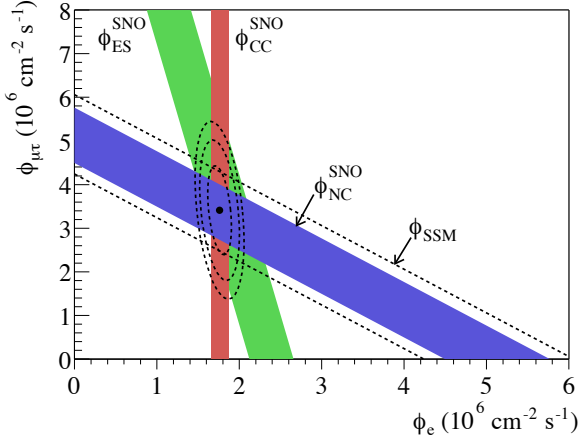


Fig. 28: Flux of  ${}^8\text{B}$  solar neutrinos which have  $\mu$  or  $\tau$  flavor versus the flux of  $\nu_e$  deduced by the three measurements of SNO. The diagonal bands show the total  ${}^8\text{B}$  flux as predicted in the SSM (dashed lines) and as measured with the NC reaction. All bands represent  $1\sigma$  uncertainties. All bands intersect, indicating that the combined flux results are consistent with neutrino flavor transformation assuming no distortion in the  ${}^8\text{B}$  neutrino energy spectrum. From [86].

- [3] A non trivial seasonal effect. In the minimal standard model, that is if neutrinos do not oscillate the solar neutrino flux does depend on the season because of the eccentricity of the Earth orbit around the sun, since the solar neutrino flux obviously is proportional to  $r_\odot^{-2}$  (where  $r_\odot$  is the sun–Earth distance). In the presence of oscillations, if the oscillation length is comparable to the average sun–Earth distance one can have more complex seasonal variations. The experimental data do not exhibit deviations from the simple  $r_\odot^{-2}$  scaling law.

#### 8.4. Interpretation

In the presence of neutrino flavor transitions the event rates for the solar neutrino detectors are suppressed because the electron neutrino flux at the Earth becomes

$$\phi_{\nu_{e,\odot}}(E) = \phi_{\nu_\odot}^{\text{SSM}}(E) \times P_{\nu_e \rightarrow \nu_e}(E), \quad (158)$$

where  $\phi_{\nu_\odot}^{\text{SSM}}(E)$  is the Standard Solar Model (SSM) prediction. In the case of electron scattering, the effective flux that can generate the scattering is a linear combination (with different weights) of the  $\nu_e$  and  $\nu_{\mu,\tau}$  fluxes that reach the earth. Therefore one has to make the substitution:

$$\phi_{\nu_\odot}^{\text{SSM}}(E) \rightarrow \phi_{\nu_\odot}^{\text{SSM}}(E) \times \left\{ P_{\nu_e \rightarrow \nu_e}(E) + [1 - P_{\nu_e \rightarrow \nu_e}(E)] \times \frac{\sigma_{\nu_{\mu,\tau}}(E)}{\sigma_{\nu_e}(E)} \right\}. \quad (159)$$

Qualitatively it is clear that neutrino oscillations is a natural candidate for explaining the data. The question is now to verify if it is possible to find values of the oscillation parameters (squared mass differences and mixing angles) that give predictions that are in quantitative agreement with the experimental data. For simplicity we will consider the case of two flavor ( $\nu_e - \nu_\mu$  or  $\nu_\mu - \nu_\tau$ ) mixing. In this case the  $\nu_e$  survival probability, averaged over all creation points of the neutrinos, will be a function of the two parameters  $\theta$  and  $\Delta m^2$ , where  $\theta \in [0, \frac{\pi}{2}]$  is the 2-flavor mixing angle, and  $\Delta m^2$  the squared mass difference. This description of the oscillation of solar  $\nu_e$  in terms of simple two-flavor mixing is actually a very good approximation of the most general case in the light of the results of atmospheric and reactor neutrinos. These results indicates that  $\nu_e$ 's do not participate in the “fast” oscillations related to the squared mass difference  $\Delta m_{\text{atm}}^2$ . This can be interpreted a rather stringent upper limit on the size of  $\theta_{13}$ . It is easy to demonstrate that in the limit of  $\theta_{13} \rightarrow 0$  the oscillation probability  $P_{\nu_e \rightarrow \nu_e}$  is *identical* to what is calculated with two-flavor mixing with the substitutions  $\Delta m^2 \rightarrow \Delta m_{12}^2$  and  $\theta \rightarrow \theta_{12}$ .

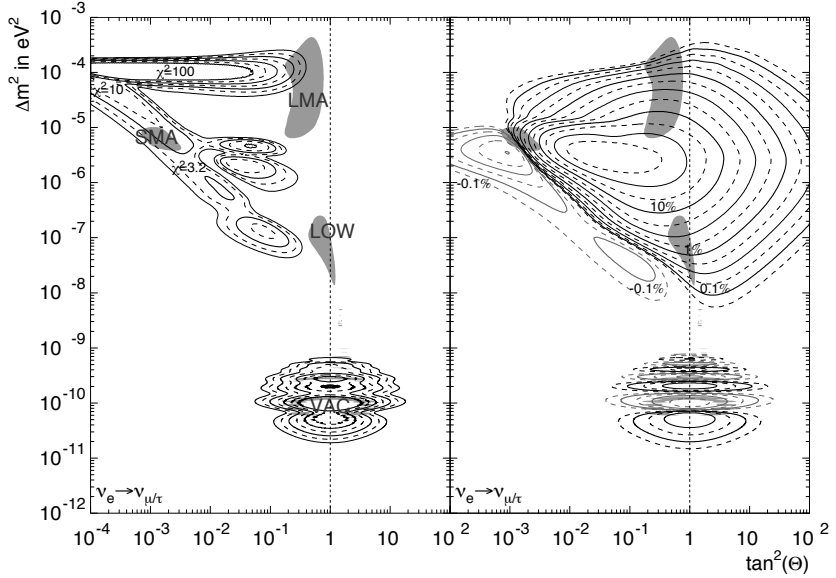


Fig. 29: Oscillation Predictions of SK Spectral Distortion (Left) and Day/Night Asymmetry (Right). The spectral distortion is depicted in contours of equal  $\chi^2$ . The shown values of both the  $\chi^2$  and the day/night asymmetry contours increase logarithmically. Superimposed in gray are the usual solution areas. From [84]

A detailed study of the parameter space (that is the plane  $(\tan^2 \theta_{12}, \Delta m_{12}^2)$ )<sup>13</sup>) reveals that there are values of the parameters that allow to reproduce the total rates measured by the different experiments. These disconnected regions are shown in Fig. 29 as dark-shaded (red) regions. The 4 disconnected parts are commonly named:

(a) **LMA**

The Large Mixing Angle solution corresponds to the region with small mixing angle  $\tan^2 \theta \simeq 10^{-3}$  and  $\Delta m^2 \in [0.9, 10] \times 10^{-5} \text{ eV}^2$ .

(b) **SMA**

The Small Mixing Angle solution corresponds to the region with large mixing angle  $\tan^2 \theta \in [0.2, 0.5]$  and  $\Delta m^2 \in [0.4, 1] \times 10^{-5} \text{ eV}^2$ .

(c) **LOW**

The so called “Low” solution corresponds to a region again with large mixing angle  $\tan^2 \theta \simeq 0.5$  but with lower  $\Delta m^2$ :  $\Delta m^2 \in [0.8, 1] \times 10^{-7} \text{ eV}^2$ .

(d) **Vacuum**

The “vacuum solution” corresponds to a subset of disconnected region with  $\tan^2 \theta$  around one (that is  $\theta \sim 45^\circ$ , and  $\Delta m^2 \sim 10^{-10} \text{ eV}^2$ ).

A detailed analysis of the data of Super-Kamiokande and SNO (including the spectral shape and the day–night differences) disfavors some of these solutions, and the LMA solution emerges as the most likely solution. This is indicated in Fig. 29 and Fig. 30.

The complexity of the shape of the parameter space region that can explain the detected rates of the solar neutrino experiments, is due to some remarkable features of the flavor transition probabilities in matter with a varying density that are discussed in the following.

It is simple to see that because of the shape of the oscillation probability in matter for fixed neutrino

<sup>13</sup>Note that since the mixing angle  $\theta_{12}$  is defined in the interval  $\theta \in [0, \frac{\pi}{2}]$ ,  $\sin^2 2\theta$  is not a good variable because two physically different points ( $\theta$  and  $\pi - \theta$ ) are mapped into the same value. On the other hand  $\sin^2 \theta_{12}$  or  $\tan^2 \theta_{12}$  are good variables.

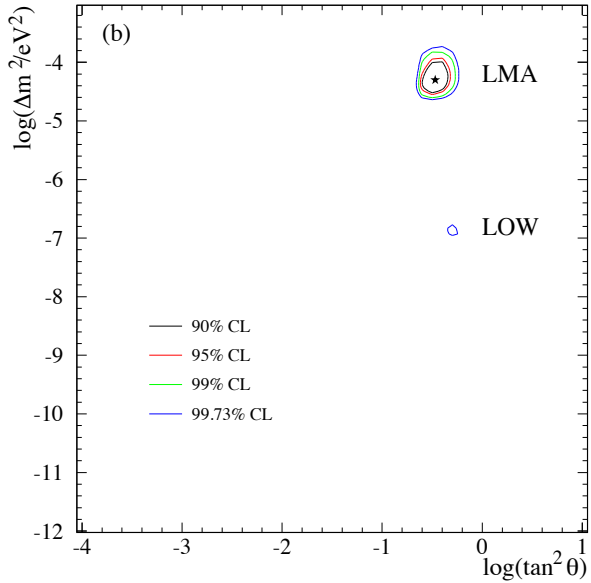


Fig. 30: Allowed regions in the parameter space  $\Delta m_{12}^2$ ,  $\tan^2 2\theta_{12}$  (assuming  $\theta_{13} \simeq 0$ ) including all measurements of solar neutrinos. The best fit point is:  $\Delta m_{12}^2 = 5 \times 10^{-5}$  eV<sup>2</sup>, and  $\tan^2 \theta_{12} = 0.32$ . From [87].

energy  $E_\nu$ , the set of points in the parameter space  $(\sin^2 2\theta, \Delta m^2)$  that give a desired survival probability  $\langle P_{\nu_e \rightarrow \nu_e} \rangle = P^*$  has the shape of a “triangle” (see Fig. 31).

The allowed region in parameter space has recently been very much reduced thanks to the data of SNO. The results are shown in Fig. 30 (from [87]). The top panel shows the allowed region obtained from the SNO data alone. The bottom panel gives the allowed region including all existing data. The best fit point is:

$$\begin{aligned} \Delta m_{12}^2 &= 5 \times 10^{-5} \text{ eV}^2, \\ \tan^2 \theta_{12} &= 0.32. \end{aligned} \quad (160)$$

## 9. REACTOR NEUTRINOS

Nuclear reactors are intense, isotropic sources of  $\bar{\nu}_e$  produced in their core as  $\beta$ -decay products of fission fragments (for a review and extensive references see [88]). In commercial nuclear reactors the energy is released in neutron induced fissions with a nuclear fuel constituted by uranium enriched (to 2–5 %) in the isotope  $^{235}\text{U}$ . The most important processes are of type



and result in the production of typically two neutrons (that can therefore sustain a chain reaction) and two fragments  $X_1$  and  $X_2$ . The fragments of the fission are too rich in neutrons (a  $^{235}\text{U}$  nucleus has 92 protons and 142 neutrons) and to reach stability must undergo a succession of beta decays (on average a total of six), therefore emitting an average of 6 electron anti-neutrinos. Considering that each decay releases 204 MeV, it is possible to obtain the number of anti-neutrinos emitted in a plant as:

$$\dot{N}_{\bar{\nu}_e} \simeq 6 \times \left( \frac{\text{Power}}{204 \text{ MeV}} \right) \simeq 8.9 \times 10^{20} \left( \frac{\text{Power}}{10 \text{ GigaWatt thermal}} \right) \bar{\nu}_e \text{ sec}^{-1}. \quad (162)$$

From a knowledge of nuclear physics it is possible to compute in detail the decay chains that are generated by the nuclear fissions, and estimate the flux and energy spectrum of the emitted  $\bar{\nu}_e$ . The  $\bar{\nu}_e$

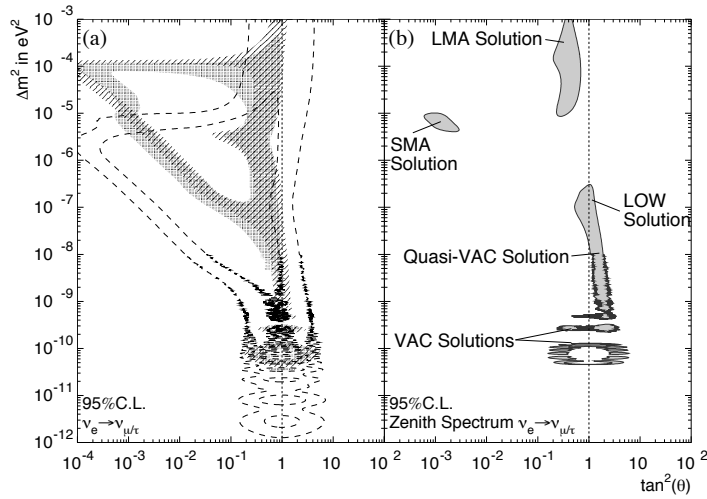


Fig. 31: Left panel: allowed areas from single solar neutrino experiments. The shaded area uses only Homestake data, while the hatched area uses only the SNO charged-current rate. Overlaid (inside dashed lines) is the region allowed by Gallex/GNO and SAGE. Right panel: allowed regions from a combined fit to these charged-current rates. All contours in this and other figures are 95% C.L.

energy is below 10 MeV, with an average value  $\sim 3$  MeV. The neutrinos above the detection threshold ( $E_{\bar{\nu}_e} > 1.8$  MeV) are produced only in the decay of short lived fission fragments and therefore the flux is very strongly correlated with the thermal power output of the nuclear reactor. For a detailed estimate one has to consider the composition of the fuel, since four types of nuclei can undergo fission  $^{235}\text{U}$ ,  $^{238}\text{U}$ ,  $^{239}\text{Pu}$ , and  $^{241}\text{Pu}$ . The chemical composition of the nuclear fuel slowly evolves with time, and this must be also be taken into account. Taking into account all uncertainties a nuclear reactor  $\bar{\nu}_e$  flux can be estimated with an uncertainty of  $\simeq 3\%$ .

The  $\bar{\nu}_e$  produced in the nuclear reactions can be detected with the reaction:

$$\bar{\nu}_e + p \rightarrow e^+ + n. \quad (163)$$

This reaction has a threshold of 1.8 MeV and gives rise to two detectable signals: a prompt one from  $e^+$  production and the annihilation into two photons; and a delayed photon signal from neutron capture (after neutron thermalization). The energy of the photon emitted in  $n$  capture is 2.2 MeV for the reaction  $np \rightarrow d\gamma$ ; it is often convenient to “dope” the scintillator with nuclei that have a large  $n$  capture cross section, and result in higher energy photons, for example from  $n$  capture by Gadolinium one obtains  $E_\gamma \simeq 8$  MeV.

### 9.1. Chooz and Palo Verde

Recent important measurements of reactor  $\bar{\nu}_e$  have been performed by two detectors: Chooz [89] (in France), and Palo Verde [90] (in the USA) with a baseline of approximately 1 Km. A scheme of the set-up of the Chooz detector is shown in Fig. 32. The source of neutrinos was composed of two nuclear reactors, each with the thermal power of 4.2 GWatt. During a significant fraction of the data taking only one of the reactors was in operation, and this allowed to study the backgrounds not-related to the neutrino flux that are independent from the reactor power while the signal is linear with the instantaneous power generated in the reactors cores.

The results of the Chooz experiments [89] are shown in Fig. 32 as the measured energy spectrum of the detected positrons, compared to a calculated prediction in the absence of neutrino oscillations. The energy spectrum extends from zero to 10 MeV with a maximum at approximately 3 MeV. The ratio

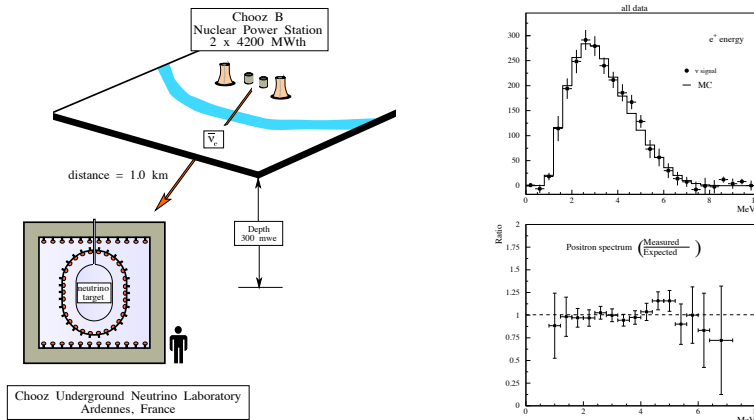


Fig. 32: Left: the Chooz detector for reactor neutrinos. Top right: background-subtracted positron energy spectrum in the Chooz data. Error bars represent statistical errors only. The solid histogram represents the expectation for the case of no oscillations. The ratio between the two curves is shown bottom right (from [89]).

between the measured spectrum and the theoretical prediction is:

$$R_{\text{Chooz}} = \frac{\text{DATA}}{\text{Prediction}} = 1.01 \pm 2.8\% \text{ (stat)} \pm 2.7\% \text{ (syst)}. \quad (164)$$

The systematic error is due to uncertainties in the prediction of the neutrino fluxes (in the absence of oscillations)<sup>14</sup>. The Palo Verde experiment [90] has obtained a similar results:

$$R_{\text{Palo Verde}} = 1.01 \pm 2.4\% \text{ (stat)} \pm 5.3\% \text{ (syst)}. \quad (165)$$

For both experiments the ratio Data/Prediction is consistent with unity. In the presence of oscillation the flux of  $\bar{\nu}_e$  at the detector would be suppressed by an energy dependent factor  $P_{\bar{\nu}_e \rightarrow \bar{\nu}_e}(E, L)$ , where  $L$  is the distance between the detector and the reactors nuclear core (the  $\bar{\nu}_\mu$  or  $\bar{\nu}_\tau$  generated by flavor transitions are below threshold to interact). The fact that no suppression of the flux is observed can be interpreted estimating an excluded region in the space of oscillation parameters. Qualitatively, it is clear that the result means that either the oscillation lengths for the transitions are longer than the distance  $L$  relevant for these experiments, or that the the oscillations can develop however their amplitude is sufficiently small that the effect remain unobservable. The simplest interpretation of the data is in terms of the “One mass scale dominance model”. This is equivalent to say that the smallest squared mass difference ( $\Delta m_{12}^2$ ) is too small to have any influence, that is:

$$\Delta m_{12}^2 \lesssim (\hbar c) \frac{1.8 \text{ MeV}}{1 \text{ Km}} \simeq 4 \times 10^{-4} \text{ eV}^2. \quad (166)$$

In this case the oscillation probability can be written as:

$$P_{\bar{\nu}_e \rightarrow \bar{\nu}_e} = 1 - \sin^2 2\theta_{13} \sin^2 \left[ 1.27 \frac{\Delta m^2(\text{eV}^2) L(\text{meters})}{E(\text{MeV})} \right]. \quad (167)$$

This formula depends on two parameters:  $\Delta m^2 \simeq \Delta m_{23}^2 \simeq \Delta m_{13}^2$  the ‘large’ neutrino squared mass difference and the mixing parameter  $\sin^2 2\theta_{13}$ . As discussed in Section 4. one has that  $\sin^2 \theta_{13} = |\langle \nu_e | \nu_3 \rangle|^2$ , and therefore the oscillations vanish (that is  $\sin^2 2\theta_{13} = 0$  and  $P_{\bar{\nu}_e \rightarrow \bar{\nu}_e} = 1$ ) when  $\theta_{13} = 0$ , that is when the state  $|\nu_3\rangle$  has no overlap with  $|\nu_e\rangle$ , or when the  $\theta_{13} = \pi/2$  and the state  $|\nu_3\rangle$  coincides with  $|\nu_e\rangle$ ; however this last possibility is not consistent with the atmospheric neutrino data that give evidence for the

<sup>14</sup>Note how the detector has collected data until it has obtained a statistical error of the same order as the systematic uncertainty.

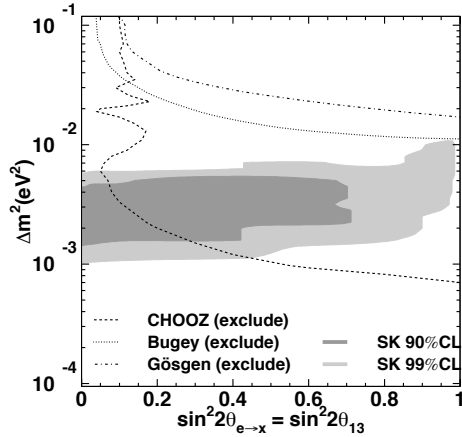


Fig. 33: Neutrino Mixing with three parameters. (a) Allowed area of  $\sin^2 \theta_{13}$  and  $\sin^2 \theta_{23}$ . At 90% C.L. SK data allows up to about 40% of  $e$ -type content of the atmospheric oscillation. (b) Allowed range of the atmospheric  $\nu_e$  disappearance probability compared to the limits for  $\bar{\nu}_e$  obtained from various reactor experiments. The most stringent limit comes from the CHOOZ experiment.

fact that the state  $|\nu_3\rangle$  has large overlaps with  $|\nu_\mu\rangle$  and  $|\nu_\tau\rangle$ . Equation (167) is formally identical to the two vacuum two flavor formula, and therefore a simple two-flavor analysis coincides with a three-flavor one performed the one mass scale approximation. Note also that equation (167) neglects the matter effects. In this case this is a good approximation, since for ordinary matter (with density  $\rho \simeq 2.7 \text{ g cm}^{-3}$ ) the effective potential is  $V \simeq 1.02 \times 10^{-13} \text{ eV}$ , and for  $E_\nu \lesssim 10 \text{ MeV}$ , we have that:

$$2 E_\nu V \simeq 10^{-8} \text{ eV}^2 \ll \Delta m^2 \quad (168)$$

for all values of  $\Delta m^2$  that can be explored. Since the experimental results are consistent with the *absence* of oscillations, the results can be interpreted as an *exclusion* region in the space of the parameters  $\Delta m^2$  and  $\sin^2 2\theta_{13}$ . These regions are shown in Fig. 33 together with the region that is *allowed* by the analysis of the atmospheric neutrino data in Super-Kamiokande [44]. The qualitative shape of the curves is simple to understand. Reactor experiments can exclude a region of high  $\Delta m^2$  (corresponding to fast oscillations) and large  $\sin^2 2\theta_{13}$  (corresponding to large amplitude oscillations). For  $\sin^2 2\theta \simeq 1$   $\Delta m^2$  must be smaller than a minimum value:

$$\Delta m_{\min}^2 \sim (\hbar c) \left( \frac{3 \text{ MeV}}{1 \text{ Km}} \right) \simeq 6 \times 10^{-4}, \quad (169)$$

while for large  $\Delta m^2$  the oscillation probability after the average over fast oscillations become a constant  $P_{\bar{\nu}_e \rightarrow \bar{\nu}_e} \simeq 1 - \frac{1}{2} \sin^2 2\theta_{13}$ , and one obtains a  $\Delta m^2$  independent limit determined by the statistical and systematic error  $\sin^2 2\theta_{13} \leq 0.10$ .

The atmospheric neutrino data determines an allowed interval for  $\Delta m^2$  that, as discussed in Section 7., is determined by the observed distortion of the  $\mu$ -like data. Since the atmospheric neutrino data for  $e$ -like events are consistent with a no oscillation prediction, then the value  $\sin^2 2\theta_{13} = 0$  is allowed (and in fact corresponds to approximately the best fit point for the atmospheric neutrino data). The lack of measurable deviations from the no-oscillation prediction for atmospheric  $e$ -like events allows to set a limit on the maximum value of  $\sin^2 2\theta_{13} \lesssim 0.75$ . As discussed in Section 7. this limit is not very stringent because of a cancellation between appearance and disappearance effects.

The combination of the results from atmospheric neutrinos (that determine the range of  $\Delta m^2$ ) and reactor neutrinos allows to determine a lower limit on the value of  $\sin^2 2\theta_{13} \lesssim 0.25$ : or equivalently

$$\sin^2 \theta_{13} \leq 0.065 \quad (90\% \text{ C.L.}) . \quad (170)$$

## 9.2. The KamLAND detector

The evidence for the oscillations of solar neutrinos has been recently dramatically confirmed by the KamLand experiment [91] with a measurement of the flux of reactor neutrinos for long ( $L \sim 180$  Km) distance. The sensitive volume of the KamLand detector (see Fig. 34) is a sphere of 6.5 meters radius that contains 1000 tons of liquid scintillator, instrumented with Photomultipliers. Electron anti-neutrinos can

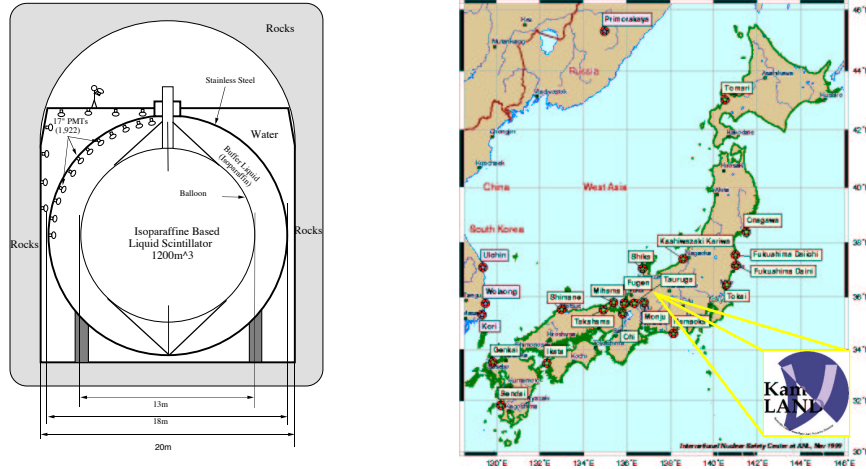


Fig. 34: Left panel: scheme of the KamLand detector. The sensitive volume is the inner sphere of 6.5 meters that contains 1000 tons of liquid scintillator, instrumented with Photomultipliers. Right panel: location of the power plants that provide the  $\bar{\nu}_e$ .

be detected with the usual reaction:  $\bar{\nu}_e + p \rightarrow e^+ + n$ , measuring the positron in the liquid scintillator, the photon emitted in the neutron capture is also observable. The  $\bar{\nu}_e$  flux is provided by an ensemble of approximately 70 reactors cores located at a distance between 150 and 210 Km from the detector in several commercial nuclear plants (see Fig. 34).

Recently the collaboration has published the results of the first 162 ton·year (145.1 days) of exposure. For this exposure the expected event rate was  $86.8 \pm 5.6$  events (for the chosen threshold of 2.6 MeV). This has to be compared with a detected rate of 54 events, with a ratio

$$\frac{N_{\text{obs}} - N_{\text{BG}}}{N_{\text{expected}}} = 0.611 \pm 0.085(\text{stat}) \pm 0.041(\text{syst}). \quad (171)$$

The probability that this ratio consistent with unity is only 0.05%, and therefore the result is clear evidence for the existence of transitions  $\bar{\nu}_e \rightarrow \bar{\nu}_x$ . Fig. 35 shows the measured/expected ratio of different reactor neutrino experiments plotted as a function of the distance between the reactor and the detector. The solid dot is the KamLAND point plotted at the flux-weighted average distance (the dot size is indicative of the spread in reactor distances). One can clearly see that the ratio is compatible with unity (that is with the absence of oscillations) for pathlength  $L \lesssim 1$  Km, while the KamLand ( $L \simeq 180$  Km) indicates that the survival probability  $\langle P(\nu_e \rightarrow \nu_e) \rangle$  is significantly different from unity. This result is in fact perfectly compatible with the Large Mixing Angle (LMA) solution of the solar neutrino problem. In Fig. 35 the shaded region indicates the range of flux predictions corresponding to the 95% C.L. LMA region found in the global analysis of the solar neutrino data. The dotted curve corresponds to  $\sin^2 2\theta = 0.833$  and  $\Delta m^2 = 5.5 \times 10^{-5}$  eV<sup>2</sup> that is a representative of recent best-fit LMA predictions.

Additional information on the possible existence of oscillations can be obtained from the analysis of the energy spectrum of the observed positrons. The expected spectrum is shown in the top part of the right panel of Fig. 35. One can see that the spectrum is dominated by the reactor neutrinos, with a smaller contributions of “geophysical” neutrinos (produced by radioactive decays of unstable nuclei in the Earth

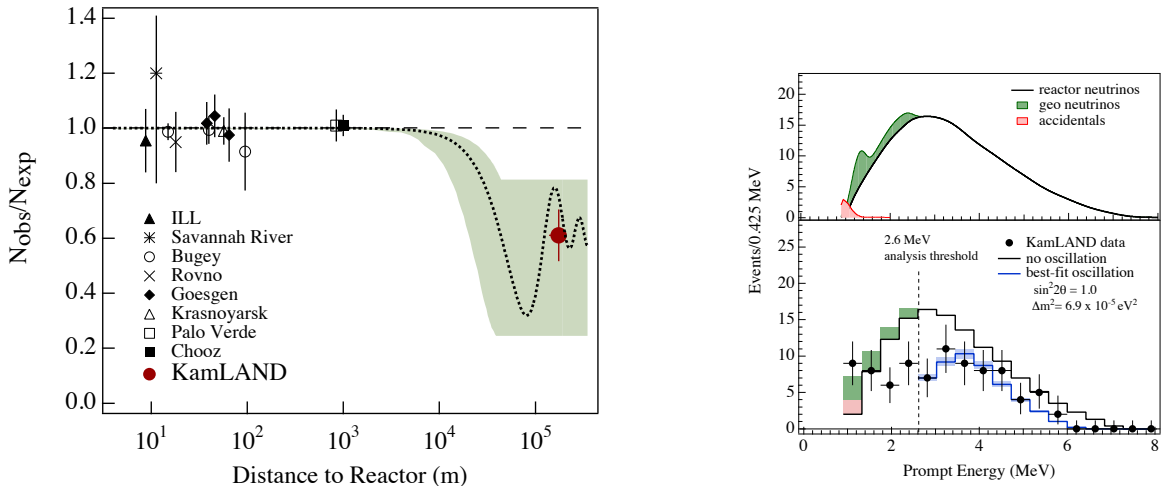


Fig. 35: The left panel shows the ratio measured/expected of the  $\bar{\nu}_e$  flux from reactor experiments. The solid dot is the KamLAND point. The shaded region indicates the range of flux predictions corresponding to the (95% C.L.) Large Mixing Angle Solution of the solar neutrino data. The dotted curve corresponds to  $\sin^2 2\theta = 0.833$  and  $\Delta m^2 = 5.5 \times 10^{-5} \text{ eV}^2$ . The right panel shows on the top the expected reactor  $\bar{\nu}_e$  energy spectrum with contributions of  $\bar{\nu}_{geo}$  and accidental background, and on the bottom the observed spectrum (solid circles with error bars), along with the expected no oscillation spectrum (upper histogram, with  $\bar{\nu}_{geo}$  and accidentals shown) and best fit (lower histogram) including neutrino oscillations. The shaded band indicates the systematic error in the best-fit spectrum. The vertical dashed line corresponds to the analysis threshold at 2.6 MeV. material), and an even smaller background of accidentals. The geophysical and accidental contributions are at low energy and can be eliminated with an analysis threshold of 2.6 MeV. The bottom part of the right panel in Fig. 35 shows (as points with error bars) the measured “prompt” energy spectrum. One can immediately see that the data is below the no-oscillation prediction (the upper histogram), while the inclusion of neutrino oscillations (lower histogram) can reconcile data and prediction. It can also be seen that there is an indication not only of a suppression of the event rate but also of a distortion of the energy spectrum: the first two bins above the analysis threshold (indicated by a vertical dashed line) seems to have a stronger suppression than the higher energy bins.

The KamLand results can be interpreted in terms of  $\nu_e \rightarrow \nu_x$  transitions, obtaining an allowed region in the plane ( $\sin^2 2\theta, \Delta m^2$ ). The results for this allowed region are shown in Fig. 36. The figure shows in the usual plane ( $\sin^2 2\theta, \Delta m^2$ ) the region excluded by previous (shorter pathlength) reactor experiments Chooz and Palo Verde (all regions are for a 95% Confidence Level), and the allowed region of the LMA solution of the solar neutrino problem. The result of KamLand are shown in two ways: as an excluded region, that takes into account only the total rate result (equation (171)); and an allowed region that takes into account both the total rate and the energy spectrum. This allowed region corresponds to several bands in  $\Delta m^2$  that can reproduce the observed distortion of the spectrum. One can see that the KamLand data excludes all oscillations solutions for the solar neutrino problem with the exception of the LMA solution.

Several authors have performed combined analysis of the KamLand and solar neutrino data to determine the  $\nu$  oscillation parameters. An example of this combined fits from Fogli et al ([92]) is shown in the right panel of Fig. 36. One can see that the LMA region is basically split into two sub-regions. The best fit point is in the lower region with  $\Delta m_{12}^2 \simeq 7.3 \times 10^{-5} \text{ eV}^2$  and  $\sin^2 \theta_{12} \simeq 0.31$ .

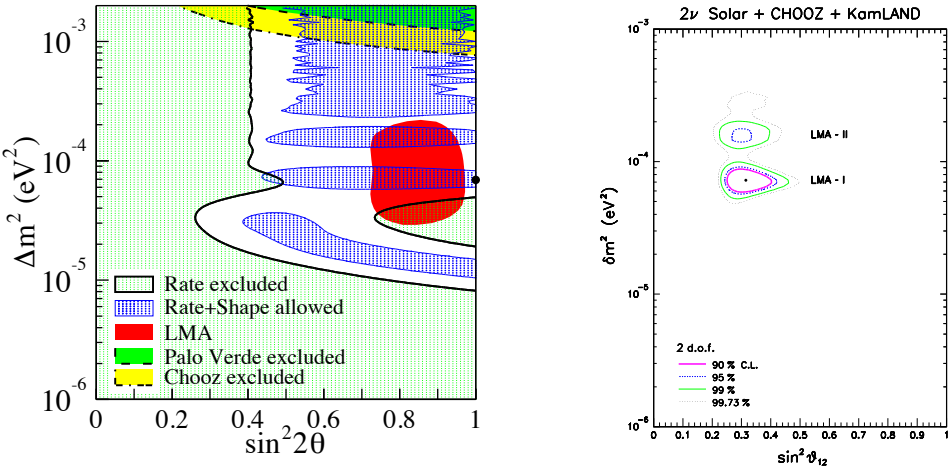


Fig. 36: The left panel shows the 95% allowed regions of neutrino oscillation parameters for the analysis of the KamLand experiment, and for the ‘Large Mixing Angle’ (LMA) solution of solar neutrino problem. The top region is excluded by Chooz and Palo Verde. The right panel shows the result of a combined fit of the Kamland and solar data performed by Fogli et al. [92]. Note that the  $x$ -axis in the case corresponds to  $\sin^2 \theta_{12}$ .

## 10. ACCELERATOR NEUTRINOS

### 10.1. Cosmologically motivated searches

Neutrino oscillations have been searched in accelerator experiments for a long time. Several dedicated searches for oscillation were motivated by cosmology and an analogy to the masses and mixing in the quark system. An explanation of the cosmological dark matter problem with neutrinos implies (see equation (36)) that the sum of the neutrino masses is of order  $\sim 30$  eV, on the other hand, an analogy with the quark sector suggests that  $m_3 \gg m_2 \gg m_1$ , and that the mixing angles are small. These considerations lead to the expectation that  $\nu_{\mu,e} \rightarrow \nu_\tau$  oscillations could be detected with a large squared mass difference  $\Delta m^2 \simeq m_3^2 \sim (30 \text{ eV})^2$ , but small mixing parameter  $\sin^2 2\theta \ll 0.1$ . Several dedicated experiment were performed searching for these oscillations. No evidence for these oscillations has been found. The best limits have been obtained by the NOMAD and CHORUS [94,95] detectors (see Fig. 37) using a neutrino beam produced by 400 GeV protons in the CERN laboratory. In these experiments the

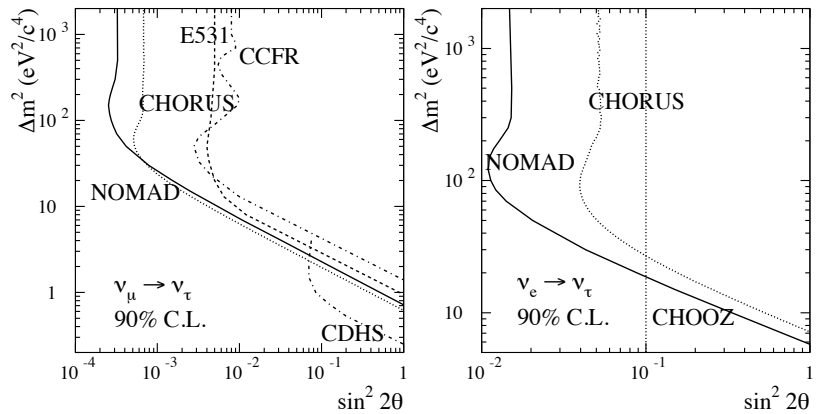


Fig. 37: The lines indicate the regions in the  $(\Delta m^2, \sin^2 2\theta)$  plane excluded (at 90% C.L.) by accelerator searches for  $\nu_\mu \leftrightarrow \nu_\tau$  oscillations (left panel) and  $\nu_e \leftrightarrow \nu_\tau$  oscillations (right panel). From [94].

distance from the detector to the target region was of order 500 meters, the average neutrino energy was

of order 50 GeV, with the minimum (threshold) energy for appearance  $E_\nu \simeq 3.5$  GeV. The region of  $\Delta m^2$  that can be explored is therefore:

$$|\Delta m^2| \gtrsim (\hbar c) \left( \frac{3.5 \text{ GeV}}{500 \text{ m}} \right) \simeq 0.7 \text{ eV}^2, \quad (172)$$

while the very large statistics allows to study very small mixing ( $\sin^2 2\theta \gtrsim 3 \times 10^{-4}$ ) at large  $|\Delta m^2|$ .

The appearance of  $\nu_\tau$  charged current events can be detected using two techniques:

(i) kinematical methods, or (ii) decay vertex identification methods. The NOMAD detector has searched for events with appropriate kinematical characteristic, in particular having missing transverse momentum, since in  $\nu_\tau$  charged current interactions some  $p_\perp$  is carried away by the neutrinos, that are always produced in  $\tau$  decay. The most attractive channel is the mode  $\tau^- \rightarrow \nu_\tau + e^- + \bar{\nu}_e$ , since it has a low background due to  $\nu_e$  charged-current interactions which are only  $\sim 1.5\%$  of the total event rate, and have a very different energy spectrum from what is expected from  $\nu_\mu \leftrightarrow \nu_\tau$  oscillations.

The CHORUS detector (see Fig. 38) was constructed using the emulsion technique that provides space resolution of  $\sim 1 \mu\text{m}$ , well matched to the average  $\tau^-$  decay length of 1 mm.

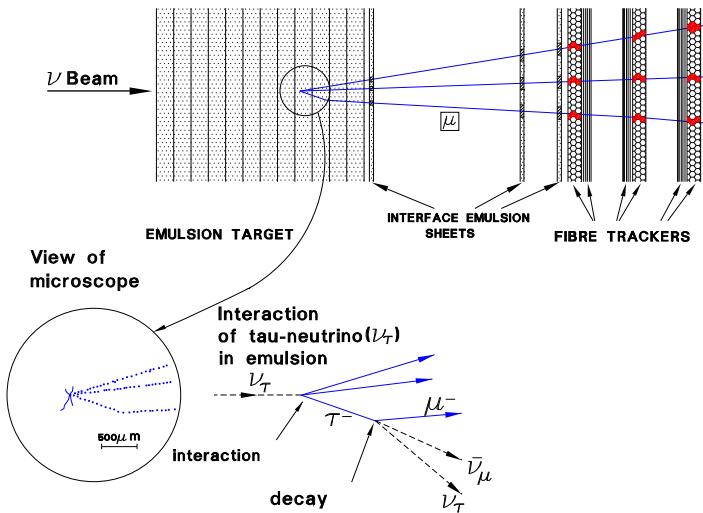


Fig. 38: Expected configuration of a typical  $\nu_\tau$  charged-current interaction event in the CHORUS emulsion. The decay length for a  $\tau^-$  ( $L_\tau \simeq 87 \mu\text{m}$   $E_{\text{GeV}}$ ) is typically a fraction of a millimeter. In this example the  $\tau^-$  decays to  $\mu^- \nu_\tau \bar{\nu}_\mu$ .

## 10.2. The LSND effect

A controversial result on neutrino flavor transitions has been obtained by the Liquid Scintillator Neutrino Detector (LSND) running at the Los Alamos Meson Physics facility [96]. The LSND collaboration has also reported evidence for neutrino flavor transitions of type  $\bar{\nu}_\mu \rightarrow \bar{\nu}_e$ . This evidence is still very controversial, and has not been confirmed by other independent measurements. The “LSND effect” is *not* consistent with the results on solar and atmospheric neutrino experiments at least in a simple three neutrino framework, since it requires  $|\Delta m^2|$  in a range much larger than what is indicated by the other experiments. If this effect is real the consequences would be very important.

The LSND  $\nu$  beam is obtained from an accelerated proton beam with momentum  $|\vec{p}| = 800$  MeV, the detector is a tank filled with 167 tons of liquid scintillator at approximately 30 meters from the neutrino source. The neutrino beam is mostly due to  $\pi^+$  that stop in target region and decay with the usual sequence  $\pi^+ \rightarrow \nu_\mu + \mu^+$  followed by  $\mu^+ \rightarrow \bar{\nu}_\mu + \nu_e + e^-$ . The contribution of  $\pi^-$  is much

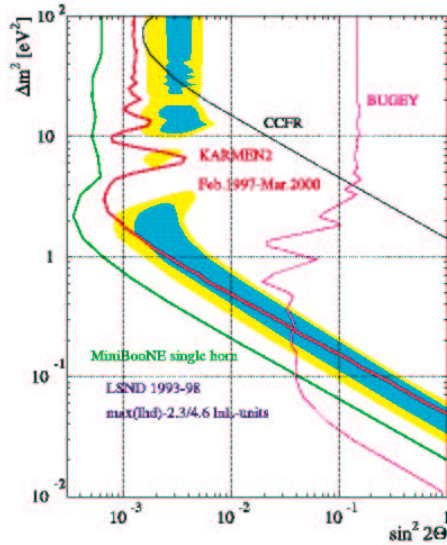


Fig. 39: The shaded areas show the allowed regions (at 90 and 99% C.L.) for  $\nu_\mu \leftrightarrow \nu_e$  oscillations from the LSND experiment. This region is compared with the (90% C.L.) excluded region (to the right of the lines) by other experiments, CCFR, BUGEY and KARMEN-2. The blue line (that entirely excludes the LSND region) is the region that can be explored with the MiniBoone experiment currently taking data.

suppressed because they are produced less abundantly in low energy  $p$  interactions, and most of them are absorbed in nuclear interactions before decay, and therefore the beam contains  $\nu_\mu, \bar{\nu}_\mu, \nu_e$  but only very few  $\bar{\nu}_e$  (in the absence of oscillations the ratio  $\bar{\nu}_e/\nu_e$  is estimated as  $7.5 \times 10^{-4}$ . The appearance of  $\bar{\nu}_e$  can be studied with the “classic” coincident observation of a positron and a delayed photon from  $n$  capture:

$$\bar{\nu}_e + p \rightarrow e^+ + n, \quad n + p \rightarrow d + \gamma \text{ (2.2 MeV)}. \quad (173)$$

After subtracting the expected sources of background The LSND collaboration [96] observes in the energy range  $E_e \in [20, 60]$  MeV an excess of  $87.9 \pm 22.4 \pm 6.0$  events. This excess can be explained assuming an average probability:

$$\langle P_{\bar{\nu}_\mu \rightarrow \bar{\nu}_e} \rangle = (2.64 \pm 0.67 \pm 0.45) \times 10^{-3}. \quad (174)$$

This result is supported by a measurement of the  $\nu_e$  flux with the process  $\nu_e + {}^{12}\text{C} \rightarrow e^- + X$ , measuring electrons in the energy region ( $60 \leq E_e \leq 200$  MeV). Neutrinos in this energy range can only be produced by the decay in flight of pions and muons. For this class of events the LSND collaboration reports an excess of  $18.1 \pm 6.6 \pm 4.0$  events consistent with  $\nu_\mu \rightarrow \nu_e$  transitions with an average probability

$$\langle P_{\nu_\mu \rightarrow \nu_e} \rangle = (2.4 \pm 1.0 \pm 0.5) \times 10^{-3} \quad (175)$$

consistent with the previous result. Interpreting these results in terms of two flavor  $\nu_\mu \leftrightarrow \nu_e$  oscillations one obtains the allowed region in the plane  $(\sin^2 2\theta, \Delta m^2)$  shown in Fig. 39. The allowed region requires a mixing parameter  $\sin^2 2\theta \simeq 2\langle P_{\bar{\nu}_\mu \rightarrow \bar{\nu}_e} \rangle \simeq 4 \times 10^{-3}$  if  $\Delta m^2$  is large. For maximal mixing ( $\sin^2 2\theta \simeq 1$ ) the  $\Delta m^2$  that can explain the data is of order

$$\Delta m^2 \gtrsim \frac{1}{3} (\hbar c) \left( \frac{20 \text{ MeV}}{30 \text{ meters}} \right) \gtrsim 0.06 \text{ eV}. \quad (176)$$

The low  $\Delta m^2$  region is however forbidden by the results of the Bugey reactor experiment. Note also that most of the allowed region of LSND is excluded by the results of the KARMEN [97], leaving only a small allowed interval.

## Sterile Neutrinos ?

The result of LSND cannot be easily reconciled with the results on atmospheric and solar neutrinos. This can be immediately understood noting that in three neutrino world there are only three independent squared mass differences  $\Delta m_{jk}^2$ , and the results

$$\begin{aligned}\Delta m_{\odot}^2 &\lesssim 10^{-4} \text{ eV}^2, \\ \Delta m_{\text{atm}}^2 &\simeq 3 \times 10^{-3} \text{ eV}^2, \\ \Delta m_{\text{LSND}}^2 &\gtrsim 0.2 \text{ eV}^2\end{aligned}$$

cannot be reconciled. The logical possibilities of course are that:

- (a) one or more of the experimental results are incorrect;
- (b) the theoretical framework used to interpret the results is incorrect or incomplete.

The addition of one or more neutrino mixed with the ordinary could explain the data, because in this case one more (independent) squared mass difference is available. The fourth light neutrino cannot be just the 4th generation neutrino similar to  $\nu_e$ ,  $\nu_\mu$  and  $\nu_\tau$  because this would be in conflict with the experimentally measured width of  $Z^0$  boson. It can only be an electroweak singlet (sterile) neutrino. The existence of such a state would of course be of the greatest importance.

Out of all experimental evidences for neutrino oscillations, the LSND result is the only one that has not yet been confirmed by other experiments. It is therefore very important to have it independently checked. This will be done by the MiniBooNE (first phase of BooNE) experiment at Fermilab. MiniBooNE will be capable of observing both  $\nu_\mu \rightarrow \nu_e$  appearance and  $\nu_\mu$  disappearance. The sensitivity of MiniBooNe is also shown in Fig. 39. MiniBooNE will begin taking data in 2002.

### 10.3. Long Baseline Experiments

In order to study neutrino oscillations with  $\Delta m^2$  in the range suggested by the atmospheric neutrino data it is necessary to have baselines of order 100–1000 Km or more, depending on the neutrino energy. A comparison between a “near” and a “far” detector can be an ideal method to determine the existence and detailed properties of  $\nu$  flavor oscillations. At present there is one project that is taking data: the K2K (or KEK to Kamioka) project, and two approved and under construction project: the Fermilab to Minos beam and the CERN to Gran Sasso beam.

In the K2K project an almost pure  $\nu_\mu$  beam is generated with a 12 GeV proton beam in the KEK laboratory. The “far” detector is Super-Kamiokande at a distance of 250 Km.

The K2K experiment had a successful start in 1999 and has accumulated  $\sim 4.8 \times 10^{19}$  “protons on target” (p.o.t.) that is approximately 40% of the goal of  $10^{20}$  p.o.t. The time distribution of the contained events recorded during this period of data taking is shown in Fig. 40. The beam has the structure of a  $1.1 \mu\text{s}$  pulse each 2.2 sec, and the analysis of fully contained events is virtually without background. Two “near” neutrino detectors are placed at the KEK site one being a one kiloton water detector that is like a miniature Super-Kamiokande, and the other a “fine-grained detector” made of scintillating fibers. These near detectors allow to monitor the intensity, stability and energy spectrum of the neutrino beam, when oscillations have not developed, and allow to extrapolate to the far (Super-Kamiokande detector).

The no-oscillation extrapolation of the near detector data predicts a rate of  $80.1^{+6.2}_{-5.4}$  events in the fiducial volume of SK, while only 56 have been measured. The probability that the observed flux at SK is a statistical fluctuation is less than 1%.

The Fermilab to MINOS project will use the proton beam of the Main Injector at Fermilab

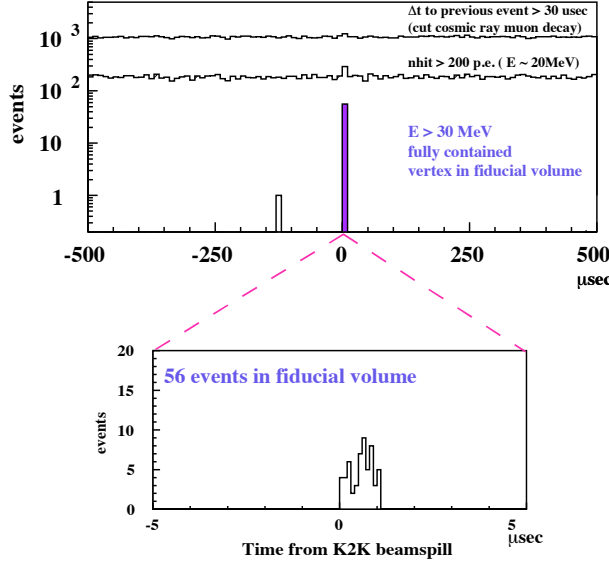


Fig. 40: Time distributions (relative to the beam arrival) of contained events events in Super-Kamiokande during the data taking with the K2K  $\nu$ -beam. From [99].

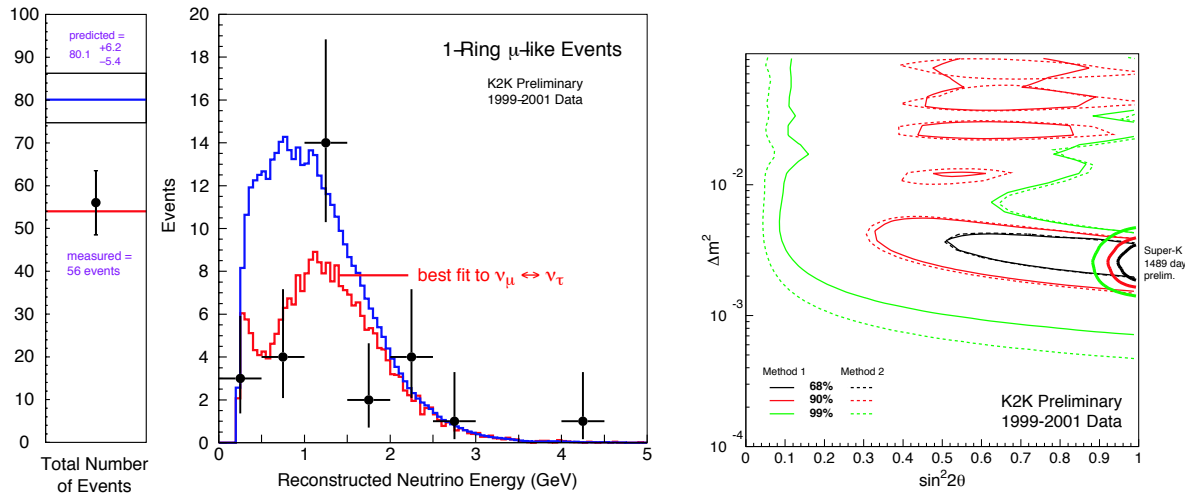


Fig. 41: The left panes shows the total event count and single-ring  $\mu$ -like neutrino spectrum overlaid with expectations for no oscillations and oscillations at the K2K best fit point. The right panel shows the allowed region in the oscillation parameter space. From [99].

( $E_p = 100$  GeV) to produce a neutrino beam that is sent to the underground site of MINOS at a distance of 730 Km. The detailed comparison of a “near” and a “far” detector functionally identical (two iron/scintillator sampling calorimeters) with toroidal magnetic field should allow to confirm the oscillation interpretation for atmospheric neutrinos, and to determine more accurately the oscillation parameters. The beginning of the data taking is scheduled for the end of 2004.

In the CERN to Gran Sasso project 450 GeV  $p$  beam is the source of a higher energy neutrino beam  $\langle E_\nu \rangle \sim 15 - 20$  GeV that will be sent to the Gran Sasso underground laboratory, again at a distance of 730 Km. The OPERA detector is designed to search for the appearance of  $\nu_\tau$  charged current interactions with a massive lead/nuclear emulsion target. The ICARUS detector is also sensitive to the  $\nu_\tau$ 's generated by the oscillations.

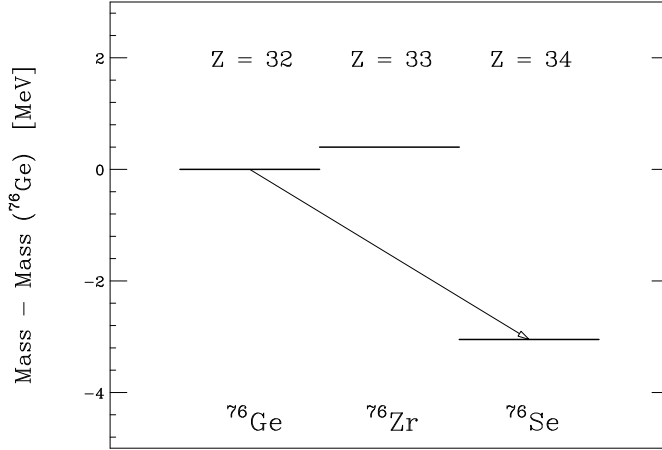


Fig. 42: Energy levels for the  $A = 76$  nuclei.

## 11. DOUBLE BETA DECAY

The most promising way to distinguish between Dirac and Majorana neutrinos is neutrinoless double beta decay (for extensive reviews see [102]). Double beta decay is the process:

$$(Z, A) \rightarrow (Z + 2, A) + 2e^- + 2\nu_e \quad (2\nu\beta\beta \text{ decay}), \quad (177)$$

that can occur when single beta decay is kinematically forbidden. For example the nucleus  $^{76}\text{Ge}$  ( $Z=32$ ) cannot have a beta decay into the  $Z=33$  state ( $^{76}\text{As}$ ) that has a mass 0.4 MeV larger, but can have a double beta decay into the  $Z=34$  state ( $^{76}\text{Se}$ ) that is 3.05 MeV lighter. The process (177) at the fundamental (quark) level (see part (a) of Fig. 43) is the transition of two  $d$  quarks into two  $u$  quarks with the emission of two electrons and two  $\bar{\nu}_e$ . The process is of second order in the weak coupling and therefore the corresponding decay rates are very low with lifetimes of order  $T \gtrsim 10^{19} - 10^{21}$  years.

In the neutrino-less process:

$$(Z, A) \rightarrow (Z + 2, A) + 2e^- \quad (0\nu\beta\beta \text{ decay}), \quad (178)$$

there is no neutrino emission. The leading order diagram of this process is shown in part (b) of Fig. 43, and can be pictured as one beta decay followed by the absorption of the emitted anti-neutrino by a different neutron in the nucleus. The process has a very clear experimental signature because while in the standard decay the sum of the energy of the two electrons in the final state has a broad distribution, in the neutrinoless case one has that the sum of the energies of the two emitted electrons is equal to the

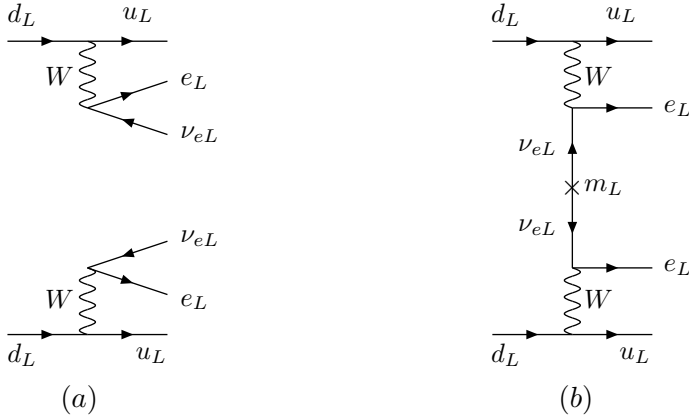


Fig. 43: Double beta decay diagrams. Diagram (a) shows the standard process when two neutrinos are emitted; diagram (b) shows the neutrinoless decay that has not been observed and is possible only if the neutrino is a massive Majorana particle.

$Q$  value of the reaction:

$$E(e_1^-) + E(e_2^-) \simeq Q \equiv M_i - M_f. \quad (179)$$

In order to have neutrinoless  $2\beta$  decays one has two conditions:

- [1] The neutrino must be its own anti-particle, that is it must be a Majorana particle.
- [2] The neutrino mass must be non zero.

The first condition can be easily understood observing that the virtual neutrino in the diagram (b) of Fig. 43 is emitted as  $\bar{\nu}_e$  and is absorbed as a  $\nu_e$ , and in fact the reaction (178) clearly violates the lepton number by two units. The second condition follows from the fact that anti-neutrino emitted in the ‘first’ decay has the wrong chirality for being absorbed. The absorption is therefore possible without violating angular momentum conservation only if  $m_\nu$  is non-vanishing. In fact the amplitude for neutrinoless double beta decay is proportional to the neutrino mass:

$$A(2\beta0\nu) \propto \sum_i U_{ei}^2 m_i \equiv \langle m_{\nu_e} \rangle_{\text{eff}}. \quad (180)$$

Note that the amplitude is proportional to a linear combination of the neutrino masses where the coefficients are  $U_{ei}^2$  rather than  $|U_{ei}|^2$ , and therefore in general cancellations are possible, and the effective mass can be smaller than the smallest neutrino mass  $m_j$ . The quantity  $\langle m_{\nu_e} \rangle_{\text{eff}}$  constitutes a lower limit on the mass of the heaviest neutrino.

The current best limits on neutrinoless double beta decay comes from Heidelberg–Moscow experiment on the double beta decay of  $^{76}\text{Ge}$  [103]. This experiment located in the Gran Sasso underground laboratory is using 11 kg of Ge enriched to 86% in the isotope with mass 76, and has achieved a very low background (of order 0.2 counts/year/Kg/KeV) at the expected position of the  $\beta\beta0\nu$  signal, and has collected an exposure of order 50 Kg years. In Fig. 44 we show the energy spectrum observed by the experiment (the experiment measures only the total released energy and cannot identify if the source of the energy is a photon, or one or more electrons). One can see the presence of several sources of background (that give a continuum and several radioactive decay lines) but also the clear contribution of a two-neutrino double decay with the predicted shape. The half-life of Germanium-76 was estimated from a fit to the background-subtracted signal in the energy range 700–2040 KeV

$$T_{1/2}^{2\nu} = [1.55 \pm 0.01(\text{stat}) \quad {}^{+0.19}_{-0.15}(\text{syst})] \times 10^{21} \text{ years}. \quad (181)$$

In the presence of a neutrino-less contribution, one would observe a line corresponding to the  $Q$ -value of the  $^{76}\text{Ge} \rightarrow {}^{76}\text{Se}$  transition ( $2038.56 \pm 0.32$  KeV). The data (see the bottom panel of Fig. 44) shows

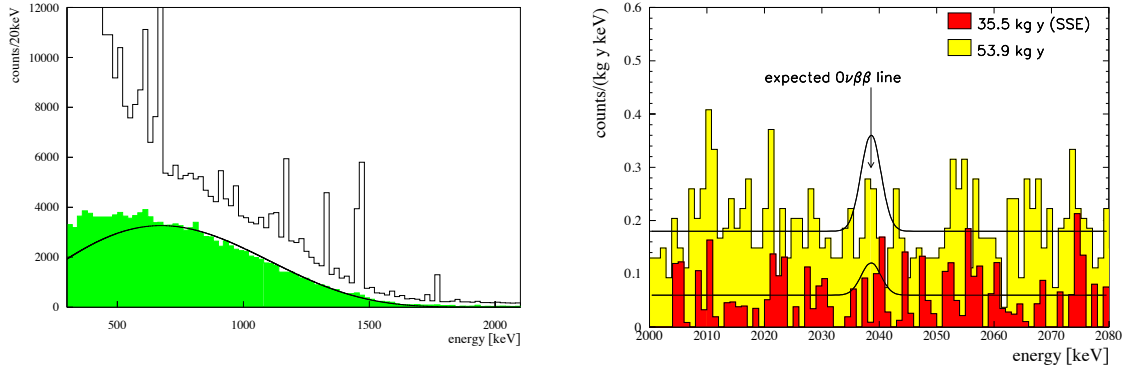


Fig. 44: Left panel: Energy spectrum (20 KeV bins) of the Heidelberg–Moscow experiment, together with the residual spectrum after subtracting all identified background components. The thick line shows the fitted  $2\nu\beta\beta$ -signal. Right panel: energy Spectrum close to the  $Q$  value of the  $^{76}\text{Ge} \rightarrow ^{76}\text{Se}$  decay. The darker histogram correspond to a smaller exposure, that uses a technique to select events where the energy is released in a single point (like in double beta decay) and not in multiple points (like in Compton scattering). The curves correspond to the excluded signals for neutrinoless double beta decay. From [103]

no peak above an approximately flat background. This can be used to extract a half-life limit for the neutrinoless mode

$$T_{1/2}^{0\nu} \geq 1.9 \times 10^{25} \text{ years} \quad 90\% \text{ C.L.} \quad (182)$$

This limits can be used to extract a limit<sup>15</sup> effective mass of the  $\nu_e$  (see equation (180)):

$$m_{\text{eff}} \leq 0.35 \text{ eV} \quad (90\% \text{C.L.}) \quad (183)$$

Recently it has been claimed [104] that the results of the Heidelberg–Moscow collaboration can be interpreted as positive evidence for the existence of neutrinoless  $\beta\beta$  decay, and implies an effective neutrino mass  $\langle m_{\nu_e} \rangle_{\text{eff}} \simeq 0.4 \text{ eV}$ . This controversial claim has been criticised in [105,106].

The discovery of  $2\beta0\nu$  decay would establish that neutrinos are Majorana particle and determine the quantity  $\langle m_{\nu_e} \rangle_{\text{eff}}$ ) that sets a *lower* limit on the absolute value of the scale of the neutrino masses.

## 12. PHENOMENOLOGICAL SUMMARY

A coherent picture has begun to emerge from the experimental studies on neutrino flavor transitions. All existing data, with the notable exception of the LSND results, can be explained assuming the existence of standard oscillations among three neutrino flavors.

Without loss of generality one can define the state  $|\nu_3\rangle$  as the “most isolated neutrino”, that is the neutrino with the largest mass difference (in absolute value) from the closest mass eigenstates. Obviously  $|\nu_3\rangle$  is either the heaviest of the lightest neutrino. It is possible and convenient to choose  $\Delta m_{12}^2 \equiv m_2^2 - m_1^2$  as positive (or  $m_2 > m_1$ ). With this we have completely defined the conventions for the labeling of the neutrino mass eigenstates. The neutrino masses and mixing matrix have the following properties:

- [1] The neutrino squared mass differences are ‘hierarchical’: there is a “small” mass difference  $\Delta m_{12}^2$ . responsible for the oscillations of solar neutrinos, that is at least one order of magnitude smaller than “large” mass difference  $|\Delta m_{23}^2|$ .

<sup>15</sup>To obtain information of the effective mass parameter from the measured lifetime limit, one needs to use the results of a difficult calculation of the matrix element between the initial and final nucleus. This introduces some uncertainty in the limit

[2] The “large” squared mass difference is measures with atmospheric neutrinos and has value:

$$\Delta m_{\text{atm}}^2 \simeq \Delta m_{23}^2 \simeq \Delta m_{13}^2 \simeq \pm 2.5 \times 10^{-3} \text{ eV}^2. \quad (184)$$

Note the ambiguity in the sign. We do not know if  $\nu_3$  is the lightest or heaviest neutrino. The 90% C.L. allowed interval for  $|\Delta m_{\text{atm}}^2|$  determined by SK is At 90% C.L. the allowed interval is

$$|\Delta m_{23}^2| \in [1.6, 4.5] \times 10^{-3} \text{ eV}^2. \quad (185)$$

[3] The eigenstate  $|\nu_3\rangle$  has the composition:

$$|\nu_3\rangle \simeq \frac{1}{\sqrt{2}}(1 \pm \epsilon) |\nu_\mu\rangle + \frac{1}{\sqrt{2}}(1 \mp \epsilon) |\nu_\tau\rangle + \epsilon' |\nu_e\rangle. \quad (186)$$

where  $\epsilon$  and  $\epsilon'$  are small quantities. That is the “isolated” state  $|\nu_3\rangle$  is a superposition with approximately equal weight of  $\nu_\mu$  and  $\nu_\tau$  with a small (or vanishing) overlap with  $\nu_e$ . In the standard parametrization of the mixing matrix we have:

$$|\nu_3\rangle = \sin \theta_{13} |\nu_e\rangle + \cos \theta_{13} \sin \theta_{23} |\nu_\mu\rangle + \cos \theta_{13} \cos \theta_{23} |\nu_\tau\rangle, \quad (187)$$

therefore we can restate the result (186) saying that  $\theta_{23} \simeq 45^\circ$  (that corresponds to maximal mixing) while  $\theta_{13}$  is small. For  $\theta_{23}$  the current 90% C.L. allowed region determined by SK is  $\sin^2 2\theta_{23} \gtrsim 0.90$  that can also be expressed as:

$$\sin^2 \theta_{23}, \cos^2 \theta_{23} \in [0.35, 0.65] \quad (90\% \text{ C.L.}). \quad (188)$$

[4] The upper limit on the value of  $\theta_{13}$  is determined by the results of the reactor experiments Chooz and Palo Verde and the non observations of  $\nu_e \rightarrow \nu_{\mu,\tau}$  transitions: The 90% C.L. limits of Chooz are:

$$\begin{aligned} \sin^2 \theta_{13} &\gtrsim 0.065 & (\Delta m^2 = [\text{SK minimum allowed}]), \\ \sin^2 \theta_{13} &\gtrsim 0.025 & (\Delta m^2 = [\text{SK best fit}]). \end{aligned} \quad (189)$$

[5] The values of  $\Delta m_{12}^2$  and of the other mixing angle  $\theta_{12}$  are determined by the solar neutrino experiments. The combination of the data of different experiments, until recently resulted in a set of disconnected regions in the plane  $(\Delta m_{12}^2, \sin^2 \theta_{12})$ , that have been given names: LMA corresponds to the “Large Mixing Angle” solution, SMA to the “Small Mixing Angle” solution, LOW to the region with large mixing angle with  $\Delta m^2$  lower than for LMA, and finally the vacuum solution to the very small  $\Delta m^2$  solution with oscillation length of the same order of the sun-earth distance. Numerically the regions are approximately:

$$\begin{cases} \Delta m_{12}^2 = (0.7 \div 8) \times 10^{-5} \text{ eV}^2, & \sin^2 \theta_{12} = (0.2 \div 0.6) & \text{LMA} \\ \Delta m_{12}^2 = (0.7 \div 2) \times 10^{-7} \text{ eV}^2, & \sin^2 \theta_{12} = (0.5 \div 0.7) & \text{LOW} \\ \Delta m_{12}^2 = (0.4 \div 1) \times 10^{-5} \text{ eV}^2, & \sin^2 \theta_{12} = (0.6 \div 3.0) \times 10^{-3} & \text{SMA} \\ \Delta m_{12}^2 = (0.5 \div 3) \times 10^{-10} \text{ eV}^2, & \sin^2 \theta_{12} = (0.25 \div 0.75) & \text{Vacuum} \end{cases}$$

The most recent data of SNO favors very clearly the LMA solution with a best point fit:

$$\begin{aligned} \Delta m_{12}^2 &= 5 \times 10^{-5} \text{ eV}^2 \\ \sin^2 \theta_{12} &= 0.24 \quad (\theta_{12} = 29.5^\circ) \end{aligned} \quad (190)$$

Note that since in the parametrization of the mixing matrix the overlap  $|\langle \nu_e | \nu_1 \rangle|^2 = \cos^2 \theta_{13} \cos^2 \theta_{12} \simeq \cos^2 \theta_{12}$ , the state  $|\nu_1\rangle$  state is *mostly* a  $\nu_e$ .

These results indicate that the mixing in the lepton sector is deeply different than in the quark sector,

where *all* mixing angles are small. These results suggest (or better “require) a number of new experimental studies to confirm and complete our knowledge of the neutrino masses and mixing. On the other hand the discovery of these remarkable “patterns” for the neutrino masses and mixing suggest several theoretical questions about what this all “means”, that is what it is teaching us about the origin of flavor, the fermion families and the particle masses.

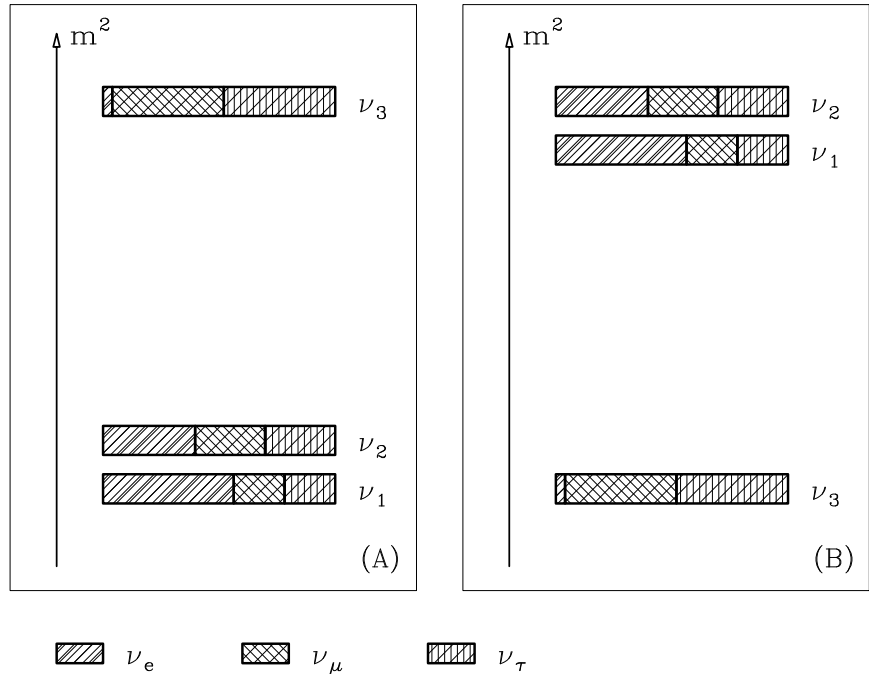


Fig. 45: Flavor composition of the  $\nu$  mass eigenstates. Each mass eigenstate is represented as a “box”, with three flavor components proportional to  $|\langle \nu_\alpha | \nu_j \rangle|^2$ . The mixing angles are chosen as  $\theta_{12} = 40^\circ$ ,  $\theta_{23} = 45^\circ$ ,  $\theta_{13} = 11^\circ$ , the phase  $\delta$  has the value  $\delta = 90^\circ$ . The value of  $\theta_{23}$  is the best fit for the atmospheric neutrino data,  $\theta_{12}$  is in the LMA solution for the solar neutrino data, while the value of  $\theta_{13}$  is just below the upper limit obtained by the Chooz reactor experiment; the phase  $\delta$  is left completely undetermined by the experimental data. The squared mass is only shown “qualitatively”. The ‘small’ mass splitting  $\Delta m_{12}^2$  is responsible for (and determined by) the oscillations of solar neutrinos, while the larger splitting  $\Delta m_{23}^2 \simeq \Delta m_{13}^2$  is responsible for the higher frequency oscillations measured with atmospheric neutrinos. Case (A) corresponds to “normal hierarchy”, case (B) to the “inverted hierarchy”.

### 12.1. Absolute value of the neutrino masses

Oscillation experiments can only determine squared mass differences, and therefore leave the question of the absolute value of the neutrino masses unanswered. Atmospheric and solar neutrino experiments have determined the two independent  $\Delta m^2$  with an important ambiguity in sign for  $\Delta m_{\text{atm}}^2$ . Using the notation  $\Delta m_{\odot}^2 \equiv \Delta m_{12}^2$  and  $\Delta m_{\text{atm}}^2 \equiv \Delta m_{23}^2$ , and taking into account the sign ambiguity the neutrino masses can be written as:

- Normal hierarchy:

$$\begin{aligned} m_1 &= m_0, \\ m_2 &= m_0 + \sqrt{\Delta m_{\odot}^2}, \\ m_3 &= m_0 + \sqrt{\Delta m_{\odot}^2} + \sqrt{\Delta m_{\text{atm}}^2}. \end{aligned} \quad (191)$$

- Inverse hierarchy:

$$\begin{aligned} m_3 &= m_0, \\ m_1 &= m_0 + \sqrt{\Delta m_{\text{atm}}^2}, \\ m_2 &= m_0 + \sqrt{\Delta m_{\odot}^2} + \sqrt{\Delta m_{\text{atm}}^2}, \end{aligned} \quad (192)$$

where  $m_0$  is an unknown minimal mass.

The experiments most sensitive to the mass  $m_0$  are the searches for neutrinoless double beta decay. The amplitude for this process is proportional to an effective neutrino mass:

$$m_{\text{eff}} = \left| \sum_j U_{ej}^2 m_j \right| \equiv \left| \sum_j |U_{ej}|^2 e^{-\varphi_j} m_j \right|, \quad (193)$$

where the phases  $\varphi_j$  are the Majorana phases that are unobservable in oscillation experiments. More explicitly, using the standard parametrization of the mixing matrix we have:

$$m_{\text{eff}} = \left| c_{13}^2 c_{12}^2 m_1 + c_{13}^2 s_{12}^2 e^{i\varphi_2} m_2 + s_{13}^2 e^{i\varphi_3} m_3 \right|. \quad (194)$$

### 13. MODELS FOR THE NEUTRINO MASS

The most striking fact about the neutrino masses is that they are so small, much smaller than the masses of the quarks and charged leptons. It is true that the fermion mass spectrum extends for several orders of magnitudes, however the size of the neutrino masses calls for a special explanation. A second remarkable fact is that the neutrino mass matrix is that the mixing is large, in sharp contrast with the quark sector where the Cabibbo–Kobayashi–Maskawa matrix  $V_{CKM}$  matrix has small deviations from the unity matrix.

Several explanations have been offered for the smallness of the neutrino masses. It is fascinating that all these explanations are based on some form of new physics beyond the standard model, and therefore the measurement of the neutrino masses and mixing can open a precious window on the physics of “Unification” giving information on the physics at mass scales beyond what can be reached directly with accelerator experiments.

A massive spin 1/2 particle has two spin states, and if it is “charged” it also has an anti-particle, with the same mass and opposite charge(s), that also has two spin states, for a total of four states with identical mass. Each quark or charged lepton (together with its own anti-particle) is in fact described as a 4-state system in a Dirac spinor. A “neutral” fermion on the other hand could be identical with its anti-particle, and have only two states. A  $CPT$  operation would transform the two states into each other. It is remarkable that it is possible to build the field theory of such a two state system described by a Majorana spinor.

Is the neutrino a Majorana or a Dirac particle ? If the neutrino is massless this question is meaningless. This can be understood easily observing that a zero mass particle moves with the speed of light, and if it has helicity  $-1$  (that is spin anti-parallel to the momentum) in one system of reference it will have the same helicity in *all frames*, and of course the same is true for a  $+1$  helicity particle. In the minimal standard model, each neutrino flavor has two states, the one with helicity  $-1$  is called by convention “neutrino” and the one with helicity  $+1$  “antineutrino”. The question if the neutrino is a Dirac or Majorana particle is equivalent to the question if the reversal of the spin of a neutrino would turn it into an antineutrino or not. For a massless particle the spin reversal is impossible, and the question has no meaning. On the other hand if the neutrino has a non zero mass the question becomes not only meaningful but also natural and important. For a massive neutrino, with a Lorentz transformation, one

can “overtake” a neutrino produced in the laboratory with helicity  $-1$ , and study its behaviour in a new reference frame where it has the opposite helicity. If the boosted frame the neutrino behaves as a non-interacting singlet under the  $SU(2) \otimes U(1)$  group it is the component of a four state Dirac spinor; if it behaves as an antineutrino it is the component of a two state Majorana spinor.

The possibility that the neutrino is a Majorana particle has suggested what is probably the most interesting explanation of the smallness of the neutrino mass, the “seesaw” mechanism. In the seesaw mechanism ([93]) (discussing for simplicity one single flavor) a four-state Dirac neutrino is split by “Majorana mass terms” into a pair of two-states Majorana neutrinos ( $\nu$  and  $N$ ). One of these Majorana neutrinos (the state  $N$ ) becomes very massive taking a mass  $m_N \sim M$  of the same order as a high mass scale  $M$  characteristic of some new physics beyond the range of current experiments (for example a Grand Unification scale), while the other Majorana neutrino, that is identified with the observed light neutrinos, obtains a light mass  $m_\nu$  that is of order  $m_\nu \sim m_D^2/M$  where  $m_D$  is the Dirac mass characteristic of the other fermions in the same generation. So the reason why the neutrino is light is that it is associated with a very massive particle, in the same way as in the game of the seesaw (see Fig. 46) a massive participant will push “up” the other one.

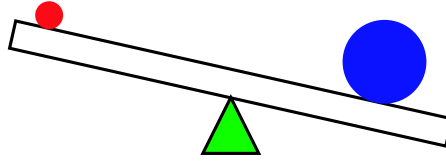


Fig. 46: Scheme of a see-saw.

A technical and detailed description of this mechanism is beyond the scope of these lectures (see [10,4] for more discussion), however the basic formulae in the model are very simple and instructive. A 4-components Dirac spinor can be represented as the combination of a pair of two-components spinors (the left-handed and right-handed part). In the standard (Weyl or chiral representation) one has:

$$\psi = \begin{pmatrix} \psi_L \\ \psi_R \end{pmatrix}, \quad (195)$$

where  $\psi_{L,R}$  are the two components Weyl spinors with left and right chirality. The operation of particle–antiparticle conjugation for a Dirac spinor corresponds to  $\psi \rightarrow \psi^c$  with:

$$\psi^c = C \bar{\psi}^T = [i\gamma^2\gamma^0] \bar{\psi}^T = i\gamma^2\psi^* = \begin{pmatrix} +i\sigma^2 \psi_R^* \\ -i\sigma^2 \psi_L^* \end{pmatrix}, \quad (196)$$

where  $\bar{\psi} = \psi^\dagger\gamma^0$ , the asterisk indicates complex conjugation, and we have used the explicit form of the Dirac matrices in the chiral representation and  $\sigma^2$  is the second one of the three Pauli matrices. Note that the conjugate of a left-handed spinor has only a right-handed component and viceversa, in fact particle–antiparticle conjugation transform a left (right) handed particle in a right (left) handed anti-particle; it is also easy to verify that  $(\psi^c)^c = \psi$ . The standard Dirac mass term in the Lagrangian has the form:

$$-\mathcal{L}_{\text{mass}}^{\text{Dirac}} = m_D \bar{\psi} \psi = m_D [(\psi_L)^\dagger \psi_R + (\psi_R)^\dagger \psi_L] \quad (197)$$

and combines the left and right handed parts of the spinor. A Majorana particle with only two degrees of freedom is described by one single Weyl spinor, and therefore a Dirac mass term such as (197) cannot

exist, however one can still construct a different mass term. If  $\psi_L$  is a left-handed spinor, one can obtain an object that transform as a right handed one as:  $(\psi_L)^c = -i\sigma^2 \psi_L^*$ . Note that one can then represent a Majorana spinor also as a 4-component object as:

$$\psi_M = \begin{pmatrix} \psi_L \\ -i\sigma^2 \psi_L^* \end{pmatrix} = \begin{pmatrix} \psi_L \\ (\psi_L)^c \end{pmatrix}. \quad (198)$$

This form has obviously only two independent components and under a charge conjugation operation (as described in equation (196)) one has  $(\psi_M)^c = \psi_M$ . A mass term with a single Weyl spinor (left or right-handed) can then be constructed as:

$$-\mathcal{L}_{\text{mass}}^{\text{Majorana}} = \frac{m_M}{2} \{ [(\psi_L)^c]^\dagger \psi_L + \text{h.c.} \} = \frac{m_M}{2} [(\psi_L)^T i\sigma^2 \psi_L + \text{h.c.}]. \quad (199)$$

Such a Majorana mass term violates (by two units) the conservation of the “charges” associated to the fermion considered, therefore it is only possible for “neutral” particles. Since neutrinos have no known charges, in principle they can have a Dirac mass term *and* a Majorana mass term. One can write this combination in matrix form as:

$$-\mathcal{L}_{\text{mass}}^\nu = \frac{1}{2} [\nu_L \quad (\nu_R)^c] C \begin{pmatrix} m_{M,L} & m_D \\ m_D & m_{M,R} \end{pmatrix} \begin{bmatrix} \nu_L \\ (\nu_R)^c \end{bmatrix} + \text{h.c.}, \quad (200)$$

where we have included a Dirac mass term, and two Majorana masses for the left and right component. Now it is possible to observe that:

- [1] The Dirac mass term can be naturally expected to be of the same order of magnitude as for the other fermions in the family.
- [2] The mass term  $m_{M,L}$  is small ( $m_{M,L} \ll m_D$ ), because it can be generated only by a triplet of Higgs scalars, that is absent in the standard model.
- [3] A right-handed neutrino is completely neutral under the standard-model gauge group, and therefore it can have any mass at all without breaking the gauge symmetry. In other words the mass  $m_{M,R}$  is not connected to the symmetry breaking scale ( $v = 246$  GeV) of  $SU(2) \otimes U(1)$  but is associated to a different higher mass scale  $M$  (connected for example with unification).

We therefore have a mass matrix of type:

$$\mathcal{M} \simeq \begin{pmatrix} 0 & m_D \\ m_D & M \end{pmatrix}. \quad (201)$$

This matrix can be diagonalized, obtaining two eigenvalues that are approximately  $M$  and  $-m_D^2/M$  (the minus sign is irrelevant and can be reabsorbed by a redefinition of the neutrino field). The two eigenvectors are two physical Majorana Particles with masses  $m_N \simeq M$  and  $m_\nu \simeq m_D^2/M$ . In summary we have used two ingredients: (i) the possibility to include a Majorana like mass term, and (ii) the existence of a large mass scale  $M$ , to obtain the result that the neutrino splits naturally into two Majorana states one very massive and one very light. As an illustration, one could extract a new mass scale from the atmospheric neutrino data using :

$$|\Delta m_{\text{atm}}^2| \simeq m_3^2 - m_1^2 \simeq m_3^2 \simeq \left( \frac{m_{\text{top}}^2}{M} \right)^2, \quad (202)$$

obtaining:

$$M \sim \frac{m_{\text{top}}^2}{\sqrt{|\Delta m_{\text{atm}}^2|}} \sim 0.6 \times 10^{15} \text{ GeV}, \quad (203)$$

that is close to the Grand Unification scale<sup>16</sup>.

More in general, considering the case with  $n$  generations of neutrinos, the mass matrix (201) becomes of order  $(2n \times 2n)$  (each entry has 2 components). The diagonalization of this matrix results in  $n$  light Majorana neutrinos and  $n$  super heavy ones, however now the light neutrinos are mixed with each other (with negligible admixtures with the heavy ones of order  $m_D/M$ ). The mixing clearly depends on various assumptions about the masses. Can this procedure reproduce the patterns of mixing observed in nature? The original predictions of lepton mixing in the framework of the seesaw model predicted that in analogy with the quark sector, the mixing between light neutrinos would be small, and the experimental results came as big surprise for (essentially all) the theory community. It is now understood that the seesaw model can predict also large mixing. Several non-seesaw models for the neutrino masses also exist, also making use of physics beyond the standard model. This is a very active field of research that cannot be summarized here (see for example [93] for a discussion and additional references). We list below some possible questions for model builders:

- [1] Why some of the  $\nu$  mixing angles are large while all quark mixing angles small?
- [2] Why two of the  $\nu$  angles are (probably) large while one ( $\theta_{13}$  is small)?
- [3] Why  $\theta_{23}$  is so close to the “maximal” value of  $45^\circ$ ? How close it is to this special value?
- [4] How large is  $\theta_{13}$ ?
- [5] Are the neutrino masses nearly degenerate with small splittings or “hierarchical”?
- [6] Is the ordering of the neutrino masses “normal” (with the state  $\nu_1$  that is prevalently  $e$ -like as the lightest state) or “inverted”?
- [7] Is the phase  $\delta$  predictable?

Research on these (and other) questions is very active, and hopefully the answers will shed light on the physics of unification.

## 14. CONCLUSIONS

The field of neutrino Physics has lived during the last decade a period of remarkable developments, and the perspectives for future studies are exciting. Future solar and long-baseline experiments will provide new and important knowledge, and should determine the neutrino squared mass differences and mixing; double beta decay studies and/or cosmological studies can also determine the absolute scale of the  $\nu$  masses. Neutrinos may also bring us new surprises, as they have done several times in the past, revealing some new properties, or the existence of additional states. Theoretically, the challenge of understanding the deeper meaning of the neutrino properties in a unification scheme remains an open problem of fundamental importance.

## Acknowledgments

It was a great pleasure to participate to the CLAF school, and I'm very grateful to the students and the organizers for the stimulating and pleasant atmosphere. A special thanks to prof. Bernard Marechal, Maurizio Lusignoli, Carlo Bernardini and Andrea Donini for criticism and discussions.

---

<sup>16</sup>Replacing  $m_{\text{top}}$  with  $m_\tau$  reduces the scale  $M$  by 4 orders of magnitude to  $M \simeq 6 \times 10^{11}$  GeV, and one can speculate about the significance of this new mass scale

## References

- [1] B. Pontecorvo, *Sov. Phys. JETP* **26** (1968) 984 [Zh. Eksp. Teor. Fiz. **53**, 1717 (1968)].
- [2] N. Cabibbo, *Phys. Rev. Lett.* **10** (1963) 531;  
M. Kobayashi and T. Maskawa, *Prog. Theor. Phys.* **49** (1973) 652.
- [3] Z. Maki, M. Nakagawa and S. Sakata, *Prog. Theor. Phys.* **28** (1962) 870.
- [4] C.W. Kim and A. Pevsner, “*Neutrinos in Physics and Astrophysics*”, Harwood Academic Press, (1993).
- [5] R.N. Mohapatra and P.B. Pal, “*Massive Neutrinos in Physics and Astrophysics. Second Edition*”, World Sci. Lect. Notes Phys. **60** (1998) 1.
- [6] F. Boehm and P. Voegel, “*Physics of Massive Neutrinos*”, Cambridge University Press, (1992).
- [7] W.C. Haxton and B.R. Holstein, *Am. J. Phys.* **68** (2000) 15, [hep-ph/9905257].
- [8] P. Fisher, B. Kayser, K.S. McFarland, *Ann. Rev. Nucl. Part. Sci.* **49** (1999) 481, [hep-ph/9906244].
- [9] G.G. Raffelt and W. Rodejohann, hep-ph/9912397.
- [10] E.Kh. Akhmedov, hep-ph/0001264.
- [11] B. Kayser, hep-ph/0104147.
- [12] S.M. Bilenky, physics/0103091.
- [13] M.C. Gonzalez-Garcia and Y. Nir, hep-ph/0202058.
- [14] <http://www.to.infn.it/giunti/NU/>
- [15] <http://www.hep.anl.gov/ndk/hypertext/nuindustry.html>
- [16] E. Fermi, “*Versuch einer Theorie der  $\beta$ -Strahlen*”, *Z. Phys.* **88** (1934) 161.
- [17] C.L. Cowan, F. Reines, F.B. Harrison, E.C. Anderson and F.N. Hayes, *Science* **124** (1956) 103.
- [18] G. Danby, *et al. Phys. Rev. Lett.* **9** (1962) 36.
- [19] D.E. Groom *et al.* [Particle Data Group Collaboration], *Eur. Phys. J.* **C15** (2000) 1.
- [20] WMAP coll., C.L. Bennett *et al.*, astro-ph/0302207; D.N. Spergel *et al.*, astro-ph/0302209.
- [21] R. Foot, R.R. Volkas *Phys. Rev.* **D52** (1995) 6595, [hep-ph/9505359].
- [22] A.D. Dolgov and Y.B. Zeldovich, *Rev. Mod. Phys.* **53** (1981) 1.
- [23] M.S. Turner and J.A. Tyson, *Rev. Mod. Phys.* **71** (1999) S145, [astro-ph/9901113].
- [24] J.R. Primack, astro-ph/0112255.
- [25] D.N. Schramm and M.S. Turner, *Rev. Mod. Phys.* **70** (1998) 303, [astro-ph/9706069].

- [26] O. Elgaroy *et al.*, astro-ph/0204152.
- [27] <http://www.sdss.org/>
- [28] A.D. Dolgov, *Phys. Rep.* **370** (2002) 333, [hep-ph/0202122].
- [29] G.G. Raffelt, hep-ph/0201099.
- [30] K.S. Hirata *et al.* (Kamiokande Collaboration), *Phys. Rev.* **D38** (1988) 448; C.B. Bratton *et al.*, (IMB Collaboration), *Phys. Rev.* **D37** (1988) 3361.
- [31] R.S. Raghavan *et al.*, *Phys. Rev. Lett.* **80** (1998) 635.
- [32] F. Halzen, astro-ph/0103195.
- [33] J.G. Learned and K. Mannheim, *Ann. Rev. Nucl. Part. Sci.* **50** (2000) 679.
- [34] T.K. Gaisser, F. Halzen and T. Stanev, *Phys. Rept.* **258** (1995) 173, [Erratum-ibid. **271** (1995) 355], [hep-ph/9410384].
- [35] A. Roberts, *Rev. Mod. Phys.* **64** (1992) 259.
- [36] F. Halzen, astro-ph/0111059.
- [37] C. Giunti and C.W. Kim, hep-ph/0011074; see also <http://www.to.infn.it/giunti/neutrino/qmno/>
- [38] C. Giunti, *Mod. Phys. Lett.* **A16** (2001) 2363, [hep-ph/0104148].
- [39] C. Giunti, hep-ph/0105319.
- [40] M. Zralek, *Acta Phys. Polon.* **B29** (1998) 3925, hep-ph/9810543.
- [41] Y. Srivastava, A. Widom and E. Sassaroli, *Eur. Phys. J.* **C2** (1998) 769.
- [42] S.P. Mikheyev and A.Y. Smirnov, *Sov. Jour. Nucl. Phys.* **42** (1985) 913; L. Wolfenstein, *Phys. Rev.* **D17** (1978) 2369.
- [43] T.K. Kuo and J. Pantaleone, *Rev. Mod. Phys.* **61** (1989) 937.
- [44] T. Kajita and Y. Totsuka, *Rev. Mod. Phys.* **73** (2001) 85.
- [45] P. Lipari, *Nucl. Phys. Proc. Suppl.* **91** (2001) 159.
- [46] T.K. Gaisser and M. Honda, hep-ph/0203272.
- [47] T.K. Gaisser and T. Stanev, *Phys. Rev.* **D57** (1998) 1977, [astro-ph/9708146].
- [48] K.S. Hirata *et al.* [Kamiokande Collaboration], *Phys. Lett.* **B280** (1992) 146; E.W. Beier *et al.*, [Kamiokande Collaboration], *Phys. Lett.* **B283** (1992) 446.
- [49] Y. Fukuda *et al.* [Kamiokande Collaboration], *Phys. Lett.* **B335** (1994) 237.
- [50] Kamiokande Collaboration, *Phys. Lett.* **B335** (1994) 237.
- [51] Super-Kamiokande Collaboration, *Phys. Rev. Lett.* **81** (1998) 1562, [hep-ex/9807003].

- [52] SuperKamiokande Collaboration, *Phys. Rev. Lett.* **82** (1999) 2644, [hep-ex/9812014].
- [53] Super-Kamiokande Collaboration, *Phys. Rev. Lett.* **85** (2000) 3999, [hep-ex/0009001].
- [54] C.V. Achar *et al.*, *Phys. Lett.* **18** (1965) 196; *Phys. Lett.* **19** (1965) 78;  
F. Reines *et al.*, *Phys. Rev. Lett.* **15** (1965) 429.
- [55] Baksan collaboration, *Nucl. Phys. Proc. Suppl.* **70** (1999) 371.
- [56] Frejus Collaboration, *Phys. Lett.* **B245** (1990) 305; *Z. Phys.* **C66** (1995) 417.
- [57] MACRO Collaboration, *Phys. Lett.* **B434** (1998) 451, [hep-ex/9807005].
- [58] MACRO Collaboration, *Phys. Lett.* **B478** (2000) 5.
- [59] MACRO Collaboration, *Phys. Lett.* **B517** (2001) 59, [hep-ex/0106049]
- [60] P. Lipari and M. Lusignoli, *Phys. Rev.* **D60** (1999) 013003;  
G.L. Fogli, E. Lisi, A. Marrone, and G. Scioscia, *Phys. Rev.* **D59** (1999) 117303.
- [61] G.L. Fogli, E. Lisi, A. Marrone and D. Montanino, hep-ph/0009269.
- [62] V. Barger, *et al.*, *Phys. Lett.* **B462** (1999) 109.
- [63] M. Gasperini, *Phys. Rev.* **D38** (1988) 2635.
- [64] S. Coleman and S.L. Glashow, *Phys. Lett.* **B405** (1997) 249;  
S.L. Glashow *et al.*, *Phys. Rev.* **D56** (1997) 2433.
- [65] M.C. Gonzalez-Garcia *et al.*, *Phys. Rev. Lett.* **82** (1999) 3202;  
M.M. Guzzo *et al.*, *Funchal, Nucl. Phys. (Proc. Suppl.)* **B87** (2000) 201.
- [66] R. Barbieri, P. Creminelli, and A. Strumia, hep-ph/0002199.
- [67] G.R. Dvali and A.Y. Smirnov, *Nucl. Phys.* **B563** (1999) 63, [hep-ph/9904211].
- [68] K.R. Dienes, E. Dudas and T. Gherghetta, *Nucl. Phys.* **B557** (1999) 25, [hep-ph/9811428];  
N. Arkani-Hamed, S. Dimopoulos, G.R. Dvali and J. March-Russell, hep-ph/9811448;  
Y. Grossman and M. Neubert, *Phys. Lett.* **B474** (2000) 361, [hep-ph/9912408].
- [69] E. Lisi, A. Marrone and E. Montanino, *Phys. Rev. Lett.* **85** (2000) 1166.
- [70] Donald Clayton “*Principles of Stellar Evolution and Nucleosynthesis*”, The University of Chicago Press, 1983.
- [71] J.N. Bahcall, “*Neutrino Astrophysics*”, Cambridge University Press, 1989.
- [72] J.N. Bahcall, M.H. Pinsonneault and S. Basu, *Ap.J.* **555** (2001) 990, [astro-ph/0010346]
- [73] J. Bahcall home page: <http://www.sns.ias.edu/jnb/>
- [74] S. Turck-Chièze and I. Lopes, *Ap.J.* **408** (1993) 347.
- [75] B.T. Cleveland *et al.*, *Ap.J.* **496** (1998) 505.

- [76] GALLEX Collaboration, *Phys. Lett.* **B447** (1999) 127.
- [77] SAGE Collaboration, *Phys. Rev.* **C60** (1999) 055801.
- [78] E. Bellotti et al. (GNO Collaboration) in *Proc. of the XIX International Conference on Neutrino Physics Astrophysics*, Sudbury, Canada, June 2000 (Amsterdam: Elsevier Science Publishers).
- [79] K.S. Hirata *et al.*, [Kamiokande Collaboration], *Phys. Rev.* **D44** (1991) 2241, [Erratum-*ibid.* **D45** (1991) 2170].
- [80] K.S. Hirata *et al.* [Kamiokande Collaboration], *Phys. Rev. Lett.* **65** (1990) 1297.
- [81] K.S. Hirata *et al.*, [Kamiokande Collaboration], *Phys. Rev. Lett.* **65** (1990) 1301.
- [82] Kamiokande Collaboration, *Phys. Rev. Lett.* **77** (1996) 1683.
- [83] Super-Kamiokande Collaboration, *Phys. Rev. Lett.* **86** (2001) 5651, [hep-ex/0103032]; *Phys. Rev. Lett.* **86** (2001) 5656, [hep-ex/0103033]; *Phys. Lett.* **B539** (2002) 179, [hep-ex/0205075].
- [84] M.B. Smy, [Super-Kamiokande collaboration], hep-ex/0208004.
- [85] SNO collaboration, *Phys. Rev. Lett.* **87** (2001) 071301, [nucl-ex/0106015].
- [86] SNO collaboration, nucl-ex/0204008.
- [87] SNO collaboration, nucl-ex/0204009.
- [88] C. Bemporad, G. Gratta and P. Vogel, hep-ph/0107277.
- [89] M. Apollonio *et al.* [CHOOZ Collaboration], *Phys. Lett.* **B466** (1999) 415, [hep-ex/9907037].
- [90] F. Boehm *et al.*, *Phys. Rev.* **D641** (2001) 11200, [hep-ex/0107009].
- [91] KamLand collaboration, hep-ex/0212021.
- [92] G.L. Fogli *et al.*, hep-ph/0212127.
- [93] G. Altarelli and F. Feruglio, hep-ph/9905536; G. Altarelli, hep-ph/0106085.
- [94] P. Astier *et al.*, [NOMAD Collaboration], *Nucl. Phys.* **B611** (2001) 3, [hep-ex/0106102].
- [95] L. Ludovici (for the Chorus collaboration), *Nucl. Phys. Proc. Suppl.* **91** (2001) 177.
- [96] LSND Collaboration, *Phys. Rev. Lett.* **77** (1996) 3082; *ibid.* **81** (1998) 1774.
- [97] KARMEN Collaboration, hep-ex/0203021.
- [98] MiniBooNE Collaboration, *Nucl. Phys. Proc. Suppl.* **91** (2000) 210, [hep-ex/0009056]; See the MiniBooNE home page at <http://www-boone.fnal.gov/>
- [99] K2K Collaboration, *Phys. Lett.* **B511** (2001) 178, [hep-ex/0212007].
- [100] See the MINOS home page: <http://www-numi.fnal.gov/>
- [101] See the CNGS home page: <http://proj-cngs.web.cern.ch/proj-cngs/>

- [102] H.V. Klapdor-Kleingrothaus, H. Päs, and A.Y. Smirnov, *Phys. Rev.* **D63** (2001) 073005, [hep-ph/0003219].
- [103] H.V. Klapdor-Kleingrothaus *et al.*, hep-ph/0103062.
- [104] H.V. Klapdor-Kleingrothaus, A. Dietz, H.L. Harney and I.V. Krivosheina, *Mod. Phys. Lett.* **A16** (2002) 2409, [hep-ph/0201231].
- [105] F. Feruglio, A. Strumia and F. Vissani, hep-ph/0201291.
- [106] C.E. Aalseth *et al.*, hep-ex/0202128.

# Neutrino Physics

P. Hernández

IFIC, Universidad de València and CSIC, E-46071 Valencia, Spain

## Abstract

This is the writeup of the lectures on neutrino physics delivered at various schools: TASI and Trieste in 2013 and the CERN-Latin American School in 2015. The topics discussed in this lecture include: general properties of neutrinos in the SM, the theory of neutrino masses and mixings (Dirac and Majorana), neutrino oscillations both in vacuum and in matter, as well as an overview of the experimental evidence for neutrino masses and of the prospects in neutrino oscillation physics. We also briefly review the relevance of neutrinos in leptogenesis and in beyond-the-Standard-Model physics.

## Keywords

Neutrino; particle physics; lectures; neutrino oscillations; mixing; standard model.

## 1 Introduction

The history of neutrinos is tightly linked to that of the Standard Model. The discovery of neutrinos and the measurement of their tiny masses has been a scientific *tour de force*.

Neutrinos made their appearance at the beginning of the 20th century as *dark* particles in radioactive  $\beta$ -decay. In this process a nucleus undergoes a transition

$${}_{Z}^{A}X \rightarrow {}_{Z+1}^{A}X' + e^- \quad (1)$$

emitting an electron, which, by energy conservation, should have an energy equal to the difference of the parent and daughter nuclear masses,  $Q$ , see Fig. 1.

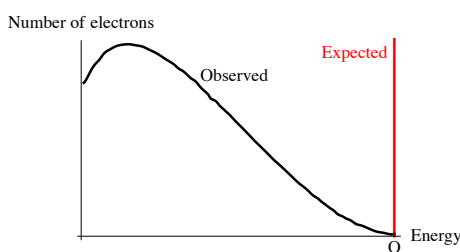


**Fig. 1:** Electron spectrum of  $\beta$ -decay.

The spectrum of the electrons was measured to be instead continuous with an end-point at  $Q$ . It took almost 20 years to come up with an explanation to this apparent violation of energy conservation. W. Pauli called for a *desperate remedy*, proposing that in the decay, a neutral and relatively light particle was being emitted together with the electron and escaped undetected. In that case the spectrum of the electron would indeed be continuous since only the sum of the energy of the electron and the phantom particle should equal  $Q$ . The dark particle got an Italian name: *neutrino* in honour of E. Fermi, who was among the first to take seriously Pauli's hypothesis, from which he constructed the famous theory of  $\beta$ -decay [1]. In this theory, the interaction responsible for  $\beta$ -decay can be depicted as in Fig. 2,

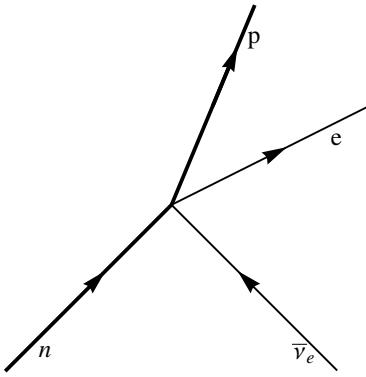


**Fig. 2:** Fermi four-fermion coupling responsible for  $\beta$ -decay.

a four-fermion interaction with strength given by  $G_F$ , the fermi constant. Such interaction implies that neutrinos should also scatter off matter through the inverse beta process,  $\bar{\nu} p \rightarrow n e^+$ . Bethe and Pearls [2] estimated the cross section for such process to be

$$\sigma_{\bar{\nu}} \leq 10^{-44} \text{ cm}^2, \quad E_{\bar{\nu}} \simeq 2 \text{ MeV} \quad (2)$$

and concluded that "*it is absolutely impossible to observe processes of this kind*". Indeed this tiny cross section implies that a neutrino has a mean free path of thousands of light-years in water.

Pontecorvo [3] however was among the first to realise that it was not so hopeless. One could get a few events per day in a ton-mass scale detector with a neutrino flux of  $10^{11} \nu/\text{cm}^2/\text{s}$ . Such is the neutrino flux of a typical nuclear reactor at a few tens of meters. Reines and Cowen (RC) succeeded [4, 5]. They were able to detect neutrinos via inverse beta decay in a very massive detector thanks to the extremely robust and clean signal which combines the detection of the positron and the neutron in delayed coincidence, see Fig. 3. This experiment not only lead to the discovery of anti-neutrinos, but introduced a detection technique that is still being used today in state-of-the-art reactor neutrino experiments, that continue to make discoveries in neutrino physics.

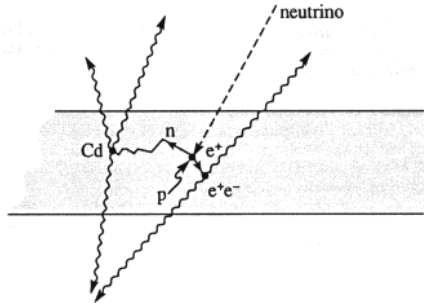


**Fig. 3:** Detection technique in the Reines-Cowan experiment.

Soon after anti-neutrinos were discovered, it was realised that they come in flavours. The muon had been discovered in cosmic rays much earlier, but it took a long time to understand that this particle was a heavier version of the electron and not the pion. The analogous of the  $\beta$ -process involving muons is pion decay

$$\pi^- \rightarrow \mu^- \bar{\nu}_\mu. \quad (3)$$

It was understood that also in this case a neutrino was being emitted but that such neutrino, accompanying the  $\mu$ , had a different identity to that in  $\beta$ -decay. Since the energies involved in this process are higher than in  $\beta$ -decay and neutrino cross-sections grow fast with energy in the Fermi theory, it would actually be easier to detect this new type of neutrinos.

In 1962 Lederman, Schwartz and Steinberger (LSS) achieved this goal by creating the first accelerator neutrino beam [6]. In such a beam, an boosted proton beam hits a target producing pions and other hadrons that decay into neutrinos and other particles, mimicking what happens in cosmic rays. If a thick shield intercepts the beam, all particles except the neutrinos can be stopped, see Fig. 4. A neutrino detector is located behind the shield. A neutrino event will be seen from the appearance of a muon in the detector. Again this was such a great idea that we are still making discoveries with the modern versions of the LSS experiment, in the so-called conventional accelerator neutrino beams.

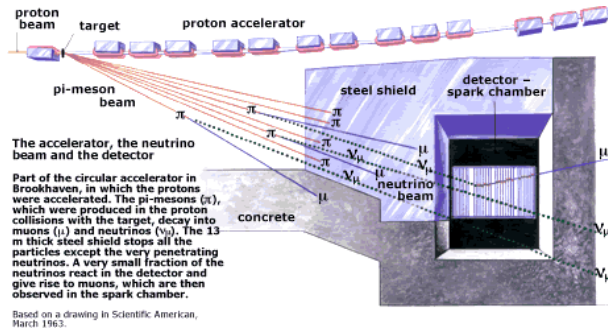


**Fig. 4:** Lederman, Schwartz, Steinberger experiment.

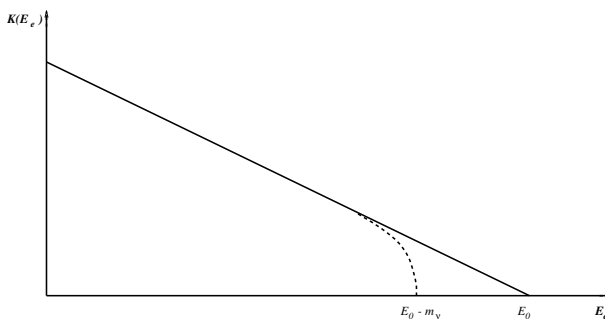
Kinematical effects of neutrino masses were searched for by measuring very precisely the end-point of the lepton energy spectrum in weak decays, that gets modified if neutrinos are massive. In particular the most stringent limit is obtained from tritium  $\beta$ -decay for the "electron" neutrino:



Fig. 5 shows the effect of a neutrino mass in the end-point electron energy spectrum in this decay. The best limit has been obtained by the Mainz and Troitsk experiments. The PDG combination gives [7]:

$$m_{\nu_e} < 2 \text{ eV}(95\% \text{ CL}) . \quad (5)$$

The direct limits from processes involving  $\mu, \tau$  leptons are much weaker. The best limit on the  $\nu_\mu$  mass ( $m_{\nu_\mu} < 170 \text{ keV}$  [8]) was obtained from the end-point spectrum of the decay  $\pi^+ \rightarrow \mu^+ \nu_\mu$ , while that



**Fig. 5:** Effect of a neutrino mass in the end-point of the lepton energy spectrum in  $\beta$  decay.

$(\mathbf{1}, \mathbf{2})_{-\frac{1}{2}}$	$(\mathbf{3}, \mathbf{2})_{-\frac{1}{6}}$	$(\mathbf{1}, \mathbf{1})_{-1}$	$(\mathbf{3}, \mathbf{1})_{-\frac{2}{3}}$	$(\mathbf{3}, \mathbf{1})_{-\frac{1}{3}}$
$\begin{pmatrix} \nu_e \\ e \end{pmatrix}_L$	$\begin{pmatrix} u^i \\ d^i \end{pmatrix}_L$	$e_R$	$u_R^i$	$d_R^i$
$\begin{pmatrix} \nu_\mu \\ \mu \end{pmatrix}_L$	$\begin{pmatrix} c^i \\ s^i \end{pmatrix}_L$	$\mu_R$	$c_R^i$	$s_R^i$
$\begin{pmatrix} \nu_\tau \\ \tau \end{pmatrix}_L$	$\begin{pmatrix} t^i \\ b^i \end{pmatrix}_L$	$\tau_R$	$t_R^i$	$b_R^i$

**Table 1:** Irreducible fermionic representations in the Standard Model:  $(d_{SU(3)}, d_{SU(2)})_Y$ .

on the  $\nu_\tau$  mass was obtained at LEP ( $m_{\nu_\tau} < 18.2$  MeV [9]) from the decay  $\tau \rightarrow 5\pi\nu_\tau$ . Neutrinos in the SM were therefore conjectured to be massless.

## 2 Neutrinos in the Standard Model

The Standard Model (SM) is a gauge theory based on the gauge group  $SU(3) \times SU(2) \times U_Y(1)$ . All elementary particles arrange in irreducible representations of this gauge group. The quantum numbers of the fermions  $(d_{SU(3)}, d_{SU(2)})_Y$  are listed in table 1.

Under gauge transformations neutrinos transform as doublets of  $SU(2)$ , they are singlets under  $SU(3)$  and their hypercharge is  $-1/2$ . The electric charge, given by  $Q = T_3 + Y$ , vanishes. They are therefore the only particles in the SM that carry no conserved charge.

The two most intriguing features of table 1 are its left-right or chiral asymmetry, and the three-fold repetition of family structures. Neutrinos have been essential in establishing both features.

### 2.1 Chiral structure of the weak interactions

The left and right entries in table 1 have well defined chirality, negative and positive respectively. They are two-component spinors or Weyl fermions, that is the smallest irreducible representation of the Lorentz group representing spin 1/2 particles. Only fields with negative chirality (i.e. eigenvalue of  $\gamma_5$  minus one) carry the  $SU(2)$  charge. For free fermions moving at the speed of light (i.e., massless), it is easy to see that the chiral projectors are equivalent to the projectors on helicity components:

$$P_{R,L} \equiv \frac{1 \pm \gamma_5}{2} = \frac{1}{2} \left( 1 \pm \frac{\mathbf{s} \cdot \mathbf{p}}{|p|} \right) + O\left(\frac{m_i}{E}\right), \quad (6)$$

where the helicity operator  $\Sigma = \frac{\mathbf{s} \cdot \mathbf{p}}{|p|}$  measures the component of the spin in the direction of the momentum. Therefore for massless fermions only the left-handed states (with the spin pointing in the opposite direction to the momentum) carry  $SU(2)$  charge. This is not inconsistent with Lorentz invariance, since for a fermion travelling at the speed of light, the helicity is the same in any reference frame. In other words, the helicity operator commutes with the Hamiltonian for a massless fermion and is thus a good quantum number.

The discrete symmetry under CPT (charge conjugation, parity, and time reversal), which is a basic building block of any Lorentz invariant and unitary quantum field theory (QFT), requires that for any left-handed particle, there exists a right-handed antiparticle, with opposite charge, but the right-handed particle state may not exist. A Weyl fermion field represents therefore a particle of negative helicity and an antiparticle with positive one.

Parity however transforms left and right fields into each other, thus the left-handedness of the weak interactions implies that parity is maximally broken in the SM. The breaking is nowhere more obvious than for neutrinos where the parity partner of the neutrino does not exist. All the remaining fermions in the SM come in parity pairs, albeit with different  $SU(2) \times U(1)$  charges. Since this gauge symmetry is spontaneously broken, the left and right fields combine into massive Dirac fermions, that is a four component representation of the Lorentz group and parity, which represents a particle and an antiparticle with either helicity.

The SM resolved the Fermi interaction as being the result of the exchange of the  $SU(2)$  massive  $W$  boson as in Fig. 6.

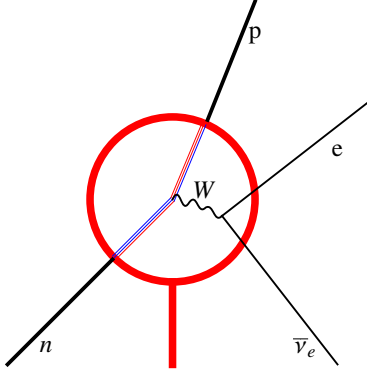


**Fig. 6:**  $\beta$ -decay process in the SM.

Neutrinos interact in the SM via charged and neutral currents:

$$\mathcal{L}_{SM} = \frac{g}{\sqrt{2}} \sum_{\alpha} \bar{\nu}_{\alpha} \gamma_{\mu} P_L l_{\alpha} W_{\mu}^+ - \frac{g}{2 \cos \theta_W} \sum_{\alpha} \bar{\nu}_{\alpha} \gamma_{\mu} P_L \nu_{\alpha} Z_{\mu}^+ + h.c. \quad (7)$$

The weak current is therefore  $V-A$  since it only couples to the left fields:  $\gamma_{\mu} P_L \propto \gamma_{\mu} - \gamma_{\mu} \gamma_5$ . This structure is clearly seen in the kinematics of weak decays involving neutrinos, such as the classic example of pion decay to  $e \bar{\nu}_e$  or  $\mu \bar{\nu}_{\mu}$ . In the limit of vanishing electron or muon mass, this decay is forbidden, because the spin of the initial state is zero and thus it is impossible to conserve simultaneously momentum and angular momentum if the two recoiling particles must have opposite helicities, as shown in Fig. 7. Thus the ratio of the decay rates to electrons and muons, in spite of the larger phase space in the former, is strongly suppressed by the factor  $\left(\frac{m_e}{m_{\mu}}\right)^2 \sim 2 \times 10^{-5}$ .

Another profound consequence of the chiral nature of the weak interaction is anomaly cancellation. The chiral coupling of fermions to gauge fields leads generically to inconsistent gauge theories due to chiral anomalies: if any of the diagrams depicted in Fig. 8 is non-vanishing, the weak current is conserved at tree level but not at one loop, implying a catastrophic breaking of gauge invariance. Anomaly cancellation is the requirement that all these diagrams vanish, which imposes strong constraints on the hypercharge assignments of the fermions in the SM, which are *miraculously* satisfied:

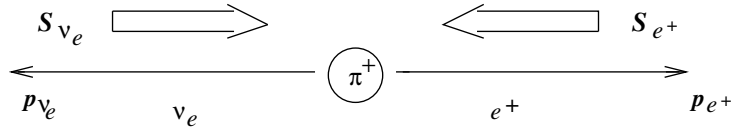


**Fig. 7:** Kinematics of pion decay.

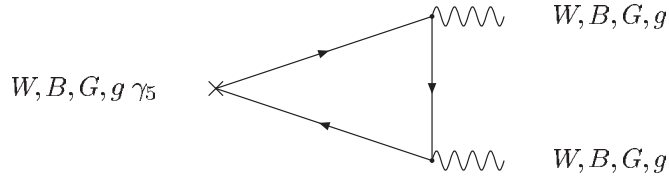


**Fig. 8:** Triangle diagrams that can give rise to anomalies.  $W, B, G$  are the gauge bosons associated to the  $SU(2), U_Y(1), SU(3)$  gauge groups, respectively, and  $g$  is the graviton.

$$\overbrace{\sum_{i=\text{quarks}}^{GGB} Y_i^L - Y_i^R} = \overbrace{\sum_{i=\text{doublets}}^{WWB} Y_i^L} = \overbrace{\sum_i^{Bgg} Y_i^L - Y_i^R} = \overbrace{\sum_i^{B^3} (Y_i^L)^3 - (Y_i^R)^3} = 0, \quad (8)$$

where  $Y_i^{L/R}$  are the hypercharges of the left/right components of the fermionic field  $i$ , and the triangle diagram corresponding to each of the sums is indicated above the bracket.

## 2.2 Family structure

Concerning the family structure, we know, thanks to neutrinos, that there are exactly three families in the SM. An extra SM family with quarks and charged leptons so heavy that cannot be produced, would also have massless neutrinos that would contribute to the invisible  $Z^0$  decay:

$$Z^0 \rightarrow \bar{\nu}_\alpha \nu_\alpha. \quad (9)$$

The invisible width of the  $Z^0$  has been measured at LEP with an impressive precision, as shown in Fig. 9. This measurement excludes any number of standard families different from three [7]:

$$N_\nu = \frac{\Gamma_{\text{inv}}}{\Gamma_{\bar{\nu}\nu}} = 2.984 \pm 0.008. \quad (10)$$

## 3 Massive Neutrinos

Neutrinos are ubiquitous in our surroundings. If we open our hand, it will be crossed each second by about  $\mathcal{O}(10^{12})$  neutrinos from the sun, about  $\mathcal{O}(10)$  from the atmosphere, about  $\mathcal{O}(10^9)$  from natural radioactivity in the Earth and even  $\mathcal{O}(10^{12})$  relic neutrinos from the Big Bang. In 1987, the Kamiokande detector in Japan observed the neutrino burst from a SuperNova that exploded in the Large Magellanic Cloud, at a distance of 168 thousand light years from Earth. For a few seconds, the supernova flux was of the same order of magnitude as the flux of solar neutrinos!

Using many of these sources as well as others man-made, a decade of revolutionary neutrino experiments have demonstrated that, for the time being, neutrinos are the less standard of the SM particles. They have tiny masses and this necessarily requires new degrees of freedom with respect to those in table 1.

A massive fermion necessarily has two states of helicity, since it is always possible to reverse the helicity of a state that moves at a slower speed than light by looking at it from a boosted reference frame. What is the right-handed state of the neutrino? It turns out there are two ways to proceed.

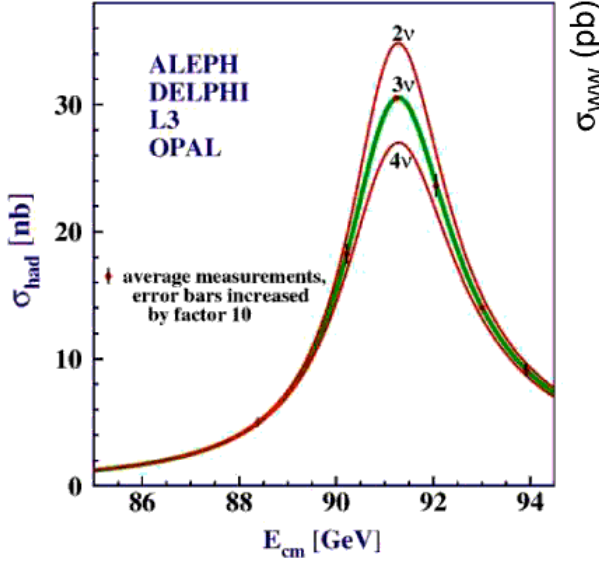


**Fig. 9:**  $Z^0$  resonance from the LEP experiments. Data are compared to the case of  $N_\nu = 2, 3$  and  $4$ .

Let us consider the case of free fermions. A four-component Dirac fermion can be made massive adding the following mass term to the Lagrangian:

$$-\mathcal{L}_m^{Dirac} = m\bar{\psi}\psi = m(\overline{\psi_L + \psi_R})(\psi_L + \psi_R) = m(\overline{\psi_L}\psi_R + \overline{\psi_R}\psi_L). \quad (11)$$

A Dirac mass term couples the left-handed and right-handed chiral components of the fermion field, and therefore this coupling vanishes identically in the case of a Weyl fermion.

Can one give a mass to a two-component Weyl fermion ? As first realized by Majorana, this indeed can be done with the following mass term:

$$-\mathcal{L}_m^{Majorana} = \frac{m}{2}\overline{\psi^c}\psi + \frac{m}{2}\overline{\psi}\psi^c = \frac{m}{2}\psi^T C\psi + \frac{m}{2}\bar{\psi}C\bar{\psi}^T, \quad (12)$$

where

$$\psi^c \equiv C\bar{\psi}^T = C\gamma_0\psi^*. \quad (13)$$

It is easy to check that the Majorana mass term satisfies the required properties:

- 1) It can be constructed with a two-component spinor or Weyl fermion: if  $\psi = P_L\psi \equiv (\psi_L, 0)$

$$\psi^T C\psi = \psi_L^T i\sigma_2 \psi_L, \quad (14)$$

and it does not vanish in the absence of the right chiral component.

- 2) It is Lorentz invariant. It is easy to show, using the properties of the gamma matrices that under a Lorentz transformation  $\psi$  and  $\psi^c$  transform in the same way,

$$\psi \rightarrow e^{-\frac{i}{4}\omega_{\mu\nu}\sigma^{\mu\nu}}\psi \equiv S(\Lambda)\psi, \quad \psi^c \rightarrow S(\Lambda)\psi^c, \quad (15)$$

with  $\sigma_{\mu\nu} \equiv \frac{i}{4}[\gamma_\mu, \gamma_\nu]$ , and therefore the bilinear  $\overline{\psi^c}\psi$  is Lorentz invariant.

- 3) The equation of motion derived from eq. (12) for a free majorana fermion has plane wave solutions satisfying the relativistic relation for a massive fermion:

$$E^2 - \mathbf{p}^2 = m^2.$$

In the SM none of the mass terms of eqs. (11) and (12) are gauge invariant. Spontaneous symmetry breaking allows to generate the Dirac mass term from Yukawa couplings for all fermions in the SM, while the Majorana mass term can only be generated for neutrinos.

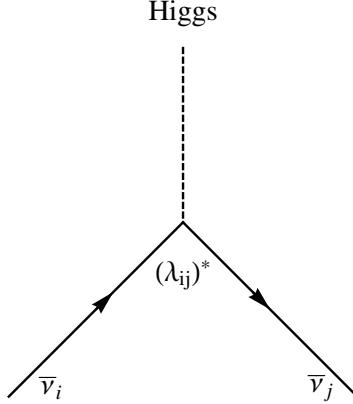


**Fig. 10:** Neutrino Yukawa coupling.

### 3.1 Massive Dirac neutrinos

We can enlarge the SM by adding a set of three right-handed neutrino,  $\nu_R$  states, with quantum numbers  $(1, 1)_0$ , ie singlets under all the gauge groups. A new Yukawa (Fig. 10) coupling of these new states with the lepton doublet is exactly gauge invariant and therefore can be added to the SM:

$$-\mathcal{L}_m^{Dirac} = \bar{L} \lambda \tilde{\Phi} \nu_R + \text{h.c.} \quad (16)$$

where  $L = (\nu l)$  is the lepton doublet,  $\tilde{\Phi} \equiv i\sigma_2 \phi^*$  and  $\phi$  is the Higgs field, with quantum numbers  $(\mathbf{1}, \mathbf{2})_{-\frac{1}{2}}$ . Upon spontaneous symmetry breaking the scalar doublet gets a vacuum expectation value  $\langle \tilde{\Phi} \rangle = (\frac{v}{\sqrt{2}} \ 0)$ , and therefore a neutrino Dirac mass term is generated

$$-\mathcal{L}_m^{Dirac} \rightarrow -\bar{\nu}_L \lambda \frac{v}{\sqrt{2}} \nu_R + \text{h.c.} \quad (17)$$

The neutrino mass matrix is proportional to the Higgs vev, in complete analogy to the remaining fermions:

$$m_\nu = \lambda \frac{v}{\sqrt{2}}. \quad (18)$$

There are two important consequences of Dirac neutrinos. First, there is a new hierarchy problem in the SM to be explained: why are neutrinos so much lighter than the remaining leptons, even those in the same family (see Fig. 11), if they get the mass in the same way? Secondly, an accidental global symmetry, lepton number L, that counts the number of leptons minus that of antilepton, remains exactly conserved at the classical level<sup>1</sup>, just as baryon number, B, is.

### 3.2 Massive Majorana neutrinos

Since the combination  $\bar{L}\tilde{\phi}$  is a singlet under all gauge groups, the Majorana-type contraction (see Fig. 12):

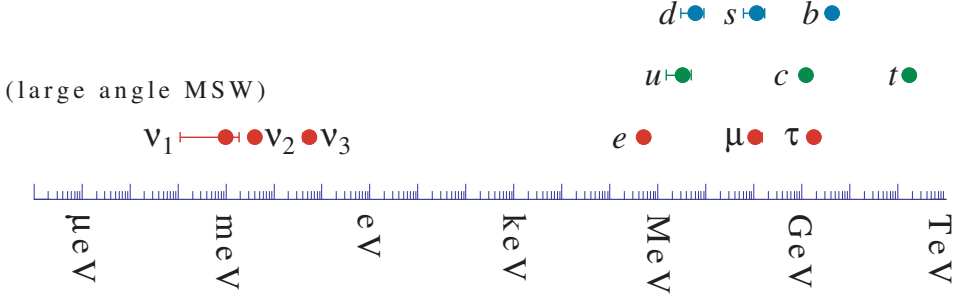
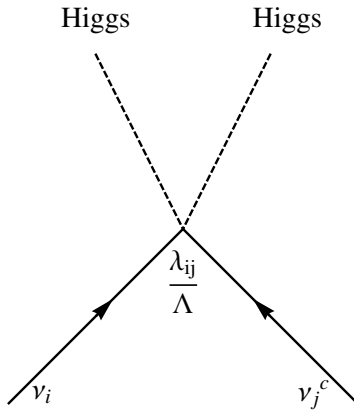
$$-\mathcal{L}_m^{Majorana} = \bar{L}\tilde{\phi} \alpha C \tilde{\phi}^T \bar{L}^T + \text{h.c.}, \quad (19)$$

is gauge invariant. This term, first written down by Weinberg [10], gives rise to a Majorana mass term for neutrinos upon spontaneous symmetry breaking:

$$-\mathcal{L}_m^{Majorana} \rightarrow \bar{\nu}_L \alpha \frac{v^2}{2} C \bar{\nu}_L^T + \text{h.c.}, \quad (20)$$

---

<sup>1</sup>As usual  $B + L$  is broken by the anomaly and only  $B - L$  remains exact at all orders.

**Fig. 11:** Fermion spectrum in the Standard Model.**Fig. 12:** Weinberg operator.

The neutrino mass matrix in this case is given by:

$$m_\nu = \alpha v^2. \quad (21)$$

The Weinberg operator has dimension 5, and therefore the coupling  $[\alpha] = -1$ . We can write it in terms of a dimensionless coupling as

$$\alpha = \frac{\lambda}{\Lambda}, \quad (22)$$

where  $\Lambda$  is a new physics scale, in principle unrelated to the electroweak scale.

The consequences of the SM neutrinos being massive Majorana particles are profound.

If the scale  $\Lambda$  is much higher than the electroweak scale  $v$ , a strong hierarchy between the neutrino and the charged lepton masses arises naturally. If all dimensionless couplings  $\lambda$  are of the same order, neutrino masses are suppressed by a factor  $v/\Lambda$  with respect to the charged fermions. On the other hand, Weinberg's operator violates lepton number L and provides a new seed for generating the matter/antimatter asymmetry in the Universe as we will see.

Even though the Majorana mechanism to generate neutrino masses does not involve any extra degree of freedom with respect to those in the SM, the existence of the Weinberg coupling implies that cross sections involving for example the scattering of neutrinos and the higgs will grow with energy, ultimately violating unitarity. The situation is analogous to that of the Fermi interaction of Fig. 2. The SM resolved this interaction at higher energies as being the result of the interchange of a heavy vector boson, Fig. 6. The Majorana coupling, if it exists, should also represent the effect at low-energies of the exchange of one or more unknown massive states. What those states are remains one of the most interesting open questions in neutrino physics.

Finally, it is interesting to note that the anomaly cancellation conditions fix all the hypercharges in this case (i.e., there is only one possible choice for the hypercharges that satisfies Eqs. (8)), which implies that electromagnetic charge quantization is the only possibility in a field theory with the same matter content as the SM.

### 3.3 Neutrino masses and physics beyond-the-standard-model

Any new physics beyond the standard model (BSM) characterized by a high scale,  $\Lambda$ , will induce effects at low energies  $E \ll \Lambda$  that can be described by an effective field theory [11, 12]:

$$\mathcal{L}_{\text{eff}} = \mathcal{L}_{\text{SM}} + \sum_i \frac{\alpha_i}{\Lambda} O_i^{d=5} + \sum_i \frac{\beta_i}{\Lambda^2} O_i^{d=6} + \dots \quad (23)$$

It is the most general Lagrangian which includes the SM and an infinite tower of operators constructed out of the SM fields respecting Lorentz and gauge symmetries. In principle such a theory depends on infinite new couplings, one per new independent operator, and it is therefore not predictive. However, if the energy we are interested in effects at a given finite order,  $n$ , in  $(\frac{E}{\Lambda})^n$ , we can truncate the series to include only operators of dimension  $d \leq n + 4$ . The operators of lowest dimension are the most relevant at low energies.

It turns out that there is only one such operator of the lowest possible dimension,  $d = 5$ , which is precisely the Weinberg operator of eq. (19). In this perspective, it is natural to expect that the first indication of BSM physics is precisely Majorana neutrino masses, and while many types of BSM theories can give rise to neutrino masses, generically they will induce other new physics effects represented by the operators of  $d = 6$  or higher.

## 4 Neutrino masses and lepton mixing

Neutrino masses, whether Dirac or Majorana, imply lepton mixing [13, 14]. The Yukawa couplings in eq. (16) is a generic complex matrix in flavour space, while that in eq. (19) is a generic complex symmetric matrix, and therefore the same holds for the corresponding mass matrices:

$$-\mathcal{L}_m^{\text{Dirac}} = \overline{\nu_L^i} (M_\nu)_{ij} \nu_R^j + \overline{l_L^i} (M_l)_{ij} l_R^j + \text{h.c.} \quad (24)$$

$$-\mathcal{L}_m^{\text{Majorana}} = \frac{1}{2} \overline{\nu_L^i} (M_\nu)_{ij} \nu_L^{cj} + \overline{l_L^i} (M_l)_{ij} l_R^j + \text{h.c.} \quad (25)$$

In the Dirac case, the two mass matrices can be diagonalized by a bi-unitary rotation:

$$M_\nu = U_\nu^\dagger \text{Diag}(m_1, m_2, m_3) V_\nu, \quad M_l = U_l^\dagger \text{Diag}(m_e, m_\mu, m_\tau) V_l, \quad (26)$$

while in the Majorana case, the neutrino mass matrix, being symmetric, can be taken to a diagonal form by

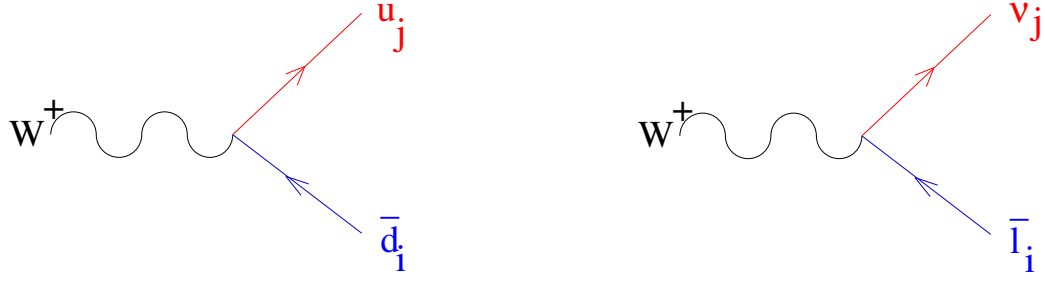
$$M_\nu = U_\nu^\dagger \text{Diag}(m_1, m_2, m_3) U_\nu^*. \quad (27)$$

We can go to the mass basis by rotating the fields as:

$$\nu'_R = V_\nu \nu_R, \quad \nu'_L = U_\nu \nu_L, \quad l'_R = V_l l_R, \quad l'_L = U_l l_L. \quad (28)$$

In this basis the charged current interactions are no longer diagonal, in complete analogy with the quark sector (see Fig. 13):

$$\mathcal{L}_{CC}^{\text{lepton}} = -\frac{g}{\sqrt{2}} \bar{l}_i \gamma_\mu P_L W_\mu^+ \underbrace{(U_l^\dagger U_\nu)_{ij}}_{U_{\text{PMNS}}} \nu'_j + \text{h.c.} \quad (29)$$

**Fig. 13:** Quark and lepton mixing.

The mixing matrix in the lepton sector is referred to as the Pontecorvo-Maki-Nakagawa-Sakata (PMNS) matrix, analogous to the CKM one in the quark sector.

The number of physical parameters in the lepton mixing matrix,  $U_{\text{PMNS}}$ , can easily be computed by counting the number of independent real and imaginary elements of the Yukawa matrices and eliminating those that can be absorbed in field redefinitions. The allowed field redefinitions are the unitary rotations of the fields that leave the rest of the Lagrangian invariant, only those that are not symmetries of the full Lagrangian when lepton masses are included.

	Yukawas	Field redefinitions	No. $m$	No. $\theta$	No. $\phi$
Dirac	$\lambda_l, \lambda_\nu$ $4n^2$	$U(n)^3/U(1)$ $\frac{3(n^2-n)}{2}, \frac{3(n^2+n)-1}{2}$	$2n$	$\frac{n^2-n}{2}$	$\frac{(n-2)(n-1)}{2}$
Majorana	$\lambda_l, \alpha_\nu^T = \alpha_\nu$ $3n^2 + n$	$U(n)^2$ $n^2 - n, n^2 + n$	$2n$	$\frac{n^2-n}{2}$	$\frac{n^2-n}{2}$

**Table 2:** Number of real and imaginary parameters in the Yukawa matrices, of those that can be absorbed in field redefinitions. The difference between the two is the number of observable parameters: the lepton masses ( $m$ ), mixing angles ( $\theta$ ), and phases ( $\phi$ ).

In the Dirac case, it is possible to rotate independently the left-handed lepton doublet, together with the right-handed charged leptons and neutrinos, that is  $U(n)^3$ , for a generic number of families  $n$ . However, this includes total lepton number which remains a symmetry of the massive theory and thus cannot be used to reduce the number of physical parameters in the mass matrix. The parameters that can be absorbed in field redefinitions are thus the parameters of the group  $U(n)^3/U(1)$  (that is  $\frac{3(n^2-n)}{2}$  real,  $\frac{3(n^2+n)-1}{2}$  imaginary).

In the case of Majorana neutrinos, there is no independent right-handed neutrino field, nor is lepton number a good symmetry. Therefore the number of field redefinitions is the number of parameters of the elements in  $U(n)^2$  (that is  $n^2 - n$  real and  $n^2 + n$  imaginary).

The resulting real physical parameters are the mass eigenstates and the mixing angles, while the resulting imaginary parameters are CP-violating phases. All this is summarized in Table 2. Dirac and Majorana neutrinos differ only in the number of observables phases. For three families ( $n = 3$ ), there is just one Dirac phase and three in the Majorana case.

A standard parametrization of the mixing matrices for Dirac,  $U_{\text{PMNS}}$ , and Majorana,  $\tilde{U}_{\text{PMNS}}$ , is given by

$$\begin{aligned} U_{\text{PMNS}} &= \begin{pmatrix} 1 & 0 & 0 \\ 0 & c_{23} & s_{23} \\ 0 & -s_{23} & c_{23} \end{pmatrix} \begin{pmatrix} c_{13} & 0 & s_{13}e^{-i\delta} \\ 0 & 1 & 0 \\ -s_{13}e^{i\delta} & 0 & c_{13} \end{pmatrix} \begin{pmatrix} c_{12} & s_{12} & 0 \\ -s_{12} & c_{12} & 0 \\ 0 & 0 & 1 \end{pmatrix}, \\ \tilde{U}_{\text{PMNS}} &= U_{\text{PMNS}}(\theta_{12}, \theta_{13}, \theta_{23}, \delta) \begin{pmatrix} 1 & 0 & 0 \\ 0 & e^{i\alpha_1} & 0 \\ 0 & 0 & e^{i\alpha_2} \end{pmatrix}, \end{aligned} \quad (30)$$

where in all generality  $\theta_{ij} \in [0, \pi/2]$  and  $\delta, \alpha_1, \alpha_2 \in [0, 2\pi]$ .

## 5 Majorana versus Dirac

It is clear that establishing the Majorana nature of neutrinos is of great importance, since it would imply the existence of a new physics scale. In principle there are very clear signatures, such as the one depicted in Fig. 14, where a  $\nu_\mu$  beam from  $\pi^+$  decay is intercepted by a detector. In the Dirac case, the interaction of neutrinos on the detector via a charged current interaction will produce only a  $\mu^-$  in the final state. If neutrinos are Majorana, a wrong-sign muon in the final state is also possible. Unfortunately the rate for  $\mu^+$  production is suppressed by  $m_\nu/E$  in amplitude with respect to the  $\mu^-$ . For example, for  $E_\nu = \mathcal{O}(1)$  GeV and  $m_\nu \sim \mathcal{O}(1)$  eV the cross-section for this process will be roughly  $10^{-18}$  times the usual CC neutrino cross-section.

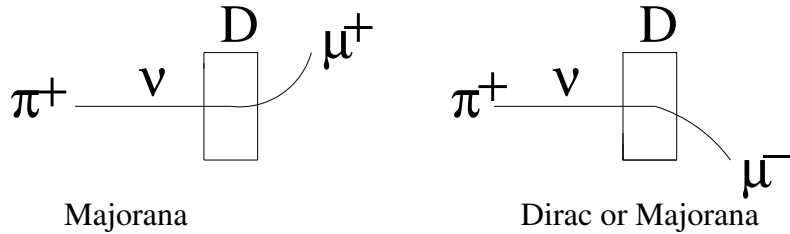


**Fig. 14:** A neutrino beam from  $\pi^+$  decay ( $\nu_\mu$ ) could interact in the magnetized detector producing a  $\mu^+$  only if neutrinos are Majorana.

The best hope of observing a rare process of this type seems to be the search for neutrinoless double-beta decay ( $2\beta0\nu$ ), the right diagram of Fig. 15. The background to this process is the standard double-beta decay depicted on the left of Fig. 15, which has been observed to take place for various isotopes with a lifetime of  $T_{2\beta2\nu} > 10^{19}\text{--}10^{21}$  years.

If the source of this process is just the Majorana  $\nu$  mass, the inverse lifetime for this process is given by

$$T_{2\beta0\nu}^{-1} \simeq \underbrace{G^{0\nu}}_{\text{Phase}} \underbrace{|M^{0\nu}|^2}_{\text{NuclearM.E.}} \underbrace{\left| \sum_i \left( \tilde{U}_{\text{PMNS}}^{ei} \right)^2 m_i \right|^2}_{|m_{ee}|^2}. \quad (31)$$

In spite of the suppression in the neutrino mass (over the energy of this process), the neutrinoless mode has a phase factor orders of magnitude larger than the  $2\nu$  mode, and as a result present experiments searching for this rare process have already set bounds on neutrino masses in the eV range as shown in Table 3.

**Fig. 15:**  $2\beta$  decay: normal (left) and neutrinoless (right).

Experiment	Nucleus	$ m_{ee} $
EXO-200	$^{136}\text{Xe}$	< 0.19–0.45 eV
NEMO-3	$^{100}\text{Mo}$	< 0.33–0.87 eV
GERDA	$^{76}\text{Ge}$	< 0.2–0.4 eV
KamLAND-Zen	$^{136}\text{Xe}$	< 0.12–0.25 eV
CUORICINO	$^{130}\text{Te}$	< 0.2–0.7 eV

**Table 3:** Present bounds at 90%CL from some recent neutrinoless double-beta-decay experiments [7].

## 6 Neutrino Oscillations

The most spectacular implication of neutrino masses and mixings is the macroscopic quantum phenomenon of neutrino oscillations, first introduced by B. Pontecorvo [15]. The Nobel prize in 2015 has been awarded to T. Kajita (from the SuperKamiokande collaboration) and A. B. McDonald (from the SNO collaboration) for the *discovery of neutrino oscillations, which shows that neutrinos have a mass*.

We have seen that the neutrino flavour fields ( $\nu_e, \nu_\mu, \nu_\tau$ ) that couple via CC to the leptons ( $e, \mu, \tau$ ) are unitary combinations of the mass eigenstates fields ( $\nu_1, \nu_2, \nu_3$ ):

$$\begin{pmatrix} \nu_e \\ \nu_\mu \\ \nu_\tau \end{pmatrix} = U_{\text{PMNS}}(\theta_{12}, \theta_{13}, \theta_{23}, \text{phases}) \begin{pmatrix} \nu_1 \\ \nu_2 \\ \nu_3 \end{pmatrix}. \quad (32)$$

In a neutrino oscillation experiment, neutrinos are produced by a source (e.g. pion or  $\mu$  decays, nuclear reactions, etc) and are detected some macroscopic distance,  $L$ , away from the production point. They are produced and detected via weak processes in combination with a given lepton flavour, that is in flavour states. As these states propagate undisturbed in space-time from the production to the detection regions, the different mass eigenstates, having slightly different phase velocities, pick up different phases, resulting in a non-zero probability that the state that arrives at the detector is in a different flavour combination to the one originally produced, see Fig. 16. The probability for this flavour transition oscillates with the distance travelled.

Two ingredients are mandatory for this phenomenon to take place:

- neutrinos must keep quantum coherence in propagation over macroscopic distances, which is only possible because they are so weakly interacting



**Fig. 16:** Neutrino oscillations.

- there is sufficient uncertainty in momentum at production and detection so that a coherent flavour state can be produced<sup>2</sup>

The master formula for the oscillation probability of  $\nu_\alpha$  turning into a  $\nu_\beta$  is

$$P(\nu_\alpha \rightarrow \nu_\beta) = \sum_{i,j} U_{\alpha i}^* U_{\beta i} U_{\alpha j} U_{\beta j}^* e^{-i \frac{\Delta m_{ji}^2 L}{2|\mathbf{p}|}}, \quad (33)$$

where  $\Delta m_{ji}^2 \equiv m_i^2 - m_j^2$ ,  $U_{\alpha i}$  are the elements of the PMNS matrix,  $L$  is the baseline and  $\mathbf{p}$  is the neutrino momentum.

There are many ways to derive this formula. The simplest way that appears in most textbooks uses simple quantum mechanics, where neutrinos are treated as plane waves. A slightly more rigorous method treats neutrinos as wave packets. Finally, it is also possible to derive it from QFT, where neutrinos are treated as intermediate virtual states. The different methods make more or less explicit the basic necessary conditions of neutrino oscillations mentioned above, and therefore are more or less prone to quantum paradoxes.

### 6.1 Plane wave derivation

Let us suppose that a neutrino of flavor  $\alpha$  is produced at  $t_0$ . It is therefore a superposition of the mass eigenstates that we assume to be plane waves with spatial momentum  $\mathbf{p}$ :

$$|\nu_\alpha(t_0)\rangle = \sum_i U_{\alpha i}^* |\nu_i(\mathbf{p})\rangle. \quad (34)$$

The mass eigenstates are eigenstates of the free Hamiltonian:

$$\hat{H}|\nu_i(\mathbf{p})\rangle = E_i(\mathbf{p})|\nu_i(\mathbf{p})\rangle, \quad E_i(\mathbf{p})^2 = \mathbf{p}^2 + m_i^2. \quad (35)$$

The time evolution operator from  $t_0 \rightarrow t$  is given by  $e^{-i\hat{H}(t-t_0)}$  and therefore the state at time  $t$  is given by

$$|\nu_\alpha(t)\rangle = e^{-i\hat{H}(t-t_0)}|\nu_\alpha(t_0)\rangle = \sum_i U_{\alpha i}^* e^{-iE_i(\mathbf{p})(t-t_0)} |\nu_i(\mathbf{p})\rangle. \quad (36)$$

---

<sup>2</sup>If the momentum uncertainty is sufficiently small one could kinematically distinguish the mass eigenstate being produced/detected.

The probability that at time  $t$  the state is in flavour  $\beta$  is

$$P(\nu_\alpha \rightarrow \nu_\beta)(t) = |\langle \nu_\beta | \nu_\alpha(t) \rangle|^2 = \left| \sum_i U_{\beta i} U_{\alpha i}^* e^{-iE_i(\mathbf{p})(t-t_0)} \right|^2, \quad (37)$$

where we have used the orthogonality relation  $\langle \nu_i(\mathbf{p}) | \nu_j(\mathbf{p}) \rangle = \delta_{ij}$ .

Since the neutrinos are ultrarelativistic, we can approximate

$$E_i(\mathbf{p}) - E_j(\mathbf{p}) \simeq \frac{1}{2} \frac{m_i^2 - m_j^2}{|\mathbf{p}|} + \mathcal{O}(m^4), \quad (38)$$

and  $L \simeq (t - t_0)$ , so that the master formula in eq. (33) is recovered.

The well-founded criticism to this derivation can be summarized in the following questions: 1) why are all mass eigenstates of equal spatial momentum,  $\mathbf{p}$  ? 2) is the plane wave treatment justified when the production and detection regions are localized ? 3) why is it necessary to do the  $t - t_0 \rightarrow L$  conversion ?

A number of quantum paradoxes can be formulated from these questions, that can be resolved only when the two basic conditions for neutrino oscillations above are made explicit. This can be achieved in a wave packet treatment.

## 6.2 Wave packet derivation

Many authors have derived the master formula treating neutrinos involved as wave packets. For some recent references see [16, 17].

A neutrino of flavour  $\alpha$  is produced at time and position  $(t_0, \mathbf{x}_0) = (0, \mathbf{0})$  as a superposition of *source* wave packets,  $f_i^S(\mathbf{p})$ , one for each mass eigenstate. The state at time and position  $(t, \mathbf{x})$  is therefore

$$|\nu_\alpha(t)\rangle = \sum_i U_{\alpha i}^* \int_{\mathbf{p}} f_i^S(\mathbf{p}) e^{-iE_i(\mathbf{p})t} |\nu_i(\mathbf{p})\rangle. \quad (39)$$

For simplicity we will assume gaussian wave packets, with an average momentum  $\mathbf{Q}_i$  and width  $\sigma_S$ :

$$f_i^S(\mathbf{p}) \propto e^{-(\mathbf{p}-\mathbf{Q}_i)^2/2\sigma_S^2}. \quad (40)$$

Note that we have lifted the assumption that all mass eigenstates have the same spatial momentum.

A neutrino of flavour  $\beta$  is detected at time and position  $(T, \mathbf{L})$  as a superposition of *detector* wave packets,  $f_j^D(\mathbf{p})$ , created at this space-time position. The state detected is therefore

$$|\nu_\beta(t)\rangle = \sum_j U_{\beta j}^* \int_{\mathbf{p}} f_j^D(\mathbf{p}) e^{-iE_j(\mathbf{p})(t-T)} e^{-i\mathbf{p}\mathbf{L}} |\nu_j(\mathbf{p})\rangle, \quad (41)$$

where we also assume gasussian wave packets at detection, with average momentum  $\mathbf{Q}'_j$  and width  $\sigma_D$ :

$$f_j^D(\mathbf{p}) \propto e^{-(\mathbf{p}-\mathbf{Q}'_j)^2/2\sigma_D^2}. \quad (42)$$

The probability amplitude for the first state to turn into the second is therefore

$$\mathcal{A}(\nu_\alpha \rightarrow \nu_\beta) = \langle \nu_\beta(t) | \nu_\alpha(t) \rangle = \sum_i U_{\alpha i}^* U_{\beta i} \int_{\mathbf{p}} e^{-iE_i(\mathbf{p})T} e^{i\mathbf{p}\mathbf{L}} f_i^S(\mathbf{p}) f_i^{D*}(\mathbf{p}) \quad (43)$$

For gaussian wave packets we can rewrite the product of the  $S$  and  $D$  wave packets as a gaussian wave packet:

$$f_i^{D*}(\mathbf{p}) f_i^S(\mathbf{p}) \propto f_i^{ov}(\mathbf{p}) e^{-(\mathbf{Q}_i - \mathbf{Q}'_i)^2 / 4(\sigma_S^2 + \sigma_D^2)}, \quad (44)$$

where the overlap wave packet

$$f_i^{ov}(\mathbf{p}) \equiv e^{-(\mathbf{p} - \bar{\mathbf{Q}}_i)^2 / 2\sigma_{ov}^2}, \quad \bar{\mathbf{Q}}_i \equiv \left( \frac{\mathbf{Q}_i}{\sigma_S^2} + \frac{\mathbf{Q}'_i}{\sigma_D^2} \right) \sigma_{ov}^2, \quad \sigma_{ov}^2 \equiv \frac{1}{1/\sigma_S^2 + 1/\sigma_D^2}. \quad (45)$$

The momentum integral in eq. (43) can be done analytically if we approximate

$$E_i(\mathbf{p}) \simeq E_i(\bar{\mathbf{Q}}_i) + \sum_k \frac{\partial E_i}{\partial p_k} \Big|_{\bar{\mathbf{Q}}_i} (p_k - (\bar{Q}_i)_k) + \dots = E_i(\bar{\mathbf{Q}}_i) + \mathbf{v}_i(\mathbf{p} - \bar{\mathbf{Q}}_i) + \dots, \quad (46)$$

where  $\mathbf{v}_i$  is the overlap wave packet group velocity.

The amplitude obtained is

$$\mathcal{A}(\nu_\alpha \rightarrow \nu_\beta) \propto \sum_i U_{\alpha i}^* U_{\beta i} e^{-i E_i(\bar{\mathbf{Q}}_i) T} e^{i \bar{\mathbf{Q}}_i \mathbf{L}} e^{-(\mathbf{Q}_i - \mathbf{Q}'_i)^2 / 4(\sigma_S^2 + \sigma_D^2)} e^{-(\mathbf{L} - \mathbf{v}_i T)^2 \sigma_{ov}^2 / 2}. \quad (47)$$

Note that the two last exponential factors impose momentum conservation (the average momentum of the source and detector wave packets should be equal up to the momentum uncertainty) and the classical relation  $\mathbf{L} = \mathbf{v}_i T$  within the spatial uncertainty,  $\sigma_{ov}^{-1}$ .

Since we usually do not measure the detection time  $T$  in a neutrino oscillation experiment, we should integrate the probability over this variable. For simplicity we assume  $\mathbf{Q}_i \simeq \mathbf{Q}'_i$  and parallel to  $\mathbf{L}$ . In this case, the integral gives:

$$\begin{aligned} P(\nu_\alpha \rightarrow \nu_\beta) &\propto \int_{-\infty}^{\infty} dT |\mathcal{A}(\nu_\alpha \rightarrow \nu_\beta)|^2 \\ &\propto \sum_{i,j} U_{\alpha i}^* U_{\beta i} U_{\alpha j} U_{\beta j} e^{-i \frac{\Delta m_{ji}^2 L}{2|\mathbf{p}|}} \underbrace{e^{-\left(\frac{L}{L_{coh}(i,j)}\right)^2}}_{\text{coherence}} \underbrace{e^{-\left(\frac{E_i(\bar{\mathbf{Q}}_i) - E_j(\bar{\mathbf{Q}}_j)}{2\sigma_{ov}}\right)^2}}_{\text{momentum uncertainty}} \end{aligned} \quad (48)$$

where the coherence length

$$L_{coh}(i,j) \simeq \sigma_{ov} \frac{|\mathbf{v}_i - \mathbf{v}_j|}{\sqrt{|\mathbf{v}_i^2 + \mathbf{v}_j^2}}, \quad (49)$$

represents the distance travelled by the two wave packets, moving at slightly different group velocities  $v_i$  and  $v_j$ , such that the center of the two wave packets have separated spacially a distance of the order of the spatial uncertainty  $\sigma_{ov}^{-1}$ . For  $L \geq L_{coh}(i,j)$  the coherence between the wave packets  $i, j$  is lost and the corresponding terms in the oscillation probability exponentially suppressed. The last exponential factor in eq. (48) leads to a suppression of the oscillation probability when the difference in average energies of the two wave packets  $i, j$  is larger than the momentum uncertainty of the overlap wave packet,  $\sigma_{ov}$ . Note that  $\sigma_{ov}$  is dominated by the smallest of the production and detection uncertainties, and therefore both should be large enough to ensure that the wave packets of the different mass eigenstates remain coherent. To the extent that  $L \ll L_{coh}$  and  $|E_i - E_j| \ll \text{Min}(\sigma_S, \sigma_D)$ , the probability reduces to the master formula, with one caveat: we have lost the normalization along the way. This is usually unavoidable in the wave packet derivation. The right normalization can be imposed only a posteriori, for example, from unitarity,  $\sum_\beta P(\nu_\alpha \rightarrow \nu_\beta) = 1$ .

In summary, the wave packet derivation is clearly more physical, as it makes explicit the two necessary conditions for neutrino oscillations to take place: coherence and sufficient momentum uncertainty.

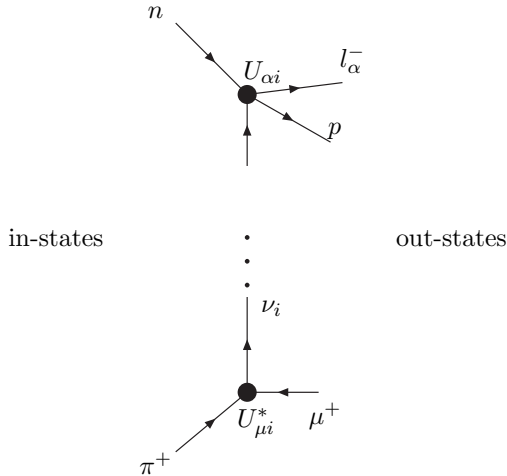


**Fig. 17:** Neutrino oscillations in QFT.

### 6.3 QFT derivation

Since we are dealing with relativistic quantum mechanics, QFT should be the appropriate framework to derive the oscillation probability.

In QFT we consider scattering processes where some asymptotic *in-states* that we can prepare in the infinite past come close together at some finite time in an interaction region and scatter off into other asymptotic *out-states* at time  $t \rightarrow \infty$ . The probability amplitude for this process is just the scalar product of the in and out states. In computing this amplitude we usually idealise the asymptotic states as plane waves, which is a good approximation provided the interaction region is small compared to the Compton wavelength of the scattering states. In reality however the proper normalization of the scattering probability as a probability per unit time and volume requires that the initial states are normalized wave packets.

In a neutrino oscillation experiment, the asymptotic states are not the neutrinos, we cannot really prepare the neutrino states, but the particles that produce the neutrino at the source and those that interact with the neutrino in the detector. The neutrino is just a virtual particle being exchanged between the source and detector, see Fig. 17, and in this perspective the interaction region is as large as the baseline and therefore macroscopic, in particular much larger than the Compton wavelength of the asymptotic states involved. It is mandatory therefore to consider the in-states as wave packets to ensure the localization of the source and detector.

Consider for example a neutrino beam produced from pions at rest and a detector some distance apart, where neutrinos interact with nucleons that are also at rest, via a quasi-elastic event:

$$\pi n \rightarrow p \mu l_\beta. \quad (50)$$

The in-states therefore will be the two wave packets representing a static pion that decays and is localized at time and position  $(0, \mathbf{0})$  within the uncertainty better defined than the decay tunnel, and a nucleon that is static and localized within the detector, at time and position  $(T, \mathbf{L})$ , when the interaction takes place. The out-states are the muon produced in pion decay and the lepton and hadron produced in the quasi-elastic event. The probability amplitude for the whole process includes the pion decay amplitude, the neutrino propagation and the scattering amplitude at the detector. Therefore in order to extract from the full amplitude an oscillation probability, it must be the case that there is factorization of the whole probability into three factors that can be identified with the flux of neutrino from pion decay, an oscillation probability and a neutrino cross section.

By explicit calculation [18], it is possible to show that such factorization does indeed take place as long as kinematical effects of neutrino masses can be neglected. The oscillation probability defined as the ratio of the probability for the whole process and the product of the neutrino flux from pion decay and the neutrino scattering cross-section is properly normalized.

#### 6.4 Neutrino oscillations in vacuum

Let us analyse more closely the master formula eq. (33). The probability is a superposition of oscillatory functions of the baseline with wavelengths that depend on the neutrino mass differences  $\Delta m_{ij}^2 = m_j^2 - m_i^2$ , and amplitudes that depend on different combinations of the mixing matrix elements. Defining  $W_{\alpha\beta}^{ij} \equiv [U_{\alpha i} U_{\beta i}^* U_{\alpha j}^* U_{\beta j}]$  and using the unitarity of the mixing matrix, we can rewrite the probability in the more familiar form:

$$\begin{aligned} P(\nu_\alpha \rightarrow \nu_\beta) &= \delta_{\alpha\beta} - 4 \sum_{j>i} \operatorname{Re}[W_{\alpha\beta}^{ij}] \sin^2 \left( \frac{\Delta m_{ij}^2 L}{4E_\nu} \right) \\ &\mp 2 \sum_{j>i} \operatorname{Im}[W_{\alpha\beta}^{ij}] \sin \left( \frac{\Delta m_{ij}^2 L}{2E_\nu} \right), \end{aligned} \quad (51)$$

where the  $\mp$  refers to neutrinos/antineutrinos and  $|\mathbf{q}| \simeq E_\nu$ .

We refer to an *appearance* or *disappearance* oscillation probability when the initial and final flavours are different ( $\alpha \neq \beta$ ) or the same ( $\alpha = \beta$ ), respectively. Note that oscillation probabilities show the expected GIM suppression of any flavour changing process: they vanish if the neutrinos are degenerate.

In the simplest case of two-family mixing, the mixing matrix depends on just one mixing angle:

$$U_{\text{PMNS}} = \begin{pmatrix} \cos \theta & \sin \theta \\ -\sin \theta & \cos \theta \end{pmatrix}, \quad (52)$$

and there is only one mass square difference  $\Delta m^2$ . The oscillation probability of Eq. (51) simplifies to the well-known expression where we have introduced convenient physical units:

$$\begin{aligned} P(\nu_\alpha \rightarrow \nu_\beta) &= \sin^2 2\theta \sin^2 \left( 1.27 \frac{\Delta m^2 (\text{eV}^2) L (\text{km})}{E_\nu (\text{GeV})} \right), \quad \alpha \neq \beta. \\ P(\nu_\alpha \rightarrow \nu_\alpha) &= 1 - P(\nu_\alpha \rightarrow \nu_\beta). \end{aligned} \quad (53)$$

The probability is the same for neutrinos and antineutrinos, because there cannot be CP violation when there are only two families. Indeed CPT implies that the disappearance probabilities are the same for neutrinos and antineutrinos, and therefore according to eq. (53) the same must hold for the appearance probability. The latter is a sinusoidal function of the distance between source and detector, with a period determined by the oscillation length:

$$L_{\text{osc}} (\text{km}) = \pi \frac{E_\nu (\text{GeV})}{1.27 \Delta m^2 (\text{eV}^2)}, \quad (54)$$

which is proportional to the neutrino energy and inversely proportional to the neutrino mass square difference. The amplitude of the oscillation is determined by the mixing angle. It is maximal for  $\sin^2 2\theta = 1$  or  $\theta = \pi/4$ . The oscillation probability as a function of the baseline is shown on the left plot of Fig. 18.

In many neutrino oscillation experiments the baseline is not varied but the oscillation probability can be measured as a function of the neutrino energy. This is shown on the right plot of Fig. 18. In this case, the position of the first maximum contains information on the mass splitting:

$$E_{\text{max}} (\text{GeV}) = 1.27 \frac{\Delta m^2 (\text{eV}^2) L (\text{km})}{\pi/2}. \quad (55)$$

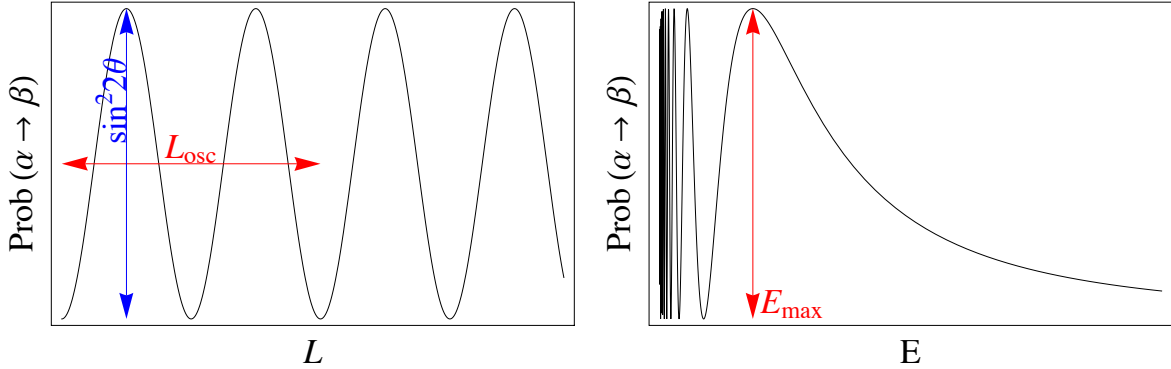


**Fig. 18:** Left: two-family appearance oscillation probability as a function of the baseline of  $L$  at fixed neutrino energy. Right: same probability shown as a function of the neutrino energy for fixed baseline.

An optimal neutrino oscillation experiment in vacuum is such that the ratio of the neutrino energy and baseline are tuned to be of the same order as the mass splitting,  $E/L \sim \Delta m^2$ . If  $E/L \gg \Delta m^2$ , the oscillation phase is small and the oscillation probability depends on the combination  $P(\nu_\alpha \rightarrow \nu_\beta) \propto \sin^2 2\theta (\Delta m^2)^2$ , and the mixing angle and mass splitting cannot be disentangled. The opposite limit  $E/L \ll \Delta m^2$  is the fast oscillation regime, where one can only measure an energy or baseline-smeared oscillation probability

$$\langle P(\nu_\alpha \rightarrow \nu_\beta) \rangle \simeq \frac{1}{2} \sin^2 2\theta. \quad (56)$$

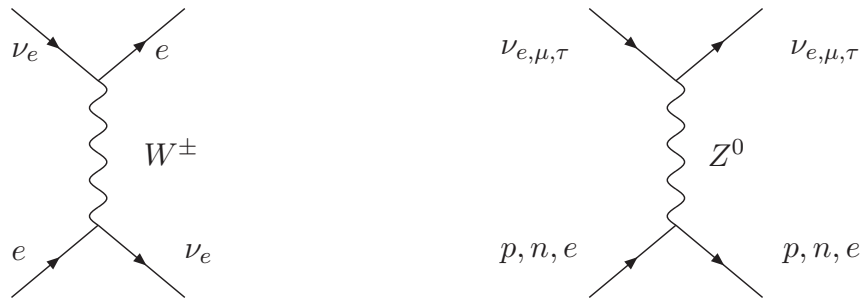
It is interesting, and reassuring, to note that this averaged oscillation regime gives the same result as the flavour transition probability in the case of incoherent propagation ( $L \gg L_{\text{coh}}$ ):

$$P(\nu_\alpha \rightarrow \nu_\beta) = \sum_i |U_{\alpha i} U_{\beta i}|^2 = 2 \cos^2 \theta \sin^2 \theta = \frac{1}{2} \sin^2 2\theta. \quad (57)$$

Flavour transitions via incoherent propagation are sensitive to mixing but not to the neutrino mass splitting. The 'smoking gun' for neutrino oscillations is not the flavour transition, which can occur in the presence of neutrino mixing without oscillations, but the peculiar  $L/E_\nu$  dependence. An optimal experiment that intends to measure both the mixing and the mass splitting requires running  $E/L \sim \Delta m^2$ .

## 6.5 Neutrino propagation in matter

When neutrinos propagate in matter (Earth, sun, etc.), their propagation is modified owing to coherent forward scattering on electrons and nucleons [19]:



The effective Hamiltonian density resulting from the charged current interaction is

$$\mathcal{H}_{CC} = 2\sqrt{2}G_F [\bar{e}\gamma_\mu P_L \nu_e][\bar{\nu}_e \gamma^\mu P_L e] = 2\sqrt{2}G_F [\bar{e}\gamma_\mu P_L e][\bar{\nu}_e \gamma^\mu P_L \nu_e]. \quad (58)$$

Since the medium is not polarized, the expectation value of the electron current is simply the number density of electrons:

$$\langle \bar{e}\gamma_\mu P_L e \rangle_{\text{unpol.medium}} = \delta_{\mu 0} \frac{N_e}{2}. \quad (59)$$

Including also the neutral current interactions in the same way, the effective Hamiltonian for neutrinos in the presence of matter is

$$\langle \mathcal{H}_{CC} + \mathcal{H}_{NC} \rangle_{\text{medium}} = \bar{\nu} V_m \gamma^0 (1 - \gamma_5) \nu \quad (60)$$

$$V_m = \begin{pmatrix} \frac{G_F}{\sqrt{2}} \left( N_e - \frac{N_n}{2} \right) & 0 & 0 \\ 0 & \frac{G_F}{\sqrt{2}} \left( -\frac{N_n}{2} \right) & 0 \\ 0 & 0 & \frac{G_F}{\sqrt{2}} \left( -\frac{N_n}{2} \right) \end{pmatrix}, \quad (61)$$

where  $N_n$  is the number density of neutrons. Due to the neutrality of matter, the proton and electron contributions to the neutral current potential cancel.

The plane wave solutions to the modified Dirac equation satisfy a different dispersion relation and as a result, the phases of neutrino oscillation phenomena change. The new dispersion relation becomes

$$E - V_m - M_\nu = (\pm |\mathbf{p}| - V_m) \frac{1}{E + M_\nu - V_m} (\pm |\mathbf{p}| - V_m) \quad h = \pm, \quad (62)$$

where  $h = \pm$  indicate the two helicity states and we have neglected effects of  $\mathcal{O}(VM_\nu)$ . This is a reasonable approximation since  $m_\nu \gg V_m$ . For the positive energy states we then have

$$E > 0 \quad E^2 = |\mathbf{p}|^2 + M_\nu^2 + 4EV_m \quad h = - \quad E^2 = |\mathbf{p}|^2 + M_\nu^2, \quad h = +, \quad (63)$$

while for the negative energy ones  $V_m \rightarrow -V_m$  and  $h \rightarrow -h$ .

The effect of matter can be simply accommodated in an effective mass matrix:

$$\tilde{M}_\nu^2 = M_\nu^2 \pm 4EV_m. \quad (64)$$

The effective mixing matrix  $\tilde{V}_{\text{MNS}}$  is the one that takes us from the original flavour basis to that which diagonalizes this effective mass matrix:

$$\begin{pmatrix} \tilde{m}_1^2 & 0 & 0 \\ 0 & \tilde{m}_2^2 & 0 \\ 0 & 0 & \tilde{m}_3^2 \end{pmatrix} = \tilde{V}_{\text{MNS}}^\dagger \begin{pmatrix} M_\nu^2 \pm 4E & 0 & 0 \\ 0 & V_\mu & 0 \\ 0 & 0 & V_\tau \end{pmatrix} \tilde{V}_{\text{MNS}}. \quad (65)$$

The effective mixing angles and masses depend on the energy.

The matter potential in the center of the sun is  $V_m \sim 10^{-12}$  eV and in the Earth  $V_m \sim 10^{-13}$  eV. In spite of these tiny values, these effects are non-negligible in neutrino oscillations.

## 6.6 Neutrino oscillations in constant matter

In the case of two flavours, the effective mass and mixing angle have relatively simple expressions:

$$\Delta \tilde{m}^2 = \sqrt{\left( \Delta m^2 \cos 2\theta \mp 2\sqrt{2}E G_F N_e \right)^2 + (\Delta m^2 \sin 2\theta)^2}, \quad (66)$$

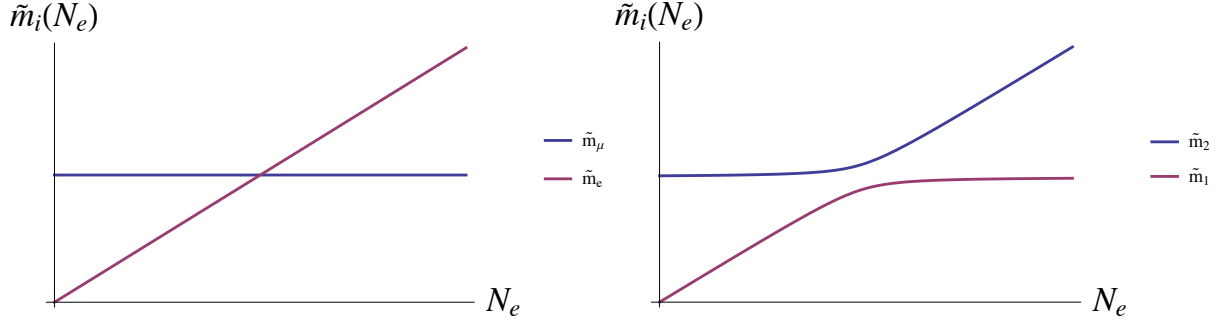


**Fig. 19:** Mass eigenstates as a function of the electron number density at fixed neutrino energy for  $\theta = 0$  (left) and  $\theta \neq 0$  (right).

$$\sin^2 2\tilde{\theta} = \frac{(\Delta m^2 \sin 2\theta)^2}{(\Delta \tilde{m}^2)^2} \quad (67)$$

where the sign  $\mp$  corresponds to neutrinos/antineutrinos. The corresponding oscillation amplitude has a resonance [20], when the neutrino energy satisfies

$$\sqrt{2} G_F N_e \mp \frac{\Delta m^2}{2E} \cos 2\theta = 0 \Rightarrow \sin^2 2\tilde{\theta} = 1, \quad \Delta \tilde{m}^2 = \Delta m^2 \sin 2\theta. \quad (68)$$

The oscillation amplitude is therefore maximal, independently of the value of the vacuum mixing angle.

We also note that

- oscillations vanish at  $\theta = 0$ , because the oscillation length becomes infinite for  $\theta = 0$ ;
- the resonance is only there for  $\nu$  or  $\bar{\nu}$  but not both;
- the resonance condition depends on the sign( $\Delta m^2 \cos 2\theta$ ):

$$\begin{aligned} &\text{resonance observed in } \nu \rightarrow \text{sign}(\Delta m^2 \cos 2\theta) > 0, \\ &\text{resonance observed in } \bar{\nu} \rightarrow \text{sign}(\Delta m^2 \cos 2\theta) < 0. \end{aligned}$$

The origin of this resonance is a would-be level crossing in the case of vanishing mixing. In the case of two families, for  $\theta = 0$ , the mass eigenstates as a function of the electron number density, at fixed neutrino energy, are depicted in Fig. 19 for  $\Delta m^2 > 0$ . As soon as the mixing is lifted from zero, no matter how small, the crossing cannot take place. The resonance condition corresponds to the minimum level-splitting point.

## 6.7 Neutrino oscillations in variable matter

In the sun the density of electrons is not constant. However, if the variation is sufficiently slow, the eigenstates will change slowly with the density, and we can assume that the neutrino produced in an eigenstate in the center of the sun, remains in the same eigenstate along the trajectory. This is the so-called *adiabatic approximation*.

We consider here two-family mixing for simplicity. At any point in the trajectory, it is possible to diagonalize the Hamiltonian fixing the matter density to that at the given point. The resulting eigenstates can be written as

$$|\tilde{\nu}_1\rangle = |\nu_e\rangle \cos \tilde{\theta} - |\nu_\mu\rangle \sin \tilde{\theta}, \quad (69)$$

$$|\tilde{\nu}_2\rangle = |\nu_e\rangle \sin \tilde{\theta} + |\nu_\mu\rangle \cos \tilde{\theta}. \quad (70)$$

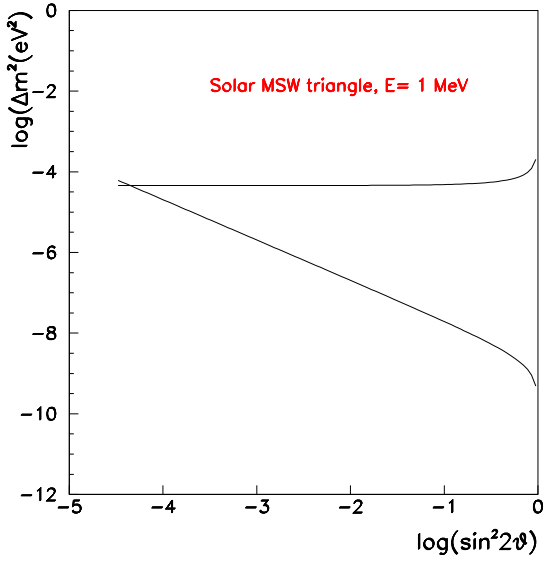


**Fig. 20:** MSW triangle: in the region between the two lines the resonance and adiabaticity conditions are both satisfied for neutrinos of energy 1 MeV.

Neutrinos are produced close to the centre  $x = 0$  where the electron density is  $N_e(0)$ . Let us suppose that it satisfies

$$2\sqrt{2}G_F N_e(0) \gg \Delta m^2 \cos 2\theta. \quad (71)$$

Then the diagonalization of the mass matrix at this point gives

$$\tilde{\theta} \simeq \frac{\pi}{2} \Rightarrow |\nu_e\rangle \simeq |\tilde{\nu}_2\rangle, \quad (72)$$

in such a way that an electron neutrino is mostly the second mass eigenstate. When neutrinos exit the sun, at  $x = R_\odot$ , the matter density falls to zero,  $N_e(R_\odot) = 0$ , and the local effective mixing angle is the one in vacuum,  $\tilde{\theta} = \theta$ . If  $\theta$  is small, the eigenstate  $\tilde{\nu}_2$  is mostly  $\nu_\mu$  according to Eq. (70).

Therefore an electron neutrino produced at  $x = 0$  is mostly the eigenstate  $\tilde{\nu}_2$ , but this eigenstate outside the sun is mostly  $\nu_\mu$ . There is maximal  $\nu_e \rightarrow \nu_\mu$  conversion if the adiabatic approximation is a good one. This is the famous MSW effect [19, 20]. The conditions for this to happen are:

- *Resonant condition*: the density at the production is above the critical one

$$N_e(0) > \frac{\Delta m^2 \cos 2\theta}{2\sqrt{2}E G_F}. \quad (73)$$

- *Adiabaticity*: the splitting of the levels is large compared to energy injected in the system by the variation of  $N_e(r)$ . A measurement of this is given by  $\gamma$  which should be much larger than one:

$$\gamma = \frac{\sin^2 2\theta}{\cos 2\theta} \frac{\Delta m^2}{2E} \frac{1}{|\nabla \log N_e(r)|} > \gamma_{\min} > 1, \quad (74)$$

where  $\nabla = \partial/\partial r$ .

At fixed energy both conditions give the famous MSW triangles, if plotted on the plane  $(\log(\sin^2 2\theta), \log(\Delta m^2))$

$$\log(\Delta m^2) < \log\left(\frac{2\sqrt{2}G_F N_e(0)E}{\cos 2\theta}\right) \quad (75)$$

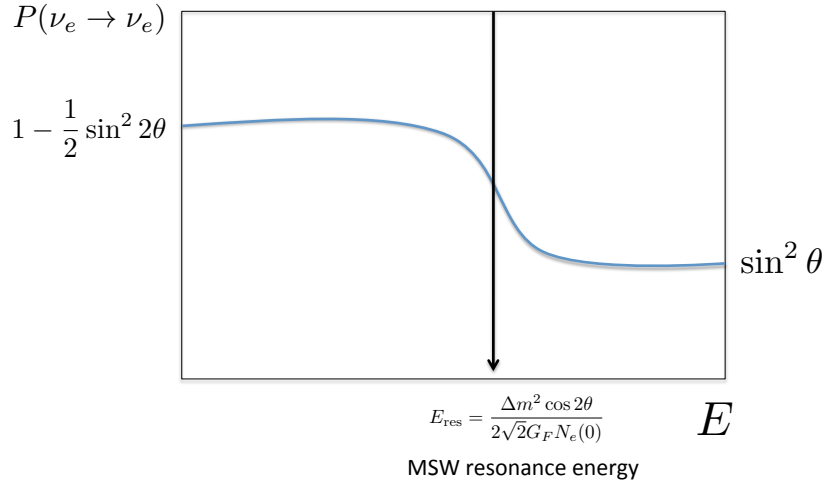


**Fig. 21:** Schematic survival probability of solar neutrinos as a function of the energy.

$$\log(\Delta m^2) > \log\left(\gamma_{\min} 2E \nabla \log N_e \frac{\cos 2\theta}{\sin^2 2\theta}\right). \quad (76)$$

For example, taking  $N_e(r) = N_c \exp(-r/R_0)$ ,  $R_0 = R_\odot/10.54$ ,  $N_c = 1.6 \times 10^{26} \text{ cm}^{-3}$ ,  $E = 1 \text{ MeV}$ , these curves are shown in Fig. 20.

It should be stressed that neutrino oscillations are not responsible for the flavour transition of solar neutrinos. The survival probability of the solar  $\nu_e$  in the adiabatic approximation is the incoherent sum of the contribution of each of the mass eigenstates:

$$P(\nu_e \rightarrow \nu_e) = \sum_i |\langle \nu_e | \tilde{\nu}_i(R_\odot) \rangle|^2 |\langle \tilde{\nu}_i(0) | \nu_e \rangle|^2, \quad (77)$$

where  $\tilde{\nu}_i(r)$  is the  $i$ -th mass eigenstate for the electron number density,  $N_e(r)$ , at a distance  $r$  from the center of the sun. If the mass eigenstates contribute incoherently, how can we measure the neutrino mass splitting? The answer is that the resonance condition of eq. (73) depends on the neutrino energy. If we define

$$E_{\text{res}} \equiv \frac{\Delta m^2 \cos 2\theta}{2\sqrt{2}G_F N_e(0)}, \quad (78)$$

the MSW effect will affect neutrinos with  $E > E_{\text{res}}$ , while for  $E < E_{\text{res}}$ , the oscillation probability is close to that in vacuum for averaged oscillations. The spectrum of the solar neutrino flux includes energies both above and below  $E_{\text{res}}$ :

$$\begin{aligned} P(\nu_e \rightarrow \nu_e) &\simeq 1 - \frac{1}{2} \sin^2 2\theta, & E \ll E_{\text{res}} \\ P(\nu_e \rightarrow \nu_e) &\simeq \sin^2 \theta, & E \gg E_{\text{res}} \end{aligned} \quad (79)$$

The sensitivity to  $\Delta m^2$  relies on the ability to locate the resonant energy. This behaviour is esquematically depicted in Fig. 21.

## 7 Evidence for neutrino oscillations

Nature has been kind enough to provide us with two natural sources of neutrinos (the sun and the atmosphere) where neutrino flavour transitions have been observed in a series of ingenious experiments, that started back in the 1960s with the pioneering experiment of R. Davies. This effort was rewarded with the Nobel prize of 2002 to R. Davies and M. Koshiba *for the detection of cosmic neutrinos*.

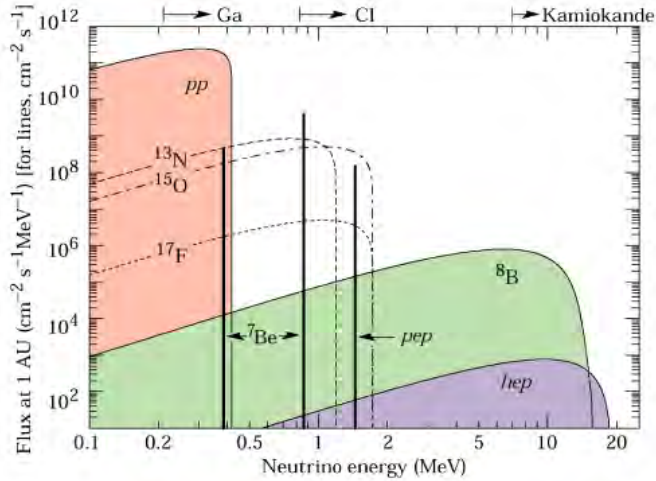


**Fig. 22:** Spectrum of solar neutrinos [22]. The arrows indicate the threshold of the different detection techniques.

## 7.1 Solar neutrinos

The sun, like all stars, is an intense source of neutrinos produced in the chain of nuclear reactions that burn hydrogen into helium:



The theory of stellar nucleosynthesis was established at the end of the 30's by H. Bethe [21]. The spectrum of the solar  $\nu_e$ , for massless neutrinos, is shown in Fig. 22. The prediction of this flux, obtained by J. Bahcall and collaborators [22], is the result of a detailed simulation of the solar interior and has been improved over many years. It is the so-called standard solar model (SSM).

Neutrinos coming from the sun have been detected with several experimental techniques that have a different neutrino energy threshold as indicated in Fig. 22. On the one hand, the radiochemical techniques, used in the experiments Homestake (chlorine,  ${}^{37}\text{Cl}$ ) [23], Gallex/GNO [24] and Sage [25] (using gallium,  ${}^{71}\text{Ga}$ , and germanium,  ${}^{71}\text{Ge}$ , respectively), can count the total number of neutrinos with a rather low threshold ( $E_\nu > 0.81$  MeV in Homestake and  $E_\nu > 0.23$  MeV in Gallex and Sage), but they cannot get any information on the directionality, the energy of the neutrinos, nor the time of the event.

On the other hand, Kamiokande [26] pioneered a new technique to observe solar neutrinos using water Cherenkov detectors that can measure the recoil electron in elastic neutrino scattering on electrons:  $\nu_e + e^- \rightarrow \nu_e + e^-$ . This is a real-time experiment that provides information on the directionality and the energy of the neutrinos. The threshold on the other hand is much higher,  $\sim 5$  MeV. All these experiments have consistently observed a number of solar neutrinos between 1/3 and 1/2 of the number expected in the SSM and for a long time this was referred to as the *solar neutrino problem or deficit*.

The progress in this field over the last decade has been enormous culminating in a solution to this puzzle that no longer relies on the predictions of the SSM. There have been three milestones.

**1998:** The experiment SuperKamiokande [27] measured the solar neutrino deficit with unprecedented precision, using the elastic reaction (ES):



The measurement of the direction of the events demonstrated that the neutrinos measured definitely come from the sun: the left plot of Fig. 23 shows the distribution of the events as a function of the zenith angle of the sun. A seasonal variation of the flux is expected since the distance between the Earth and the sun

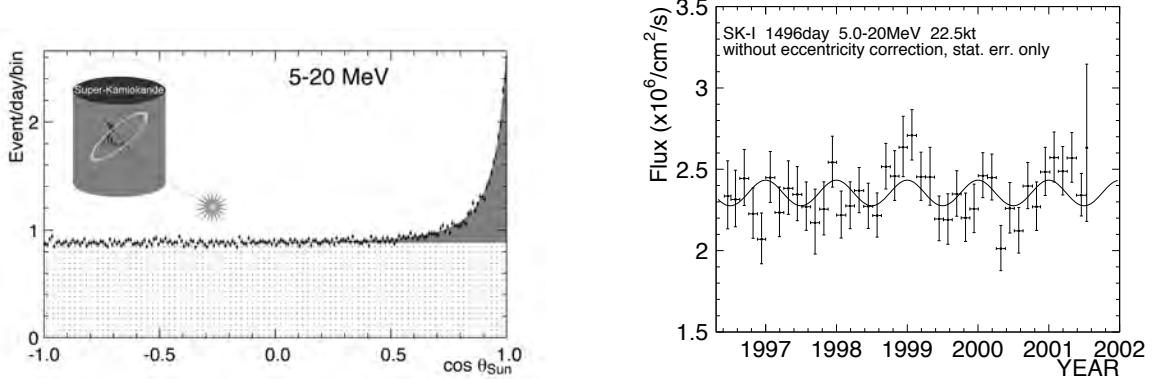


**Fig. 23:** Left: distribution of solar neutrino events as a function of the zenith angle of the sun. Right: seasonal variation of the solar neutrino flux in SuperKamiokande (from Ref. ([28])).

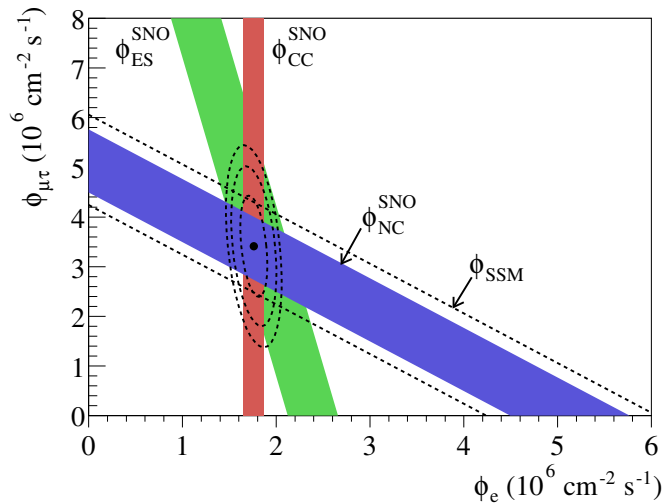


**Fig. 24:** Flux of  $\nu_\mu$  and  $\nu_\tau$  versus the flux of  $\nu_e$  in the solar neutrino flux as measured from the three reactions observable in the SNO experiment. The dashed band shows the prediction of the SSM, which agrees perfectly with the flux measured with the NC reaction (from Ref. [30]).

varies seasonally. The right plot of Fig. 23 shows that the measured variation is in perfect agreement with that expectation.

**2001:** The SNO experiment [29, 30] measured the flux of solar neutrinos using also the two reactions:

$$(CC) \quad \nu_e + d \rightarrow p + p + e^- \quad E_{\text{thres}} > 5 \text{ MeV} \quad (82)$$

$$(NC) \quad \nu_x + d \rightarrow p + n + \nu_x \quad x = e, \mu, \tau \quad E_{\text{thres}} > 2.2 \text{ MeV} \quad (83)$$

Since the CC reaction is only sensitive to electron neutrinos, while the NC one is sensitive to all the types that couple to the  $Z^0$  boson, the comparison of the fluxes measured with both reactions can establish if there are  $\nu_\mu$  and  $\nu_\tau$  in the solar flux independently of the normalization given by the SSM. The result is shown on the Nobel-prize-winning plot Fig. 24. These measurements demonstrate that the sun shines  $(\nu_\mu, \nu_\tau)$  about twice more than it shines  $\nu_e$ , which constitutes the first direct demonstration of flavour transitions in the solar flux! Furthermore the NC flux that measures all active species in the solar flux, is compatible with the total  $\nu_e$  flux expected according to the SSM.

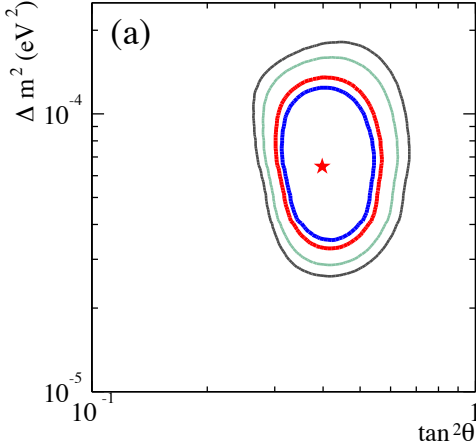


**Fig. 25:** Analysis of all solar data at SNO in terms of neutrino oscillations (from Ref. [29]).

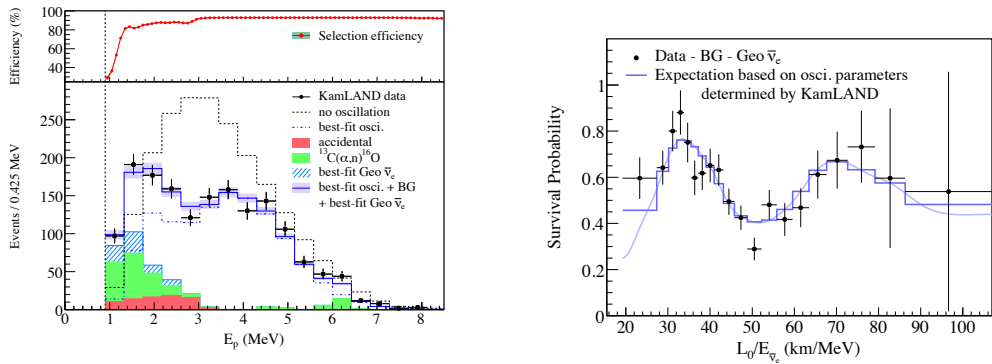


**Fig. 26:** Spectral distribution of the  $\bar{\nu}_e$  events in KamLAND (left) and  $E_\nu/L$  dependence (right). The data are compared to the expectation in the absence of oscillations and to the best fit oscillation hypothesis (from Ref. [32]).

All solar neutrino data can be interpreted in terms of neutrino masses and mixings. The analysis in terms of two neutrino families is shown in the left plot of Fig. 25. The solar  $\nu_e$  deficit can be explained for a  $\Delta m_{\text{solar}}^2 \simeq 7-8 \times 10^{-5} \text{ eV}$  and a relatively large mixing angle. The fortunate circumstance that

$$\Delta m_{\text{solar}}^2 \sim \langle E_\nu(1 \text{ MeV}) \rangle / L(100 \text{ km}) \quad (84)$$

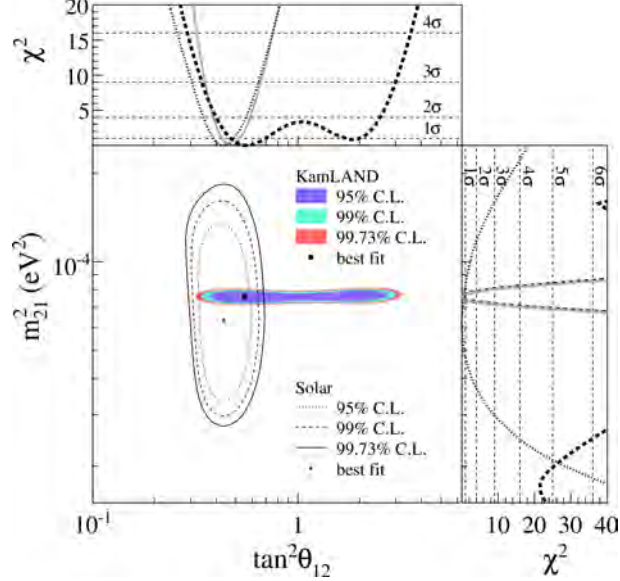
implies that one could look for this oscillation measuring reactor neutrinos at baselines of  $\sim 100$  km. This was the third milestone.

**2002:** The solar oscillation is confirmed with reactor neutrinos in the KamLAND experiment [31]. This is 1kton of liquid scintillator which measures the flux of reactor neutrinos produced in a cluster of nuclear plants around the Kamioka mine in Japan. The average distance is  $\langle L \rangle = 175$  km. Neutrinos are detected via inverse  $\beta$ -decay which has a threshold energy of about 2.6 MeV:

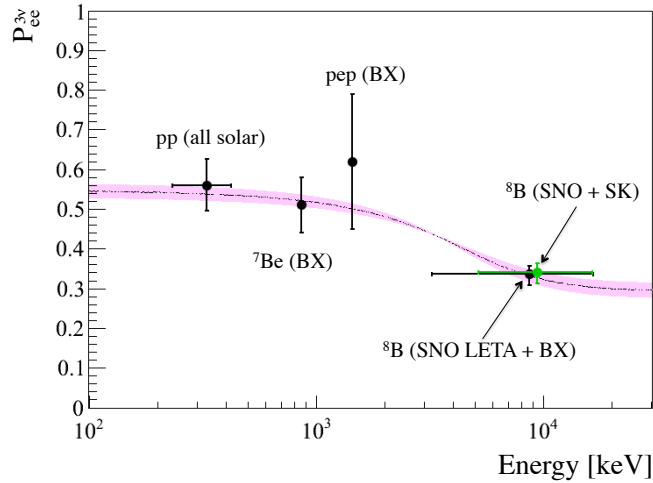
$$\bar{\nu}_e + p \rightarrow e^+ + n \quad E_{\text{th}} > 2.6 \text{ MeV}. \quad (85)$$

Figure 26 shows the KamLAND results [32] on the antineutrino spectrum, as well as the survival probability as a function of the ratio  $E_\nu/L$ . The low-energy contribution of geoneutrinos is clearly visible. This measurement could have important implications in geophysics.

Concerning the sensitivity to the oscillation parameters, Fig. 27 shows the present determination of the solar oscillation parameters from KamLAND and other solar experiments. The precision in the



**Fig. 27:** Analysis of all solar and KamLAND data in terms of oscillations (from Ref. [32]).



**Fig. 28:** Comparison of solar neutrino fluxes measured by the different solar neutrino experiments ( from Ref. [33]).

determination of  $\Delta m_{\text{solar}}^2$  is spectacular and shows that solar neutrino experiments are entering the era of precision physics.

The last addition to this success story is the Borexino [33] experiment. This is the lowest-threshold real-time solar neutrino experiment and the only one capable of measuring the flux of the monocromatic  ${}^7\text{Be}$  neutrinos and pep neutrinos. Their recent results are shown in Fig. 28. The result is in agreement with the oscillation interpretation of other solar and reactor experiments and it adds further information to disfavour alternative exotic interpretations of the data. In summary, solar neutrinos experiments have made fundamental discoveries in particle physics and are now becoming useful for other applications, such as a precise understanding of the sun and the Earth.

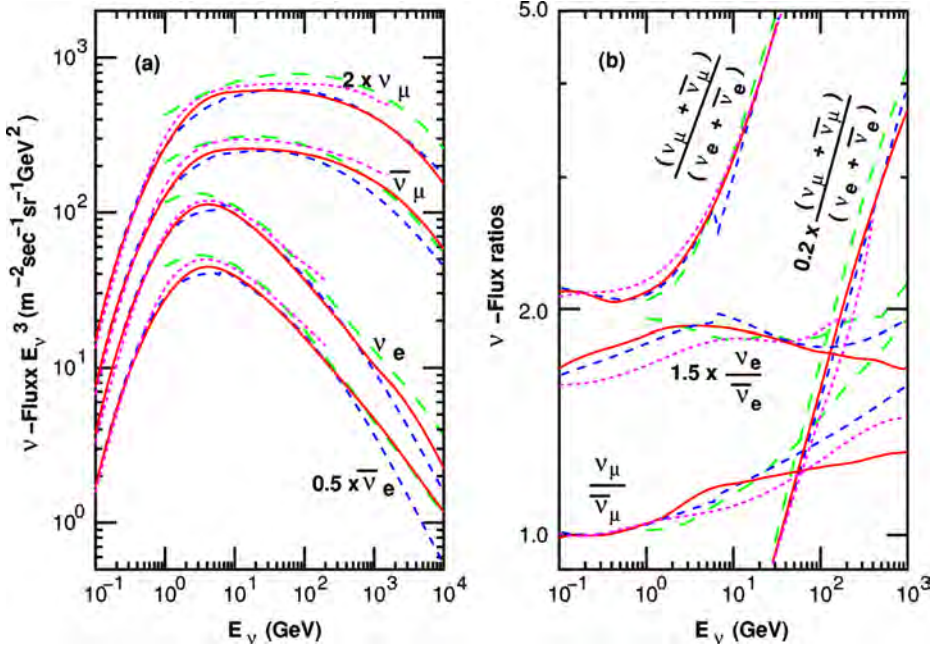


**Fig. 29:** Comparison of the predictions of different Monte Carlo simulations of the atmospheric neutrino fluxes averaged over all directions (left) and of the flux ratios  $(\nu_\mu + \bar{\nu}_\mu)/(\nu_e + \bar{\nu}_e)$ ,  $\nu_\mu/\bar{\nu}_\mu$ , and  $\nu_e/\bar{\nu}_e$  (right). The solid line corresponds to a recent full 3D simulation. Taken from the last reference in Ref. [34].

## 7.2 Atmospheric neutrinos

Neutrinos are also produced in the atmosphere when primary cosmic rays impinge on it producing  $K, \pi$  that subsequently decay. The fluxes of such neutrinos can be predicted within a 10–20% accuracy to be those in the left plot of Fig. 29.

Clearly, atmospheric neutrinos are an ideal place to look for neutrino oscillation since the  $E_\nu/L$  span several orders of magnitude, with neutrino energies ranging from a few hundred MeV to  $10^3$  GeV and distances between production and detection varying from  $10$ – $10^4$  km, as shown in Fig. 30 (right).

Many of the uncertainties in the predicted fluxes cancel when the ratio of muon to electron events is considered. The first indication of a problem was found when a deficit was observed precisely in this ratio by several experiments: Kamiokande, IMB, Soudan2 and Macro.

In 1998, SuperKamiokande clarified the origin of this anomaly [35]. This experiment can distinguish muon and electron events, measure the direction of the outgoing lepton (the zenith angle with respect to the Earth's axis) which is correlated to that of the neutrino (the higher the energy the higher the correlation), in such a way that they could measure the variation of the flux as a function of the distance travelled by the neutrinos. Furthermore, they considered different samples of events: sub-GeV (lepton with energy below 1 GeV), multi-GeV (lepton with energy above 1 GeV), together with stopping and through-going muons that are produced on the rock surrounding Superkamiokande. The different samples correspond to different parent neutrino energies as can be seen in Fig. 30 (left). The number of events for the different samples as a function of the zenith angle of the lepton are shown in the Nobel-prize-winning plot Fig. 31.

While the electron events observed are in rough agreement with predictions, a large deficit of muon events was found with a strong dependence on the zenith angle: the deficit was almost 50% for those events corresponding to neutrinos coming from below  $\cos \theta = -1$ , while there is no deficit for those coming from above. The perfect fit to the oscillation hypothesis is rather non-trivial given the sensitivity

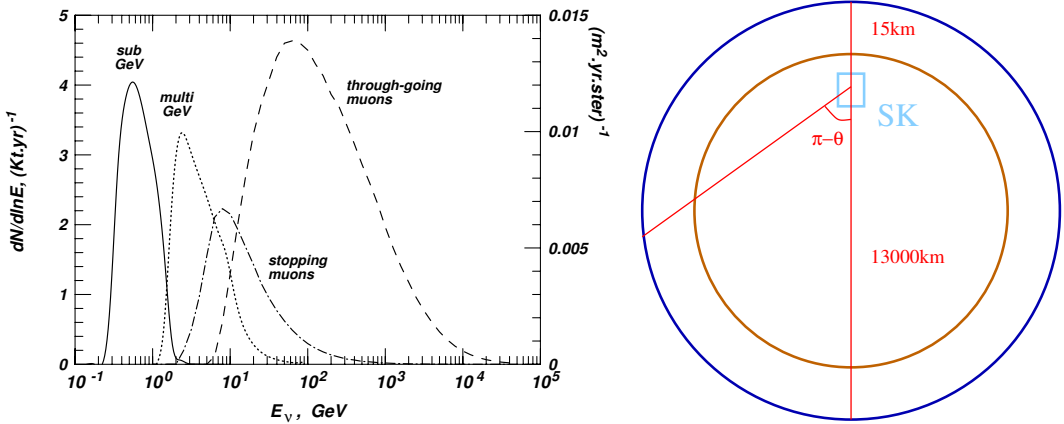


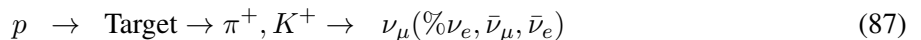
**Fig. 30:** Left: Parent neutrino energies of the different samples considered in Superkamiokande: sub-GeV, multi-GeV, stopping and through-going muons. Right: Distances travelled by atmospheric neutrinos as a function of the zenith angle.

of this measurement to the  $E_\nu$  (different samples) and  $L$  (zenith angle) dependence. The significance of the  $E_\nu/L$  dependence has also been measured by the SuperKamiokande Collaboration [37], as shown in Fig. 32. The best fit value of the oscillation parameters indicate  $\Delta m^2 \simeq 3 \times 10^{-3} \text{ eV}^2$  and maximal mixing.

Appropriate neutrino beams to search for the atmospheric oscillation can easily be produced at accelerators if the detector is located at a long baseline of a few hundred kilometres, and also with reactor neutrinos in a baseline of  $\mathcal{O}(1)\text{km}$ , since

$$|\Delta m_{\text{atmos}}^2| \sim \frac{E_\nu(1 - 10 \text{ GeV})}{L(10^2 - 10^3 \text{ km})} \sim \frac{E_\nu(1 - 10 \text{ MeV})}{L(0.1 - 1 \text{ km})}. \quad (86)$$

A *conventional* accelerator neutrino beam, as the one used in the FSS experiment, is produced from protons hitting a target and producing  $\pi$  and  $K$ :



$$\nu_\mu \rightarrow \nu_x. \quad (88)$$

Those of a selected charge are focused and are left to decay in a long decay tunnel producing a neutrino beam of mostly muon neutrinos (or antineutrinos) with a contamination of electron neutrinos of a few per cent. The atmospheric oscillation can be established by studying, as a function of the energy, either the disappearance of muon neutrinos, the appearance of electron neutrinos or, if the energy of the beam is large enough, the appearance of  $\tau$  neutrinos.

Three conventional beams confirmed the atmospheric oscillation from the measurement of the disappearance of  $\nu_\mu$  neutrinos: K2K ( $L = 235$  km), MINOS ( $L = 730$  km) and from the appearance of  $\nu_\tau$  OPERA ( $L = 730$  km). Fig. 33 shows the measurement of the  $\nu_\mu$  survival probability as a function of the reconstructed neutrino energy in the MINOS experiment.

Three reactor neutrino experiments, Daya Bay [39], RENO [40] and Double Chooz [41], have discovered that the electron neutrino flavour also oscillates with the atmospheric wavelength: electron antineutrinos from reactors disappear at distances of  $\mathcal{O}(1 \text{ km})$ , but with a small amplitude.

Finally the T2K experiment has measured for the first time the appearance of  $\nu_e$  in an accelerator  $\nu_\mu$  beam [42] in the atmospheric range.

The agreement of all these measurements with the original atmospheric oscillation signal was excellent.

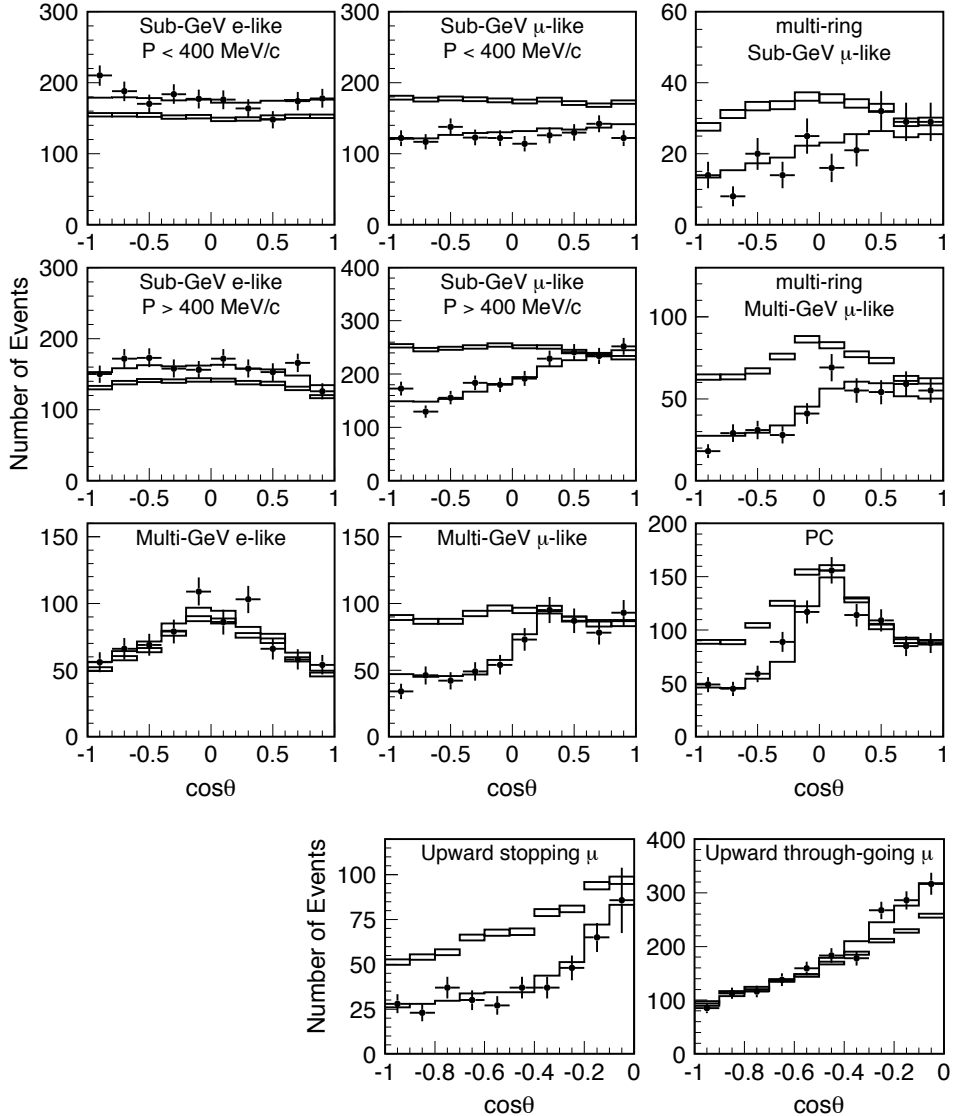


**Fig. 31:** Zenith angle distribution for fully-contained single-ring  $e$ -like and  $\mu$ -like events, multi-ring  $\mu$ -like events, partially contained events, and upward-going muons. The points show the data and the boxes show the Monte Carlo events without neutrino oscillations. The solid lines show the best-fit expectations for  $\nu_\mu \leftrightarrow \nu_\tau$  oscillations (from Ref. [36]).

## 8 The three-neutrino mixing scenario

As we have seen the evidence summarized in the previous section points to two distinct neutrino mass square differences related to the solar and atmospheric oscillation frequencies:

$$\underbrace{|\Delta m_{\text{solar}}^2|}_{\sim 8 \cdot 10^{-5} \text{ eV}^2} \ll \underbrace{|\Delta m_{\text{atmos}}^2|}_{\sim 2.5 \cdot 10^{-3} \text{ eV}^2} \quad (89)$$

The mixing of the three standard neutrinos  $\nu_e, \nu_\mu, \nu_\tau$  can accommodate both. The two independent neutrino mass square differences are conventionally assigned to the solar and atmospheric ones in the following way:

$$\Delta m_{13}^2 = m_3^2 - m_1^2 = \Delta m_{\text{atmos}}^2, \quad \Delta m_{12}^2 = m_2^2 - m_1^2 = \Delta m_{\text{solar}}^2. \quad (90)$$

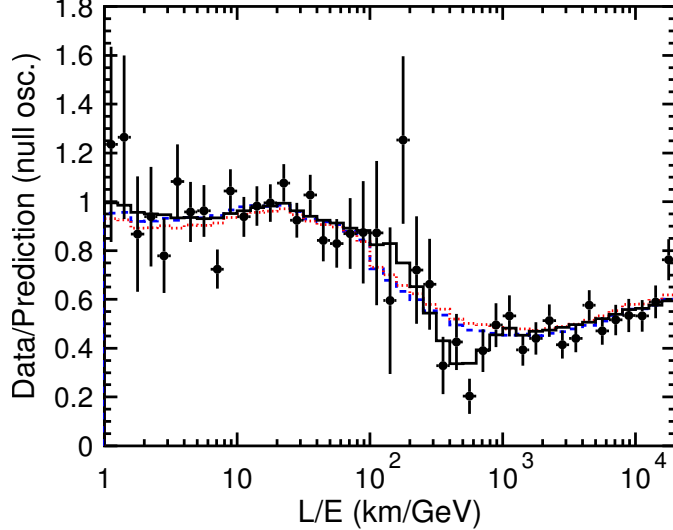


**Fig. 32:** Ratio of the data to the non-oscillated Monte Carlo events (points) with the best-fit expectation for 2-flavour  $\nu_\mu \leftrightarrow \nu_\tau$  oscillations (solid line) as a function of  $E_\nu/L$  (from Ref. [37]).

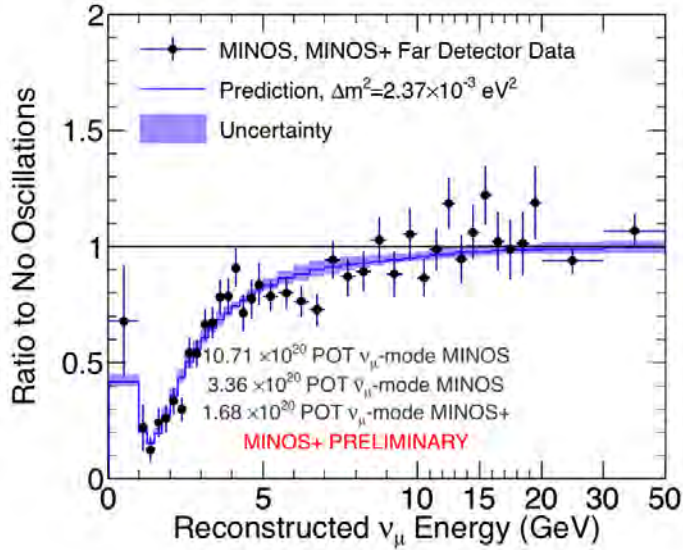


**Fig. 33:** Ratio of measured to expected (in absence of oscillations) neutrino events in MINOS as a functions of neutrino energy compared to the best fit oscillation solution (from Ref. [38]).

The PMNS mixing matrix depends on three angles and one or more CP phases (see eq. (30) for the standard parametrization). Only one CP phase, the so-called Dirac phase  $\delta$ , appears in neutrino oscillation probabilities.

With this convention, the mixing angles  $\theta_{23}$  and  $\theta_{12}$  in the parametrization of Eq. (30) correspond approximately to the ones measured in atmospheric and solar oscillations, respectively. This is because solar and atmospheric anomalies approximately decouple as independent 2-by-2 mixing phenomena thanks to the hierarchy between the two mass splittings,  $|\Delta m_{\text{atmos}}^2| \gg |\Delta m_{\text{solar}}^2|$ , on the one hand, and the fact that the angle  $\theta_{13}$ , which measures the electron component of the third mass eigenstate element  $\sin \theta_{13} = (U_{\text{PMNS}})_{e3}$ , is small.

To see this, let us first consider the situation in which  $E_\nu/L \sim |\Delta m_{\text{atmos}}^2|$ . We can thus neglect

the solar mass square difference in front of the atmospheric one and  $E_\nu/L$ . The oscillation probabilities obtained in this limit are given by

$$P(\nu_e \rightarrow \nu_\mu) \simeq s_{23}^2 \sin^2 2\theta_{13} \sin^2 \left( \frac{\Delta m_{13}^2 L}{4E_\nu} \right), \quad (91)$$

$$P(\nu_e \rightarrow \nu_\tau) \simeq c_{23}^2 \sin^2 2\theta_{13} \sin^2 \left( \frac{\Delta m_{13}^2 L}{4E_\nu} \right), \quad (92)$$

$$P(\nu_\mu \rightarrow \nu_\tau) \simeq c_{13}^4 \sin^2 2\theta_{23} \sin^2 \left( \frac{\Delta m_{13}^2 L}{4E_\nu} \right). \quad (93)$$

The results for antineutrinos are the same. All flavours oscillate therefore with the atmospheric frequency, but only two angles enter these formulae:  $\theta_{23}$  and  $\theta_{13}$ . The latter is the only one that enters the disappearance probability for  $\nu_e$  or  $\bar{\nu}_e$  in this regime:

$$P(\nu_e \rightarrow \nu_e) = P(\bar{\nu}_e \rightarrow \bar{\nu}_e) = 1 - P(\nu_e \rightarrow \nu_\mu) - P(\nu_e \rightarrow \nu_\tau) \simeq \sin^2 2\theta_{13} \sin^2 \left( \frac{\Delta m_{13}^2 L}{4E_\nu} \right). \quad (94)$$

This is precisely the measurement of reactor neutrino experiments like Chooz, Daya Bay, RENO and Double Chooz. Therefore the oscillation amplitude of these experiments is a direct measurement of the angle  $\theta_{13}$ , which has been measured to be small.

Note that in the limit  $\theta_{13} \rightarrow 0$ , the only probability that survives in Eq. (93) is the  $\nu_\mu \rightarrow \nu_\tau$  one, which has the same form as a 2-family mixing formula Eq. (53) if we identify

$$(\Delta m_{\text{atmos}}^2, \theta_{\text{atmos}}) \rightarrow (\Delta m_{13}^2, \theta_{23}). \quad (95)$$

Therefore the close-to-maximal mixing angle observed in atmospheric neutrinos and the accelerator neutrino experiments like MINOS is identified with  $\theta_{23}$ .

Instead if we consider experiments in the solar range,  $E_\nu/L \sim \Delta m_{\text{solar}}^2$ , the atmospheric oscillation is too rapid and gets averaged out. The survival probability for electrons in this limit is given by:

$$P(\nu_e \rightarrow \nu_e) = P(\bar{\nu}_e \rightarrow \bar{\nu}_e) \simeq c_{13}^4 \left( 1 - \sin^2 2\theta_{12} \sin^2 \left( \frac{\Delta m_{12}^2 L}{4E_\nu} \right) \right) + s_{13}^4. \quad (96)$$

Again it depends only on two angles,  $\theta_{12}$  and  $\theta_{13}$ , and in the limit in which the latter is zero, the survival probability measured in solar experiments has the form of two-family mixing if we identify

$$(\Delta m_{\text{solar}}^2, \theta_{\text{solar}}) \rightarrow (\Delta m_{12}^2, \theta_{12}). \quad (97)$$

The results that we have shown in the previous section of solar and atmospheric experiments have been analysed in terms of 2-family mixing. The previous argument indicates that when fits are done in the context of 3-family mixing nothing changes too much.

On the other hand, the fact that reactor experiments have already measured the disappearance of reactor  $\bar{\nu}_e$  in the atmospheric range implies that the effects of  $\theta_{13} \simeq 9^\circ$  are not negligible, and therefore a proper analysis of all the oscillation data requires performing global fits in the 3-family scenario. Figure 34 shows the  $\Delta\chi^2$  as a function of each of the six parameters from a recent global analysis [43]. There are two parameters in which we observe two distinct minima, these correspond to degeneracies that cannot be resolved with present data. The first corresponds to the neutrino mass ordering or hierarchy: present data cannot distinguish between the normal (NH or NO) and inverted ordering (IH or IO) represented in Fig. 35. Note that we denote by  $\Delta m_{13}^2 = \Delta m_{\text{atmos}}^2$  the atmospheric splitting for NO and  $\Delta m_{23}^2 = -\Delta m_{\text{atmos}}^2$ . The second degeneracy corresponds to the octant choice of  $\theta_{23}$ . Present data are mostly sensitive to  $\sin^2 2\theta_{23}$ . If this angle is not maximal, there are two possible choices that are roughly

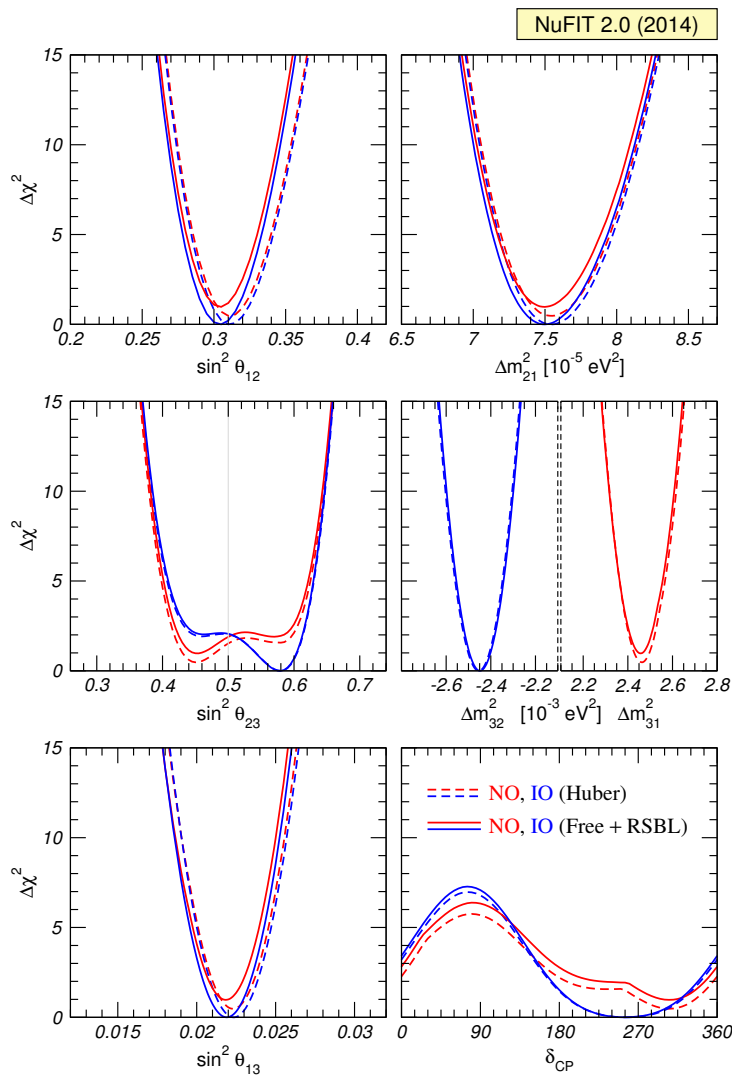


**Fig. 34:** Fits to the standard  $3\nu$ -mixing scenario including all available neutrino oscillation data (from Ref. [43]).

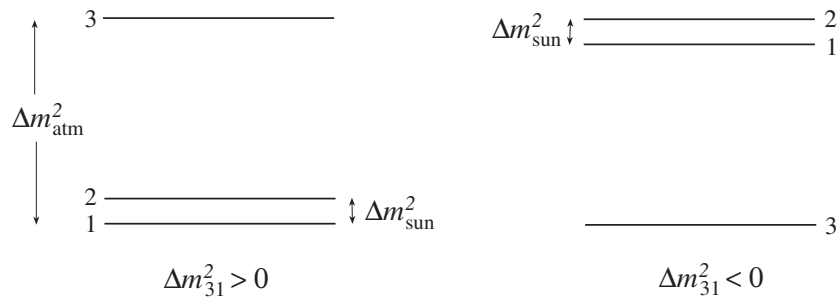


**Fig. 35:** Possible neutrino spectra consistent with solar and atmospheric data.

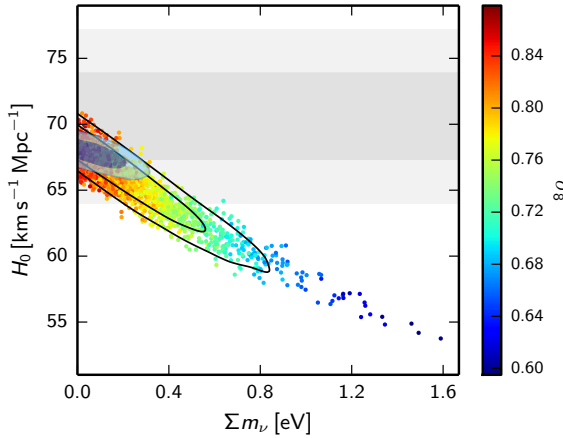


**Fig. 36:** Constraints on the sum of neutrino masses (in the standard  $3\nu$  scenario from cosmology [44]).

equivalent  $\theta_{23} \leftrightarrow \pi/4 - \theta_{23}$ . Due to this degeneracy, the largest angle is also the one less accurate. The  $1\sigma$  limits for NO are:

$$\begin{aligned} \theta_{23}/^\circ &= 42^{+3}_{-1.6}, & \theta_{12}/^\circ &= 33.5^{+0.78}_{-0.75}, & \theta_{13}/^\circ &= 8.5(2), \\ \Delta m_{12}^2 &= 7.5(2) \times 10^{-5} \text{ eV}^2, & \Delta m_{13}^2 &= 2.46(5) \times 10^{-3} \text{ eV}^2. \end{aligned} \quad (98)$$

The CP phase  $\delta$  remains completely unconstrained at  $3\sigma$ . As we will see, the dependence on the phase requires sensitivity to both frequencies simultaneously. There is however at  $2\sigma$  some hint of a preference for  $\delta > 180^\circ$ . For more details see [43].

Neutrino oscillations cannot provide information on the absolute neutrino mass scale. The best sensitivity to this scale is at present coming from cosmology. Indeed neutrinos properties are imprinted in the history of the universe. In particular the features of the cosmic microwave background (CMB) and the large scale galaxy distribution depends sizeably on the sum of neutrino masses. The last results from Planck [44] are shown in Fig. 36. Their conservative limit at 95%CL is impressive:

$$\sum_i m_i \leq 0.23 \text{ eV}. \quad (99)$$

## 9 Prospects in neutrino oscillation experiments

An ambitious experimental program is underway to pin down the remaining unknowns and reach a 1% precision in the lepton flavour parameters. The neutrino ordering, the octant of  $\theta_{23}$  and the CP violating phase,  $\delta$ , can be search for in neutrino oscillation experiments with improved capabilities.

Concerning the neutrino ordering, the best hope to identify the spectrum exploits the MSW effect in the propagation of GeV neutrinos through the Earth matter. In the case of three neutrinos propagating in matter, the  $\nu$  mass eigenstates as a function of the electron density for vanishing  $\theta_{12}, \theta_{13}$  are depicted in Fig. 37 for NO and IO. For NO we see that there are two level crossings giving rise to two MSW resonances. The first one is essentially the one relevant for solar neutrinos, as it affects the smallest mass splitting, with the resonance condition:

$$E_{\text{res}}^{(1)} = \frac{\Delta m_{12}^2 \cos 2\theta_{12}}{2\sqrt{2}G_F N_e}. \quad (100)$$

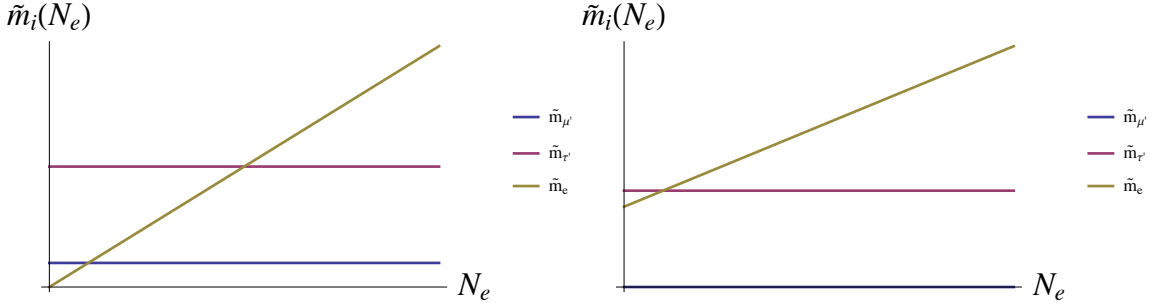


**Fig. 37:** Level crossings for  $\nu$  in the three neutrino scenario for NO (left) and IO (right) at vanishing  $\theta_{12}$  and  $\theta_{13}$ .

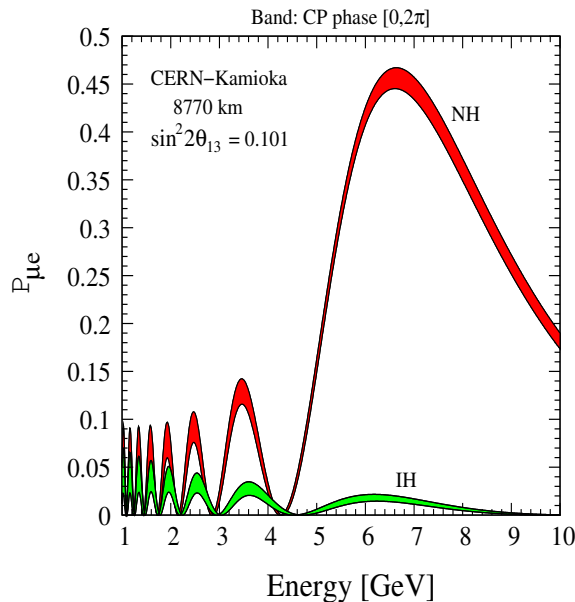


**Fig. 38:**  $P_{\mu e}$  as a function of neutrino energy for  $L$  corresponding to the distance CERN-Kamioka for NH/IH. The bands corresponds to the uncertainty in  $\delta$  (from Ref. [45]).

The second one affects the largest mass splitting

$$E_{\text{res}}^{(2)} = \frac{\Delta m_{13}^2 \cos 2\theta_{13}}{2\sqrt{2}G_F N_e}. \quad (101)$$

For IO, only the first resonance appears in the  $\nu$  channel.

For  $\bar{\nu}$  the dependence on  $N_e$  of the first eigenstate has a negative slope and therefore only the second resonance appears for IO.

The existence of the atmospheric resonance implies a large enhancement of the oscillation probability  $P(\nu_e \leftrightarrow \nu_\mu)$  for NO for energies near the resonant energy and at sufficiently long baseline. For IO the enhancement occurs in  $P(\bar{\nu}_e \leftrightarrow \bar{\nu}_\mu)$  instead. For the typical matter densities of the Earth crust and mantle and the value of the atmospheric mass splitting, the resonant energy for neutrinos travelling through Earth is  $\simeq 6$  GeV, an energy that can be reached in accelerator neutrino beams. The measurement of the neutrino ordering becomes almost a digital measurement sending a conventional  $\nu$  beam sufficiently far as shown in Fig. 38, which shows the oscillation probability  $P(\nu_\mu \rightarrow \nu_e)$  as a function of the neutrino energy at a distance corresponding to the baseline from CERN-Kamioka (8770 km).

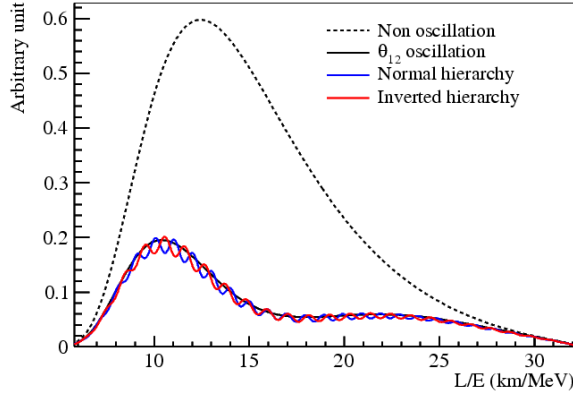


**Fig. 39:** Reactor neutrino spectrum in JUNO for NO/IO ( from Ref. [48]).

The first experiment that will be sensitive to this effect is the NOvA experiment, optimized like T2K to see the  $\nu_e$  appearance signal, with a baseline of 810km, which is however a bit short to see a large enhancement. Nevertheless if lucky NOvA could discriminate the ordering at  $3\sigma$ .

The atmospheric resonance must also affect atmospheric neutrinos at the appropriate energy and baseline. Unfortunately the atmospheric flux contains both neutrinos and antineutrinos in similar numbers, and the corresponding events cannot be tell apart, because present atmospheric neutrino detectors cannot measure the lepton charge. If we superimpose the neutrino and antineutrino signals, both orderings will give rise to an enhancement in the resonance region, since no matter what the ordering is, either the neutrino or antineutrino channel will have a resonance. Nevertheless with sufficient statistics, there is discrimination power and in fact the biggest neutrino telescopes, ICECUBE and KM3NeT have proposed to instrument more finely some part of their detectors (PINGU and ORCA projects) to perform this measurement. Also the next generation of atmospheric neutrino detectors, such as HyperKamiokande, with a factor  $\mathcal{O}(20)$  more mass than the present SuperKamiokande, or the INO detector that is designed to measure the muon charge in atmospheric events, could discriminate between the two orderings.

A very different strategy has been proposed for reactor neutrino experiments (e.g JUNO project). The idea is to measure very precisely the reactor neutrinos at a baseline of roughly 50 km, where the depletion of the flux due to the solar oscillation is maximal. At this optimal distance, one can get a superb measurement of the solar oscillation parameters,  $(\theta_{12}, \Delta m_{12}^2)$ , and, with sufficient energy resolution, one could detect the modulation of the signal due to the atmospheric oscillation [46, 47]. Fig. 39 shows how this modulation is sensitive to the neutrino ordering. A leap ahead is needed to reach the required energy resolution.

### 9.1 Leptonic CP violation

As we have seen, the CP phase,  $\delta$ , in the mixing matrix induces CP violation in neutrino oscillations, that is a difference between  $P(\nu_\alpha \rightarrow \nu_\beta)$  and  $P(\bar{\nu}_\alpha \rightarrow \bar{\nu}_\beta)$ , for  $\alpha \neq \beta$ . As we saw in the general expression of Eq. (51), CP violation is possible if there are imaginary entries in the mixing matrix that make  $\text{Im}[W_{\alpha\beta}^{jk}] \neq 0$ . By CPT, disappearance probabilities cannot violate CP however, because under CPT

$$P(\nu_\alpha \rightarrow \nu_\beta) = P(\bar{\nu}_\beta \rightarrow \bar{\nu}_\alpha), \quad (102)$$

so in order to observe a CP or T-odd asymmetry the initial and final flavour must be different,  $\alpha \neq \beta$ :

$$A_{\alpha\beta}^{CP} \equiv \frac{P(\nu_\alpha \rightarrow \nu_\beta) - P(\bar{\nu}_\alpha \rightarrow \bar{\nu}_\beta)}{P(\nu_\alpha \rightarrow \nu_\beta) + P(\bar{\nu}_\alpha \rightarrow \bar{\nu}_\beta)}, \quad A_{\alpha\beta}^T \equiv \frac{P(\nu_\alpha \rightarrow \nu_\beta) - P(\nu_\beta \rightarrow \nu_\alpha)}{P(\nu_\alpha \rightarrow \nu_\beta) + P(\nu_\beta \rightarrow \nu_\alpha)}. \quad (103)$$

In the case of 3-family mixing it is easy to see that the CP(T)-odd terms in the numerator are the same for all transitions  $\alpha \neq \beta$ :

$$A_{\nu_\alpha \nu_\beta}^{\text{CP(T)-odd}} = \frac{\sin \delta c_{13} \sin 2\theta_{13} \sin 2\theta_{12} \overbrace{\frac{\Delta m_{12}^2 L}{4E_\nu}}^{\text{solar}} \overbrace{\sin 2\theta_{23} \sin^2 \frac{\Delta m_{13}^2 L}{4E_\nu}}^{\text{atmos}}}{P_{\nu_\alpha \nu_\beta}^{\text{CP-even}}}. \quad (104)$$

As expected, the numerator is GIM suppressed in all the  $\Delta m_{ij}^2$  and all the angles, because if any of them is zero, the CP-odd phase becomes unphysical. Therefore an experiment which is sensitive to CP violation must be sensitive to both mass splittings simultaneously. In this situation, it is not clear a priori what the optimization of  $E/L$  should be.

It can be shown that including only statistical errors, the signal-to-noise for this asymmetry is maximized for  $\langle E_\nu \rangle / L \sim |\Delta m_{\text{atmos}}^2|$ . In this case, only two small parameters remain in the CP-odd terms: the solar splitting,  $\Delta m_{\text{solar}}^2$  (i.e., small compared to the other scales,  $\Delta m_{\text{atmos}}^2$  and  $\langle E_\nu \rangle / L$ ), and the angle  $\theta_{13}$ . The asymmetry is then larger in the subleading transitions:  $\nu_e \rightarrow \nu_\mu (\nu_\tau)$ , because the CP-even terms in the denominator are also suppressed by the same small parameters. A convenient approximation for the  $\nu_e \leftrightarrow \nu_\mu$  transitions is obtained expanding to second order in both small parameters [49]:

$$\begin{aligned} P_{\nu_e \nu_\mu (\bar{\nu}_e \bar{\nu}_\mu)} &= s_{23}^2 \sin^2 2\theta_{13} \sin^2 \left( \frac{\Delta m_{13}^2 L}{4E_\nu} \right) \equiv P^{\text{atmos}} \\ &+ c_{23}^2 \sin^2 2\theta_{12} \sin^2 \left( \frac{\Delta m_{12}^2 L}{4E_\nu} \right) \equiv P^{\text{solar}} \\ &+ \tilde{J} \cos \left( \pm \delta - \frac{\Delta m_{13}^2 L}{4E_\nu} \right) \frac{\Delta m_{12}^2 L}{4E_\nu} \sin \left( \frac{\Delta m_{13}^2 L}{4E_\nu} \right) \equiv P^{\text{inter}}, \end{aligned} \quad (105)$$

where  $\tilde{J} \equiv c_{13} \sin 2\theta_{13} \sin 2\theta_{12} \sin 2\theta_{23}$ . The first term corresponds to the atmospheric oscillation, the second one is the solar one and there is an interference term which has the information on the phase  $\delta$  and depends on both mass splittings.

These results correspond to vacuum propagation, but usually these experiments require the propagation of neutrinos in the Earth matter. The oscillation probabilities in matter can also be approximated by a similar series expansion [49]. The result has the same structure as in vacuum:

$$\begin{aligned} P_{\nu_e \nu_\mu (\bar{\nu}_e \bar{\nu}_\mu)} &= s_{23}^2 \sin^2 2\theta_{13} \left( \frac{\Delta_{13}}{B_\pm} \right)^2 \sin^2 \left( \frac{B_\pm L}{2} \right) \\ &+ c_{23}^2 \sin^2 2\theta_{12} \left( \frac{\Delta_{12}}{A} \right)^2 \sin^2 \left( \frac{A L}{2} \right) \\ &+ \tilde{J} \frac{\Delta_{12}}{A} \sin \left( \frac{A L}{2} \right) \frac{\Delta_{13}}{B_\pm} \sin \left( \frac{B_\pm L}{2} \right) \cos \left( \pm \delta - \frac{\Delta_{13} L}{2} \right), \end{aligned} \quad (106)$$

where

$$B_\pm = |A \pm \Delta_{13}| \quad \Delta_{ij} = \frac{\Delta m_{ij}^2}{2E_\nu} \quad A = \sqrt{2}G_F N_e. \quad (107)$$

The oscillation probability for neutrinos and antineutrinos now differ not just because of leptonic CP violation, but also due to the matter effects, that as we have seen can be resonant. In particular, the atmospheric term which is the dominant one, shows the expected resonant enhancement in the neutrino or antineutrino oscillation probability (depending on the ordering).

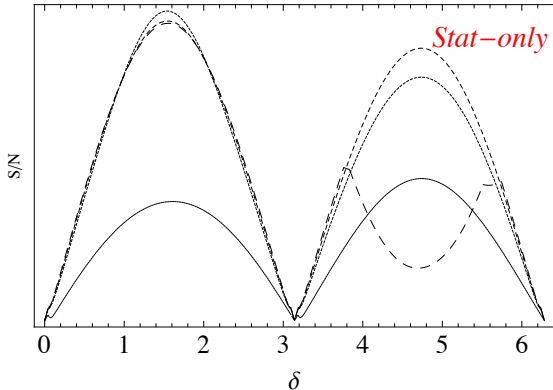


**Fig. 40:** Signal-to-noise for the discovery of CP violation at fixed  $E/L \sim |\Delta m_{\text{atm}}^2|$  as a function of the true value of  $\delta$  for  $L = 295\text{km}$  (long-dashed),  $L = 650\text{km}$  (short-dashed),  $L = 1300\text{km}$  (dotted),  $L = 2300\text{km}$  (solid). The ordering is assumed to be unknown.

The sensitivity to the interference term requires very good knowledge of the leading atmospheric term and the present degeneracies (the octant and the neutrino ordering) directly affect the leading term compromising therefore the  $\delta$  sensitivity. Either both uncertainties are solved before this measurement, or there must be sufficient sensitivity from the energy dependence of the signal to resolve all unknowns simultaneously.

A rough optimization of  $L$  for fixed  $E/L$  for discovering CP violation is shown in Fig. 40. It shows the signal-to-noise as a function of the true value of  $\delta$ , assuming only statistical errors, but including the expected dependence of the cross sections and fluxes. At very short baselines, the sensitivity is compromised due to the lack of knowledge of the neutrino ordering. In a wide intermediate region around  $\mathcal{O}(1000)\text{km}$  the sensitivity is optimal, and at much larger baselines the sensitivity deteriorates because the matter effects completely hide CP-violation.

Several projects have been proposed to search for leptonic CP violation, including conventional beams, but also novel neutrino beams from muon decays (neutrino factories), from radioactive ion decays ( $\beta$ -beams) or from spallation sources (ESS). The relatively large value of  $\theta_{13}$  has refocussed the interest in using the less challenging conventional beams and two projects are presently being developed: the HyperKamiokande detector, an upscaled version of SuperKamiokande that will measure atmospheric neutrinos with unprecedent precision, and also intercept a neutrino beam from JPARC at a relatively short baseline  $L = 295\text{km}$ , and the DUNE project that involves a  $\sim 30$  kton liquid argon neutrino detector and a neutrino beam from Fermilab to the Soudan mine at a baseline of  $L = 1500\text{km}$ . The expected sensitivities to the neutrino ordering and to CP violation of both projects are shown in Figs. 41., 42.

## 10 Outliers: the LSND anomaly

The long-standing puzzle brought by the LSND experiment is still unresolved. This experiment [52] observed a surplus of electron events in a muon neutrino beam from  $\pi^+$  decaying in flight (DIF) and a surplus of positron events in a neutrino beam from  $\mu^+$  decaying at rest (DAR). The interpretation of this data in terms of neutrino oscillations, that is a non-vanishing  $P(\nu_\mu \rightarrow \nu_e)$ , gives the range shown by a coloured band in Fig. 44.

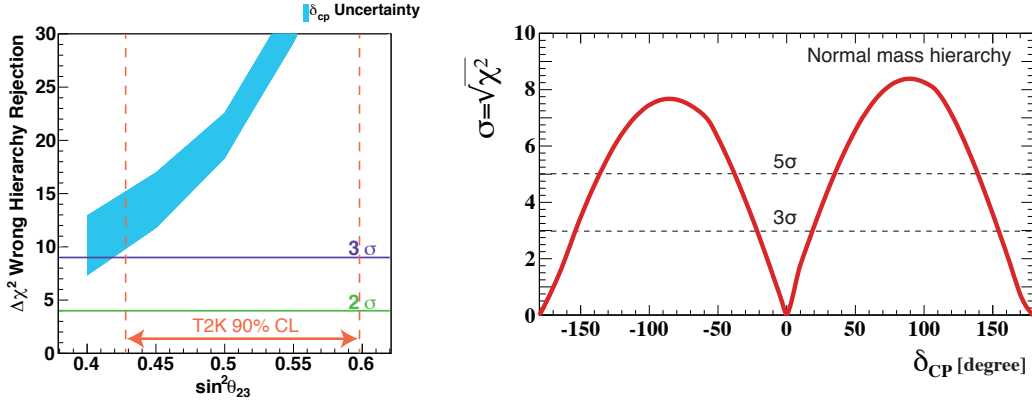


**Fig. 41:** Prospects for determining the ordering (left) and discovering CP violation (right) in HyperKamiokande (from Ref. [50]).

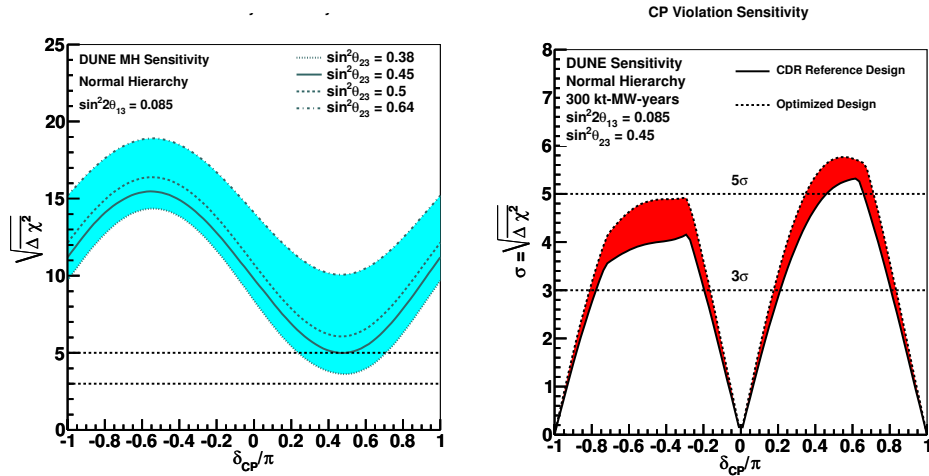


**Fig. 42:** Prospects for determining the ordering (left) and discovering CP violation (right) in DUNE ( from Ref. [51]).

$$\begin{aligned} \pi^+ &\rightarrow \mu^+ \nu_\mu \\ \nu_\mu &\rightarrow \nu_e \quad \text{DIF } (28 \pm 6/10 \pm 2) \\ \mu^+ &\rightarrow e^+ \nu_e \bar{\nu}_\mu \\ \bar{\nu}_\mu &\rightarrow \bar{\nu}_e \quad \text{DAR } (64 \pm 18/12 \pm 3) \end{aligned}$$

A significant fraction of this region was already excluded by the experiment KARMEN [53] that has unsuccessfully searched for  $\bar{\nu}_\mu \rightarrow \bar{\nu}_e$  in a similar range.

The experiment MiniBOONE was designed to further investigate the LSND signal, with inconclusive results [54]. They did not confirm the anomaly, but found some anomaly at lower energies.

On the other hand, recently the results of various short baseline (tens of meters) reactor neutrino experiments were revised, after an update on the reactor neutrino flux predictions [55–57], which increased these fluxes by a few per cent. While the measured neutrino flux was found to be in agreement with predictions before, after this revision some reactor neutrinos seem to disappear before reaching near detectors,  $L = \mathcal{O}(10)\text{m}$ . This is the so-called reactor anomaly shown in Fig. 43. This result brought some excitement because if this disappearance is due to oscillations, it might reinforce the oscillation interpretation of the LSND anomaly.

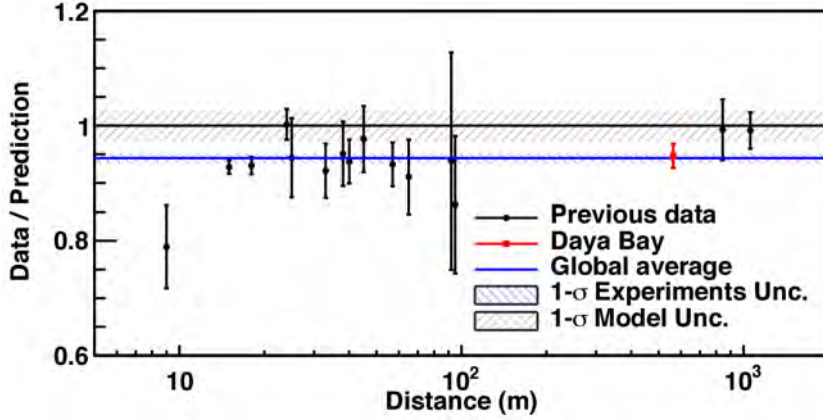


**Fig. 43:** Reactor neutrino flux measured by various near detectors compared with the recent flux predictions (from Ref. [58]).

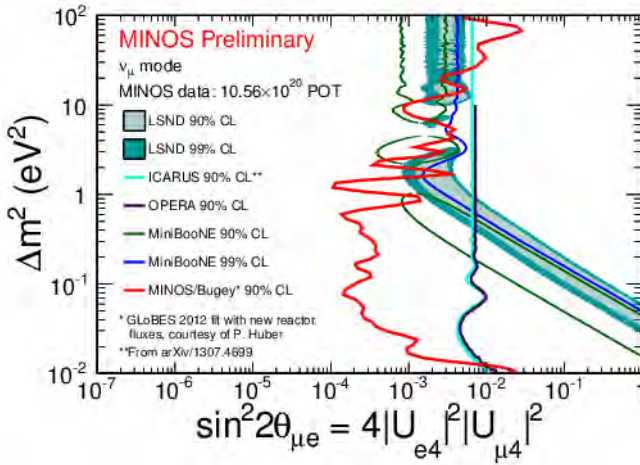


**Fig. 44:** Sterile neutrino search in the disappearance of  $\nu_\mu$ 's in MINOS (from Ref. [59]).

The required mass splitting to describe both anomalies is  $\Delta m_{\text{LSND}}^2 \simeq 1 \text{ eV}^2$ , which is much larger than the solar and atmospheric, and therefore requires the existence of at least a fourth neutrino mass eigenstate,  $i$ . If such a state can explain the LSND anomaly, it must couple to both electrons and muons. Unfortunately the smoking gun would require that also accelerator  $\nu_\mu$  disappear with the same wavelength and this has not been observed:

$$\begin{aligned} P(\nu_\mu \rightarrow \nu_e) &\propto |U_{ei} U_{\mu i}|^2 && \text{LSND} \\ 1 - P(\nu_e \rightarrow \nu_e) &\propto |U_{ei}|^4 && \text{reactor} \\ 1 - P(\nu_\mu \rightarrow \nu_\mu) &\propto |U_{\mu i}|^4 && \text{not observed} \end{aligned}$$

The strongest constraint on the disappearance of  $\nu_\mu$  in the LSND range has been recently set by MINOS+ [59] and is shown in Fig. 44 together with the region favoured by the LSND anomaly. An improvement of this sensitivity is expected also from the measurement of atmospheric neutrinos in ICECUBE.

A number of experiments are being constructed to clarify the reactor anomaly. Hopefully in the near future they will settle this long-standing puzzle.

## 11 Neutrinos and BSM Physics

The new lepton flavour sector of the SM has opened new perspectives into the flavour puzzle. As we have seen neutrinos are massive but significantly lighter than the remaining charged fermions. Clearly the gap of Fig. 11 calls for an explanation. The leptonic mixing matrix is also very different to that in the quark sector. The neutrino mixing matrix is approximately given by [43]

$$|U_{\text{PMNS}}|_{3\sigma} \simeq \begin{pmatrix} 0.80 - 0.84 & 0.51 - 0.58 & 0.137 - 0.158 \\ 0.22 - 0.52 & 0.44 - 0.70 & 0.61 - 0.79 \\ 0.25 - 0.53 & 0.46 - 0.71 & 0.59 - 0.78 \end{pmatrix}. \quad (108)$$

The CKM matrix is presently constrained [7] to be:

$$|V_{\text{CKM}}| \simeq \begin{pmatrix} 0.97427(14) & 0.22536(61) & 0.00355(15) \\ 0.22522(61) & 0.97343(15) & 0.0414(12) \\ 0.00886(33) & 0.0405(12) & 0.99914(5) \end{pmatrix}. \quad (109)$$

There is a striking difference between the two (and not only in the precision of the entries...). The CKM matrix is close to the unit matrix:

$$V_{\text{CKM}} \simeq \begin{pmatrix} 1 & O(\lambda) & O(\lambda^3) \\ O(\lambda) & 1 & O(\lambda^2) \\ O(\lambda^3) & O(\lambda^2) & 1 \end{pmatrix}, \quad \lambda \sim 0.2, \quad (110)$$

while the leptonic one has large off-diagonal entries. With a similar level of precision, it is close to the tri-bimaximal mixing pattern [60]

$$U_{\text{PMNS}} \simeq V_{\text{tri-bi}} \simeq \begin{pmatrix} \sqrt{\frac{2}{3}} & \sqrt{\frac{1}{3}} & 0 \\ -\sqrt{\frac{1}{6}} & \sqrt{\frac{1}{3}} & \sqrt{\frac{1}{2}} \\ \sqrt{\frac{1}{6}} & -\sqrt{\frac{1}{3}} & \sqrt{\frac{1}{2}} \end{pmatrix}.$$

Discrete flavour symmetries have been extensively studied as the possible origin of this pattern. For recent review see [61].

While we do not have yet a compelling explanation of the different mixing patterns, we do have one for the gap between neutrino and other fermion masses. We saw that if the light neutrinos are Majorana particles and get their mass via the Weinberg interaction of Fig. 12, they are signalling BSM physics. Neutrino masses are suppressed because they arise from a new scale of physics that could be  $\Lambda \gg v$ . Generically such BSM would induce not only neutrino masses but also other effects represented at low-energies by the  $d = 6$  effective operators of eq. (23). Unfortunately the list of  $d = 6$  operators is too long to be of guidance: which one might be more relevant is to a large extent model dependent.

We could argue that there is not better motivated BSM physics than the one that gives rise to the Weinberg operator. The simplest possibility is that Weinberg's operator, like the Fermi one in Fig. 2, arises from the exchange of a massive particle at tree level. The classification of what particles can induce the Weinberg operator at tree level has been done, and reproduces the three types of seesaw models, as depicted in Fig. 45:

- type I see-saw: SM+ heavy singlet fermions [62–65],
- type II see-saw: SM + heavy triplet scalar [66–70],
- type III see-saw: SM + heavy triple fermions [71, 72],

or combinations. The masses of the extra states define the scale  $\Lambda$ .

It is also possible that Weinberg's interaction is generated by new physics at higher orders, such as in the famous Zee model [73] and related ones [74, 75]. In this case, neutrino masses have an additional suppression by loop factors  $1/(16\pi^2)$ .

The  $d = 6$  operators induced at tree level in see-saw models of Types I to III have been worked out [76]. They give rise to a rich phenomenology that could help discriminate between the models. In particular, they could induce beyond-the-standard-model signals in  $Z$  and  $W$  decays, deviations in the  $\rho$  parameter or the  $W$  mass, and mediate rare lepton decays, as well as violations of universality and unitarity of the neutrino mass matrix. It would therefore be extremely important to search for these effects. Whether they are large enough to be observed or not depends strongly on how high the scale  $\Lambda$  is, since all these effects are suppressed by two powers of  $\Lambda$ .

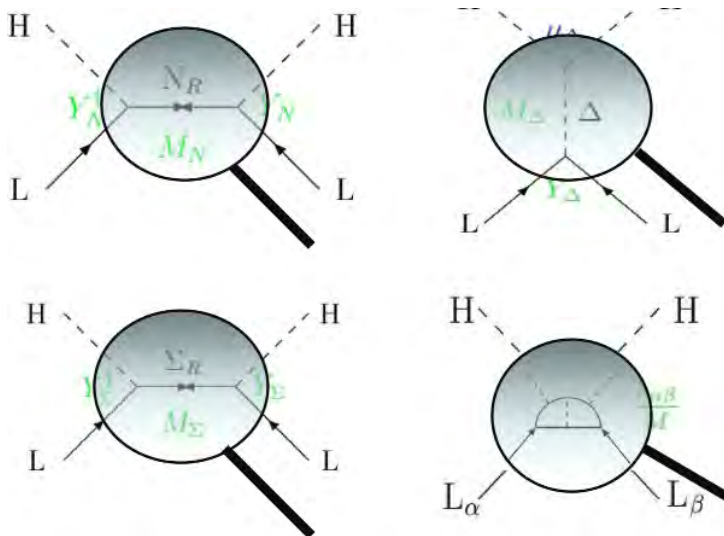


**Fig. 45:** Magnifying-glass view of Weinberg operator in see-saws Type I (top left), Type II (top right), Type III (bottom left) and Zee–Babu model (bottom right).

Unfortunately, the measurement of Weinberg's interaction leaves behind an unresolved  $\lambda \leftrightarrow \Lambda$  degeneracy that makes it impossible to know what the scale of the new physics is, even if we were to know the absolute value of neutrino masses.

The recent discovery of the Higgs field and in particular the value of its mass  $m_H = 125$  GeV [77] suggests that the SM is as healthy as ever. In spite of the Landau poles, the value of the SM couplings surprisingly conspire to make the model consistent up to arbitrarily large scales [78].

The most popular choice for  $\Lambda$  has traditionally been a grand-unification scale, given the intriguing fact that the seesaw-type ratio  $\frac{v^2}{M_{\text{GUT}}} \sim 0.01\text{--}0.1$  eV, in the right ballpark of the neutrino mass scale. However, in the absence of any stabilizing mechanism such as supersymmetry, however, the electroweak scale needs to be fine-tunned [79, 80] since the Higgs mass receives quadratic loop corrections in  $\Lambda$ . A naturalness argument would then imply that  $\Lambda < 10^7$  GeV. The opposite is not true however, the scale  $\Lambda$  would not get corrections from the electroweak scale: any value of  $\Lambda \leq v$  is technically natural.

The possibility that the scale  $\Lambda$  might be of the order of the EW scale or lower has recently been studied in more detail, with special emphasis on establishing the existing experimental constraints, and the possibility that this new physics could explain other open problems in the SM such as: the LSND and reactor anomalies, dark matter, leptogenesis, etc. The type I seesaw model is the case better studied so we will concentrate on pinning down the scale  $\Lambda$  in this context.

### 11.1 Type I seesaw model

It is arguably the minimal extension of the SM allowing for neutrino masses [62–65]. It involves the addition of  $n_R \geq 2$  singlet Weyl fermions,  $\nu_R$ , to the SM. The most general renormalizable Lagrangian which satisfies Lorentz and the gauge symmetries is given by:

$$\mathcal{L}_{\text{TypeI}} = \mathcal{L}_{\text{SM}} - \sum_{\alpha,i} \bar{L}^\alpha Y_\nu^{\alpha i} \tilde{\Phi} \nu_R^i - \sum_{i,j}^{n_R} \frac{1}{2} \bar{\nu}_R^{ic} M_N^{ij} \nu_R^j + \text{h.c.}, \quad (111)$$

where the new parameters involved are a  $3 \times n_R$  neutrino Yukawa matrix and a  $n_R \times n_R$  symmetric Majorana mass matrix for the singlet fields. Upon spontaneous symmetry breaking these couplings become mass terms, that can be written in the Majorana basis  $(\nu_L^c, \nu_R)$  as

$$\mathcal{L}_{\text{TypeI}} \rightarrow \mathcal{L}_{\text{SM}} - \frac{1}{2} (\bar{\nu}_L \quad \bar{\nu}_R^c) \begin{pmatrix} 0 & m_D \\ m_D^T & M_N \end{pmatrix} \begin{pmatrix} \nu_L^c \\ \nu_R \end{pmatrix} + \text{h.c.} + \dots \quad (112)$$

where

$$m_D = Y_\nu \frac{v}{\sqrt{2}}. \quad (113)$$

Note that Dirac neutrinos are a particular case of the model. If we invoke a global lepton number symmetry to force  $M_N = 0$ , the singlets are exactly equivalent to the right-handed neutrinos in the Dirac case described in sec. 3.1. In the opposite limit  $M_N \gg v$ , the singlets can be integrated out and give rise to the Weinberg interaction as well as others at  $d = 6$ , etc. For finite  $M_N$ , the spectrum of this theory contains in general  $3 + n_R$  Majorana neutrinos, which are admixtures of the active ones and the extra singlets. It is easy to diagonalize the mass matrix in eq. (112) in an expansion in  $m_D/M_N$ . The result to leading order in this expansion is

$$U^T \begin{pmatrix} 0 & m_D \\ m_D^T & M_N \end{pmatrix} U \simeq \begin{pmatrix} -m_D \frac{1}{M_N} m_D^T & 0 \\ 0 & M_N \end{pmatrix} + \mathcal{O}(\theta^2), \quad U = \begin{pmatrix} 1 & \theta \\ -\theta^\dagger & 1 \end{pmatrix}, \quad (114)$$

where

$$\theta = m_D^* \frac{1}{M_N}. \quad (115)$$

To this order therefore the light neutrino and heavy neutrino masses are given by

$$m_l = \text{Diag} \left[ -m_D \frac{1}{M_N} m_D^T \right], \quad M_h = \text{Diag}[M_N]. \quad (116)$$

Fig. (46) depicts the spectrum for the case of  $n_R = 3$  as a function of a common  $M_N$ . In the limit  $M_N \rightarrow 0$  the states degenerate in pairs to form Dirac fermions. As  $M_N$  increases three states get more massive proportional to  $M_N$ , while three get lighter proportional to  $M_N^{-1}$ . This is why the model is called seesaw. The number of new free parameters is large. For the case  $n_R = 3$  there are 18 fundamental parameters in the lepton sector: six of them are masses, six mixing angles and six phases. The counting of parameters for general  $n_R$  is shown in Table 4. Out of these 18 parameters we have determined only 5: two mass differences and three neutrino mixing angles.

A very convenient parametrization in this model is the so-called Casas-Ibarra [81] parametrization, which allows to write in all generality (up to corrections of  $\mathcal{O}(\theta^2)$ ) the Lagrangian parameters in terms of the parameters that can be measured at low energies: light neutrino masses and mixings, and others that cannot. In particular the phenomenology of this model depends on the spectrum of neutrino mass

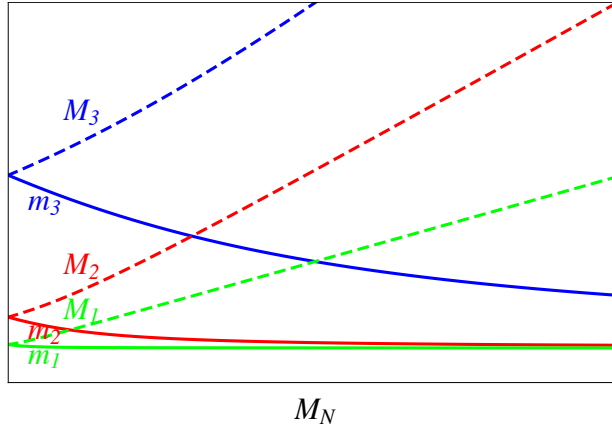


**Fig. 46:** Spectrum of th type I seesaw model for  $n_R = 3$  as a function of a common  $M_N$ .

	Yukawas	Field redefinitions	No. $m$	No. $\theta$	No. $\phi$
see-saw $E \geq M_i$	$Y_l, Y_\nu, M_R = M_R^T$ $5n^2 + n$	$U(n)^3$ $\frac{3(n^2-n)}{2}, \frac{3(n^2+n)}{2}$	$3n$	$n^2 - n$	$n^2 - n$
see-saw $E \ll M_i$	$Y_l, \alpha_\nu^T = \alpha_\nu$ $3n^2 + n$	$U(n)^2$ $n^2 - n, n^2 + n$	$2n$	$\frac{n^2-n}{2}$	$\frac{n^2-n}{2}$

**Table 4:** Number of physical parameters in the see-saw model with  $n$  families and the same number of right-handed Majorana neutrinos at high and low energies.

eigenstates, that we denote by  $(\nu_1, \nu_2, \nu_3, N_1, N_2, \dots N_{n_R})$ , and their admixture in the flavour neutrino states which is given by:

$$\begin{pmatrix} \nu_e \\ \nu_\mu \\ \nu_\tau \end{pmatrix} = U_{ll} \begin{pmatrix} \nu_1 \\ \nu_2 \\ \nu_3 \end{pmatrix} + U_{lh} \begin{pmatrix} N_1 \\ N_2 \\ .. \\ N_{n_R} \end{pmatrix}. \quad (117)$$

In the Casas-Ibarra parametrization we have

$$\begin{aligned} U_{ll} &= U_{\text{PMNS}} + \mathcal{O}(\theta^2), \\ U_{lh} &= iU_{\text{PMNS}}\sqrt{m_l}R\frac{1}{\sqrt{M_h}} + \mathcal{O}(\theta^2). \end{aligned} \quad (118)$$

where  $R$  is a general complex orthogonal matrix,  $R^T R = 1$ , which together with the heavy neutrino masses,  $M_h$ , parametrizes the parameter space inaccessible to neutrino oscillation experiments. Note that  $U_{ll}$  is the mixing matrix that we measure in neutrino oscillation experiments, assuming the heavy states are too heavy to play a role. This matrix is however no longer unitary, but the unitarity violations are parametrically of  $\mathcal{O}(\theta^2) \sim m_l/M_h$ .

The Casas-Ibarra parametrization needs to be modified in the presence of large unitarity violations. A similar parametrization valid to all orders in  $\theta$  is given in [82].

Eqs. (118) indicate that in this model there is a strong correlation between flavour mixings of the heavy states,  $U_{lh}$ , and the ratio of light-to-heavy neutrino masses. However the presence of the unknown matrix  $R$ , which is not bounded, implies that the naive seesaw scaling,  $|U_{lh}|^2 \sim m_l/M_h$ , that would hold exactly for one neutrino family, is far too naive for  $n_R > 1$ . In fact there are regions of parameter space where these mixings can be much larger than suggested by the naive scaling, and these are precisely the regions with more phenomenological interest, as we will see below.

In this model we can ask the question. What is the value of the  $M_N$  scale to avoid the hierarchy between neutrinos and the remaining fermions. If we plot the distribution of Yukawa couplings instead of the masses, we find that neutrino masses can be explained with a scale  $M_N \simeq \text{GUT}$ , if the neutrino yukawa couplings are of  $O(1)$  like the top. However if the yukawas are of the order of the electron yukawa, a scale  $M_N \sim \text{TeV}$  can also explain neutrino masses. Clearly, in both cases we have avoided making neutrinos especial, and the flavour puzzle is no worse than in the charged fermion sector. Note that this wide range of scales between TeV-GUT is the result of the quadratic dependence of the light neutrino masses on the yukawas, as opposed to the linear dependence in the Dirac case.

Let us discuss some phenomenological implications of the different choices of the scale  $M_N$ .

### Neutrinoless double-beta decay

For  $M_N \geq 100$  MeV, the model implies the presence of neutrinoless double beta decay at some level. The amplitude for this process gets contribution from the light and heavy states:

$$m_{\beta\beta} \equiv \sum_{i=1}^3 (U_{PMNS})_{ei}^2 m_i + \sum_{j=1}^{n_R} (U_{lh})_{ej}^2 M_j \frac{\mathcal{M}^{\beta\beta0\nu}(M_j)}{\mathcal{M}^{\beta\beta0\nu}(0)}, \quad (119)$$

where the ratio of matrix elements  $\mathcal{M}^{\beta\beta0\nu}$  for heavy and light mediators satisfy [83]:

$$\frac{\mathcal{M}^{\beta\beta0\nu}(M_j)}{\mathcal{M}^{\beta\beta0\nu}(0)} \propto \left( \frac{100 \text{ MeV}}{M_j} \right)^2, \quad M_j \rightarrow \infty. \quad (120)$$

If all the heavy state masses  $\gg 100$  MeV, the second term is suppressed and the amplitude contains only the light neutrino masses and mixings:

$$m_{\beta\beta} \simeq |c_{13}^2(m_1 c_{12}^2 + m_2 e^{i\alpha_1} s_{12}^2) + m_3 e^{i\alpha_2} s_{13}^2|, \quad (121)$$

and is quite well constrained from neutrino oscillation experiments. Figure 47 shows the present allowed regions for  $m_{\beta\beta}$  neglecting the heavy state contributions as a function of the sum of the light neutrino masses, that can be constrained from cosmology:

$$\Sigma \equiv m_1 + m_2 + m_3. \quad (122)$$

If the neutrino ordering would be inverted or  $\Sigma$  not much smaller than 0.1 eV, there is a good chance that the next generation of  $\beta\beta0\nu$  experiments will see a signal. A plethora of experiments using different technologies have been proposed to reach a sensitivity in  $m_{\beta\beta}$  in the range of  $10^{-2}$  eV, which could be sufficient to explore the full parameter space in the case of the IO. The importance of this measurement can hardly be overstated. A non-zero  $m_{\beta\beta}$  will imply that neutrinos are Majorana and therefore a new physics scale must exist, that lepton number is violated, and might give very valuable information on the lightest neutrino mass, and even help establishing the neutrino mass ordering. If the heavy states are not too heavy, within 100 MeV-few GeV, they could also contribute to the process significantly and even dominate over the light neutrino contribution for both orderings [85–87].

### Mini-seesaw and oscillations

If the scale  $M_N \leq$  eV (mini-seesaw models [88]), the extra heavy states could affect neutrino oscillations significantly. Strong constraints can be derived therefore from neutrino oscillation experiments

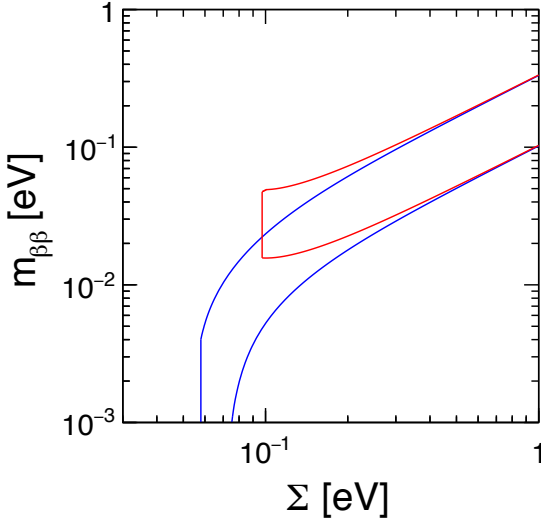


**Fig. 47:** Allowed region for  $m_{\beta\beta}$  for NO (blue contour) and IO (red contour) from a global analysis of neutrino data (from Ref. [84]).

which essentially exclude the possibility that  $M_N \in [10^{-9}(10^{-11}) \text{ eV}, 1 \text{ eV}]$  for NO(IO) [89–91]. The possibility that  $M_N \sim 1 \text{ eV}$  could explain the LSND and reactor anomalies has also been studied. It is intriguing that the best fit to the LSND and reactor anomalies [92, 93] point to mixings and masses of the extra neutrino(s) that nicely match the naive seesaw scaling. In fact mini-seesaw models provide similar fits to data [82], with much less parameters, than general phenomenological models with  $3 + N$  neutrino mixing. Both are affected however by the tension in data between the anomalies and the non-observation of  $\nu_\mu$  disappearance.

### Cosmology and the seesaw scale

For  $M_N \leq 100 \text{ MeV}$ , the heavy states in seesaw models can sizeably modify the history of the Universe: the abundance of light elements, the fluctuations in the CMB and the galaxy distribution at large scales. This is the case because these extra states contribute to the expansion either as a significant extra component of dark matter ( $\Omega_m$ ) or radiation ( $\Delta N_{\text{eff}}$ ).

The singlet states in this mass range are produced at  $T$  below the electroweak phase transition via mixing. A simple estimate of their production rate is

$$\Gamma_{s_i}(T) \simeq \sum_{\alpha} |(\tilde{U}_{lh})_{\alpha i}|^2 \times \Gamma_{\nu_{\alpha}}(T), \quad (123)$$

where  $\Gamma_{\nu_{\alpha}}$  is the interaction rate of the active neutrinos and the  $\tilde{U}_{lh}$  is the light-heavy mixing at  $T$ , strongly modified by forward scattering on the plasma particles [94]. The state  $i$  will reach thermal equilibrium if  $\Gamma_{s_i}(T)$  is larger than the Hubble parameter at some  $T$ . If this is the case, the extra species will contribute like one extra neutrino for  $T > M_i$  or like an extra component of dark matter for  $T < M_i$ . The latest results from Planck strongly constrain an extra radiation component at CMB:

$$N_{\text{eff}}(\text{CMB}) = 3.2 \pm 0.5. \quad (124)$$

and also measures the dark matter component to be  $\Omega_m = 0.308 \pm 0.012$ . Similar bounds are obtained from the abundance of light elements, BBN. These bounds exclude the possibility of having essentially any extra fully thermalized neutrino that is sufficiently long-lived to survive BBN. It can be shown that

the ratio  $\frac{\Gamma_{s_i}(T)}{H(T)}$  reaches a maximum at  $T_{max}$  [95, 96] and

$$\frac{\Gamma_{s_i}(T_{max})}{H(T_{max})} \sim \frac{\sum_\alpha |(U_{lh})_{\alpha i}|^2 M_i}{\sqrt{g_*(T_{max})}}. \quad (125)$$

The naive seesaw scaling  $U_{lh}^2 M_h \sim m_l$ , would seem to imply that the thermalization condition depends only on the light neutrino masses and is independent on the seesaw scale. In fact a detailed study shows that indeed this naive expectation holds.

For  $n_R = 2$ , the heavy states must be  $M_i \geq 100$  MeV [97], so that they might decay before BBN. For  $n_R = 3$  two things can happen [98]. If the lightest neutrino mass  $m_{\text{lightest}} \geq 3 \times 10^{-3}$  eV, all the three heavy states thermalize so  $M_i \geq 100$  MeV. If  $m_{\text{lightest}} \leq 3 \times 10^{-3}$  eV two states must be above this limit, but one of the states with mass  $M_1$  might not thermalize and therefore be sufficiently diluted.  $M_1$  may take any value provided  $m_{\text{lightest}}$ , which is presently unconstrained, is tuned accordingly.

The states that could explain the LSND and reactor anomalies will imply  $\Delta N_{\text{eff}} \geq 1$  which is essentially excluded by cosmology. For a recent detailed analysis see [99]. Exotic extensions involving hidden interactions of the extra singlet states would be needed to make them compatible.

### Warm dark matter

For  $m_{\text{lightest}} \leq 10^{-5}$  eV,  $M_1$  might be  $\mathcal{O}(\text{keV})$ , and a viable warm dark matter candidate [100, 101]. This scenario is the so-called  $\nu$ MSM model [101]. The most spectacular signal of this type of Dark Matter is a monochromatic X-ray line. Two recent analyses [102, 103] have recently shown some evidence for an unexplained X-ray line in galaxy clusters that might be compatible with a 7 keV neutrino. These results are under intense debate. If interpreted in terms of a keV neutrino, the mixing however is too small and some extra mechanism is needed to enhance the production so that it matches the required dark matter density, such as the presence of large primordial lepton asymmetries [104].

### Direct searches

In summary, cosmology and neutrino oscillations restrict a huge range of  $M_N \in [10^{-17} - 10^2]$  MeV. Naturalness arguments on the other hand point to a scale  $M_N \leq 10^{10}$  MeV, suggesting that maybe the scale of  $M_N$  is not far from the electroweak scale. States with masses in this range could be produced on the lab and searched for as peaks in meson decays, in beam dump experiments, colliders, etc. [105]. The present experimental bounds on the  $e, \mu$  mixings of these heavy states are shown in Figs. 48. The shaded regions correspond to existing constraints and the unshaded ones to prospects of various new experiments. For masses below a few GeV, the best constraints come from peak searches in meson decays. In particular the new beam dump experiment SHiP [106] can improve considerably the sensitivity in the region above kaon decays. For the lighter hadrons, improvements can be achieved with the more intense beams expected in long-baseline accelerator neutrino projects such as DUNE [107]. For

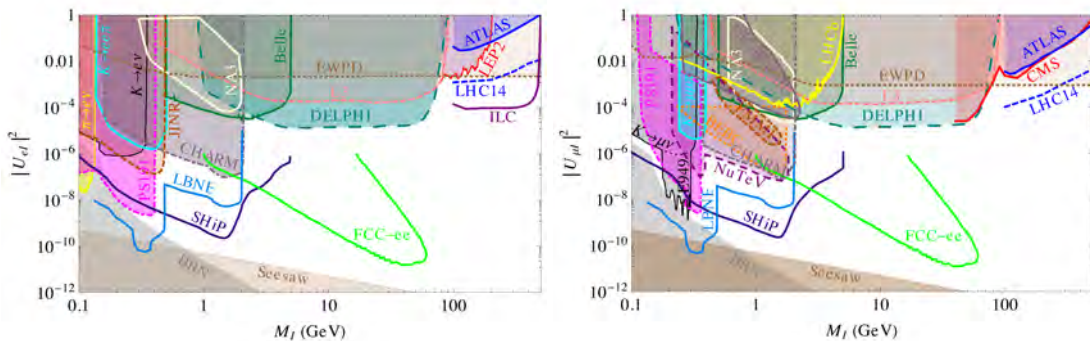


**Fig. 48:** Constraints from present and future experiments on a heavy neutrino with mixing to the electron (left) and muon (right). Shaded regions are existing bounds and the empty ones are prospects (from Ref. [106]).

masses above the  $W, Z$  masses the best constraints are presently coming from LHC searches. Processes with three leptons in the final state as in Fig. 49 seem most promising [108], although other production mechanisms like  $W\gamma$  fusion can dominate at higher masses [109]. For a recent review and further references see [106]. For masses below the  $W$  mass, it has been pointed out recently that LHC might also improve the present constraints by looking for displaced vertices in the range 1mm-1m [110–112].

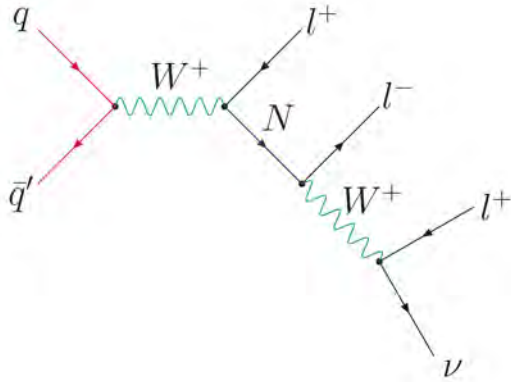


**Fig. 49:** Process to search for heavy Majoranas at LHC.

Note that present sensitivities are very far from the naive seesaw scaling  $|U_{lh}|^2 \sim m_l/M_h$ , so they are only exploring a relatively small corner of parameter space.

#### Lepton flavour violating processes

Massive neutrinos imply that lepton flavour violating processes, such as  $\mu \rightarrow e\gamma$ ,  $eee$  or  $\mu - e$  conversion in atoms, must exist at some level. Heavy Majorana neutrinos around the EW scale can significantly enhance these rates. The constraints on the mixing and mass coming from these searches cannot be included in Figs. 48 without further assumptions, since they depend on the different combination,  $|\sum_i U_{ei} U_{\mu i}^*|$ . They are shown in Fig. 50 and compared with other present constraints. Future searches will significantly improve present constraints for  $M_N \in [1, 100]$  GeV.

## 11.2 Approximate Lepton Number

Type I seesaw models with a scale around the electroweak scale are very hard to test unless  $|U_{lh}|^2 \gg m_l/M_h$ . Although this is possible in some corners of parameter space for  $n_R \geq 2$ , being in such corners might be enforced and technically natural by an approximate lepton number symmetry [113, 114].

Let us consider the simplest case  $n_R = 2$  [115]. If the two singlet states have opposite lepton charges and we impose an exact  $U(1)$  global symmetry, the  $3 \times 2$  Yukawa matrix, and the Majorana mass matrix have the following structures:

$$Y_\nu = \begin{pmatrix} Y_{e1} & 0 \\ Y_{\mu 1} & 0 \\ Y_{\tau 1} & 0 \end{pmatrix}, \quad M_N = \begin{pmatrix} 0 & M \\ M & 0 \end{pmatrix}. \quad (126)$$

For this texture, the heavy states form a Dirac pair, while the light neutrino masses vanish identically. The global symmetry can be only approximate if the zero entries in these matrices are small compared to the non-zero ones, but non vanishing. For example if we lift the zero in the 22 element of the  $M_N$  matrix to be  $\mu \ll M$ , we get the type of texture found in the so-called inverse seesaw models<sup>3</sup> [116, 117]. In

<sup>3</sup>In order to get at least two non-zero light neutrino masses by lifting the zeros of  $M_N$  only, it is necessary to have two pairs of singlets, each pair with +1 or -1 lepton charge, ie.  $n_R = 4$ . For  $n_R = 2$ , the zero's in the Yukawa matrix must be lifted aswell.

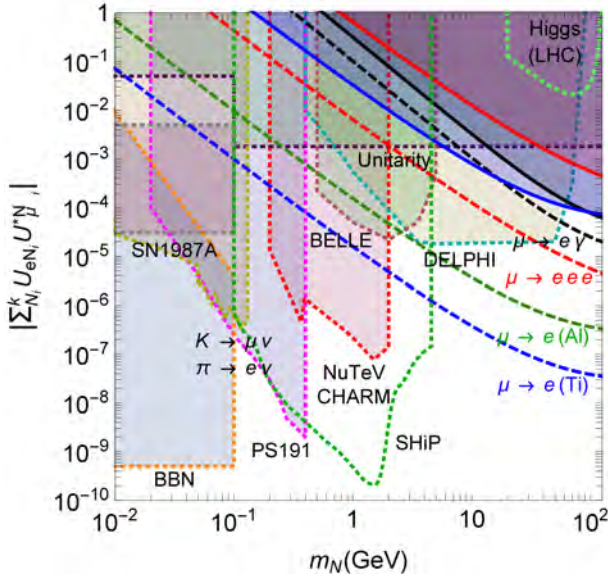


**Fig. 50:** Present bounds and prospects from lepton  $\mu \rightarrow e\gamma$ ,  $\mu \rightarrow eee$  and  $\mu - e$  conversion searches (from Ref. [106]).

this case the light neutrino mass satisfies  $m_l \propto \frac{\mu}{M^2}$ . If we integrate out the scale  $M$ , the effective field theory describing this type of models is of the form

$$\mathcal{L} = \mathcal{L}_{\text{SM}} + \sum_i \frac{\alpha_i}{\Lambda_{\text{LN}}} \mathcal{O}_i^{d=5} + \sum_i \frac{\beta_i}{\Lambda_{\text{LFV}}^2} \mathcal{O}_i^{d=6} + \dots, \quad (127)$$

where the operators that break lepton number ( $d = 5$ ) and those that preserve this symmetry ( $d = 6$ ) are generically suppressed by different scales:  $\Lambda_{\text{LN}} \simeq \frac{M^2}{\mu} \gg \Lambda_{\text{LFV}} \simeq M$ . These models therefore have a richer phenomenology if  $M$  is at the EW scale, since yukawa's need not be suppressed. Future searches such as those mentioned in the previous section will be particularly important to constraint this subclass of seesaw models.

We have discussed the phenomenological implications of the minimal Type I seesaw model, which will be the hardest to test. The other types of models leading to the Weinberg operator have a richer phenomenology since the extra states couple to gauge fields (e.g the triplet scalar in type II or the fermion in type III), and therefore can be more copiously produced at colliders. In particular lepton number violation could give rise to spectacular signals at LHC, like same-sign lepton resonances in the type II seesaw model [118]:

$$pp \rightarrow H^{++} H^{--} \rightarrow l^+ l^+ l^- l^-. \quad (128)$$

Searches for triplet scalar and fermions are now standard LHC analyses.

## 12 Leptogenesis

The Universe is made of matter. The matter–antimatter asymmetry is measured to be

$$\eta_B \equiv \frac{N_b - N_{\bar{b}}}{N_\gamma} \sim 6.21(16) \times 10^{-10}. \quad (129)$$

One generic implication of neutrino mass models is that they provide a new mechanism to explain this asymmetry dynamically.

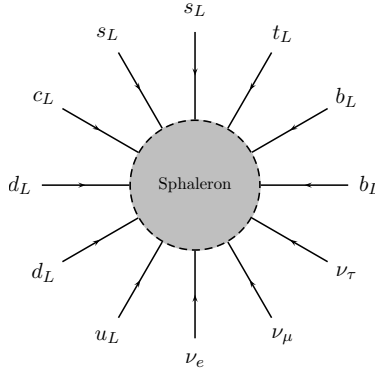


**Fig. 51:** Artistic view of a sphaleron.

It has been known for a long time that all the ingredients to generate such an asymmetry from a symmetric initial state are present in the laws of particle physics. These ingredients were first put forward by Sakharov [119]:

#### *Baryon number violation*

$B + L$  is anomalous in the SM [120] both with and without massive neutrinos. At high T in the early Universe,  $B + L$  violating transitions are in thermal equilibrium [121] due to the thermal excitation of configurations with topological charge called sphalerons, see Fig. 51.

These processes violate baryon and lepton numbers by the same amount:

$$\Delta B = \Delta L. \quad (130)$$

In seesaw models, there is generically an additional source of  $L$  violation (and  $B - L$ ). If a lepton charge is generated at temperatures where the sphalerons are still in thermal equilibrium, a baryon charge can be generated.

#### *C and CP violation*

Any lepton or baryon asymmetry can only be generated if there is  $C$  and  $CP$  violation. Seesaw models generically include new sources of  $CP$  violation. As we have seen in type I seesaw model with  $n_R = 3$  there are six new  $CP$  phases in the lepton sector. They can be absorbed in the Yukawa matrix,  $Y_\nu$  of eq. (111). For example, in the Casas-Ibarra parametrization, this matrix is written as

$$Y_\nu = U_{\text{PMNS}}^* \sqrt{m_l} R \sqrt{M_h} \frac{\sqrt{2}}{v}. \quad (131)$$

Three phases can be chosen as those in the PMNS matrix, and therefore accessible via neutrino oscillations and neutrinoless double-beta decay. The other three are the parameters of the general complex matrix  $R$ , that we cannot access at low-energies. Note that the combination  $Y_\nu^\dagger Y_\nu$  only depends on the latter.

#### *Departure from thermal equilibrium*

In seesaw models,  $B - L$  violating processes can be out-of-equilibrium at  $T \gg T_{\text{EW}}$  where the sphalerons are still in thermal equilibrium. In the type I seesaw model two possibilities of non-equilibrium  $L$  violation can be realised. In the high scale scenario  $M_i \gg v$ , the non-equilibrium condition is met at freeze out. The heavy states are thermally produced and freeze out at a temperatures similar to their masses [122]. A net lepton asymmetry can be produced if the decay rate is slower than the expansion of the Universe close to the decoupling temperature, so that the distribution functions of these states differ slightly from the thermal ones, as shown in Fig. 52. It is necessary however that  $CP$

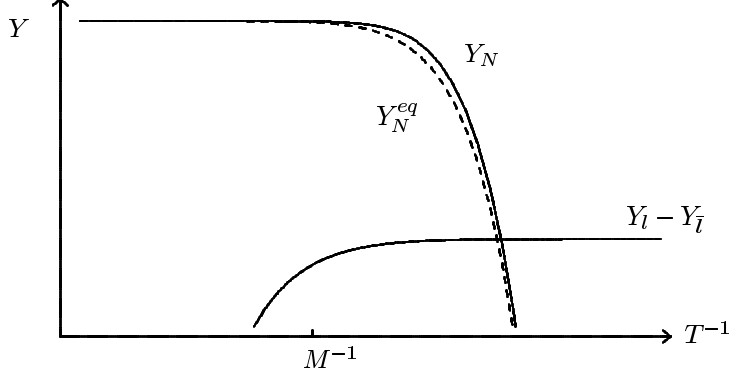


**Fig. 52:** Abundance of the heavy Majorana singlets at the decoupling temperature and the lepton number generated in the decay.

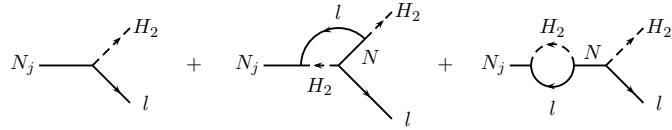


**Fig. 53:** Tree-level and one-loop diagrams contributing to heavy neutrino decays.

and C be violated in the out-of-equilibrium decays:

$$\epsilon_1 = \frac{\Gamma(N \rightarrow \Phi l) - \Gamma(N \rightarrow \Phi \bar{l})}{\Gamma(N \rightarrow \Phi l) + \Gamma(N \rightarrow \Phi \bar{l})} \neq 0. \quad (132)$$

The new CP phases in the Yukawa matrix induce an asymmetry,  $\epsilon_1$ , at the one-loop level (see Fig. 53). The final asymmetry is given by

$$Y_B = 10^{-2} \overbrace{\epsilon_1}^{\text{CP-asym}} \overbrace{\kappa}^{\text{eff. factor}}, \quad (133)$$

where  $\kappa$  is an efficiency factor which depends on the non-equilibrium dynamics. Therefore a relation between the baryon number of the Universe and the neutrino flavour parameters in  $\epsilon_1$  exists.

In the low-scale scenario, for  $M_i < v$ , the out-of-equilibrium condition is met at freeze-in [123] [101, 124]. It is possible that not all the massive states reach thermal equilibrium before  $T_{EW}$ . A non-vanishing lepton and baryon asymmetry can survive at  $T_{EW}$  and, if this is the case, sphaleron transitions that decouple at this point, can no longer wash it out. It turns out that these conditions can be met naturally in type I seesaw model for masses in the range [0.1, 100] GeV. The relevant CP asymmetries arise in the production of the heavy seesaw states via the interference of CP-odd phases from the Yukawa's with CP-even phases from propagation. A quantum treatment of the corresponding kinetic equations is mandatory in this case.

An interesting question is whether the baryon asymmetry can be predicted quantitatively from the measurements at low energies of the neutrino mass matrix. Unfortunately this is not the case generically, because the asymmetry depends on more parameters than those that are observable at low energies.

For example, in the high-scale scenario,  $\epsilon_1$  can be approximated by [125]

$$\epsilon_1 = -\frac{3}{16\pi} \sum_i \frac{\text{Im}[(Y_\nu^\dagger Y_\nu)_{i1}^2]}{(Y_\nu^\dagger Y_\nu)_{11}} \frac{M_1}{M_i}, \quad (134)$$

in the minimal model with  $M_{2,3} \gg M_1$ . It depends only on the CP phases of  $R$ , but not those in  $U_{PMNS}$ .

If the prediction of the lepton asymmetry is not possible, it is possible to constrain the neutrino mass matrix, assuming that the lepton asymmetry explains the measured baryon asymmetry. Indeed, various upper bounds can be derived on the generated asymmetry. In particular  $\epsilon_1$  has been shown [126] to satisfy

$$|\epsilon_1| \leq \frac{8}{16\pi} \frac{M_1}{v^2} |\Delta m_{\text{atm}}^2|^{1/2}, \quad (135)$$

and therefore leptogenesis in this model requires that the lightest heavy neutrino is rather heavy:

$$M_1 \geq \mathcal{O}(10^9 \text{ GeV}). \quad (136)$$

For further details and references see Ref. [125].

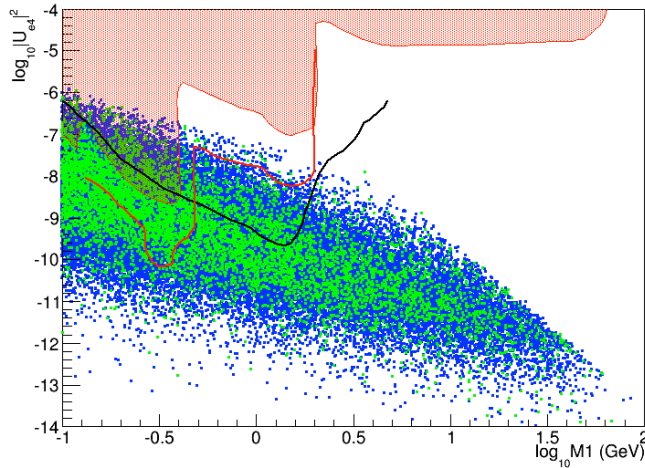


**Fig. 54:** Points on the plane  $|U_{e4}|^2$  vs  $M_1$  for which the baryon asymmetry,  $Y_B$ , is in the range  $[1/5 - 1] \times Y_B^{\text{exp}}$  (blue) and  $[1 - 5] \times Y_B^{\text{exp}}$  (green) for IO (from Ref. [127]). The red band are the present constraints [105], the solid black line shows the reach of the SHIP experiment [106] and the solid red line is the reach of LBNE near detector [107].

Interestingly, in the low-scale scenario, the states responsible for generating the baryon asymmetry might be accessible experimentally. For example, Fig. 54 shows the values of the mixing  $|(U_{lh})_{e1}|^2$  and mass  $M_1$  for which the baryon asymmetry can be explained within the type I seesaw model, compared to the sensitivity of future experiments such as SHIP and DUNE.

### 13 Conclusions

The results of many beautiful experiments in the last decade have demonstrated beyond doubt that neutrinos are massive and mix. The standard  $3\nu$  scenario can explain all available data, except that of the unconfirmed signal of LSND. The lepton flavour sector of the Standard Model is expected to be at least as complex as the quark one, even though we know it only partially.

The structure of the neutrino spectrum and mixing is quite different from the one that has been observed for the quarks: there are large leptonic mixing angles and the neutrino masses are much smaller than those of the remaining leptons. These peculiar features of the lepton sector strongly suggest that leptons and quarks constitute two complementary approaches to understanding the origin of flavour in the Standard Model. In fact, the smallness of neutrino masses can be naturally understood if there is new physics beyond the electroweak scale.

Many fundamental questions remain to be answered in future neutrino experiments, and these can have very important implications for our understanding of the Standard Model and of what lies beyond:

Are neutrinos Majorana particles? Are neutrino masses the result of a new physics scale? Is CP violated in the lepton sector? Could neutrinos be the seed of the matter–antimatter asymmetry in the Universe?

A rich experimental programme lies ahead where fundamental physics discoveries are very likely (almost warranted). We can only hope that neutrinos will keep up with their old tradition and provide a window to what lies beyond the Standard Model.

## References

- [1] E. Fermi, “Trends to a Theory of beta Radiation. (In Italian),” *Nuovo Cim.*, vol. 11, pp. 1–19, 1934. [,535(1934)].
- [2] H. Bethe and R. Peierls, “The ‘neutrino’,” *Nature*, vol. 133, p. 532, 1934.
- [3] B. Pontecorvo, “Inverse beta process,” *Camb. Monogr. Part. Phys. Nucl. Phys. Cosmol.*, vol. 1, pp. 25–31, 1991.
- [4] F. Reines and C. L. Cowan, “The neutrino,” *Nature*, vol. 178, pp. 446–449, 1956.
- [5] C. L. Cowan, F. Reines, F. B. Harrison, H. W. Kruse, and A. D. McGuire, “Detection of the free neutrino: A Confirmation,” *Science*, vol. 124, pp. 103–104, 1956.
- [6] G. Danby, J. M. Gaillard, K. A. Golianos, L. M. Lederman, N. B. Mistry, M. Schwartz, and J. Steinberger, “Observation of High-Energy Neutrino Reactions and the Existence of Two Kinds of Neutrinos,” *Phys. Rev. Lett.*, vol. 9, pp. 36–44, 1962.
- [7] K. A. Olive *et al.*, “Review of Particle Physics,” *Chin. Phys.*, vol. C38, p. 090001, 2014.
- [8] K. Assamagan *et al.*, “Upper limit of the muon-neutrino mass and charged pion mass from momentum analysis of a surface muon beam,” *Phys. Rev.*, vol. D53, pp. 6065–6077, 1996.
- [9] R. Barate *et al.*, “An Upper limit on the tau-neutrino mass from three-prong and five-prong tau decays,” *Eur. Phys. J.*, vol. C2, pp. 395–406, 1998.
- [10] S. Weinberg, “Baryon and Lepton Nonconserving Processes,” *Phys. Rev. Lett.*, vol. 43, pp. 1566–1570, 1979.
- [11] S. Weinberg, “Phenomenological Lagrangians,” *Physica*, vol. A96, pp. 327–340, 1979.
- [12] W. Buchmuller and D. Wyler, “Effective Lagrangian Analysis of New Interactions and Flavor Conservation,” *Nucl. Phys.*, vol. B268, pp. 621–653, 1986.
- [13] Z. Maki, M. Nakagawa, and S. Sakata, “Remarks on the unified model of elementary particles,” *Prog. Theor. Phys.*, vol. 28, pp. 870–880, 1962.
- [14] B. Pontecorvo, “Neutrino Experiments and the Problem of Conservation of Leptonic Charge,” *Sov. Phys. JETP*, vol. 26, pp. 984–988, 1968. [Zh. Eksp. Teor. Fiz. 53, 1717(1967)].
- [15] B. Pontecorvo, “Mesonium and anti-mesonium,” *Sov. Phys. JETP*, vol. 6, p. 429, 1957. [Zh. Eksp. Teor. Fiz. 33, 549(1957)].
- [16] E. K. Akhmedov and A. Yu. Smirnov, “Paradoxes of neutrino oscillations,” *Phys. Atom. Nucl.*, vol. 72, pp. 1363–1381, 2009, 0905.1903.
- [17] E. K. Akhmedov and J. Kopp, “Neutrino oscillations: Quantum mechanics vs. quantum field theory,” *JHEP*, vol. 04, p. 008, 2010, 1001.4815. [Erratum: JHEP10,052(2013)].
- [18] M. Cerdá, “Master Thesis University of Valencia, 2011, 0905.1903.
- [19] L. Wolfenstein, “Neutrino Oscillations in Matter,” *Phys. Rev.*, vol. D17, pp. 2369–2374, 1978.
- [20] S. P. Mikheev and A. Yu. Smirnov, “Resonance Amplification of Oscillations in Matter and Spectroscopy of Solar Neutrinos,” *Sov. J. Nucl. Phys.*, vol. 42, pp. 913–917, 1985. [Yad. Fiz. 42, 1441(1985)].
- [21] H. A. Bethe, “Energy production in stars,” *Phys. Rev.*, vol. 55, pp. 434–456, 1939.
- [22] J. N. Bahcall, M. H. Pinsonneault, and S. Basu, “Solar models: Current epoch and time dependences, neutrinos, and helioseismological properties,” *Astrophys. J.*, vol. 555, pp. 990–1012, 2001,

- astro-ph/0010346.
- [23] B. T. Cleveland, T. Daily, R. Davis, Jr., J. R. Distel, K. Lande, C. K. Lee, P. S. Wildenhain, and J. Ullman, “Measurement of the solar electron neutrino flux with the Homestake chlorine detector,” *Astrophys. J.*, vol. 496, pp. 505–526, 1998.
  - [24] W. Hampel *et al.*, “GALLEX solar neutrino observations: Results for GALLEX IV,” *Phys. Lett.*, vol. B447, pp. 127–133, 1999.
  - [25] J. N. Abdurashitov *et al.*, “Solar neutrino flux measurements by the Soviet-American Gallium Experiment (SAGE) for half the 22 year solar cycle,” *J. Exp. Theor. Phys.*, vol. 95, pp. 181–193, 2002, astro-ph/0204245. [Zh. Eksp. Teor. Fiz. 122, 211 (2002)].
  - [26] Y. Fukuda *et al.*, “Solar neutrino data covering solar cycle 22,” *Phys. Rev. Lett.*, vol. 77, pp. 1683–1686, 1996.
  - [27] Y. Fukuda *et al.*, “Measurement of the solar neutrino energy spectrum using neutrino electron scattering,” *Phys. Rev. Lett.*, vol. 82, pp. 2430–2434, 1999, hep-ex/9812011.
  - [28] J. Hosaka *et al.*, “Solar neutrino measurements in super-Kamiokande-I,” *Phys. Rev.*, vol. D73, p. 112001, 2006, hep-ex/0508053.
  - [29] Q. R. Ahmad *et al.*, “Measurement of the rate of  $\nu_e + d \rightarrow p + p + e^-$  interactions produced by  ${}^8B$  solar neutrinos at the Sudbury Neutrino Observatory,” *Phys. Rev. Lett.*, vol. 87, p. 071301, 2001, nucl-ex/0106015.
  - [30] Q. R. Ahmad *et al.*, “Direct evidence for neutrino flavor transformation from neutral current interactions in the Sudbury Neutrino Observatory,” *Phys. Rev. Lett.*, vol. 89, p. 011301, 2002, nucl-ex/0204008.
  - [31] K. Eguchi *et al.*, “First results from KamLAND: Evidence for reactor anti-neutrino disappearance,” *Phys. Rev. Lett.*, vol. 90, p. 021802, 2003, hep-ex/0212021.
  - [32] S. Abe *et al.*, “Precision Measurement of Neutrino Oscillation Parameters with KamLAND,” *Phys. Rev. Lett.*, vol. 100, p. 221803, 2008, 0801.4589.
  - [33] G. Bellini *et al.*, “Final results of Borexino Phase-I on low energy solar neutrino spectroscopy,” *Phys. Rev.*, vol. D89, no. 11, p. 112007, 2014, 1308.0443.
  - [34] M. Honda, T. Kajita, K. Kasahara, and S. Midorikawa, “A New calculation of the atmospheric neutrino flux in a 3-dimensional scheme,” *Phys. Rev.*, vol. D70, p. 043008, 2004, astro-ph/0404457.
  - [35] Y. Fukuda *et al.*, “Evidence for oscillation of atmospheric neutrinos,” *Phys. Rev. Lett.*, vol. 81, pp. 1562–1567, 1998, hep-ex/9807003.
  - [36] Y. Ashie *et al.*, “A Measurement of atmospheric neutrino oscillation parameters by SUPER-KAMIOKANDE I,” *Phys. Rev.*, vol. D71, p. 112005, 2005, hep-ex/0501064.
  - [37] Y. Ashie *et al.*, “Evidence for an oscillatory signature in atmospheric neutrino oscillation,” *Phys. Rev. Lett.*, vol. 93, p. 101801, 2004, hep-ex/0404034.
  - [38] A. Holin, “Results from the MINOS Experiment and New MINOS+ Data,” *PoS*, vol. NUFACT2014, p. 028, 2014, 1507.08564.
  - [39] F. P. An *et al.*, “Observation of electron-antineutrino disappearance at Daya Bay,” *Phys. Rev. Lett.*, vol. 108, p. 171803, 2012, 1203.1669.
  - [40] J. K. Ahn *et al.*, “Observation of Reactor Electron Antineutrino Disappearance in the RENO Experiment,” *Phys. Rev. Lett.*, vol. 108, p. 191802, 2012, 1204.0626.
  - [41] Y. Abe *et al.*, “Indication for the disappearance of reactor electron antineutrinos in the Double Chooz experiment,” *Phys. Rev. Lett.*, vol. 108, p. 131801, 2012, 1112.6353.
  - [42] K. Abe *et al.*, “Observation of Electron Neutrino Appearance in a Muon Neutrino Beam,” *Phys. Rev. Lett.*, vol. 112, p. 061802, 2014, 1311.4750.
  - [43] M. C. Gonzalez-Garcia, M. Maltoni, and T. Schwetz, “Updated fit to three neutrino mixing: status of leptonic CP violation,” *JHEP*, vol. 11, p. 052, 2014, 1409.5439.

- [44] P. A. R. Ade *et al.*, “Planck 2015 results. XIII. Cosmological parameters,” *arXiv:1502.01589[astro-ph.CO]*, 2015, 1502.01589.
- [45] S. K. Agarwalla and P. Hernandez, “Probing the Neutrino Mass Hierarchy with Super-Kamiokande,” *JHEP*, vol. 10, p. 086, 2012, 1204.4217.
- [46] S. T. Petcov and M. Piai, “The LMA MSW solution of the solar neutrino problem, inverted neutrino mass hierarchy and reactor neutrino experiments,” *Phys. Lett.*, vol. B533, pp. 94–106, 2002, hep-ph/0112074.
- [47] S. Choubey, S. T. Petcov, and M. Piai, “Precision neutrino oscillation physics with an intermediate baseline reactor neutrino experiment,” *Phys. Rev.*, vol. D68, p. 113006, 2003, hep-ph/0306017.
- [48] F. An *et al.*, “Neutrino Physics with JUNO,” *J. Phys.*, vol. G43, no. 3, p. 030401, 2016, 1507.05613.
- [49] A. Cervera, A. Donini, M. B. Gavela, J. J. Gomez Cadenas, P. Hernandez, O. Mena, and S. Rigolin, “Golden measurements at a neutrino factory,” *Nucl. Phys.*, vol. B579, pp. 17–55, 2000, hep-ph/0002108. [Erratum: Nucl. Phys.B593,731(2001)].
- [50] K. Abe *et al.*, “Physics potential of a long-baseline neutrino oscillation experiment using a J-PARC neutrino beam and Hyper-Kamiokande,” *PTEP*, vol. 2015, p. 053C02, 2015, 1502.05199.
- [51] R. Acciarri *et al.*, “Long-Baseline Neutrino Facility (LBNF) and Deep Underground Neutrino Experiment (DUNE) Conceptual Design Report Volume 2: The Physics Program for DUNE at LBNF,” *arXiv:1512.06148 [hep-ex]*, 2015, 1512.06148.
- [52] A. Aguilar-Arevalo *et al.*, “Evidence for neutrino oscillations from the observation of anti-neutrino(electron) appearance in a anti-neutrino(muon) beam,” *Phys. Rev.*, vol. D64, p. 112007, 2001, hep-ex/0104049.
- [53] B. Armbruster *et al.*, “Upper limits for neutrino oscillations muon-anti-neutrino → electron-anti-neutrino from muon decay at rest,” *Phys. Rev.*, vol. D65, p. 112001, 2002, hep-ex/0203021.
- [54] A. A. Aguilar-Arevalo *et al.*, “Improved Search for  $\bar{\nu}_\mu \rightarrow \bar{\nu}_e$  Oscillations in the MiniBooNE Experiment,” *Phys. Rev. Lett.*, vol. 110, p. 161801, 2013, 1207.4809.
- [55] T. A. Mueller *et al.*, “Improved Predictions of Reactor Antineutrino Spectra,” *Phys. Rev.*, vol. C83, p. 054615, 2011, 1101.2663.
- [56] G. Mention, M. Fechner, T. Lasserre, T. A. Mueller, D. Lhuillier, M. Cribier, and A. Letourneau, “The Reactor Antineutrino Anomaly,” *Phys. Rev.*, vol. D83, p. 073006, 2011, 1101.2755.
- [57] P. Huber, “On the determination of anti-neutrino spectra from nuclear reactors,” *Phys. Rev.*, vol. C84, p. 024617, 2011, 1106.0687. [Erratum: Phys. Rev.C85,029901(2012)].
- [58] F. P. An *et al.*, “Measurement of the Reactor Antineutrino Flux and Spectrum at Daya Bay,” *Phys. Rev. Lett.*, vol. 116, no. 6, p. 061801, 2016, 1508.04233.
- [59] A. B. Sousa, “First MINOS+ Data and New Results from MINOS,” *AIP Conf. Proc.*, vol. 1666, p. 110004, 2015, 1502.07715.
- [60] P. F. Harrison, D. H. Perkins, and W. G. Scott, “Tri-bimaximal mixing and the neutrino oscillation data,” *Phys. Lett.*, vol. B530, p. 167, 2002, hep-ph/0202074.
- [61] S. F. King and C. Luhn, “Neutrino Mass and Mixing with Discrete Symmetry,” *Rept. Prog. Phys.*, vol. 76, p. 056201, 2013, 1301.1340.
- [62] P. Minkowski, “ $\mu \rightarrow e\gamma$  at a Rate of One Out of  $10^9$  Muon Decays?,” *Phys. Lett.*, vol. B67, pp. 421–428, 1977.
- [63] M. Gell-Mann, P. Ramond, and R. Slansky, “Complex Spinors and Unified Theories,” *Conf. Proc.*, vol. C790927, pp. 315–321, 1979, 1306.4669.
- [64] T. Yanagida, “HORIZONTAL SYMMETRY AND MASSES OF NEUTRINOS,” *Conf. Proc.*, vol. C7902131, pp. 95–99, 1979.
- [65] R. N. Mohapatra and G. Senjanovic, “Neutrino Mass and Spontaneous Parity Violation,” *Phys.*

*Rev. Lett.*, vol. 44, p. 912, 1980.

- [66] M. Magg and C. Wetterich, “Neutrino Mass Problem and Gauge Hierarchy,” *Phys. Lett.*, vol. B94, p. 61, 1980.
- [67] J. Schechter and J. W. F. Valle, “Neutrino Masses in SU(2) x U(1) Theories,” *Phys. Rev.*, vol. D22, p. 2227, 1980.
- [68] C. Wetterich, “Neutrino Masses and the Scale of B-L Violation,” *Nucl. Phys.*, vol. B187, p. 343, 1981.
- [69] G. Lazarides, Q. Shafi, and C. Wetterich, “Proton Lifetime and Fermion Masses in an SO(10) Model,” *Nucl. Phys.*, vol. B181, pp. 287–300, 1981.
- [70] R. N. Mohapatra and G. Senjanovic, “Neutrino Masses and Mixings in Gauge Models with Spontaneous Parity Violation,” *Phys. Rev.*, vol. D23, p. 165, 1981.
- [71] R. Foot, H. Lew, X. G. He, and G. C. Joshi, “Seesaw Neutrino Masses Induced by a Triplet of Leptons,” *Z. Phys.*, vol. C44, p. 441, 1989.
- [72] E. Ma, “Pathways to naturally small neutrino masses,” *Phys. Rev. Lett.*, vol. 81, pp. 1171–1174, 1998, hep-ph/9805219.
- [73] A. Zee, “A Theory of Lepton Number Violation, Neutrino Majorana Mass, and Oscillation,” *Phys. Lett.*, vol. B93, p. 389, 1980. [Erratum: *Phys. Lett.* B95, 461 (1980)].
- [74] A. Zee, “Charged Scalar Field and Quantum Number Violations,” *Phys. Lett.*, vol. B161, p. 141, 1985.
- [75] K. S. Babu, “Model of ‘Calculable’ Majorana Neutrino Masses,” *Phys. Lett.*, vol. B203, p. 132, 1988.
- [76] A. Abada, C. Biggio, F. Bonnet, M. B. Gavela, and T. Hambye, “Low energy effects of neutrino masses,” *JHEP*, vol. 12, p. 061, 2007, 0707.4058.
- [77] G. Aad *et al.*, “Combined Measurement of the Higgs Boson Mass in  $pp$  Collisions at  $\sqrt{s} = 7$  and 8 TeV with the ATLAS and CMS Experiments,” *Phys. Rev. Lett.*, vol. 114, p. 191803, 2015, 1503.07589.
- [78] G. Degrassi, S. Di Vita, J. Elias-Miro, J. R. Espinosa, G. F. Giudice, G. Isidori, and A. Strumia, “Higgs mass and vacuum stability in the Standard Model at NNLO,” *JHEP*, vol. 08, p. 098, 2012, 1205.6497.
- [79] F. Vissani, “Do experiments suggest a hierarchy problem?,” *Phys. Rev.*, vol. D57, pp. 7027–7030, 1998, hep-ph/9709409.
- [80] J. A. Casas, J. R. Espinosa, and I. Hidalgo, “Implications for new physics from fine-tuning arguments. 1. Application to SUSY and seesaw cases,” *JHEP*, vol. 11, p. 057, 2004, hep-ph/0410298.
- [81] J. A. Casas and A. Ibarra, “Oscillating neutrinos and muon  $\rightarrow e, \gamma$ ,” *Nucl. Phys.*, vol. B618, pp. 171–204, 2001, hep-ph/0103065.
- [82] A. Donini, P. Hernandez, J. Lopez-Pavon, M. Maltoni, and T. Schwetz, “The minimal 3+2 neutrino model versus oscillation anomalies,” *JHEP*, vol. 07, p. 161, 2012, 1205.5230.
- [83] M. Blennow, E. Fernandez-Martinez, J. Lopez-Pavon, and J. Menendez, “Neutrinoless double beta decay in seesaw models,” *JHEP*, vol. 07, p. 096, 2010, 1005.3240.
- [84] F. Capozzi, E. Lisi, A. Marrone, D. Montanino, and A. Palazzo, “Neutrino masses and mixings: Status of known and unknown  $3\nu$  parameters,” *arXiv:1601.07777 [hep-ph]*, 2016, 1601.07777.
- [85] A. Ibarra, E. Molinaro, and S. T. Petcov, “TeV Scale See-Saw Mechanisms of Neutrino Mass Generation, the Majorana Nature of the Heavy Singlet Neutrinos and  $(\beta\beta)_{0\nu}$ -Decay,” *JHEP*, vol. 09, p. 108, 2010, 1007.2378.
- [86] M. Mitra, G. Senjanovic, and F. Vissani, “Neutrinoless Double Beta Decay and Heavy Sterile Neutrinos,” *Nucl. Phys.*, vol. B856, pp. 26–73, 2012, 1108.0004.
- [87] J. Lopez-Pavon, E. Molinaro, and S. T. Petcov, “Radiative Corrections to Light Neutrino Masses

- in Low Scale Type I Seesaw Scenarios and Neutrinoless Double Beta Decay,” *JHEP*, vol. 11, p. 030, 2015, 1506.05296.
- [88] A. de Gouvea, “See-saw energy scale and the LSND anomaly,” *Phys. Rev.*, vol. D72, p. 033005, 2005, hep-ph/0501039.
- [89] A. de Gouvea, W.-C. Huang, and J. Jenkins, “Pseudo-Dirac Neutrinos in the New Standard Model,” *Phys. Rev.*, vol. D80, p. 073007, 2009, 0906.1611.
- [90] A. de Gouvea and W.-C. Huang, “Constraining the (Low-Energy) Type-I Seesaw,” *Phys. Rev.*, vol. D85, p. 053006, 2012, 1110.6122.
- [91] A. Donini, P. Hernandez, J. Lopez-Pavon, and M. Maltoni, “Minimal models with light sterile neutrinos,” *JHEP*, vol. 07, p. 105, 2011, 1106.0064.
- [92] C. Giunti and M. Laveder, “3+1 and 3+2 Sterile Neutrino Fits,” *Phys. Rev.*, vol. D84, p. 073008, 2011, 1107.1452.
- [93] J. Kopp, P. A. N. Machado, M. Maltoni, and T. Schwetz, “Sterile Neutrino Oscillations: The Global Picture,” *JHEP*, vol. 05, p. 050, 2013, 1303.3011.
- [94] D. Notzold and G. Raffelt, “Neutrino Dispersion at Finite Temperature and Density,” *Nucl. Phys.*, vol. B307, p. 924, 1988.
- [95] R. Barbieri and A. Dolgov, “Bounds on Sterile-neutrinos from Nucleosynthesis,” *Phys. Lett.*, vol. B237, p. 440, 1990.
- [96] K. Kainulainen, “Light Singlet Neutrinos and the Primordial Nucleosynthesis,” *Phys. Lett.*, vol. B244, pp. 191–195, 1990.
- [97] P. Hernandez, M. Kekic, and J. Lopez-Pavon, “Low-scale seesaw models versus  $N_{eff}$ ,” *Phys. Rev.*, vol. D89, no. 7, p. 073009, 2014, 1311.2614.
- [98] P. Hernandez, M. Kekic, and J. Lopez-Pavon, “ $N_{eff}$  in low-scale seesaw models versus the lightest neutrino mass,” *Phys. Rev.*, vol. D90, no. 6, p. 065033, 2014, 1406.2961.
- [99] S. Hannestad, R. S. Hansen, T. Tram, and Y. Y. Y. Wong, “Active-sterile neutrino oscillations in the early Universe with full collision terms,” *JCAP*, vol. 1508, no. 08, p. 019, 2015, 1506.05266.
- [100] S. Dodelson and L. M. Widrow, “Sterile-neutrinos as dark matter,” *Phys. Rev. Lett.*, vol. 72, pp. 17–20, 1994, hep-ph/9303287.
- [101] T. Asaka and M. Shaposhnikov, “The nuMSM, dark matter and baryon asymmetry of the universe,” *Phys. Lett.*, vol. B620, pp. 17–26, 2005, hep-ph/0505013.
- [102] E. Bulbul, M. Markevitch, A. Foster, R. K. Smith, M. Loewenstein, and S. W. Randall, “Detection of An Unidentified Emission Line in the Stacked X-ray spectrum of Galaxy Clusters,” *Astrophys. J.*, vol. 789, p. 13, 2014, 1402.2301.
- [103] A. Boyarsky, O. Ruchayskiy, D. Iakubovskyi, and J. Franse, “Unidentified Line in X-Ray Spectra of the Andromeda Galaxy and Perseus Galaxy Cluster,” *Phys. Rev. Lett.*, vol. 113, p. 251301, 2014, 1402.4119.
- [104] X.-D. Shi and G. M. Fuller, “A New dark matter candidate: Nonthermal sterile neutrinos,” *Phys. Rev. Lett.*, vol. 82, pp. 2832–2835, 1999, astro-ph/9810076.
- [105] A. Atre, T. Han, S. Pascoli, and B. Zhang, “The Search for Heavy Majorana Neutrinos,” *JHEP*, vol. 05, p. 030, 2009, 0901.3589.
- [106] S. Alekhin *et al.*, “A facility to Search for Hidden Particles at the CERN SPS: the SHiP physics case,” *arXiv:1504.04855[hep-ph]*, 2015, 1504.04855.
- [107] C. Adams *et al.*, “The Long-Baseline Neutrino Experiment: Exploring Fundamental Symmetries of the Universe,” 2013, 1307.7335.
- [108] F. del Aguila and J. A. Aguilar-Saavedra, “Distinguishing seesaw models at LHC with multi-lepton signals,” *Nucl. Phys.*, vol. B813, pp. 22–90, 2009, 0808.2468.
- [109] P. S. B. Dev, A. Pilaftsis, and U.-k. Yang, “New Production Mechanism for Heavy Neutrinos at

- the LHC,” *Phys. Rev. Lett.*, vol. 112, no. 8, p. 081801, 2014, 1308.2209.
- [110] J. C. Helo, M. Hirsch, and S. Kovalenko, “Heavy neutrino searches at the LHC with displaced vertices,” *Phys. Rev.*, vol. D89, p. 073005, 2014, 1312.2900.
- [111] E. Izaguirre and B. Shuve, “Multilepton and Lepton Jet Probes of Sub-Weak-Scale Right-Handed Neutrinos,” *Phys. Rev.*, vol. D91, no. 9, p. 093010, 2015, 1504.02470.
- [112] A. M. Gago, P. Hernandez, J. Jones-Perez, M. Losada, and A. Moreno Briceño, “Probing the Type I Seesaw Mechanism with Displaced Vertices at the LHC,” *Eur. Phys. J.*, vol. C75, no. 10, p. 470, 2015, 1505.05880.
- [113] G. C. Branco, W. Grimus, and L. Lavoura, “The Seesaw Mechanism in the Presence of a Conserved Lepton Number,” *Nucl. Phys.*, vol. B312, p. 492, 1989.
- [114] J. Kersten and A. Yu. Smirnov, “Right-Handed Neutrinos at CERN LHC and the Mechanism of Neutrino Mass Generation,” *Phys. Rev.*, vol. D76, p. 073005, 2007, 0705.3221.
- [115] M. B. Gavela, T. Hambye, D. Hernandez, and P. Hernandez, “Minimal Flavour Seesaw Models,” *JHEP*, vol. 09, p. 038, 2009, 0906.1461.
- [116] D. Wyler and L. Wolfenstein, “Massless Neutrinos in Left-Right Symmetric Models,” *Nucl. Phys.*, vol. B218, p. 205, 1983.
- [117] R. N. Mohapatra and J. W. F. Valle, “Neutrino Mass and Baryon Number Nonconservation in Superstring Models,” *Phys. Rev.*, vol. D34, p. 1642, 1986.
- [118] W.-Y. Keung and G. Senjanovic, “Majorana Neutrinos and the Production of the Right-handed Charged Gauge Boson,” *Phys. Rev. Lett.*, vol. 50, p. 1427, 1983.
- [119] A. D. Sakharov, “Violation of CP Invariance, c Asymmetry, and Baryon Asymmetry of the Universe,” *Pisma Zh. Eksp. Teor. Fiz.*, vol. 5, pp. 32–35, 1967. [Usp. Fiz. Nauk 161, 61 (1991)].
- [120] G. ’t Hooft, “Symmetry Breaking Through Bell-Jackiw Anomalies,” *Phys. Rev. Lett.*, vol. 37, pp. 8–11, 1976.
- [121] V. A. Kuzmin, V. A. Rubakov, and M. E. Shaposhnikov, “On the Anomalous Electroweak Baryon Number Nonconservation in the Early Universe,” *Phys. Lett.*, vol. B155, p. 36, 1985.
- [122] M. Fukugita and T. Yanagida, “Baryogenesis Without Grand Unification,” *Phys. Lett.*, vol. B174, p. 45, 1986.
- [123] E. K. Akhmedov, V. Rubakov, and A. Y. Smirnov, “Baryogenesis via neutrino oscillations,” *Phys. Rev. Lett.*, vol. 81, pp. 1359–1362, 1998, hep-ph/9803255.
- [124] L. Canetti, M. Drewes, T. Frossard, and M. Shaposhnikov, “Dark Matter, Baryogenesis and Neutrino Oscillations from Right Handed Neutrinos,” *Phys. Rev.*, vol. D87, p. 093006, 2013, 1208.4607.
- [125] S. Davidson, E. Nardi, and Y. Nir, “Leptogenesis,” *Phys. Rept.*, vol. 466, pp. 105–177, 2008, 0802.2962.
- [126] S. Davidson and A. Ibarra, “A Lower bound on the right-handed neutrino mass from leptogenesis,” *Phys. Lett.*, vol. B535, pp. 25–32, 2002, hep-ph/0202239.
- [127] P. Hernandez, M. Kekic, J. Lopez-Pavon, J. Racker, and N. Rius, “Leptogenesis in GeV scale seesaw models,” *JHEP*, vol. 10, p. 067, 2015, 1508.03676.